Design of Halbach Permanent Magnet External Rotor Machine with Reuse & Recycle Magnet Concepts for Automotive Applications

Amit Kumar Jha

Communauté UNIVERSITÉ Grenoble Alpes

THÈSE

Pour obtenir le grade de

DOCTEUR DE LA COMMUNAUTE UNIVERSITE GRENOBLE ALPES

Spécialité : GENIE ELECTRIQUE

Arrêté ministériel : 25 mai 2016

Présentée par

Amit Kumar JHA

Thèse dirigée par **Afef LEBOUC** et codirigée par **Lauric GARBUIO**,
préprée au sein du **Laboratoire de Génie Electrique de Grenoble, G2Elab**
dans **l'École Doctorale Electronique, Electrotechnique, Automatique, Traitement du Signal (EEATS)**

Conception d'une machine à rotor externe de type Halbach pour l'électromobilité considérant la réutilisation et le recyclage des aimants permanents

Design of Halbach Permanent Magnet External Rotor Machine with Reuse & Recycle Magnet Concepts for Automotive Applications

Thèse soutenue publiquement le **28 janvier 2019**,
devant le jury composé de :

Madame AFEF LEBOUC
DIRECTRICE DE RECHERCHE CNRS au G2Elab, Directrice de thèse
Monsieur LAURIC GARBUIO
MAITRE DE CONFERENCES, GRENOBLE INP, Co-encadrant de thèse
Monsieur JEAN-MARC DUBUS
INGENIEUR, VALEO Powertrain Electrical Systems, Examinateur
Monsieur GEORGES BARAKAT
PROFESSEUR, UNIVERSITE LE HAVRE NORMANDIE, Président de jury
Monsieur CHRISTOPHE ESPANET
PROFESSEUR, UNIVERSITE DE FRANCHE-COMTE, Rapporteur
Madame ELENA LOMONOVA
PROFESSEUR, UNIVERSITE TECH. EINDHOVEN, PAYS BAS, Rapporteur
Monsieur JEAN-CLAUDE MIPO,
RESPONSABLE DES TECHNOLOGIES AVANCEES, VALEO Powertrain Electrical Systems, Invité
Madame SOPHIE PERSONNAZ,
DIRECTRICE ELECTROTECHNIQUE, VALEO Powertrain Electrical Systems, Invité
Monsieur JEAN-PAUL YONNET,
DIRECTEUR DE RECHERCHE EMERITE CNRS au G2Elab, Invité

Abstract

Electric vehicles (EVs) or Hybrid electric vehicles (HEVs) offer many advantages over the conventional IC engine vehicles. According to recent trends, the demand for efficient (H)EVs is expected to grow significantly. For a high-power range, permanent magnet based motor technology has been the preferred choice for motors deployed in (H)EVs. Growing demand of highly efficient motors is in direct correlation to the demand of strong magnets (NdFeB or SmCo), which uses rare earth elements (REE). The availability and supply of REEs specially heavy REEs is very critical. Therefore, the aim of this doctoral thesis is to design an outer rotor Halbach motor for a (H)EV application with easy recycling and reuse of the magnet. Further, the project aims to investigate and propose the manufacturing of a Halbach magnet used in a high power motor EV applications.

Firstly, the manufacturing of Halbach magnet using a sintered and a bonded NdFeB magnet was investigated. The study shows that the manufacturing of Halbach array using a bonded magnet is much easier and more cost effective than the sintered magnet. The characterisation of a bonded NdFeB magnet used for manufacturing a Halbach magnet was also performed. Various recycling routes for both sintered and bonded magnets were analysed and it can be inferred that bonded magnets are much easier to recycle in a cost effective and environment friendly manner. The thesis also proposes the recycling route for the bonded magnet used in the motor.

Secondly, a motor with bonded Halbach magnet was designed using 2D and 3D FEM. To achieve a highly efficient and compact motor, fractional slot tooth coil winding was used. The properties of Halbach magnet was calculated using FEM model and benchmarked against the analytical model. The results obtained from the two approaches were in close agreement. Further, the impact of slot pole combinations on motor losses and the subsequent torque were investigated, specifically eddy loss (considering all the design constraints). Different strategies to use recycled magnet with lower remanence is also presented. It is shown that using a recycled magnet with increased axial length of the motor could be the best choice considering different factors, specially manufacturing of the Halbach magnet. Based on different parametric studies a design of the motor was proposed and prototype was built. It was demonstrated that a high power Halbach magnet could be built economically using a bonded NdFeB magnet. The airgap flux density of the rotor, measured on the prototype is in close agreement with the calculated values.

Additionally, WIRE (Weighted Index of Recycling and Energy) methodology was presented to benchmark different motor designs on the basis of performance and recyclability. The method developed produces two indices based on:

- Ease of motor recyclability considering material, assembly and disassembly of magnets.
- Impact of a recycled magnet on the energy consumption of a motor during its operational lifetime.

Using both the above indices, one can easily analyse the pros and cons of different motor designs on the basis of recyclability and energy efficiency. The proposed motor design was evaluated using the developed method and it is shown that the motor is easy to assemble and disassemble. In addition, the motor assembly (glue free) enables easy magnet extraction and direct reuse. The evaluated energy index of the motor shows the impact of using a recycled magnet and its viability for EV applications in different scenarios.

Finally, a motor prototype was built and measurements were done. The measured results are in good agreement with the calculated values. The assembly and disassembly of the motor were done manually using standard tools with ease.

Résumé

L'invention des véhicules électriques remonte au XIXe siècle. Cependant, en raison de limitations technologiques, ces véhicules n'ont pas pu obtenir de succès commercial jusqu'ici. Les développements récents dans le domaine de l'électronique de puissance et des batteries ont fait des véhicules électriques (VE) et électriques hybrides (VEH) des options commercialement viables pour le transport. De plus, l'utilisation des VE-H est respectueuse de l'environnement et est destinée à remplacer les voitures à moteur à combustion interne. Les véhicules électriques (VE) ou les véhicules électriques hybrides (VEH) offrent de nombreux avantages par rapport aux véhicules classiques à moteur à combustion interne. Selon les tendances actuelles du marché, la demande en VE-H à haut rendement énergétique devrait augmenter considérablement. Le moteur électrique est un composant important du VE-H. Pour la gamme des moteurs électriques à puissance élevée intégrés dans les VE-H, la technologie des moteurs à aimants permanents reste le choix privilégié. La demande croissante de moteurs à haut rendement est en corrélation directe avec la demande en aimants permanents terres rares à forte densité énergétique (NdFeB ou SmCo). La disponibilité et l'offre en terres rares, particulièrement les terres rares lourdes, est très critique. C'est pourquoi le projet DEMETER (Design and Recycling of Rare-Earth Permanent Magnet Motors and Generators in Hybrid and Full Electric Vehicles) met l'accent sur le développement de méthodes innovantes de recyclage et de production d'aimants ainsi que sur la conception de moteurs en prenant en compte la réutilisation, le recyclage et l'extraction des aimants. Il s'agit enfin de considérer leur impact environnemental. L'objectif est d'étudier le cycle de vie complet de l'aimant depuis sa production en passant par le recyclage et sa réutilisation jusqu'à sa fin de vie. Le projet a identifié 3 façons de recycler les aimants. Le premier, et le plus souhaitable, est d'extraire les aimants des moteurs électriques en fin de vie et de les réutiliser directement. Pour ce faire, les moteurs/générateurs doivent être équipés d'aimants de taille standard et conçus avec le même matériau pour une extraction facile. Cette pratique n'est pas courante à l'heure actuelle. En outre, la réutilisation des aimants est difficile car les propriétés des aimants se détériorent pendant leur utilisation. Lors de la réutilisation des aimants, il est difficile d'obtenir les mêmes performances, ce qui rend ce mode de recyclage pratiquement difficile à réaliser sans être impossible. La deuxième option est le recyclage direct : les aimants sont extraits du moteur et traités par décapage à l'hydrogène, moulage plasma/bande et frittage plasma par étincèle pour produire de nouveaux aimants. Enfin, la troisième voie est nommée recyclage indirect. Les aimants extraits sont décomposés en composants chimiques élémentaires. Ces derniers sont ensuite utilisés pour fabriquer de nouveaux aimants.

15 travaux de thèse font partie du projet et portent sur les différentes étapes du cycle de vie des aimants. L'ensemble du projet DEMETER est divisé en 4 groupes de travail (GT), liés les uns aux autres. Le groupe de travail 3 (GT3) concerne le design du moteur électrique en tenant compte de la réutilisation et du recyclage des aimants dès la phase de conception du moteur. 4 topologies de moteurs pour VE-H sont étudiées et conçues en partant de différents cahiers des charges. Le moteur étudié et développé dans le cadre de cette thèse est un moteur à rotor extérieur à aimant Halbach pour une application VEH à fonctionnement 100 % électrique ZEV (Zero Emission Vehicle). Toutefois, ce moteur peut être facilement réutilisé pour un véhicule tout électrique (VE) en mettant simplement à l'échelle ses dimensions et ses propriétés.

Le but de cette thèse est de concevoir un moteur Halbach à rotor extérieur pour une application VE-H qui doit permettrait le recyclage et la réutilisation faciles de l'aimant. De plus, le projet vise à étudier et à proposer une méthode de fabrication d'un rotor à aimant de type cylindre de Halbach en vue d'utilisation dans les applications des VE des moteurs de forte puissance. Cette thèse porte sur la conception d'une machine électrique à aimants permanents (AP) à rotor extérieur avec cylindre de Halbach pour un véhicule électrique hybride à fonctionnement possible en tout électrique (mode ZEV). Du point de vue de la fabrication, le moteur à rotor extérieur n'est pas le plus adapté en raison de son assemblage complexe. Cependant, la topologie présente de nombreux avantages en ce qui concerne les performances (ex : densité de puissance) du moteur. Deux assemblages mécaniques sont examinés dans le chapitre 4 . Nous concluons que le montage n° 2 (où le flasque du stator n'est pas relié à la culasse du rotor) est le mieux adapté au cahier des charges.

De nombreuses études ont montré que l'utilisation du rotor à cylindre de Halbach présente plusieurs avantages : une densité de flux magnétique élevée, un faible bruit acoustique, une faible ondulation du couple, etc. Cependant, la fabrication complexe et coûteuse du rotor à cylindre de Halbach limite son utilisation dans différentes applications. Le cylindre de Halbach peut être fabriqué avec des aimants frittés ou des aimants liés. La fabrication d'aimants liés est plus simple et moins coûteuse que celle d'aimants frittés, en particulier pour les cylindres de Halbach. De plus, l'utilisation d'aimants liés permet d'obtenir un cylindre de Halbach idéal, alors qu'avec des aimants frittés, de nombreuses pièces magnétiques sont nécessaires, ce qui augmente la complexité de fabrication. La faible rémanence de l'aimant lié peut être légèrement améliorée en introduisant une anisotropie du matériau. C'est pourquoi le rotor Halbach en aimant anisotrope est un choix inétressant, compte tenu de son coût de fabrication et de sa complexité. La caractérisation du matériau NdFeB lié (MagFine18P du fabricant Aichi Steel) utilisé pour fabriquer le prototype a été effectuée. L'échantillon magnétique a un bon rapport d'anisotropie et les propriétés magnétiques sont très stables en température, malgré l'absence de dysprosium dans l'aimant. Le liant PPS offre une très bonne résistance mécanique à haute température, comme le montrent les résultats desmesures. Il n'y a aucun signe de détérioration des propriétés mécaniques ou magnétiques due aux températures élevées. , On peut

déduire des résultats de mesures que l'aimant est viable jusqu'à 150 %/°C. Une autre caractéristique importante de l'aimant lié est sa haute résistivité électrique. Les résistivités de quelques échantillons ont été mesurées et les valeurs obtenues se situent entre 120 et 150 $\mu\Omega$.m, soit environ 100 fois plus que les aimants NdFeB frittés. Cela implique que, même à très haute vitesse, les pertes par courants de Foucault de l'aimant devraient être très inférieures. De plus, la conductivité thermique de l'aimant a également été mesurée à différentes puissances d'entrée. La valeur moyenne de conductivité obtenue est de 1 $W.m^{-1}.K^{-1}$. La valeur est inférieure à celle de l'aimant fritté. En dernier lieu, la densité de flux magnétique dans l'air du rotor Halbach a été mesurée et les valeurs sont en bon accord avec le calcul éléments finis. De plus, la distribution du champ magnétique du cylindre de Halbach est également très proche de la répartition idéale théorique. Les différentes options de recyclage des aimants frittés et des aimants liés sont également abordées dans ce chapitre. Comparé aux aimants frittés, le processus de recyclage des aimants liés est beaucoup plus simple. Bien qu'il ne soit pas très courant d'utiliser des aimants liés dans des moteurs électriques pour applications automobiles, les aimants liés ont connu récemment un regain d'attention. Les résultats montrent qu'avec un mélange d'aimant vierge et d'aimant ancien (jusqu'à 30 %), il est possible d'obtenir un aimant recyclé sans perte significative au niveau des propriétés magnétiques. Le procédé de recyclage proposé dans cette thèse est très simple et respectueux de l'environnement. Cependant, les méthodes de recyclage nécessitent davantage d'expérimentations et d'analyses pour déterminer les propriétés optimales de l'aimant recyclé pour l'application moteur.

La thèse présente une démarche de conception de moteur électrique à rotor extérieur pour un véhicule électrique hybride de type tout électrique. Le moteur est équipé d'un rotor à cylindre de Halbach idéal fabriqué avec des aimants permanents NdFeB liés. Il est connu que la densité de flux magnétique dans l'entrefer du cylindre de Halbach augmente avec le nombre de pôles, contrairement au rotor à aimants en surface classique. Cela a pour conséquence d'augmenter le couple. L'utilisation d'une culasse rotorique augmente la densité du flux magnétique dans l'entrefer. En outre, pour obtenir une densité de couple importante et une compacité élevée, un stator à pas fractionnaire et à bobinage concentré sur dent est choisi. L'impact des combinaisons de nombres d'encoches et de pôles a également été étudié en tenant compte de toutes les contraintes de conception. Les performances du moteur varient considérablement en fonction de la combinaison. Par conséquent, le choix de la combinaison est critique. Les pertes par courants de Foucault dans les aimants ont également été étudiées à l'aide de modèles éléments finis 2D et 3D. Malgré la résistivité électrique élevée des aimants liés, les pertes par courants de Foucault dans les aimants est importante lorsqu'on utilise des bobinages concentrés sur dent à pas fractionnaire, surtout à haute vitesse. On a également constaté qu'avec l'augmentation du nombre d'encoches, les pertes par courants induits diminuent. De plus, avec un rapport D/L (diamètre sur longueur) élevé, l'impact des courants de Foucault perpendiculaires à la direction axiale est très critique et n'est pas considéré dans les calculs 2D. Par

conséquent, une grande différence a été trouvée entre les calculs des pertes en 3D et en 2D.

Sur la base des résultats de l'étude paramétrique, la combinaison 24 encoches et 26 pôles a été sélectionnée comme la meilleure.. Plusieurs dimensionnements de moteurs ont été étudiés en faisant varier la longueur axiale et l'épaisseur de l'aimant de telle sorte qu'ils répondent aux spécifications sur l'enveloppe couple-vitesse. Il a été constaté que le moteur de plus grande longueur axiale a une masse magnétique plus faible et satisfait à l'exigence de vitesse de rotation du couple. Cependant, le dimensionnement final (n° 1) a été choisi en fonction de l'espace disponible pour le moteur. Le calcul thermique montre que le moteur ne présente aucun risque en fonctionnement continu. Cependant, en court-circuit triphasé permanent à vitesse maximale, l'aimant et la température de l'enroulement atteignent la limite critique. La probabilité d'occurrence de ce défaut de fonctionnement est moindre et, par conséquent, aucun changement dans le dimensionnement n'a été apporté. L'étude de désaimantation de l'aimant montre que l'aimant devrait pas subir de s désaimantation irréversible en cas de défaut de type court-circuit transitoire. Le fonctionnement en régime permanent de type court-circuit triphasé à vitesse maximale induit une température élevée dans la machine, ce qui rend l'aimant sujet à la désaimantation. Cependant, en régime permanent, le champ de désaimantation sera beaucoup plus petit que le champ en régime transitoire et, par conséquent, aucune désaimantation irréversible n'est prévue. De plus, la droite de recul de l'aimant montre une perte de rémanence négligeable pour une désaimantation partielle et la disposition idéale du cylindre de Halbach est également un avantage pour éviter la désaimantation. La cartographie de rendement du moteur montre une large zone de rendement supérieur à 90 %, ce qui est un paramètre critique pour les moteurs des VE - H.

L'étude de l'impact de différentes stratégies d'utilisation d'aimants recyclés sur les caractéristiques couple-vitesse du moteur a également été réalisée. Nous supposons que l'induction rémanente des aimants diminue de 20 %. La première méthode consiste à augmenter la puissance du convertisseur électronique, en conservant le même dimensionnement de moteur avec des aimants recyclés, de sorte que le moteur ait la même caractéristique de couple-vitesse. Le calcul a montré qu'un courant d'alimentation supérieur de près de 5 % est nécessaire pour obtenir la caractéristique couple-vitesse souhaitée avec une induction rémanente inférieure de 5 %. Cependant, pour une réduction plus importante de la rémanence, l'augmentation du courant n'est pas linéaire et est beaucoup plus élevée. Par conséquent, le dimensionnement de moteur proposé peut être utilisé facilement pour des aimants recyclés avec une rémanence jusqu'à 5 % plus faible sans perte de performance importante. Les trois autres méthodes étudiées nécessitent une modification du dimensionnement du moteur, au lieu de la modification du convertisseur de puissance. Dans les situations où l'espace n'est pas une contrainte, nous avons montré que la longueur axiale ou le diamètre extérieur du moteur peuvent être augmentés pour obtenir la même caractéristique couple-vitesse avec des aimants recyclés ayant une induction

rémanente jusqu'à 20 % inférieure. Cependant, la fabrication d'un rotor à cylindre de de Halbach avec une longueur axiale augmentée serait beaucoup plus facile par rapport à celle avec l'augmentation du diamètre extérieur. En cas d'augmentation de la longueur axiale, le diamètre et l'épaisseur de l'anneau constitué d'aimants ne changent pas et il n'est donc pas nécessaire de modifier le processus de fabrication et les outils utilisés sur la ligne de production. L'assemblage d'un moteur à grande longueur axiale peut poser problème et nécessiter quelques modifications dans les parties non actives du moteur. D'autre part, l'augmentation du diamètre extérieur du rotor implique une augmentation du diamètre (en conservant la même épaisseur de l'aimant) du cylindre Halbach, ce qui augmente la complexité de la production et le coût. Par conséquent, les moteurs avec une diminution de 20 % de la rémanence et un diamètre plus grand seront beaucoup plus difficiles et coûteux à produire par rapport aux moteurs avec une longueur axiale augmentée. Enfin, dans les situations où ni l'espace alloué au moteur ni la puissance du convertisseur électronique ne peuvent être modifiés, on peut utiliser des aimants recyclés en modifiant le rayon intérieur du cylindre de Halbach. Les résultats montrent que la méthode peut être utilisée pour des aimants recyclés avec une induction rémanente jusqu'à 10 % plus faible sans grand changement dans la caractéristique couple-vitesse. Avec une réduction supplémentaire de la densité de flux rémanente, le couple maximal peut être atteint, mais le couple dans la zone de puissance constante est considérablement réduit. De plus, avec cette stratégie, l'épaisseur de l'aimant est augmentée, ce qui rend l'aimantation du cylindre de Halbach difficile et coûteuse. D'après nos résultats, nous pouvons conclure qu'en cas de faible variation de l'induction rémanente de l'aimant recyclé, le changement des performances nominales du convertisseur électronique de puissance peut être l'option la plus avantageuse, mais qu'en cas de réduction importante, il serait plus intéressant d'augmenter la longueur axiale du moteur.

Une nouvelle méthode dénommée WIRE pour l'évaluation de la recyclabilité et de son impact sur la performance des moteurs a été développée dans le cadre du projet. Les critères de sortie de cette méthode d'évaluation sont : un indice de recyclabilité et un indice énergétique. Ces derniers doivent être pris en compte lors de la conception du moteur en considérant le recyclage. La méthode tient compte de la standardisation, du montage et du démontage du moteur pour évaluer l'indice de recyclabilité. De nombreux processus de montage et de démontage ont été recensés et évalués une première fois. De plus, seuls les matériaux importants du moteur ont été pris en compte. Cependant, la méthode est très simple à modifier et n'importe quel processus peut être développé et évalué en fonction du groupe choisi pour la notation. L'outil est très simple et facile à modifier. Cependant, il est important d'utiliser les mêmes règles de notation pour évaluer les indices moteurs à des fins de comparaison. L'inconvénient est que cette méthode d'évaluation pénalise les designs innovants ou ceux qui ont un arrangement mécanique particulier. Le concepteur doit tenir compte de ces modalités pendant l'évaluation. L'évaluation du recyclage du moteur proposé est présentée. Ce chapitre décrit les caractéristiques du moteur qui permettent un montage et un démontage faciles du moteur. L'utilisation d'un seul

cylindre de Halbach permet un montage du rotor sans colle et, comme démontré sur un rotor échantillon, l'extraction de l'aimant est également très simple. De plus, l'aimant extrait est de très bonne qualité et peut être directement réutilisé ou recyclé. Le moteur a un score légèrement inférieur pour l'assemblage en raison du processus complexe de production du cylindre de Halbach par rapport aux aimants frittés à aimantation radiale qui sont maintenant industrialisés. Le score est également faible en raison du recyclage difficile des aimants liés en poudre magnétique. De plus, le coût du moteur en termes de matériau est faible au coût du montage et du démontage. Ceci implique que le recyclage des matériaux du moteur en termes de coût n'est pas très élevé. Dans le cadre du projet DEMETER, 4 moteurs différents sont conçus et leurs indices de recyclabilité sont évalués. Deux stratégies différentes d'utilisation d'aimants recyclés ont été étudiées et leur impact sur l'énergie a été calculé. Le moteur à aimants recyclés et associé à un courant d'alimentation augmenté (taux de conversion plus élevé) consomme moins d'énergie que le moteur à aimants vierges. Les mêmes conclusions ont été déduites du calcul de l'indice énergétique du moteur. Cela signifie qu'il serait préférable d'augmenter le courant et la tension nominales du convertisseur associé à un moteur à aimants recyclés dans le but de réduire l'énergie consommée sur le cycle de vie du produit. Cependant, il est important de noter ici que le calcul ne tient pas compte de l'impact thermique de l'augmentation du courant qui pourrait être significatif à des valeurs plus élevées de courant. L'indice énergétique relatif à l'augmentation de la puissance du convertisseur a une plus grande distribution de valeurs inférieures à 1 en comparaison à l'indice lié à l'augmentation de la longueur axiale. Cependant, si l'on compare les deux stratégies en tenant compte de l'impact thermique, le moteur ayant une longueur axiale supérieure présente un avantage par rapport à l'option qui consiste à augmenter la puissance nominale du convertisseur. Le calcul doit faire l'objet d'une étude plus approfondie et requiert une meilleure connaissance des propriétés magnétiques de l'aimant recyclé ; éléments qui ne sont malheureusement pas disponibles à l'heure actuelle. Néanmoins, nous pouvons conclure que la méthode d'évaluation reflète bien les changements apportés lors de la conception du moteur et peut être également utilisée pour comparer différents moteurs. L'indice WIRE « total » mutualisant tous les sous-indices, peut fournir un bon moyen pour comparer la recyclabilité des moteurs et pourra être enrichi pour inclure plus de détails selon les exigences futures.

Un prototype a été fabriqué à partir du dimensionnement proposé. L'induction rémanente de l'aimant utilisé dans le cylindre de Halbach produit par moulage par injection est supérieure à la valeur attendue et la densité du flux magnétique d'entrefer est presque sinusoïdale. Un bon facteur de remplissage du bobinage statorique au niveau de l'encoche a été obtenu (0,59). La hauteur supplémentaire due aux têtes de bobines est faible. L'assemblage de toutes les pièces du moteur a été réalisé à l'aide d'outils standards. Il ressort des étapes d'assemblage que le processus a été très simple à mener et peut être réalisé manuellement, à l'exception de l'assemblage du stator et du rotor. Le démontage a également été effectué selon un processus défini. De petites vibrations dans la culasse rotorique ont été observées lors du montage

du stator et du rotor. Nous avons constaté que les vibrations s'amplifiaient encore plus lors des mesures à grande vitesse. Ceci peut être dû à une flasque de maintien et une culasse rotoriques trop minces. De plus, l'assemblage rotorique n'était pas mécaniquement équilibré, ce qui pouvait également augmenter les vibrations et le bruit acoustique. Il est donc important d'analyser le design du moteur d'un point de vue mécanique en particulier d'effectuer les calculs des efforts et des vibrations ainsi que de redessiner probablement certaines pièces avant d'effectuer de nouvelles mesures à grande vitesse. En raison des vibrations et du bruit acoustique à haute vitesse, les mesures n'ont été effectuées qu'à basse vitesse. Les résistances électriques de chaque bobine ont été mesurées et sont presque les mêmes. La mesure de la résistance de l'isolant électrique a montré que la protection électrique du moteur au niveau du bobinage est adaptée à l'application. Les forces contre électromotrices mesurées pour les trois phases sont équilibrées et sont en accord avec les valeurs calculées. Le couple de détente mesuré était légèrement supérieur à la valeur calculée. Cependant, il reste faible par rapport au couple moyen nominal. De plus, le couple de détente mesuré comprend également le frottement statique dû aux roulements. Les pertes en régime à vide (perte fer et mécaniques) ont été calculées à partir d'un essai à vide par décroissance libre de vitesse (spin down). Cependant, en raison de la non-disponibilité d'un banc de test adéquat, les mesures à partir d'une décroissance de vitesse débutant à haut régime n'ont pas pu être effectuées. Néanmoins, les pertes à vide obtenues lors de l'essai à vide par diminution libre de vitesse peuvent être utilisées pour des vitesses moyennement élevées par extrapolation. L'essai à vide et l'essai en charge en mode générateur ont été effectués pour calculer les pertes fer du moteur et les pertes mécaniques. Les résultats ont montré que les pertes fer estimées à partir de l'essai à vide par décroissance de vitesse sont conformes aux essais en mode générateur en charge et à vide. La différence entre les deux mesures de perte est due aux pertes par frottement (roulement et aérauliques). Le fait que l'arbre mécanique du moteur était vertical pendant l'essai de rotation vers le bas et horizontal lors de l'essai en mode générateur à vide et en charge peut modifier le comportement du roulement. Néanmoins, il ressort des courbes de pertes que les pertes par frottement représentent la part dominante et que la raison pourrait être mécanique. Le couple maximal du moteur a été mesuré à l'aide d'une alimentation en courant continu. Les valeurs de couple mesurées sont en accord avec les valeurs calculées. Le moteur est faiblement saturé même à des courants élevés (puissance maximale). Par conséquent, les parties du moteur en matériau ferromagnétique doux peuvent être optimisées et la masse du moteur peut être réduite. L'inductance du moteur a été mesurée par deux méthodes différentes et les valeurs obtenues sont cohérentes. L'inductance mesurée est supérieure de 10 % à l'inductance calculée par éléments finis 2D. La raison principale de cette différence est l'inductance des têtes de bobines qui n'est pas prise en compte dans le calcul éléments finis 2D. Enfin, les mesures de température ont été effectuées en alimentant la machine avec un courant continu égal au courant nominal maximum, avec et sans refroidissement. Dans les deux cas, la température dans les différentes parties était inférieure à la limite. Cependant, avec un courant permanent en court-circuit triphasé, la température du bobinage doit être validée

car en fonctionnement réel, des pertes supplémentaires seront présentes. Certaines modifications peuvent être apportées à la machine pour améliorer le refroidissement du bobinage. Ces modifications n'ont pas été prises en compte lors du prototypage du moteur. Citons, par exemple, l'utilisation de joues aux extrémités en matériau feuilleté conducteur thermiquement au lieu d'isolants en PTFE. Les coefficients de transferts thermiques dans les différentes parties du moteur sont très similaires aux valeurs utilisées pour la conception du moteur. Par conséquent, le modèle thermique de type circuit équivalent paramétré peut être utilisé pour calculer la température dans différentes conditions de fonctionnement.

Acknowledgements

Many wonderful people have helped me in completing this PhD project and I would like to take this opportunity to express my gratitude and hereby, I am pleased to acknowledge them.

Firstly, I would like to express my sincere gratitude to my supervisor Dr. Afef Keduous-Lebouc for her guidance and support of my Ph.D. study. Her patience, experience, motivation and knowledge have helped me in the research and in writing of this thesis. I am also extremely thankful to my co-supervisor Dr. Lauric Garbuio for his invaluable inputs and insightful discussions throughout the course of my research. I would also like to thank Dr. Christian Chilliet for his inputs on motor modelling.

The PhD project could be possible due to the funding received from the European Community Horizon 2020 Programme ([H2010/2014-2019]) under the Grant Agreement no. 674973 (MSCA-ETN DEMETER). I would like to thank all partners and colleagues in general and specifically those from the Valeo and Aalborg University. From the Valeo, I am extremely grateful to Mr. Jean-Marc Dubus for assistance in prototyping of the motor within stipulated timelines and for hosting me for a month in Valeo. I would also like to thank Dr. Jean-Claude Mipo from Valeo for his valuable inputs and discussions during the project. I would also like to thank Mr. Anandfrancis Charles for his help in manufacturing of the motor.

I wish to express my gratitude to Prof. Peter Omand Rasmussen for sharing his experiences and guiding me in motor measurements. He was extremely kind in hosting me for 2 months during my research at the Aalborg University, Denmark.

I am very thankful to Prof. Sophie RIVOIRARD and Dr. Faustin Mandil from the NEEL/CNRS Institute, Grenoble for performing magnet characterisation which is extensively used in the project.

A big shout out to Adolfo Garcia, Pranshu Upadhayay and Ziwei Li , my co-researchers in the DEMETER project (motor design) for all the brain storming sessions and the good times throughout my research.

Special thanks to my friend Balajee Rao for proof-reading the thesis. Also, like to mention Uncle (Mr. Valon Kadriu) my ex-colleague for all the discussions and help.

Last but by no means the least, I would like to thank my family: my parents and to my brothers who were a constant source of inspiration and encouragement. I am thankful to my wife Sneha for her constant support in every possible way and her timely assistance in proof reading the thesis. My acknowledgement would be incomplete without thanking my dear baby-son Adhrit whose smile was a constant source of inspiration throughout my research.

Amit Kumar Jha
Grenoble, France
Date. April 19, 2019

Contents

List of Figures

List of Tables

Introduction

Background

The concern for rapid climate change is at its peak and urban transportation is a major sector contributing to the pollution. Therefore, it is very important to use highly efficient and a cleaner mode of transportation. The use of electric vehicles (EV) or Hybrid electric vehicles (HEV) is one of the best choices among the available solutions to curb pollution. Many countries like India, UK, France, Norway, Sweden etc. are very aggressively changing their national policy and have already announced the phasing out of diesel and petrol cars from their streets in a couple of decades and it is likely that others will follow suit. [17]. In the last one decade, the popularity of (H)EVs has grown many folds and the sale of (H)EVs is increasing steadily, see figure 1, and it is expected to increase at a higher rate in the coming years [1]. Most of the (H)EVs use permanent magnet (PM) motors for traction and with the increasing demand of vehicles, the demand of motors is subsequently increasing. [18]-[19]. The main reason for PM motor's compactness and high efficiency is the use of powerful magnets. Furthermore, the cost and performance of the motor majorly depends on the amount and quality of PM used. Currently, strong magnets like Neodymium Iron Boron (NdFeB) or Samarium Cobalt (SmCo) are used in motors and these magnets are made up of critical and rare earth elements like Neodymium (Nd), Dysprosium (Dy), Samarium (Sm), Cobalt (Co). While the use of rare earth elements (REE) especially heavy elements improve the performance of these magnets but also makes them expensive. Other than cost, the availability of REEs is also of high concern and can limit the growth of (H)EVs.

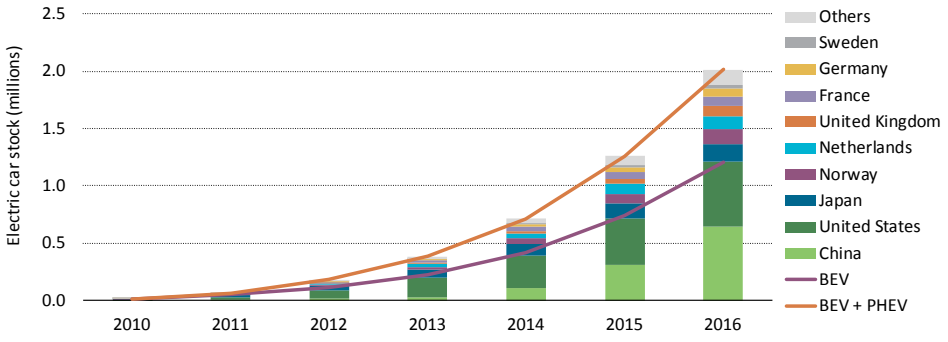

Figure 1: Growth of (H)EVs in since 2010 [1]

Rare Earth Elements : Supply and Demand Risk

The REE consists of 17 elements from the periodic table and are further divided into two categories based on their atomic weights : Light rare earth element (LREE) and Heavy rare earth element (HREE). Although, the availability of REEs are much more than some other elements like gold, uranium, etc. the quantity available for mining is very scarce. Furthermore, REEs deposits occur together with different composition across deposits and the share of HREE is much lower compared to LREE hence, the availability of HREE is further less. REEs are used in many different processes/ products like batteries, phosphors, etc. and as per an estimate from 2012, magnet consumes 20% of the total REE, see figure 2 [2]. The total consumption of REE in 2017 was around 140 kilotonne of which approximately 80% supply was controlled by China. The demand for REE is estimated to further increase 50% by 2020. This makes the REE market very much dependent on China's policy and the risk of repeating 2010-2011[1] magnet crisis has not really mitigated. Both SmCo and NdFeB magnets can be used for PM motors in (H)EVs and the availability of Samarium is not critical at present. The remanence of SmCo magnets is similar to NdFeB magnets with higher intrinsic coercivity and temperature stability. This increases the usage of SmCo magnets in motors operating at very high temperatures. Furthermore, the use of Co, which is a critical, improves the magnetic performance resource and the price of SmCo compared to NdFeB magnets are slightly higher. The NdFeB magnets match much better to the requirements of the motor in (H)EVs (both thermally and electromagnetically) and have seen major performance enhancements over the years [20], [21] & [22]. The cost and performance of PM motors largely depends on the REEs (Nd, Dy, Sm), specially HREEs, for example some high performance NdFeB magnets use 11% Dy. The risk of REE supply has been investigated and the EU has identified resolutions for the sustainable supply of REEs, are as following.

- **Mining in EU**: Nordic countries and Greenland have good deposits of REEs (both HREE & LREE) however, currently there are no active mining site for REEs in EU. After 2010-2011, EU has started EURARE project to explore mining sites considering both the commercial viability of extracting ores and separation of elements. Another, aim of the project was to investigate the environmental impact of REE production. The project concludes that the mining sites at Kvanefjeld (Greenland), Kringlerne (Norway) and Norra Karr (Sweden) can potentially start by 2025. It also concludes while primary source of REE is required; the recycling of REEs is also critical for maintaining supply.
- **REE Free Technology**: In recent years, the focus is on minimizing the use of REE in products/processes, for example many motor designs like synchronous reluctance, PM assisted synchronous reluctance motor etc. with less or no magnets are being studied. Some designs also use magnets like Ferrite. The

[1] In 2010-2011 due to change in China's supply policy the magnet (Nd & Dy) price increased by 10 folds or more

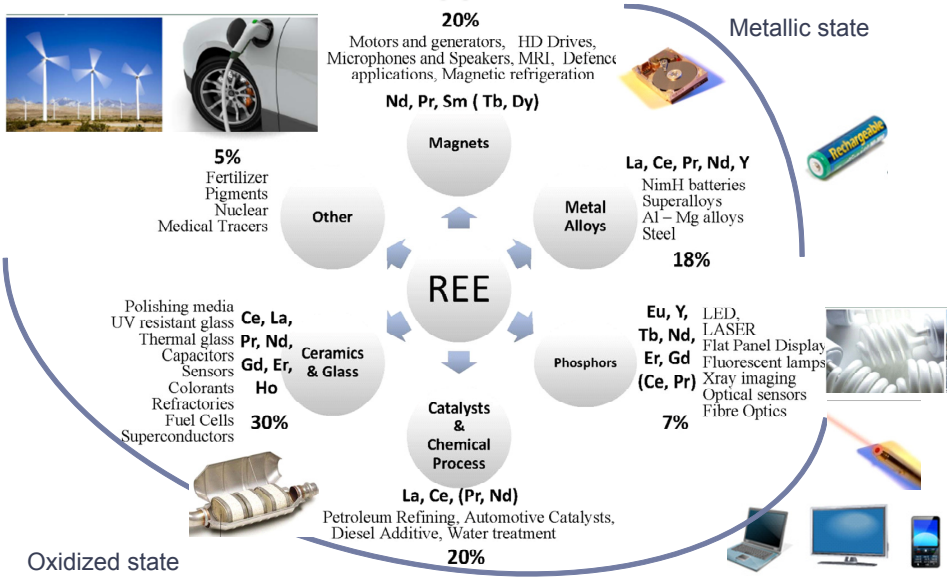

Figure 2: Application of REE in different products and processes [2]

performance of the motors has reduced and are not successful for applications with high efficiency demands. However, it is quite early stage of research and with development of new materials in future, these motor designs can be used.

- **Recycling and Reuse of REE**: Recycling /reuse of products after end of life (EoL) can provide a sustainable source of REEs. Europe is the biggest consumer/producer of products containing REEs and although there have been many studies on the methods of recycling, at present the recovery of REEs is very small. If not the primary demand of magnets, recycled magnet can fulfil the magnet demand of manufacturing industries in Europe. Although, the benefits offered by recycling in terms of economics and quantity is uncertain. the advantages it offers for the environment, reduced material cost and REEs balance problem cannot be ignored [20], [23].

DEMETER PROJECT

Industry and researchers have already started discussing and investing on the recycling of magnets. Projects like EREAN, RARE^3, etc. are focusing on developing methods to recycle magnets. The methods of recycling have been tested at labs under controlled conditions and the challenge is to up-scale them on industrial level. It is also important to ensure that the recycling route of magnets do not have a large negative environmental impact. (H)EVs have gained popularity in last decade and the number of vehicles reaching scrapyard is currently low. However, considering the sales number of (H)EVs it is expected that large number of the vehicles will reach

EoL soon and the quantity of magnets in these motors will be significant. The fact that the design and materials used in these motors is varying, the identification and reuse of magnets is an extremely difficult process. Additionally, the motor is not designed for recycling which further adds to the complexity of the extraction process and lowers the quality of the extracted magnet [18], [24].

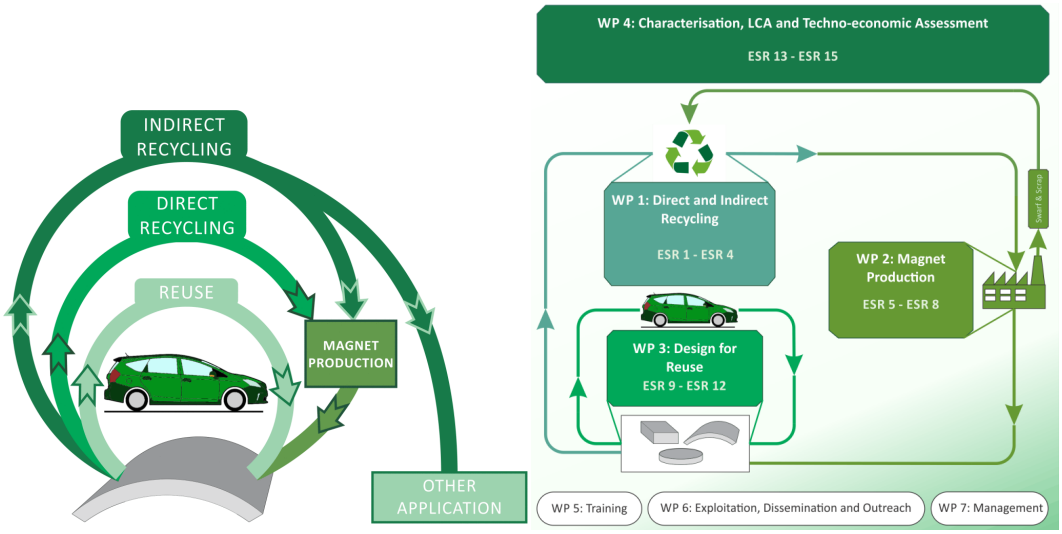

(a) Different routes to recycle/reuse REE from magnet after EoL

(b) Different work packages and their work flow

Figure 3: Project DEMETER aim and work flow [3]

Therefore, in Design and Recycling of Rare-Earth Permanent Magnet Motors and Generators in Hybrid and Full Electric Vehicles (DEMETER) project the focus is on developing innovative methods for recycling and production of magnet along with the design of motor for reuse/recycling and extraction of magnet considering the impact on environment [3]. The aim is to study the complete journey of magnet from production to EoL to recycling and reformation. The project has identified 3 ways to recycle magnet as shown in figure 3. The first and most desired route is to extract magnet and reuse them in any application after EoL of the motor. To achieve this, the motors/generators have to be designed with standard size of magnets with same material for easy extraction which is not a practice at present. Furthermore, another difficulty in reusing magnets is that the properties of magnets deteriorate during use and after EoL if magnets are reused it will be difficult to achieve the same performance which makes this route very unlikely but not impossible. The second option is direct recycling where magnets will be extracted from the motor and processed with hydrogen decrepitation, plasma/strip casting, and spark plasma sintering to produce new magnets. Lastly, the third route is called indirect recycling where extracted magnets are broken down to its elemental components and then used to make new magnets [3]. 15 PhD researches are part of the project, investigating different aspects of the magnet life cycle. The whole project is divided into 4 work

packages (WP) interlinked with each other. Figure 3b shows the flow of work between different groups within the project. The WP3 is defined for motor design considering reuse/recycling at the design phase. 4 different motor topologies are studied and designed with different specifications for (H)EVs. The designed motor presented in this thesis is a Halbach magnet outer rotor motor designed for full HEVs nevertheless, the motor can be easily scaled for an EV.

Thesis Objectives

Following are the goals of the thesis.

- **Design motor for reuse/recycling of magnets**: As mentioned earlier, the motor designs used currently in automobiles are not designed considering recycling/reuse of magnets and hence, extraction of magnets is very difficult. Therefore, the primary goal of the thesis was to design motor for easy reuse/recycling of magnets.
- **Halbach magnet motor for high power**: Despite good flux concentration of Halbach magnet, it is not used for high power motors. The reasons could be complex manufacturing process and large magnet volume. Hence, another goal of the thesis was to design an outer rotor Halbach magnet motor for high power vehicle within geometrical constraints.
- **Procedure for reuse/recycle of the magnets**: The reuse/recycling process depends on the material of magnet used in the motor. With different design features, the process of extraction of magnet can vary. Therefore, the final goal of the thesis was to define a procedure of reuse/recycling of the magnets.

Main contributions of the thesis

The contributions of the thesis are summarized below:

- The thesis proposes a high power motor design with Halbach magnet outer rotor within the given constraints for automotive applications. Furthermore, it is shown that the high torque and power density motor can be designed using bonded NdFeB magnets and the fractional slot tooth coil winding(FSTCW). Different strategies of using recycled magnet achieving the same torque speed characteristics of the motor is also presented. The thesis also presents the measurement results of the prototype motor and comparison with calculated results. Additionally, the thesis demonstrates the manufacturing of outer rotor motors for high power ratings with easy recyclability and reuse

- The thesis demonstrates the manufacturing of ideal Halbach rotor using bonded NdFeB magnets for high power application (big dimensions) and validation of the prototype with measurements. The measurement results for characterisation of bonded NdFeB magnet material is also presented. The study also proposes recycling routes for the bonded NdFeB magnet and its advantages over sintered NdFeB magnets recycling.

- Finally, a new method called WIRE, to benchmark motors recycling (focused on magnets) and the impact of recycled magnet on the motor's performance is developed in collaboration with the 3 other PhD researchers from the DEMETER project work package 3. The results show that the method can be used to compare different motors with respect to their recycling ability and the use of recycled magnets.

Thesis Outline

Chapter 1 presents different types of EVs and motors used for the application. The advantages and challenges of outer rotor topologies are also discussed. Finally, the specification of the motor design is presented.

Chapter 2 presents the theory of Halbach magnet array and the features beneficial for motor application. Different methods of manufacturing Halbach array are also discussed. The measurement results of bonded NdFeB magnet characterisation and the comparison between analytical and measured magnetic field of a Halbach ring is also presented.

Chapter 3 presents a study on the impact of different parameters on motor performance. The performance of different motor topologies is also discussed. Based on the study, a final design of the motor is proposed for the prototype. Furthermore, the impact of recycled magnets and different ways of using recycled magnets are also discussed in the chapter. Finally, the measurement of the prototype and it's comparison with calculated results is also presented.

Chapter 4 introduces the new method developed in the project DEMETER which is called WIRE. The chapter defines different terms used for the method and also presents the evaluation of the proposed motor design based on the WIRE methodology. The impact of recycled magnet on the motor performance is also discussed and the index of the motor based on both cost and energy is also presented.

Chapter 5 presents the conclusions of the thesis and recommendations for future work.

List of Publications

1. A. K. Jha, L. Garbuio, A. Kedous-Lebouc, J. P. Yonnet, and J. M. Dubus, "Design and comparison of outer rotor bonded magnets Halbach motor with different topologies," in *2017 15th International Conference on Electrical Machines, Drives and Power Systems (ELMA)*, June 2017, pp. 6–10
2. A. K. Jha, A. Kedous-Lebouc, L. Garbuio, J. P. Yonnet, and J. M. Dubus, "FEA based analysis on effect of slot pole combination on motor torque and magnet eddy current loss with bonded NdFeB Halbach rotor," in *2017 20th International Conference on Electrical Machines and Systems (ICEMS)*, Aug 2017, pp. 1–5
3. A. K. Jha, Z. Li, A. Garcia, P. Upadhayay, P. O. Rasmussen, A. Kedous-Lebouc, and L. Garbuio, "Weighted Index of Recycling and Energy (WIRE) Cost for Motors in Electric Vehicles," in *2018 International Symposium on Power Electronics, Electrical Drives, Automation and Motion (SPEEDAM)*, June 2018, pp. 1–5
4. A. Garcia, A. K. Jha, Z. Li, , P. Upadhayay, and P. O. Rasmussen, "Validation of Efficiency Maps of an Outer Rotor Surface Mounted Permanent Magnet Machine for Evaluation of Recyclability of Magnets," in *Intermag 2018*, April 2018
5. P. Upadhayay, A. Garcia, Z. Li, A. K. Jha, P. O. Rasmussen, A. Kedous-Lebouc, and J.-C. Mipo, "Evaluation of Energy Cost Index for an Electric Vehicle Motor over a particular Drive Cycle with Recycled Magnet Concept," in *XXIII rd International Conference on Electrical Machines (ICEM'2018)*, September 2018, pp. 1–7
6. A. K. Jha, A. Kedous-Lebouc, L. Garbuio, J. P. Yonnet, and J. M. Dubus, "Electric Vehicle Motor Designed for Recycling with High Torque Density And Efficiency," *IEEE Transactions on Vehicular Technology,(Submitted)*

Chapter 1

1 Motors for Electric Vehicles

The advent of electric vehicles (EV) goes back to the early 19th century. The electric vehicles were much more popular than internal combustion (IC) engine or the steam engine. However, the availability of cheap oil and the invention of the self-starter engine in the 1920s made the IC engine a more viable option both from a financial and a technological standpoint. The challenges EVs faced were primarily low specific energy of batteries, high price and the time to recharge, which are relevant even in the present times. To extend the vehicle range, power was supplied through rail or overhead lines however, creating such infrastructure proved expensive. The other method used to overcome battery limitation was to use IC engine along with a motor in the same vehicle called Hybrid electric vehicle (HEV). Nevertheless, due to low power and battery limitations it could not compete with IC engine vehicles. In last few decades, the development of power electronics and magnets many different types of motor suitable for the application are available which has brought back interest in (H)EVs. The use of variable speed AC motors has led to drastic improvement in vehicle power and efficiency of the system. Along with EVs, the HEVs have garnered traction since they offer greater flexibility in both design and operation. Despite challenges in range, cost and operation, the (H)EVs, cause negligible pollution to immediate environment and operate silently. The (H)EVs also provide greater flexibility in operability through varied energy sources like nuclear, hydro and solar as compared to the IC engine which is primarily operates on petroleum. Tackling pollution on large scale at the energy source, using some special equipments/methods, are much more easier to implement than on the vehicles. Furthermore, the (H)EVs have better efficiency[1] during start-stop operation which is best suited for city driving conditions [5]. (H)EVs being environment friendly, are an excellent solution to tackle pollution crisis, the world is facing today. Additionally, with the rapid development of batteries, motors and drives the overall cost and performance of the vehicle are expected to improve in near future [1].

[1]The overall energy consumption of the EVs might not be much lower than the IC engines.

1.1. Classification of Electric Vehicles

Depending on the source of traction force, electric vehicles are classified into two types, battery electric vehicle (BEV), also generally referred as EV and hybrid electric vehicle (HEV). The HEV can be further divided into different groups depending on the supply system or source of the energy or power train architecture i.e. μ-HEV, Mild HEV, Full HEV and PHEV (Plug-in HEV). Figure 1.1 shows the classification and different features of electric vehicles [4].

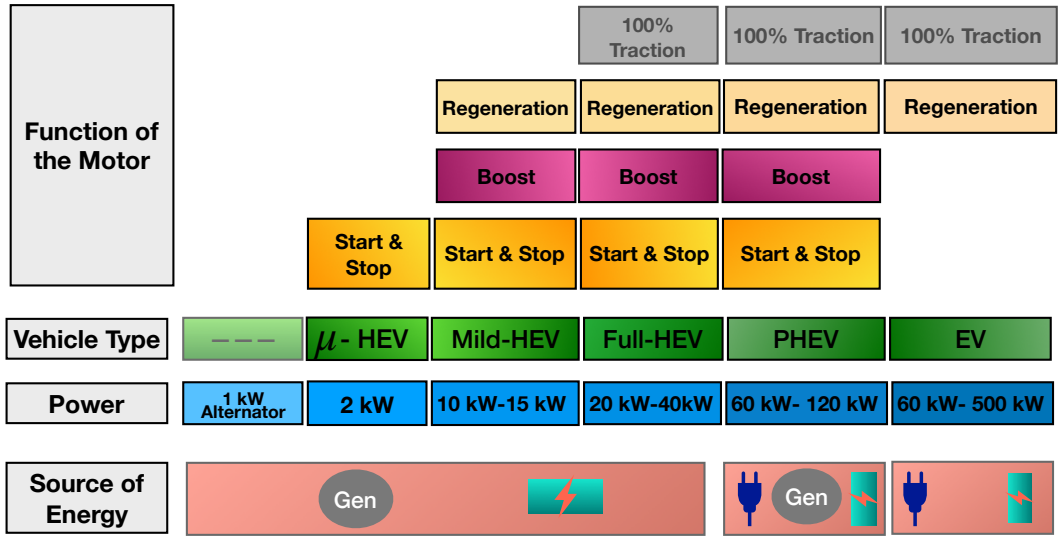

Figure 1.1: Classification of EV and HEV [4]

Battery Electric Vehicle: In battery electric vehicle all the traction force required for driving vehicle comes from electric motor (no IC engine in vehicle). The primary components of the power train are rechargeable battery (power supply unit), bi-directional converter and electric motor as shown in figure 1.2. The source of energy in this case is the rechargeable battery which can be charged from fixed outlets or dedicated stations. The source can also be an overhead supply which is not being used for automobile applications. Accordingly, the term EV is used for battery operated electric vehicles. The power supplied to the motor is controlled by the inverter depending on the torque and speed requirement. Most of the advanced controllers are bi-directional so that the regenerative power developed during braking can be used to recharge the battery. The structure and operation is simple to implement however, at present the range is limited mainly due to energy limitations of the battery.

Hybrid Electric Vehicle: A hybrid electric vehicle has both IC engine and electric motor which are used simultaneously or separately for developing traction. Depending on the arrangement, hybrid vehicles are further classified into two types : a) Series Hybrid , b) Parallel Hybrid as shown in figure 1.3. In series hybrid vehicle the power

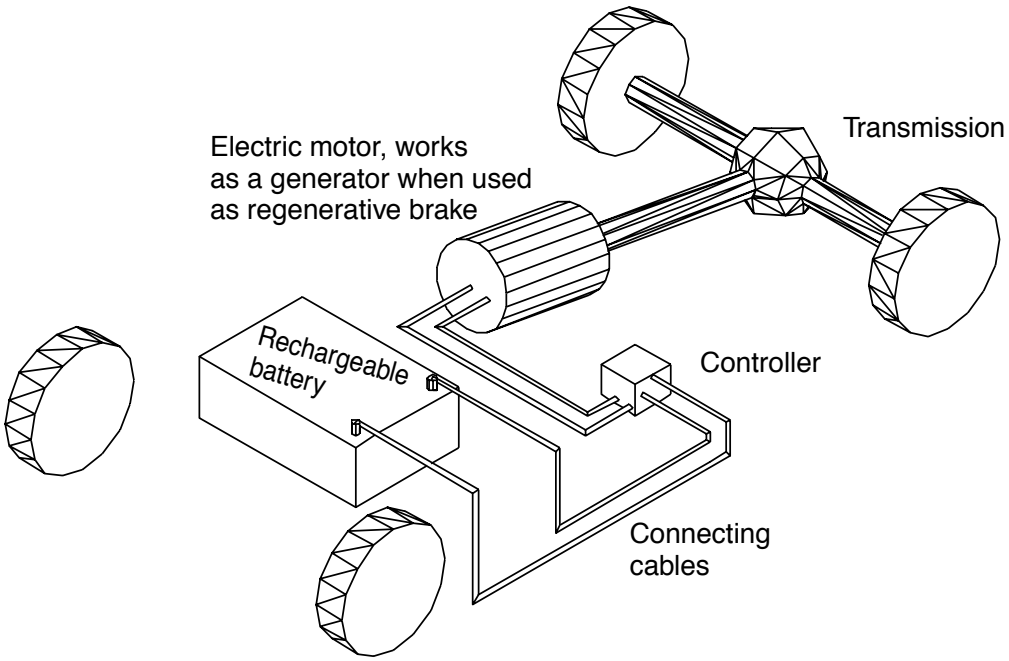

Figure 1.2: Architecture of Battery operated Electric Vehicle [5]

to the wheel is only transmitted by the motor and is powered either by a battery or an IC engine via a generator. On the other side, in parallel hybrid, either IC engine or motor or both can be used to transmit power to the wheels. In both the configurations regenerative braking is achieved by using a bi-directional converter. The series hybrid architecture is less commonly used as compared to parallel hybrid in vehicles. There are other types of HEVs configurations which can be achieved by combining series parallel combinations however, the basic operation remains the same. In comparison to EV the operation of HEV does not need large battery for the long range. The hybrid electric vehicles can operate in many ways depending on the power requirement the operation of the IC engine and motor can be varied. The operation of HEVs is much more complex than EVs due to the energy management between IC engine and the motor. Nevertheless, it also provides greater flexibility to choose and adapt the functioning depending on the operating conditions. The hybrid vehicles are further classified as micro, mild and full hybrid depending on the power shared and the function of electric motor. According to [30] & [31] the efficiency and fuel economy of HEVs improves upto 30% - 50% of motor power share and beyond that the gain is not much.

- Micro Hybrid: In micro hybrid vehicles the motor serves as both a starter and an alternator as compared to a conventional IC engine vehicle. The motor voltage and power is typically around 12 V and 2.5 kW respectively. The main function of the motor is to provide power during start and stop of the vehicle. As a result, the vehicle saves energy in the range of 5% - 10%. The system is

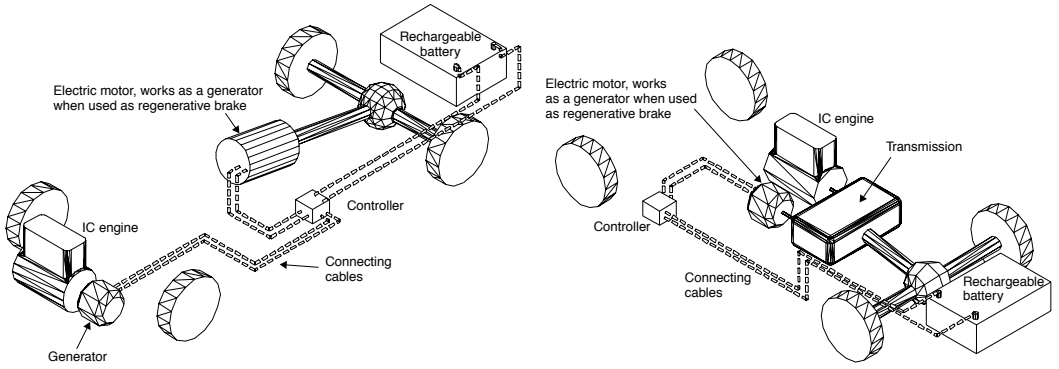

(a) Series Hybrid Vehicle *(b) Parallel Hybrid Vehicle*

Figure 1.3: Different types of Hybrid Electric Vehicle

also not very expensive as the size of the motor used is small [15]. Valeo StARS [32] system is an example of micro hybrid system used in Citroen HEVs.

- Mild Hybrid: In mild hybrid vehicles the motor voltage and power are in the range of 100-200 V and 10-15 kW respectively. In city driving, 20% - 30 % of energy can be saved however, the cost of the vehicle is also high [15]. For example, Chevrolet Silverado and Honda Civic cars use mild hybrid system.
- Full Hybrid: The motors used for full hybrid vehicles operate in the 200 -300 V range and a power output of 40 kW or higher. The system currently used for full hybrid vehicle is a mix of series-parallel configuration. As a result, a complex control system is needed to achieve optimum performance of the vehicle. In city driving, a full hybrid vehicle can save energy in the range of 30% - 50% [15]. For example Toyota Prius and BYD Song DM use a full hybrid propulsion system.

1.2. Electric Motors

The primary electrical components of an (H)EV powertrain are battery, converter (controller) and motor. The performance of each component is critical for overall vehicle performance. The main focus of the thesis is to design a motor for a (H)EV and hence, it is more interesting to discuss different types of motors used in EVs. Figure 1.4 shows a typical torque speed characteristic of a motor used for (H)EVs. The base speed is the speed at which the voltage and the current reach the supply limit and the torque remains constant. This is referred as the constant torque region. For speeds higher than the base speed, the power output of the motor remains constant and this is referred as the constant power region or flux weakening region. At very high speeds, the power and current are reduced due to the inverter switching limitations at high current and speed. The desired characteristics of an

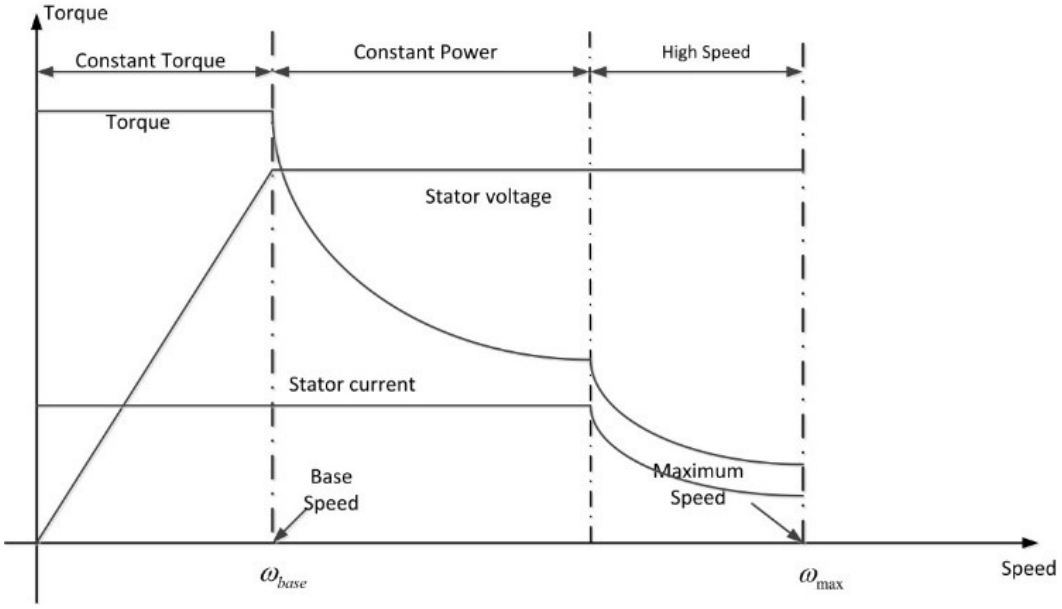

Figure 1.4: Typical Torque speed characteristic of a motor for (H)EVs [3]

Table 1.1: Sales and type of motors used in difference commercially available (H)EVs in 2017 [14]

Vehicle Name	Motor[2]	Type of Vehicle[3]	Rated Power [kW]	Torque [Nm]	Sales Unit
Chevrolet Bolt	PM	EV	150	360	27982
BYD Song PHEV	PM	HEV	220	500	30920
BMW i3	PM Syn RM	EV	125	250	31410
Renault Zoe	SB	EV	80	225	31932
Zhi Dou D2	BLDC	EV	18	82	42342
Tesla Model X	IM	EV	193	329	46535
Nissan Leaf	PM	EV	80	280	47195
Toyota Prius Prime	IPM	HEV	60	207	50830
Tesla Model S	IM	EV	193	329	54715
BAIC EC-Series	PM	EV	45	144	78079

electric motor for the vehicular application are high constant torque, high power density, wide constant power speed range, high efficiency, robust, light weight and most importantly cost efficiency. Commonly used motors in commercially available (H)EVs are direct current (DC) motor, induction motor (IM), permanent magnet synchronous motor (PMSM), switched reluctance motor (SRM) and synchronous reluctance motor (SynRM).

A comprehensive table of the various commercially available (H)EVs and the types of motors used until 2012 is presented in [7]. The study showed that induction motor was the predominant choice for the makers despite its low efficiency as compared to PMSM and reluctance motors. This may be due to the high price of permanent magnet materials used in PM motors, reluctance to accept relatively new technology or low maintenance costs of the induction motor. However, in last few years the trend has changed and the sales numbers of (H)EVs since 2010 show that most of the highest selling vehicles use synchronous motor (PM or PM assisted motor) [33]. Table 1.1 shows the sales number of (H)EVs in 2017 and the type of motors used in the vehicles. Most of the vehicles use PM motor except Tesla and Zoe. However, the new model 3 of Tesla also has PM motors.

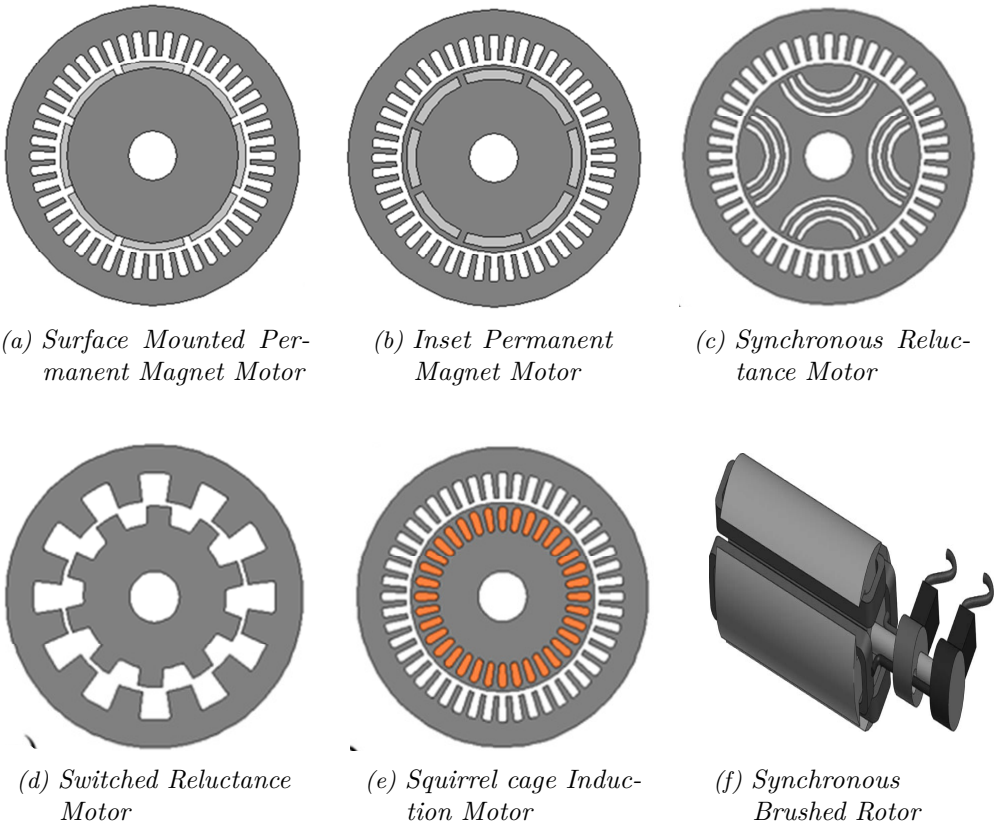

(a) Surface Mounted Permanent Magnet Motor

(b) Inset Permanent Magnet Motor

(c) Synchronous Reluctance Motor

(d) Switched Reluctance Motor

(e) Squirrel cage Induction Motor

(f) Synchronous Brushed Rotor

Figure 1.5: Cross-section of different types of motor used in electric vehicles [6],[7]

The selection of a motor for the electric vehicle depends on many factors and each motor offers different advantages and challenges. Figure 1.5 shows the cross-section view of different motors used for (H)EVs. Traditionally, DC motors were most widely

[2]PM denotes permanent magnet motor, SB denotes Synchronous brushed motor, IPM denotes inset permanent magnet motor, BLDC denotes brushless direct current motor, PMSynRM is permanent magnet assisted synchronous reluctance motor

[3]PHEV denotes plug in hybrid electric vehicle

Table 1.2: Relative evaluation of motors used for (H)EVs [15],[16]

	IM	PM Motor	DC Motor	SR Motor
Reliablity	High	Average	Low	High
Cost	Low	High	Low	Average
Technology Maturity	High	Average	High	Low
Power Density	Average	High	Low	Average
Control	Average	Low	High	Low
Flux Weakening	High	Average	High	Low
Weight	Average	Low	High	Low
Efficiency	Average	High	Low	Average
Maintenace	Low	Average	High	Low
Temperature sensitivity	Low	High	Low	Low
Noise	Low	Low	Average	High

used for trains/electric vehicles because of their torque speed characteristic, low cost and ease of control. However, with the development of new drives, the efficiency of AC motors is improved with better control specially for high power applications like EVs. For low cost and power traction systems, DC motors are still used. As mentioned earlier, with the development of drives, use of IM for variable speed operation became very common. The fact that IM manufacturing technology is highly matured, in the sense that it has low manufacturing cost and low maintenance, it is highly reliable, robust and has good constant power speed range, which makes it a very good choice for EVs. The downside of the motor is low torque density and low efficiency as compared to the PM motors, especially in constant torque region which impacts both performance and range of the vehicle. PM motors have the highest efficiency, torque density and lowest weight mainly due to powerful rare earth magnets and almost negligible rotor loss. There are many designs available for PM motors depending on PM placements and they can be broadly categorised as- surface mounted and inset PM motors. Inset PM motors are more common in high speed vehicles as compared to surface mounted motors because of their ease of manufacturing and the better protection of magnets both mechanically and electromagnetically. However, PM motors need high maintenance, special safety equipments and a complex control mechanism as compared to induction motors (IM). The motor performance varies significantly with magnet temperature and cooling of rotor is a challenge for the motor. The presence of magnets, especially heavy rare earth element magnets, makes them expensive. In recent years, magnet free reluctance motors, both synchronous and switched, have generated interest in vehicle application. These motors generally have torque density in between PM motor and IM with good flux weakening capability. The motors are robust, easy to manufacture, light weight and cost effective in the absence of magnets. Another design of reluctance motors used is PM assisted synchronous reluctance motor where small amount of magnet (generally Ferrites, bonded NdFeB) are placed in flux barriers to improve

torque density and efficiency. The drawbacks of reluctance motors are very high torque ripple and noise. Therefore they are best suited for low speed direct-drive [6]. There is another type of magnet free motor that is used in Renault Zoe car called the synchronous brushed motor. In this motor, instead of having a magnet in the rotor, coils are used for field excitation as shown in figure 1.5f. The operation of the motor is same as any PMSM motor except that the excitation field system uses DC current through a brush. The field of the rotor can easily be controlled which makes the motor efficient at high speeds. However, the torque and efficiency of the motor is lower as compared to the PM motors because of extra losses in the field winding. Like DC motor, the brushes used for field winding also require high maintenance. Table 1.2 presents the relative comparison between different motors based on different criteria. It is also important to consider system performance of the vehicle for selecting the electric motor and presently, PM motors offer the best performance to cost ratio for the overall system.

1.3. Outer Rotor Motor Topology

The thesis aims to design an outer rotor motor for EV application. Although, inner rotor motor is more common for (H)EV applications ,outer rotor motor presents the following advantages as compared to the inner rotor motor [34]. Figure 1.6 shows the cross-section of an inner and an outer rotor motor.

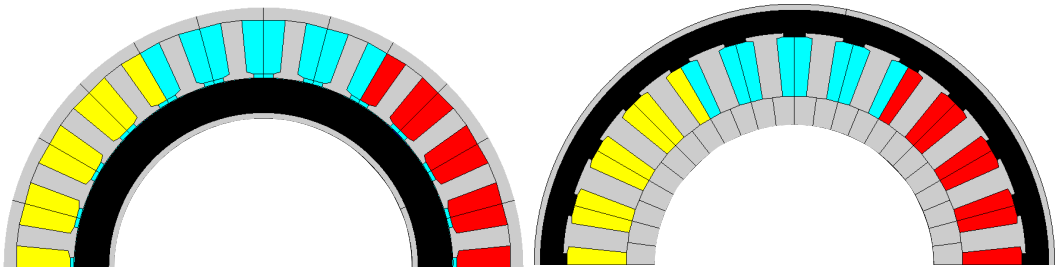

(a) Inner rotor motor *(b) Outer rotor motor*

Figure 1.6: Cross-section of inner and outer rotor motor

Advantages:

- **High Torque**: The torque of the motor varies with square of airgap diameter. Therefore, outer rotor motor develops higher torque than the inner rotor motor due to larger airgap diameter with same outer diameter and length of the motor.
- **Less glue or glue free PM arrangement**: The centrifugal force on the magnet placed in outer rotor is outward. Hence, the force helps magnet to remain attached to the rotor back unlike an inner rotor where the force pushes

the magnet out from rotor back. Therefore, less adhesive is required for the magnet in an outer rotor.

- **Thermal behaviour**: As majority of the motor loss is in the stator, the space available inside the stator, in an outer rotor assembly, can be used for cooling, see figure 1.8a. The downside of this arrangement is the lower cooling surface area. However, unlike inner rotor, with this arrangement the rotor back is exposed to ambient and with thin rotor backs magnet cooling improves.
- **Simpler Winding process**: In outer rotor, the slot opening is in the outward direction. Hence, the space is not a constraint for winding tools as compared to the inner rotor motor, especially for lower diameter motor. This makes the stator winding process relatively simpler for outer rotor topology.
- **Manufacturing Magnet**: In context of producing Halbach magnet ring, inner rotor motor has higher magnet thickness as compared to the outer rotor motor for the same volume of the magnet. The production of a thick Halbach magnet is much more difficult.

Motor assembly: The assembly of outer rotor motor is slightly more challenging as compared to the assembly of the inner rotor motor. Figure 1.7 and 1.8 show two different assemblies of outer rotor motors that are commonly used. Both commercially available motors shown in the figures are in the range of 1 - 2 kW. The outer rotor topology is much more common in lower power than higher power. Very few outer rotor topology motors with high power (50 kW- 90 kW) are available commercially like TM4- MOTIVE, Elaphe M700.

- **Assembly 1**: The assembly shown in figure 1.7a is very common for the hub/in-wheel type of motor where the wheel can be fixed on a motor housing. An example of such commercially available motors is shown in figure 1.7b. The motor housing and the two end plates are connected together and rotate with rotor. In this arrangement the shaft is stationary and hollow to route power cables to the stator winding. The drawback of the arrangement is that, due to completely closed structure, the cooling of the motor is not very good. Furthermore, the housing is rotating and in order to have inner water cooling jacket, the coolant inlet and the outlet must go through hollow shaft along with other power and sensor cables. Therefore, having liquid cooled arrangement with this assembly is very difficult to achieve and is prone to faults. This could be one of the reasons for using this assembly for low power applications like fan, bikes etc..
- **Assembly 2**: The assembly shown in figure 1.8a is also mostly used for small motors. Figure 1.8b shows a commercially available motor of assembly architecture. In this arrangement as can be seen from the figure, the motor housing is in two parts. The rotor end plate is fixed with a shaft and there is no connection between the stator and rotor end plates. The arrangement is

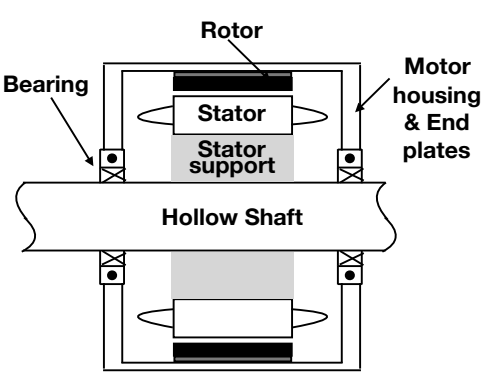

(a) Assembly with fixed shaft and closed structure

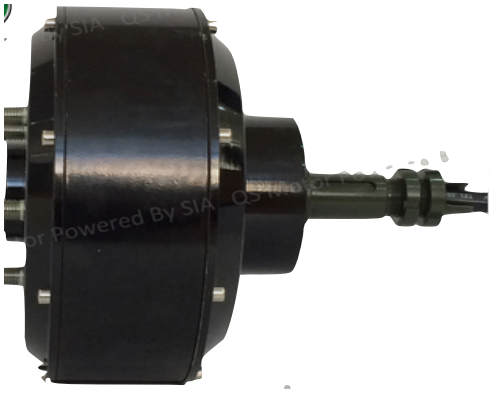

(b) Commercial Motor using Assembly 1

Figure 1.7: Schematic presentation of assembly 1 outer rotor motor and the commercially available motor using same assembly. The cross symbol is for stationary side of bearing.

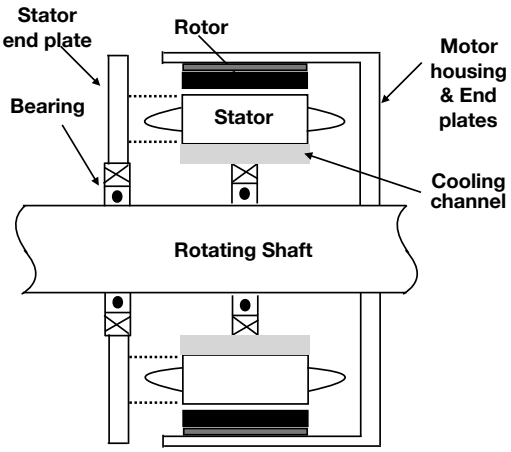

(a) Assembly with rotating shaft and open structure

(b) Commercial Motor using Assembly 2

Figure 1.8: Schematic presentation of assembly 2 outer rotor motor and the commercially available motor using same assembly. The cross symbol is for stationary side of bearing.

flexible in terms of rotating shaft or stationary shaft. In the assembly shown, the shaft is rotating however, if rotor end plate is fixed to shaft using a bearing, the shaft can be made stationary. The benefit of this assembly is that one side of the motor (stator end plate) is stationary and can be used to route power cables to the stator and cooling inlet-outlet channels. Moreover, the motor can also be suspended in car body/chassis from the stationary side. The fact that there is an opening between stator end plate and the motor housing, cooling improves. The cooling jacket can be easily placed inside the stator as shown in the figure. Another advantage of rotating shaft is that it can be used to fix

positioning encoder which is slightly more difficult with assembly 1. However, the drawback of the assembly is that the whole stator is supported on one end plate and the rotor weight is on the motor shaft. When motor is placed in the vehicle, the motor shaft is connected to the crank shaft that enhances mechanical stability. However, mechanical stability of the assembly depends a lot on the axial length given thus the assembly will be difficult for axially long motors.

1.4. Design Specification

The aim of the thesis is to design an outer rotor Halbach motor. The specification given for the motor is for a typical full hybrid electric vehicle. However, the motor application and power train architecture are of a mild hybrid EV, as shown in 1.9. The motor is placed after ICE on the crankshaft and the traction power is transmitted to the wheel through a single stage gearbox. A similar architecture is also used where the motor is placed after the clutch however, in principle the working remains same. Figure 1.10 shows the required torque in transient and continuous mode of vehicle operation. The transient mode is only for a duration of 30 s during the start or stop of the vehicle and thereafter, motor operates in a nominal mode. It can also be seen that the torque/power speed curves do not represent a typical torque speed curve of a traction motor. This is because the torque speed required in nominal operation is specified considering the energy management of the vehicle. Therefore, from a design perspective the motor was designed to deliver transient torque. However, for calculation of losses and temperature in the motor, continuous operation was considered because the motor operates for only 30 s in transient mode and will not have a significant thermal impact on the motor.

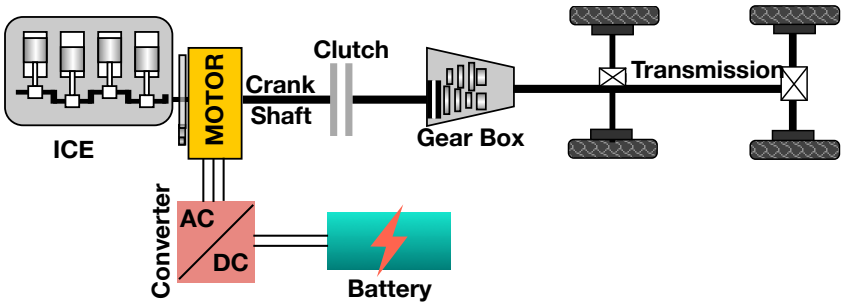

Figure 1.9: Crank Shaft mounted generator (CMG) powertrain architecture of HEV used in Valeo

For electric vehicles it is also important that the motor can handle 3 & 2 phase short circuit (SC) electromagnetically as well as thermally in both transient and steady state. The maximum slot current density for design was 13 $A.mm^{-2}$. The demagnetization of the magnet was investigated during transient phase of SC and

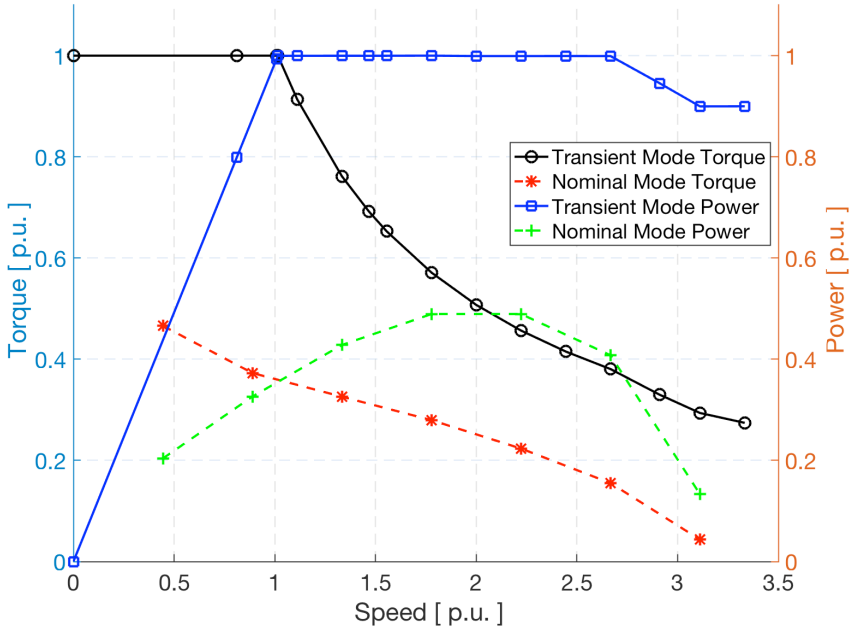

Figure 1.10: Torque specification for motor in transient and nominal mode. Transient mode is only for 30 s.

the thermal impact steady state SC was considered. The ratio of outer diameter (D_o) to maximum axial length (L) i.e. D_o/L is 3.45. The motor is designed for a water cooled system where the maximum slot current density allowed for the motor is 13 A.mm^{-2}. With specified space available and considering other constraints, assembly 2 is best suited for the motor, as discussed in section 1.3.

1.5. Summary

The invention of electric vehicles happened during the 19th century. However, due to technological limitations the vehicles could not achieve commercial success. Recent developments in the field of power electronics and the batteries have made (H)EVs a commercially viable option for transportation. Furthermore, use of (H)EVs is environment friendly and is touted to replace IC engine cars. Electric motor is an important component of a (H)EV and clearly PM motor is the preferred choice of vehicle manufacturers.

This thesis focuses on the design of an outer rotor PM machine for a full hybrid electric vehicle. The outer rotor motor is not very popular due to its complex assembly. However, the topology has many features which improve motor power density and performance. Two possible assemblies of the topology are discussed in the chapter and it is concluded that assembly 2 is better suited for the vehicle specification.

Chapter 2

2 Halbach Bonded Magnets

The Halbach array is an arrangement of magnets such that the magnetic field is concentrated on one side of the magnet and ideally, no field on the other side. To achieve the desired magnetic field distribution, the magnet with different magnetizing directions are put together as shown in figure 2.1. The concept was proposed by Dr. Klaus Halbach in the Laurance Berkeley National Laboratory in 1979 and hence, called "Halbach array", [35]. Halbach array can be manufactured using sintered or bonded magnets. Motor designs presented in various research articles predominantly has sintered Halbach array rotor with 2-5 segments per pole. The complexity of assembly increases with the increase in the number of segments per pole. In the article [36] a 8 pole rotor assembly with 2 segments/ pole Halbach sintered rotor is presented. The technique to align and magnetize an anisotropic magnet for Halbach magnet is discussed in [37]-[38]. In [39] & [40] a review of Halbach magnet and its applications is presented. In [41] a comparison between motor with Halbach array rotor and a conventional radially magnetized motor is discussed. The author presents that the motor with Halbach magnet made using bonded NdFeB magnet that can match the performance of the motor with radially magnetized sintered magnet conventional surface mounted permanent magnet [SMPM] motor.

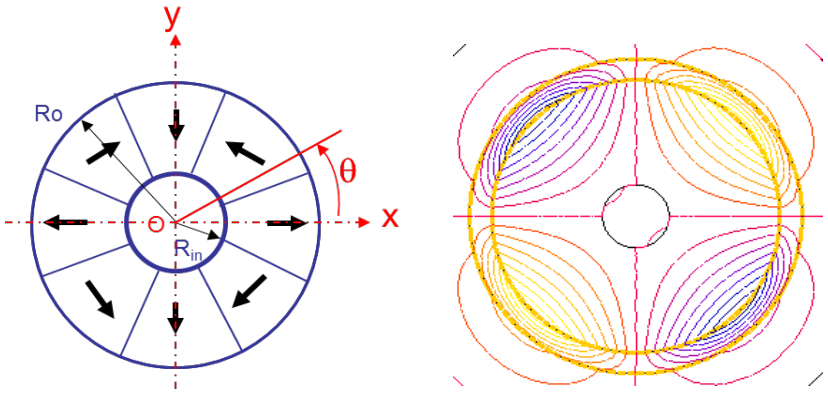

Figure 2.1: Halbach magnet arrangement and its magnetic field distribution

2.1. Principle of Halbach Arrangement

The arrangement of Halbach array can be presented mathematically using equations 2.1 - 2.5. The equations represent the ideal field distribution for an Halbach array. However, for segmented Halbach array the magnetization direction is taken at the center of the segment. Therefore, higher the number of segments per pole closer it will be to sinusoidal distribution.

$$\vec{M} = M_x\vec{x} + M_y\vec{y} + M_z\vec{z} \tag{2.1}$$

where,

$$M_x = B_r[\cos(p\theta)\cos(\theta) - \sin(p\theta)\sin(\theta)] \tag{2.2}$$

$$M_y = B_r[\cos(p\theta)\sin(\theta) + \sin(p\theta)\cos(\theta)] \tag{2.3}$$

$$M_z = 0 \tag{2.4}$$

$$\theta = \arctan(\frac{y}{x}) \tag{2.5}$$

where, p is the number of pole-pairs, B_r is magnet remanence and x,y are the coordinates of the point on the magnet.

Figure 2.2 shows the flux distribution in the airgap in 4 pole ideal Halbach arrangement as per equation 2.1 - 2.5. The flux distribution is sinusoidal in nature as compared to the conventional SMPM radially magnetized magnet arrangement. It is also interesting to note that the peak fundamental flux density of Halbach magnet is 7% higher than the SMPM with same magnet volume and magnet grade. Moreover, due to sinusoidal flux distribution in the airgap the motor with Halbach magnet will have lower harmonic losses and noise as compared with the SMPM arrangement, with better performance.

2.2. Manufacturing of Halbach Array

The primary discouraging factor in the use of Halbach array magnet is its manufacturing. In the following section an overview of manufacturing Halbach along with its advantages and challenges is presented.

The Halbach array can be realized by two ways as following [39].

(a) **Segmented Halbach**: The Halbach array magnet is achieved by assembling pre-magnetized segments of magnet with different orientation defined by equation 2.1 - 2.5, for example figure 2.1. As there are discrete magnet sections the orientation at the middle of the magnet is taken for the magnet segment.

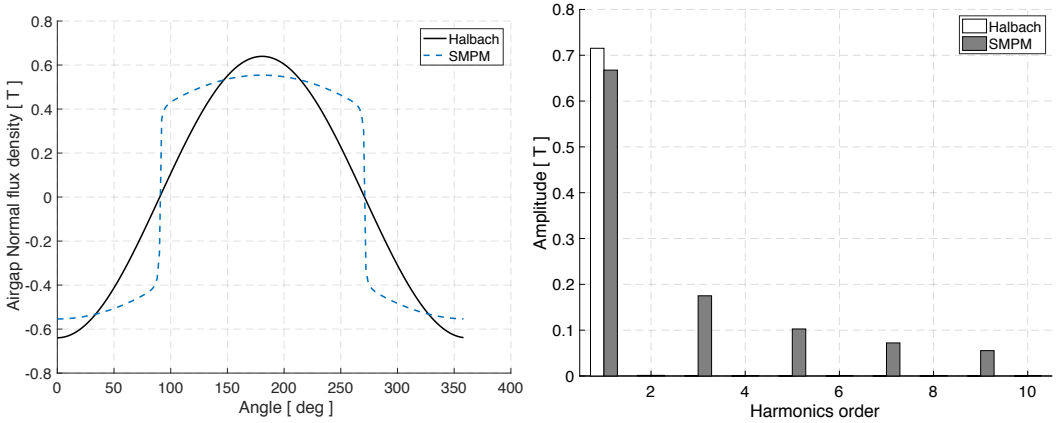

(a) Airgap filed distribution *(b) Harmonic spectrum of airgap field*

Figure 2.2: Comparison of airgap flux density between 4 pole Halbach and radial SMPM with same magnet material and volume

The sinusoidal quality of the airgap field distribution depends on the number of magnet segments per pole. Therefore, to achieve a sinusoidal airgap field distribution very high number magnet segments per pole should be used [39]-[42]. Moreover, with higher number of segments per pole the resistance against demagnetization also increases [43]. In this method sintered magnet with high remanence can be used. However, high number of segments increases the complexity and cost of manufacturing. It further increases the material cost as segment with different orientation causes large material waste. This could be one reason that most of the motor designs presented in articles with segmented Halbach rotor used 3 segments per pole i.e. radial and transverse.

(b) **Bonded Halbach**: The Halbach rotor is made by using either injection molded or compression bonded magnets and then magnetized according to the requirement. The manufacturing of Halbach rotor with bonded magnet is much easier. Furthermore, with bonded magnets the ideal Halbach field distribution can be achieved which assists in improving the motor performance essentially for motors in automobile/traction applications. Moreover, a sinusoidal field distribution also reduces motor noise. Unlike sintered magnets, the resistivity of bonded magnets is very high which eliminates the eddy current loss in magnets and hence, is suitable for high speed applications. The main drawback of bonded magnets is lower remanence caused due to binders. Therefore, to achieve certain level of torque, a higher volume of magnet is required as compared to sintered magnets. The manufacturing of bonded Halbach magnet can be further achieved in two ways [39].

(i) Isotropic Bonded: The Halbach magnet rotor is formed by molding the mixture of binder and magnet powder and then magnetized with sinusoidal

MMF producing impulse magnetizer [37]. Injection or compression method can be used to produce magnet ring. The manufacturing process is relatively easy however, the remanence of the magnet is quite low in the range of 0.3 T - 0.4 T.

(ii) Anisotropic Bonded: The process of producing anisotropic magnet ring is the same as that of isotropic bonded magnet except that the magnetic powder is oriented during the injection molding process [38]-[44]. The remanence of anisotropic bonded magnets lies in between anisotropic sintered magnet and isotropic bonded magnet. In other words, the anisotropic bonded magnets offer good compromise between performance and cost of the Halbach magnet.

2.2.1. Anisotropic Bonded NdFeB Halbach Magnet

To maintain a good balance between cost and performance, it was decided to use anisotropic bonded magnets for the motor design. In this section the manufacturing of Injection molding anisotropic bonded magnet is presented. Apart from cost and performance, bonded magnets have good features for recycling also, it will be discussed in section 2.4. Majority of bonded magnets can be formed by 4 methods: calendering, compression, injection and extrusion. Figure 2.3 shows the different steps in manufacturing of bonded magnets. Calendering is not included as it is used to produce flexible sheet of bonded magnets which is not applicable for motor.

In **Injection molding process** the magnetic powder is mixed with a binder and heated. The molten mix is then filled in a mold cavity and left for solidification. For anisotropic bonded magnet the aligning field is applied while mixing the magnet powder and binder according to the required orientation. The aligning and magnetization process for the Halbach magnet is described in [38] and [37] respectively. The most common type of binders used for magnets for motors are Polyamide 11 or 12 (Nylon), Polyphenolyne sulfide (PPS), Polyamides like PA6, PA12. The selection of binder is very important for mechanical strength and thermal behaviour. The typical density range of injection mold bonded magnets is 5 - 5.5 g/cm^3 and the recommended operating temperature is in the range of 100 °C - 150 °C. The magnets have a lower energy product due to the low magnet powder density, something in the range of 55 - 66 % by volume [8]. Table 2.1 presents a comparison between injection molded and compression bonded magnets. Although, injection molding yields lower remanence magnets, for production of Halbach bonded rotor it is much easier than compression molding. Moreover, using anisotropic injection molding, the remanence of the magnets can be improved close of compression molding.

Another advantage of using Injection molding is that one can easily manufacture any shape and hence, producing small magnet rings is very easy even at larger

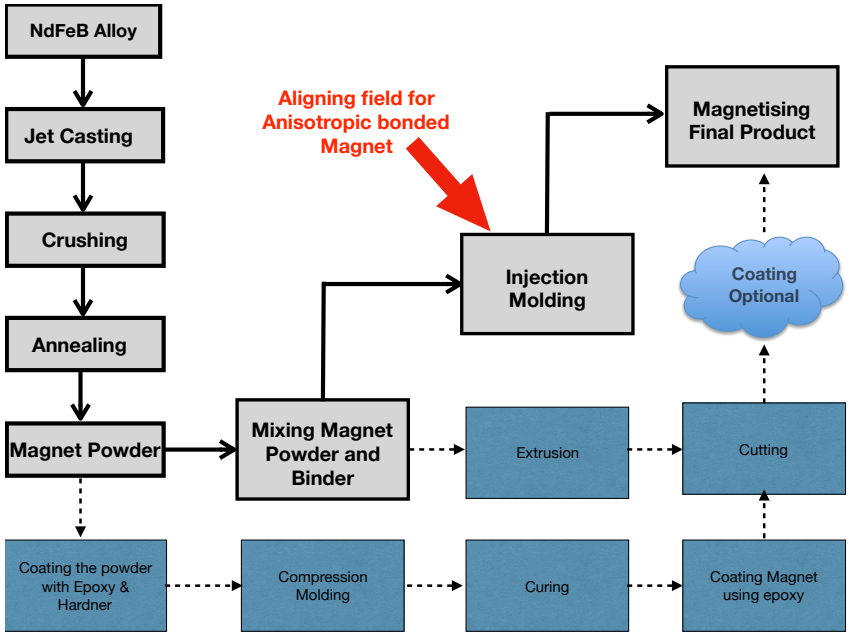

Figure 2.3: Chart showing manufacturing processes of different Bonded Magnets. Dark arrow is for Injection molding Bonded magnets. Dotted line shows process for other types of Bonded magnets

Table 2.1: Advantages and disadvantages of Injection and Compression molding processes

	Injection Molding	**Compression Molding**
Pros	Easy to make any Shape Good Quality products Easy manufacturing Process	Low tooling Cost High magnet power density
Cons	High Tooling Cost Low magnet powder volume Mainly for NdFeB and Ferrite	Only Simple Shapes are possible Mainly NdFeB Difficult to add any process while pressing

volumes. However, for high torque/ power application motor the required magnet volume (dimensions) is high. Manufacturing a single Halbach magnet ring rotor with such large dimensions is very difficult, with the present technology, even with inject molding. Large magnet ring diameter or thickness causes cracks/damages in the magnet [11]. Furthermore, the tooling cost of such large magnets is also very high. The use of segment bonded Halbach magnet does not have a very significant impact on the flux density, mainly because the magnets can be produced in arcs and can be magnetized in Halbach array. The main disadvantage of using segments is the use of glue to hold magnets on rotor which decreases recyclability of the rotor.

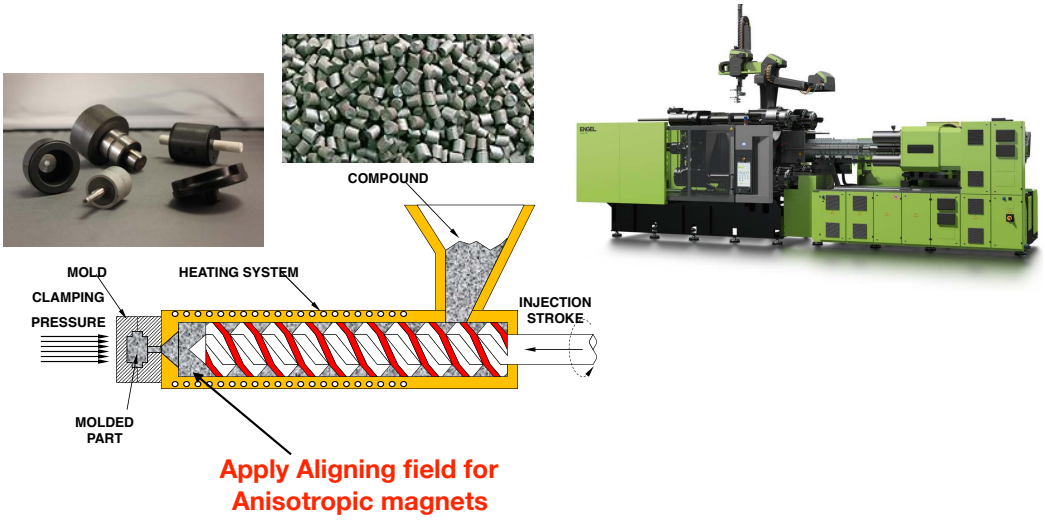

Figure 2.4: Picture of Injection Molding Machine [8]

2.3. Characterization of the Bonded NdFeB material

The magnet material used for manufacturing Halbach rotor is called Magfine MF18P from Aichi Steel. The material comprises of NdFeB magnet powder and PPS binder. The PPS is used to build thermal and mechanical capabilities required for electric vehicle applications. The samples of MF18P was characterized at Neel Institute, Grenoble, France. The magnet sample diameter and length is 20 mm and 13 mm respectively.

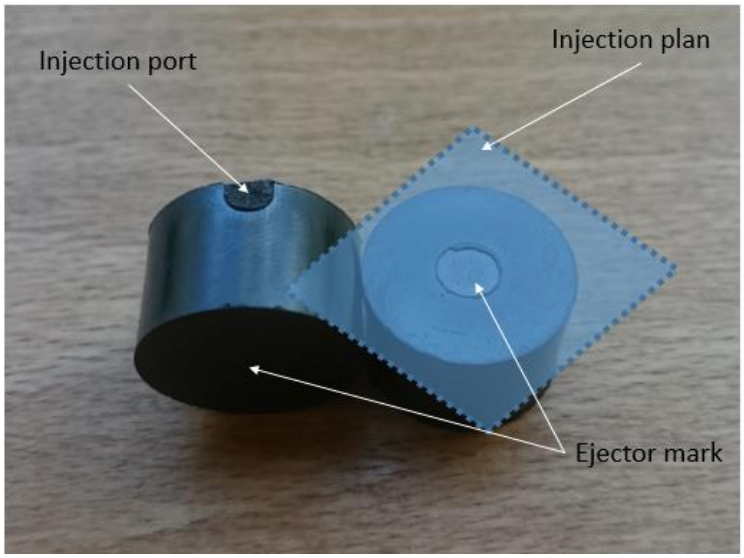

Figure 2.5: Picture of Magfine MF18P sample used for characterization [9]

2.3.1. Magnet Density

The density was measured by Archimedes thrust method in both water and ethanol. The average measured density is 4.978 $g.cm^{-3}$. If it assumed that the density of NdFeB powder and PPS binder is 7.6 g.cm^{-3} and 1.35 g.cm^{-3} respectively. The sample magnet has 89 % NdFeB powder by weight (or 58 % by volume).

2.3.2. Magnet Resistivity

The eddy current loss of the magnet depends on the resistivity of the magnet. Its importance increases even more when a single magnet is used as a rotor. The resistivity of magnet was measured using 4 wire method and the schematic is shown in Figure 2.6. The magnet sample size was very small and hence, needed special preparation before measurement. Figure 2.7 shows the preparation of sample for the measurement. The expected measured resistance was very low therefore, 4 wire method is mandatory along with good measurement contact.

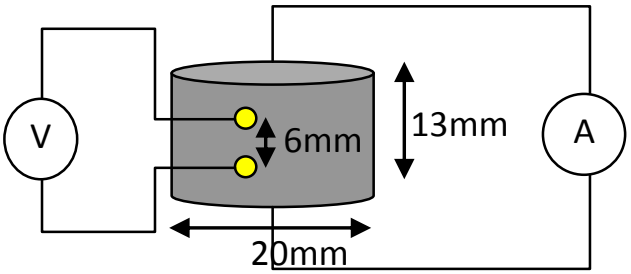

Figure 2.6: Schematic of resistivity measurement

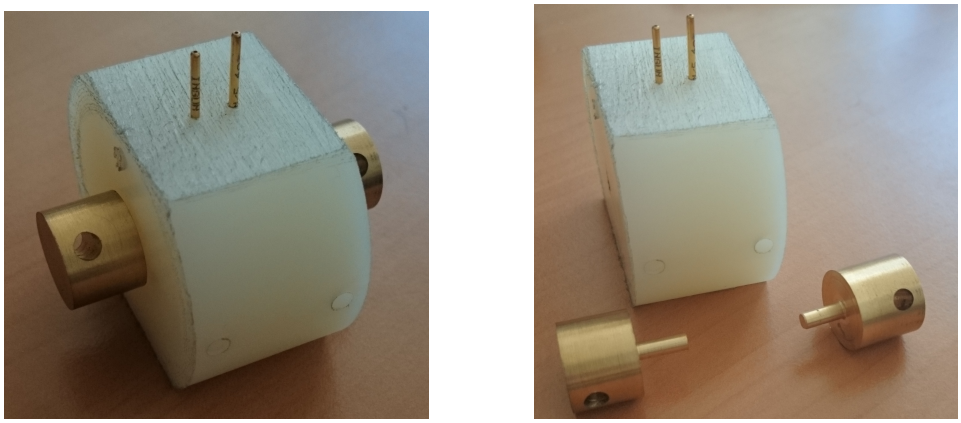

Figure 2.7: Pictures of preparation of sample for resistivity measurement [9]

Table 2.2: Variation of magnet resistivity with current [11]

		Electrical resistivity [$\mu\Omega$.m]		
	Current [mA]	Average	Maximum	Minimum
53 vol%	100	213	231	179
	600	178	201	141
	3000	196	249	166
57 vol%	100	151	153	148
	600	135	149	123
	3000	127	143	114

The measurement was performed both at Neel Institute, Grenoble and Aichi Steel, Japan. Figure 2.8 shows the resistivity values calculated from measured resistance. The selection of the measurement method has a significant impact on the measured resistivity. As expected a higher % NdFeB magnet has lower resistivity. It is interesting to note that the value measured at Aichi Steel is lower than the value measured at Neel Institute, Grenoble. The difference could be because of the sample and the measurement setup. The resistivity of the bonded magnets is greatly influenced by the production method and the sample obtained. Nevertheless, considering the worst case scenario the resistivity of the magnet can be taken as 120 $\mu\Omega$.m for 57 % volume magnet.

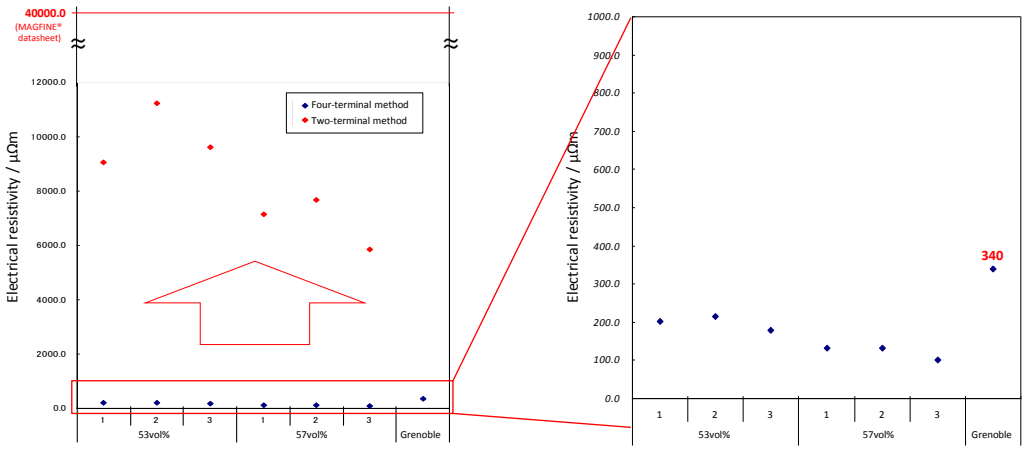

Figure 2.8: Results from the resistivity performed at Neel Institute, Grenoble and Aichi Steel

Table 2.2 presents the variation of resistivity with current. It can be seen that the variation in resistivity is not large by varying current from 100 mA to 3000 mA. The resistivity of the magnet depends on many factors like material, granule size, resin, etc.

2.3.3. Magnetic Properties

The magnetic properties of the sample were measured at NEEL institute, Grenoble (France), using extraction magnetometer which can apply field up to 7 T and temperature in the range of 300 K to 800 K (27 to 527 °C). To perform measurement a sample of 3 mm cube was made from the magnet piece shown in figure 2.5. The sample was saturated by applying field of 7 T and demagnetization in each direction was measured. The measured values are shown in figure 2.9. The figure shows that the magnet is very anisotropic. The direction named Prep 1R has high magnetic field compared to other axes and is the easy magnetization axis. The other two hard magnetization axes have very similar magnetic behaviour. The remanence of easy axis is almost 230 % higher than the other two axes. The anisotropic ratio of the magnet was around 0.42.

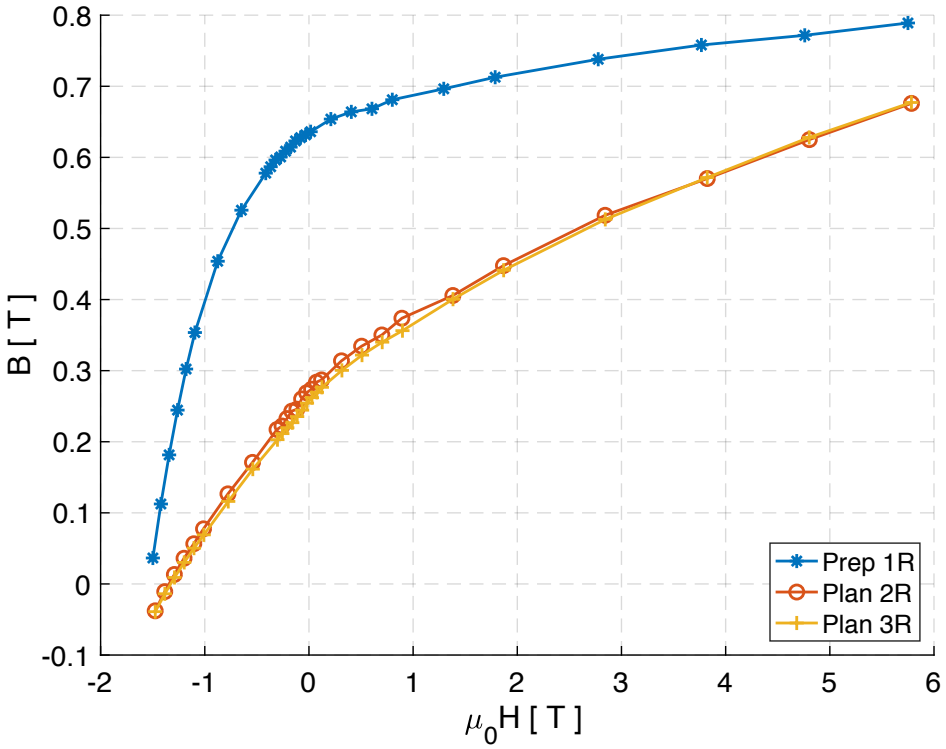

Figure 2.9: Field density of sample in different direction [9]

Figure 2.10 and 2.11 shows the variation of the magnet remanence and coercivity with temperature. The values were measured for the difficult magnetic axis of the magnet sample. The thermal coefficient of remanence and coercivity of magnet is -0.066 %/°C and 0.58 %/°C respectively. For simple approximate calculation, the thermal coefficient of remanence for the easy axis can be calculated from the hard axis value and was estimated to be -0.157 %/°C (-0.066 %/°C /0.42). The

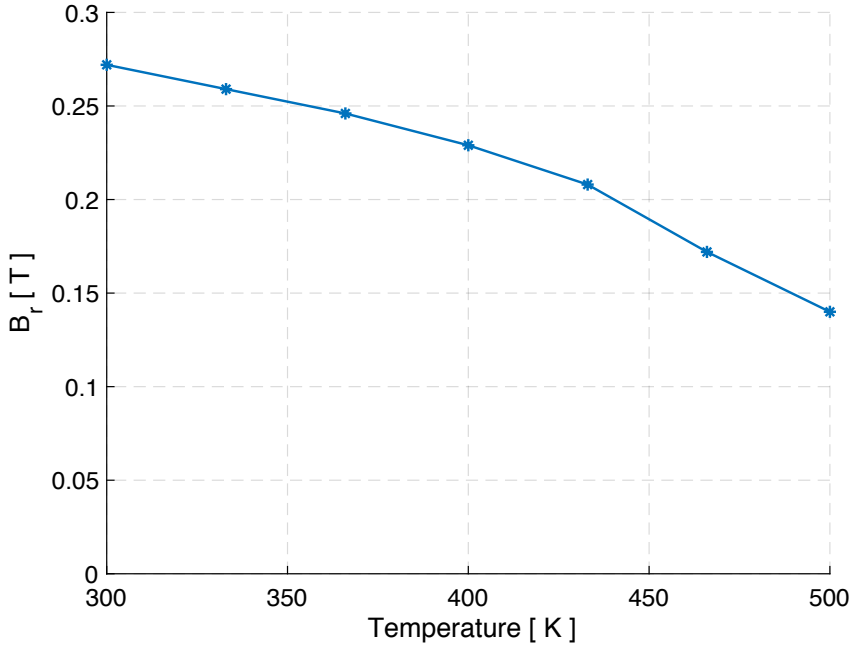

Figure 2.10: Variation of remanence field density with temperature [9]

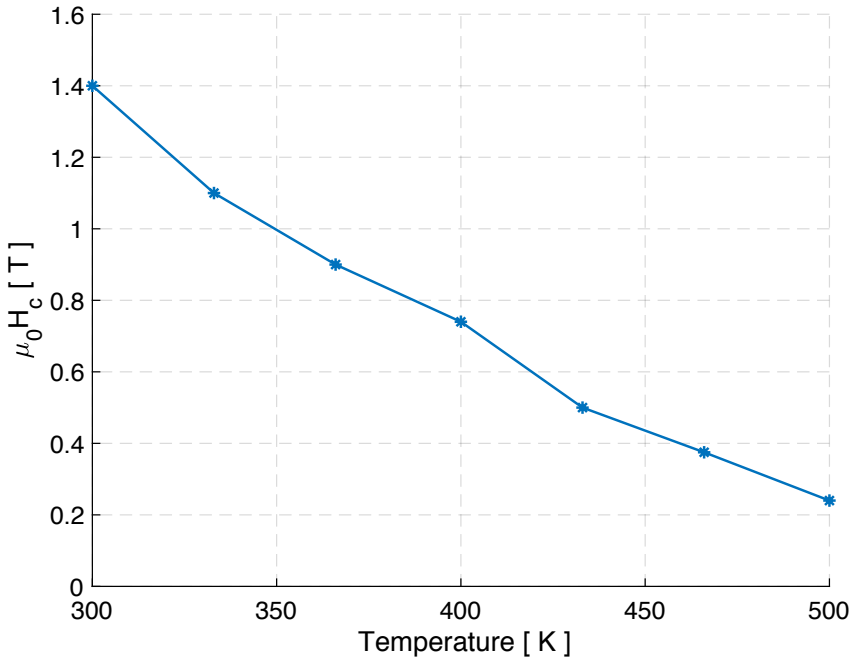

Figure 2.11: Variation of coercivity with temperature [9]

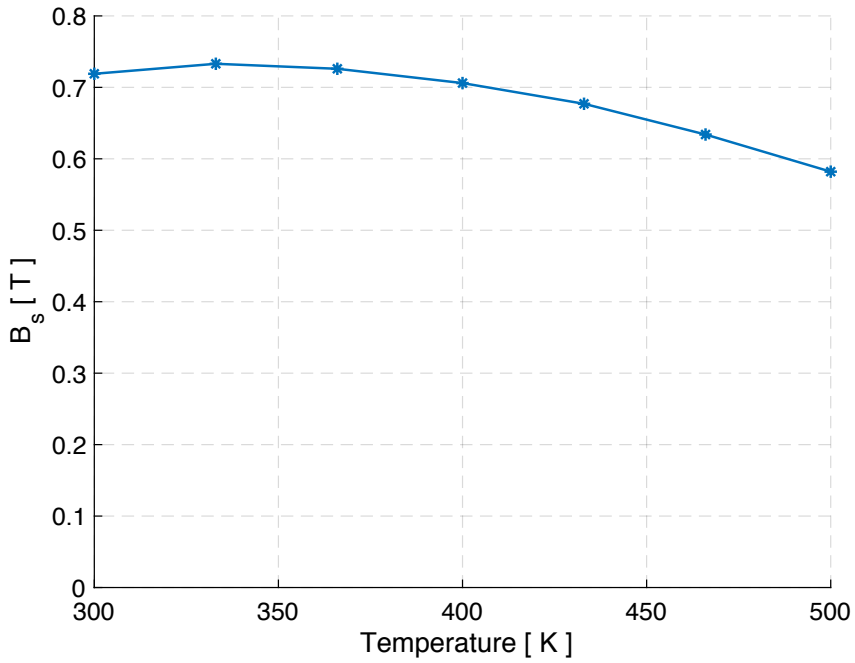

Figure 2.12: Variation of saturation field density with temperature [9]

smooth nature of curve also suggests that there is no drastic chemical or mechanical degradation of the magnet. However, as the high temperature was not applied for a very long duration the behaviour of the magnet in those conditions is unknown. The variation of saturation magnetic field also shows similar trend of decrease in the value with increase in temperature. For instance, at 500 K it requires only 0.58 T to magnetize the magnet which would be much easier to produce.

2.3.4. Thermal Conductivity

The performance of motor is highly dependent on the behaviour of the magnet under different operating temperature. Moreover, the maximum allowed temperature of bonded magnets is in the range of 100 - 150 °C depending on the binder. To have a good estimation of the thermal behaviour of the magnet, thermal conductivity is very critical.

Figure 2.13 shows the experimental setup of the measurement of the thermal conductivity of the bonded NdFeB magnets. The magnet sample's inner and outer radius are 27.3 mm and 33.4 mm respectively. The height of the sample is 45 mm. 8 T-Type thermal sensors were used to measure the temperature at different positions on the magnet cylinder. 4 sensors were placed inside the cylinder and 4 outside making 4 pairs radially as shown in figure 2.13b. A cylindrical heater was used to heat the magnet and cover around the magnet sample. The heater was supplied

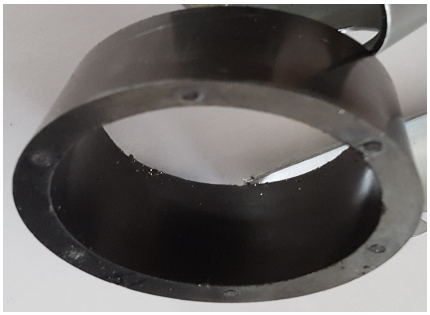

(a) Magnet Sample

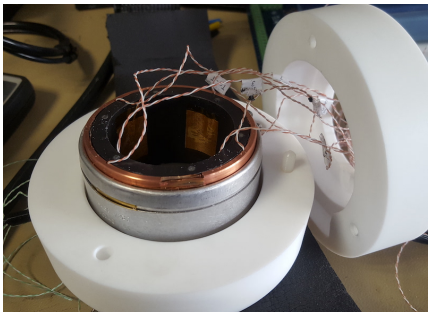

(b) Magnet sample insulated from outside

(c) Placement of temperature sensors

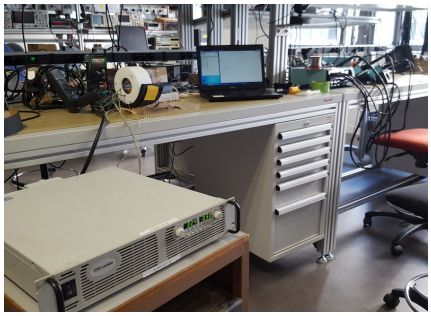

(d) Measurement Unit for temperature

Figure 2.13: Experimental setup for thermal conductivity of the bonded NdFeB magnet

with a controlled DC source and the input power was measured. The sample was insulated from outside so that there was no loss of heat from outer surface as shown in figure 2.13c. The thermal conductivity of the magnet is calculated using equation 2.6 - 2.7.

$$\Delta T = R_{th} \times P_{in} \tag{2.6}$$

$$\lambda_{th} = \frac{L}{A \times R_{th}} \tag{2.7}$$

where, ΔT is the temperature difference between outer and inner temperature sensor at any position, R_{th} is the thermal conductivity, P_{in} is the input power from the heater, λ_{th} is the specific thermal conductivity of the magnet, L is the height of the magnet sample and A is the cross-section area of the magnet.

The supply DC voltage of the heater was maintained such that the P_{in} was 7 W and 10 W. The supply was kept on till the temperatures reached steady state. Figure 2.14 shows the measured temperature and the temperature difference (ΔT) at steady state at different positions. From the figure it can be seen that different positions

Table 2.3: ΔT at different positions on the magnet and the specific thermal conductivity of the magnet

P_{in} [W]	Pos 1 [K]	Pos 2 [K]	Pos 3 [K]	Pos 4 [K]	Average [K]	Specific Thermal Conductivity (λ_{th}) [$W.m^{-1}.K^{-1}$]
7.00	5.64	4.43	4.79	5.26	5.02	1.00
9.92	9.24	5.72	5.97	6.92	6.96	1.03
12.94	8.94	7.43	10.4	8.70	8.87	1.05
20.05	13.24	11.33	15.44	12.49	13.12	1.10
24.87	14.91	13.50	18.74	15.14	15.63	1.18

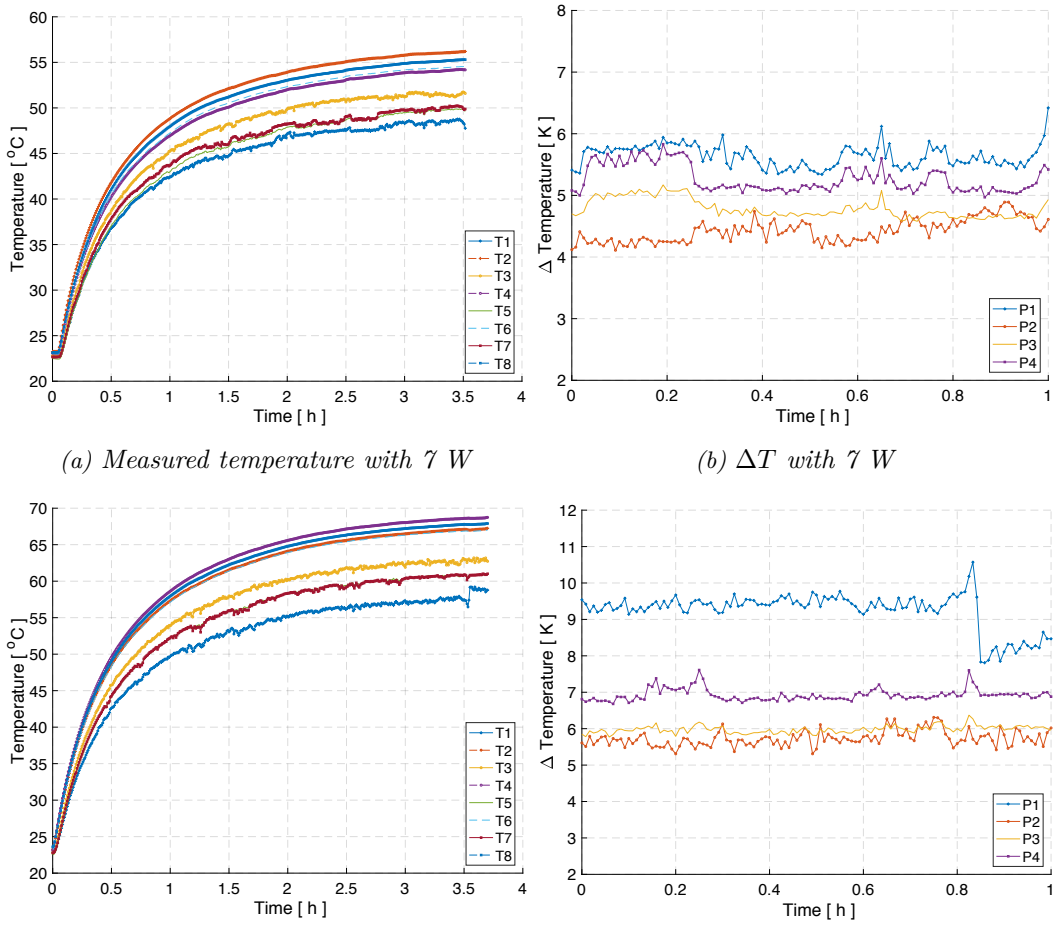

(a) Measured temperature with 7 W

(b) ΔT with 7 W

(c) Measured temperature with 10 W

(d) ΔT with 10 W

Figure 2.14: Measured temperature at different points with 7 W & 10 W Input power

have different temperatures which could be due to non-uniformity in the heating. Furthermore, the difference in ΔT at different positions suggest the non-uniformity in the magnet thermal conductivity. However, the difference is not very large and

hence, an average value of the thermal conductivity can be used to study the thermal behaviour of the magnet in different operating conditions. The average temperature difference for 7 W and 10 W is 5.02 K and 6.96 K and the corresponding specific thermal conductivity is 1 $W.m^{-1}.K^{-1}$ and 1.03 $W.m^{-1}.K^{-1}$. The resistivity of the magnet is increasing slightly with increase in power due to leakage in heat through the insulator around magnet.

2.3.5. Validation of Halbach Rotor

The flux density of a 6 pole Halbach magnet cylinder was measured to analyse the field distribution. Furthermore, the validation of FEM model was also done against the measurement. The material used for Halbach cylinder was Magfine MF18P and was produced by injection molding as discussed in section 2.2. Figure 2.15a shows the Halbach rotor for the measurement. The spatial measurements were recorder with a radial Hall probe mounted with the fixture on the vertical drill press. The probe was moved in all three XYZ axis. To avoid any interference of environment a plastic base was used. Figure 2.15b shows the setup used for measuring magnetic field density inside the cylinder.

(a) 6 pole Halbach cylinder *(b) Measurement setup of Halbach cylinder*

Figure 2.15: Halbach magnet sample and magnetic filed sample measurement setup [9]

Figure 2.16 shows the flux density inside the Halbach cylinder at different vertical (Z direction) positions from the top. It can be seen that the axial position does not have a significant impact on the flux density. In figure 2.17 the comparison of measured and FEM calculated flux density inside the cylinder is shown. The calculated values are in very good agreement with measured ones. The measured flux density around the circumference is sinusoidal which is very close to ideal Halbach cylinder.

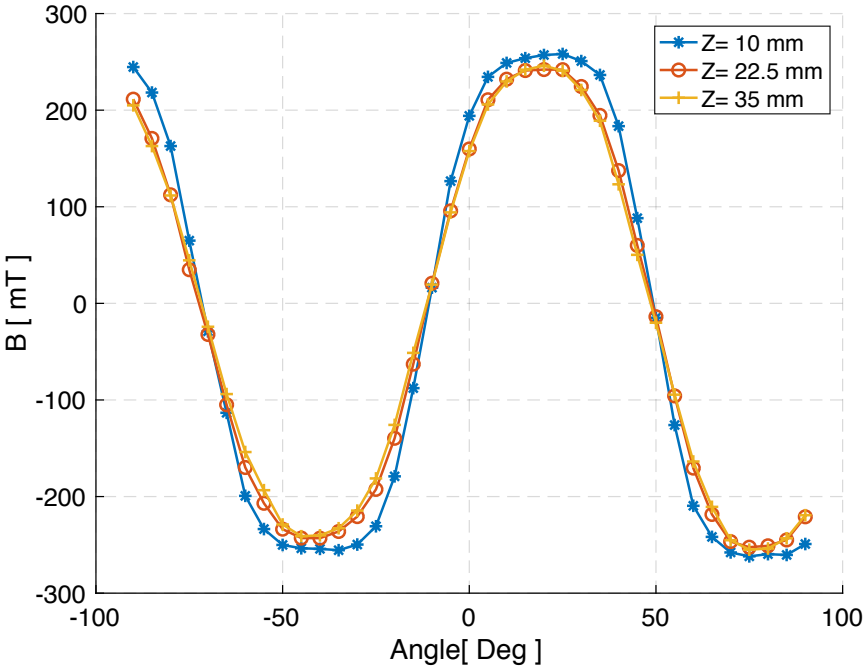

Figure 2.16: Magnetic flux density at different vertical positions

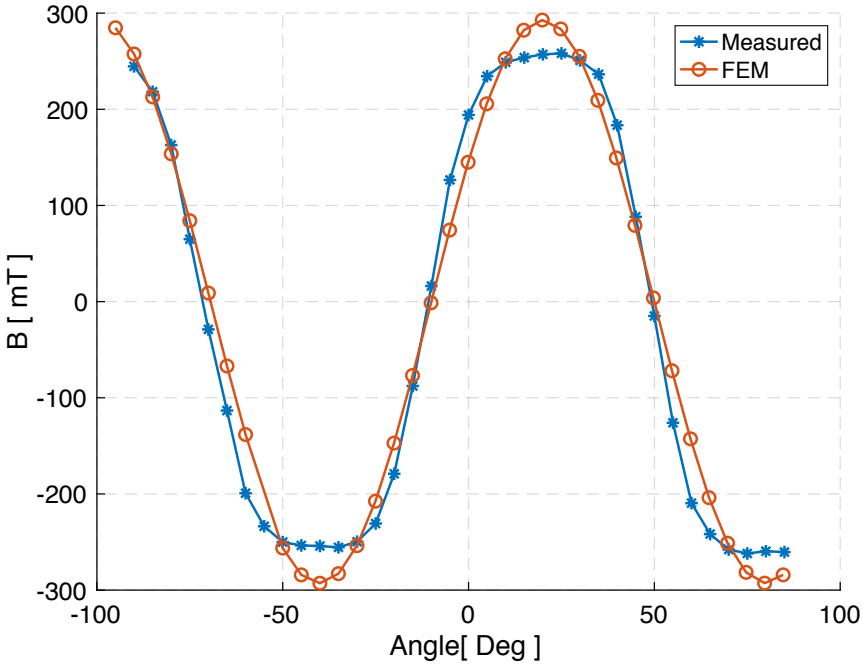

Figure 2.17: Magnetic flux density at different vertical positions

2.4. Recycling of Magnets

The NdFeB magnets contain rare earth elements and it is important to recycle them to have sustainable supply of magnets for growing demands of PM motors. In DEMETER project different routes of recycling like reuse, direct and indirect recycling of magnets are identified. In [45] a summary of results obtained from different articles regarding properties of recycled magnet is presented. Almost all of the methods and results presented are for developing new recycled sintered magnets from old sintered magnets except [46] where bonded NdFeB was produced from old sintered magnets. The variation of remanence of recycled magnet is between 0% to 20% using different recycling methods. Therefore, making estimation of the motor performance with recycled magnet is very difficult. Another challenge associated with magnet recycling as mentioned in [18] is that the motors are not designed for recycling. Hence, it very difficult to extract very good recyclable used magnets from motors. The quality of yield largely depends on the quality[1] of magnet extracted from the machine. The recycling of sintered NdFeB magnets from the motor designs at present have following challenges.

(a) **Glue / Band Aid**: The motors in automobile application are designed to handle heavy mechanical stress with high speed and hence, glue or band aid is used to fix magnets on rotor. Higher the operating speed more glue or band aid is required in an conventional SMPM motor. Even in interior permanent magnet (IPM) motor glue is used to fill the any space left in the magnet slot. Furthermore, small segments of magnets are used to reduce the eddy current loss and glue is used to put them together. The use of glue not only reduces recycling, but also reduces the effective volume of magnet.

(b) **Magnet Coating**: Sintered NdFeB magnets are very prone to corrosion. Therefore, to protect magnets coating is used [47]. The presence of coating is not desirable for magnet recycling and effects the magnetic properties of recycled magnets.

The use of glue makes extraction of magnet from the rotor very difficult. Furthermore, the magnets are either given heat or chemical treatment to remove coating/glue before recycling.

2.4.1. Recycling of Sintered NdFeB Magnets

Sintered NdFeB magnets is one of the most used magnets in different applications and higher than 90% is produced using sintering. Figure 2.18 shows different routes for recycling sintered magnet [10], [48]. As discussed in the chapter Introduction , the Demeter project has identified three different ways to recycle magnets. In this section only alloy recycling (Direct Recycling) is discussed where the scrap magnet

[1]The term quality means how good extracted magnet is for recycling

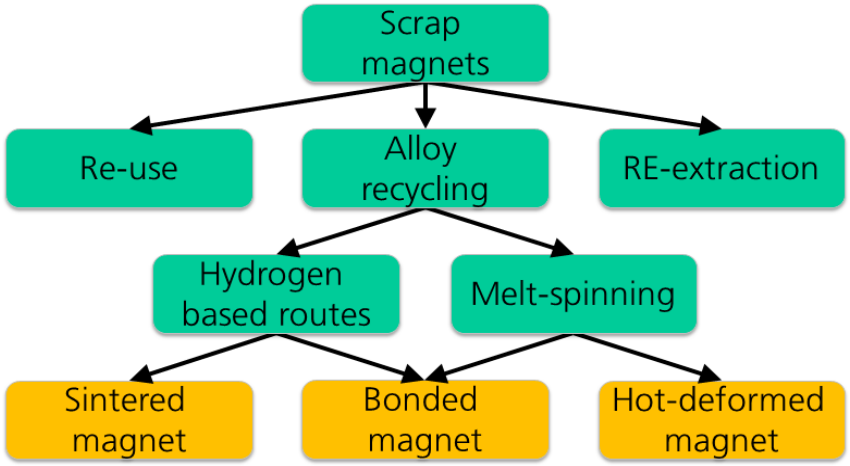

Figure 2.18: Different routes of recycling/reusing recycling NdFeB sintered magnets [10]

is recycled as an alloy of Nd, Dy etc. and new magnets can be produced in fewer process. The challenge with the route is that before recycling the scrap magnet, composition and alloy of the magnet must be know. Furthermore, the quality of the reproduced magnet is highly impacted by any impurities like glue, coating etc. and hence have to be removed [49]. Figure 2.19 shows the flow chart for recycling of sintered NdFeB magnets [10].

Hydrogen Based Routes: The recycling of magnet using hydrogen can be done in two ways Hydrogen Decrepitation (HD) and Hydrogenation, disproportionation, desorption, recombination (HDDR). In HD process the scrap magnet is processed in Hydrogen followed by blending and milling of powder along with adding extra REE (if required). Subsequently, magnetic alignment and isostatic pressing is done to form green compacts. Thereafter, sintering is done at $\sim$ 1080 °C. The downside of the process is the increases in oxygen content which lowers the density of the magnet. To achieve full dense magnet $NdH_{2.7}$ is added which additionally enhances the coercivity of the magnet [50]. The HDDR process is similar to the sintered magnet production process except temperature and pressure are shifted to optimize magnet performance. Following that by using either cold pressing or injection molding with aligning field anisotropic bonded magnet can be produced. In [45] properties of magnet following different recycling routes are presented and it can be that the variation is very large and the magnet remanence is reduced as high as 20%.

Melt Spinning : The melt spinning process, also known as rapid quenching, is being used for many years to produce primary magnetic alloys. The same process is used to reproduce new magnets from scrap magnets. The scrap is inductively heated on higher temperature than 1200°C and the molten is cast on a rotating copper wheel with fast cooling. The cooling solidifies the molten into thin flakes [48]. The process produces very homogeneous micro structure of NdFeB. However, when used for recycling the content of carbon and oxygen in scrap magnet causes 20 - 30

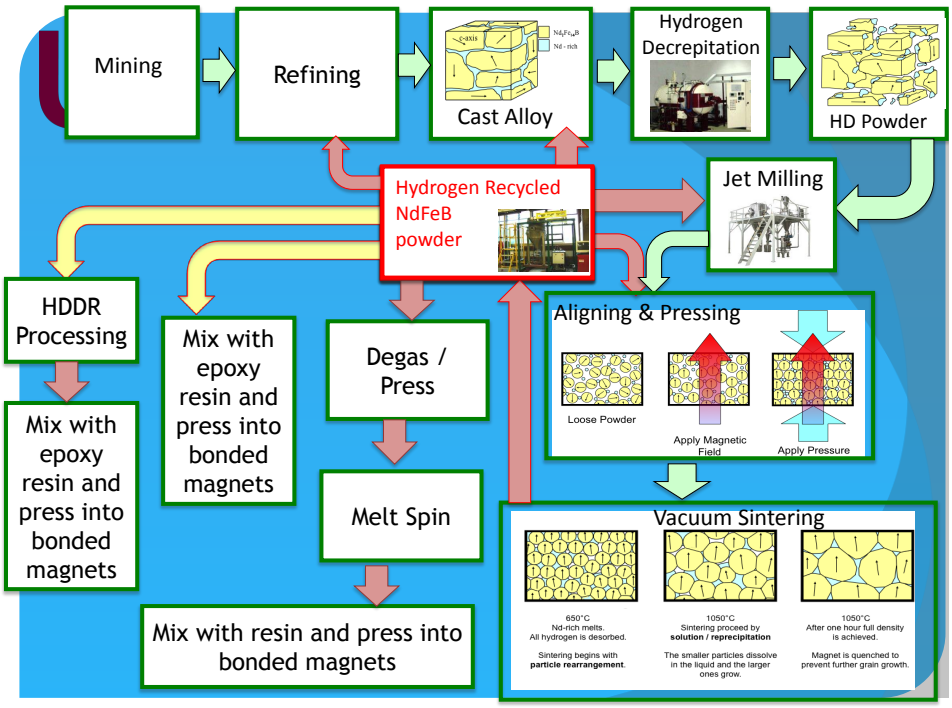

Figure 2.19: Flow chart for recycling of NdFeB sintered magnets [10]

% reduction in the yield. Furthermore, the loss of REE's also causes reduction in remanence of recycled magnets [49]. Nevertheless, Fraunhofer Project Group IWKS lab has demonstrated that this method can be used on lab as well as on industrial level to reproduce magnets from scrap [48].

2.4.2. Recycling of Bonded NdFeB Magnets

Bonded NdFeB magnets offer many advantages over sintered NdFeB magnets for recycling. Bonded magnets do not have corrosion issue and hence, do not need any coating. Furthermore, with bonded Halbach rotor the motor can be designed to avoid any glue. However, due to binder the bonded magnets cannot be recycled the same way as of sintered magnets.

Figure 2.20 shows different ways of recycling bonded NdFeB magnets. Process marked (a) and (b) differ by the method binder is removed from the power. Following is the description of different processes of recycling.

(a) Recycling by Heating: The process involves heating bonded magnet to decompose resin used. The magnet is heated to 500 - 1200 ° C. Furthermore, the process is done in inert gas atmosphere like nitrogen, argon, etc. to prevent oxidation of the magnetic powder. The process may deteriorate the magnetic properties due to

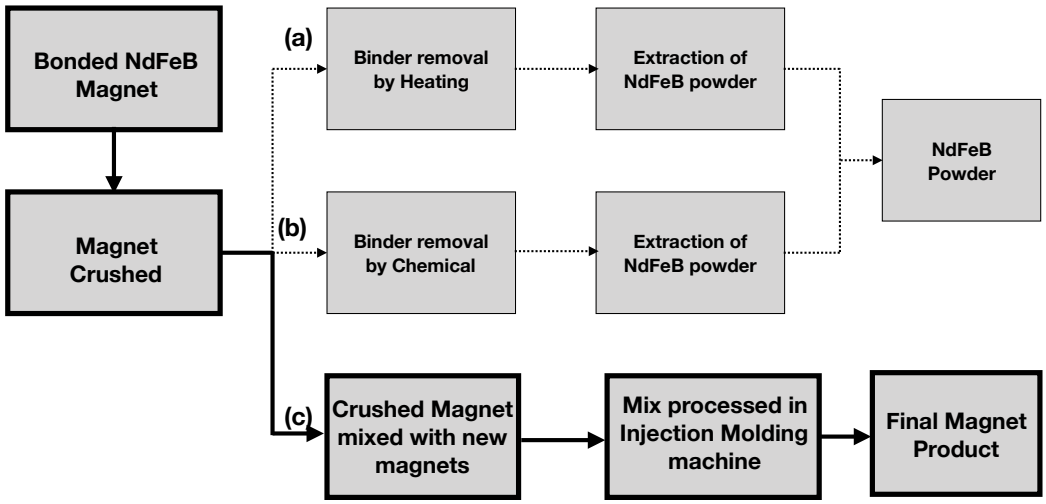

Figure 2.20: Simple flow chart for different ways of recycling bonded magnet

high temperatures. It can be applied to both thermoplastic or thermosetting type of binder [51].

(b) Recycling by Chemical Cleaning: The process involves putting the magnet in a decomposing solution or keeping the magnet in the gas phase of the decomposing solvent. The solvent can be tetralin, napthalene, methylnapthalene etc. After chemical decomposition the magnet is heated to 230 °C or higher. To protect magnet from oxidizing inert gas chamber is used same as heating recycling method. It is further recommended to use 20% of recycled magnet with new magnetic powder to maintain magnetic properties [51].

(c) Recycling by Crushing and Mixing: The process involves crushing bonded magnet and then mixing a fix ratio of old magnet with the virgin magnet powder and then put in the molding machine. Crushing helps to demagnetize the old/used magnet. However, like other two methods, this process also has risk of deteriorating magnetic properties of the magnet powder. Another critical necessity of the process is that the new and old magnet binder should be the same. This issue can be handled for defective magnet in the production however, this is very difficult task to identify binder for the magnets extracted from the used motor. Furthermore, like other recycling process mentioned above, the amount of old recovered magnet powder should not exceed certain ratio in the mix [52]. The ratio of new and old magnet is very important for the final magnet performance.

Figure 2.21 shows the steps of recycling process followed at Aichi Steel. Figure 2.22 shows the magnetic properties of recycled magnet with 30 % and 50 % of old magnet mixed with new magnet [11]. It is interesting to note that after few recycling cycles the magnetic properties do not change, in this case it is 3. Further, there is not impact of mix ratio on the remanence however, the coercivity of the magnet is decreasing

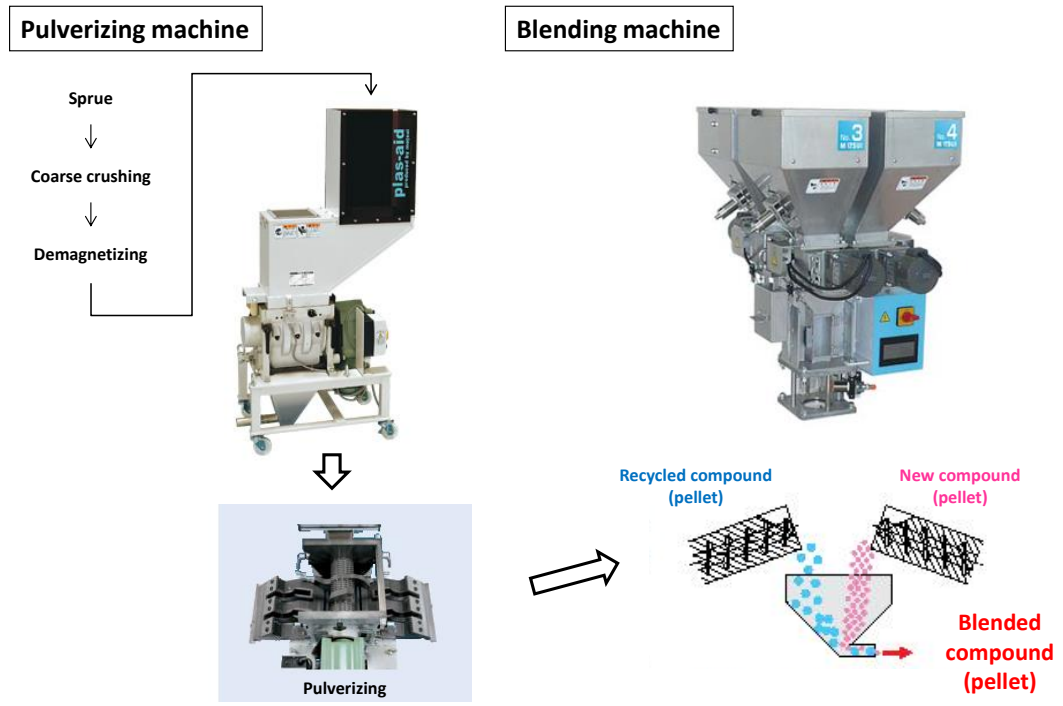

Figure 2.21: Process for magnet recycling used at Aichi Steel [11]

with higher percent of recycled magnet powder. With 30 % recycled magnet powder the coercivity drops by 2 % and hence, it is a good compromise between easy recycling process and magnet performance. Furthermore, if the motor is designed considering final recycled magnetic properties (R5), the motor can easily operate with recycled magnet without any degradation in the motor performance.

2.5. Summary

Many studies have shown that the use of Halbach magnet for motor application has several advantages like, high flux density, low noise, low torque ripple, etc. However, complex and expensive manufacturing of Halbach magnet limits its use in different applications. The Halbach magnet can be made using either sintered magnets or bonded magnets. The manufacturing of bonded magnets is simpler and less expensive compared to sintered magnets, especially for Halbach magnet. Moreover, using bonded magnets ideal Halbach magnet can be achieved, whereas with sintered magnet many magnet pieces are required which further increases manufacturing complexity. The low remanence of bonded magnet can be improved slightly by introducing anisotropic. Therefore, Halbach rotor made from anisotropic magnet is a good choice for motors considering both manufacturing cost and complexity.

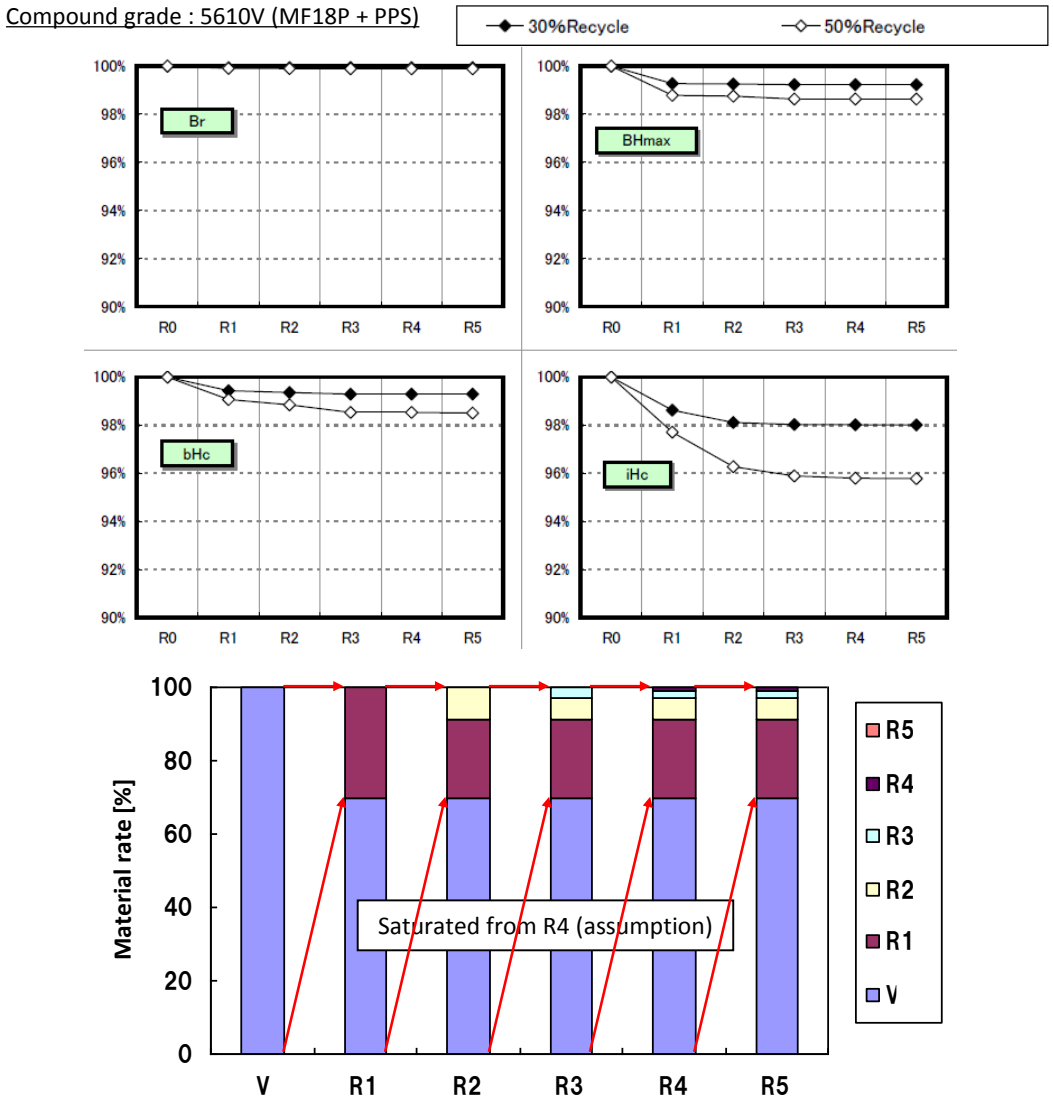

Figure 2.22: Magnetic properties of recycled magnet with different ratio of old and new magnet powder. R1, R2, R3, R4 and R5 denotes the successive recycling cycle and V for virgin magnet [11]

The characterization of bonded NdFeB material (MagFine18P from Aichi Steel) used, to manufacture the prototype, was done. The magnet sample has a good anisotropic ratio and the magnetic properties are very stable with respect to temperature, despite no Dysprosium in the magnet. The PPS binder used in the magnet provides very good mechanical strength even at high temperature, as shown in measurement results. There is no sign of deterioration either in the mechanical or magnetic properties due to high temperature. From the measurement results it can be inferred that the magnet can easily operate upto 150 °C. Another, main feature of bonded magnet

is its high resistivity. The resistivity of few samples were measured and the values obtained are in the range of 120 - 150 $\mu\Omega$.m which is roughly 100 times higher than the sintered NdFeB magnets. This implies that even at very high speed magnet's eddy loss should be very less. In addition, the thermal conductivity of the magnet was also measured at different input power and the average value of conductivity obtained was 1 $W.m^{-1}.K^{-1}$. The value is lower when compared with sintered magnet. At the end, the flux density of the sample Halbach rotor in the air was measured and the values are in good agreement with the FEM calculation. Moreover, the field distribution of the sample Halbach magnet is also very close to the ideal Halbach field distribution.

Different recycling routes of sintered and bonded magnets are also discussed in this chapter. Compared to sintered magnet, the recycling process of bonded magnet is much simpler. Although, bonded magnets are not very common to use for the motors in automotive application, but lately there has been some shift in focus towards bonded magnet. The results show that with a mix of virgin and old magnet (up to 30 %) it is possible to achieve recycled magnet without significant loss of magnetic properties. The process proposed in the thesis for recycling is very simple and environment friendly. However, the recycling methods require more experiments and analysis to determine optimum properties of the recycled magnet for the motor application.

Chapter 3

3 Design and Performance of Motor with Outer Halbach Rotor

The Halbach magnet arrangement has many features which improve motor performance as discussed in chapter 2. Despite many advantages, the use of Halbach array especially ideal Halbach magnets is not common for the motor application due to the complex and expensive manufacturing process. Furthermore, the designs presented in articles has sintered magnet which were not designed for electric vehicles (EV) or hybrid EVs [43]- [41]. In recent years, the application of fractional slot tooth coil winding (FSTCW) in motors is gaining traction specially for high torque density motor due to shorter end windings. In [53] the main advantages and disadvantages of the windings along with the different methods of windings to increase slot fill factor and its manufacturing are discussed. In [54] comparison of motor's performance with different slots poles combinations for a SMPM motor is presented. The thesis also presents the winding configuration of the stator with different combinations of slots poles. In [34] the impact of combination of slots poles on different parameters like winding factor, back EMF, torque ripple etc is presented. However, both the theses present the analysis of a radial permanent magnet motor for low speed application. The use of FSTCW for high speed application i.e. high operating frequency has many challenges mainly due to induction of many low sub and higher harmonics. These harmonics cause excess loss in rotor, specially in magnets.

In this chapter a motor design with outer rotor Halbach magnet and a FSTCW stator is presented for an (hybrid) electric vehicle. The 2D and 3D FEM models were used to dimension and calculate performance of the motor. The motor designed has an ideal Halbach magnet rotor proposed to be manufactured by injection molding process using bonded NdFeB magnet. The use of the bonded magnet helps in reducing eddy loss. The ideal Halbach magnet can be easily produced as compared to sintered magnets. This chapter also presents the impact of different parameters on the motor's performance. Different strategy to use recycled magnets with the proposed motor design were studied and results are discussed. Finally, a prototype was produced for the proposed motor designs and measurement results are also presented and compared with the calculated values.

3.1. Motor Design Parameters

3.1.1. Number of Poles

The airgap flux density of an ideal Halbach magnet for outer rotor (internal field) is given by the equation 3.1, derived from equations in [42], [37] & [55]. It was assumed, that the iron core has infinite permeability i.e. no saturation and also for the simplification the relative permeability (μ_r) of magnet was assumed 1, which is not far from the actual value. Figure 3.1 shows the model used for calculating airgap flux density of an ideal Halbach cylinder.

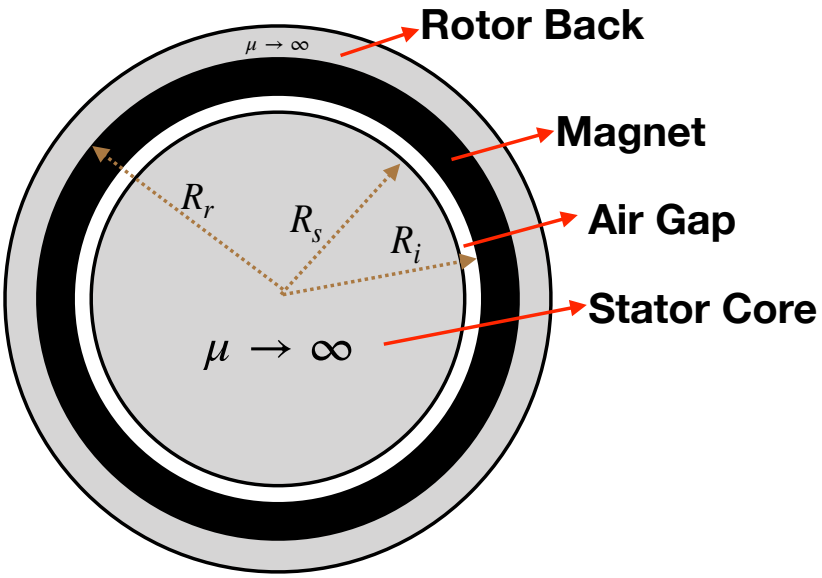

Figure 3.1: Analytical model used for calculation airgap flux density of ideal Halbach cylinder

$$B_\delta = \frac{B_r p}{(p-1)} \frac{1 - \left(\frac{R_i}{R_r}\right)^{p-1}}{k} \left[1 + \left(\frac{R_s}{r}\right)^{2p}\right] \times \left(\frac{r}{R_i}\right)^{p-1} \tag{3.1}$$

k is defined as

$$k = \begin{cases} 1 & \text{for air core rotor back} \\ [1 - (R_s/R_r)^{2p}]^{-1} & \text{for iron core rotor back} \end{cases} \tag{3.2}$$

where, B_δ is the peak fundamental airgap flux density, R_s is the stator outer radius, R_i and R_r are the inner and outer radius of the Halbach cylinder, p is the number of pole pairs and r is the radius of the flux density calculation point.

Figure 3.2 and 3.3 shows the variation of airgap flux density with number of poles for an iron-core and air-core rotor respectively. There is very good agreement between analytical and FEM calculated flux density in both the cases. Unlike, conventional SMPM the airgap flux density is increasing with number of poles for both iron-core and air-core rotors. Therefore, it is advantageous to use higher poles for the motor with Halbach rotor. Furthermore, from the equation 3.1 it can be deduced that airgap flux density increases with increase in ratio of R_r and R_i [39].

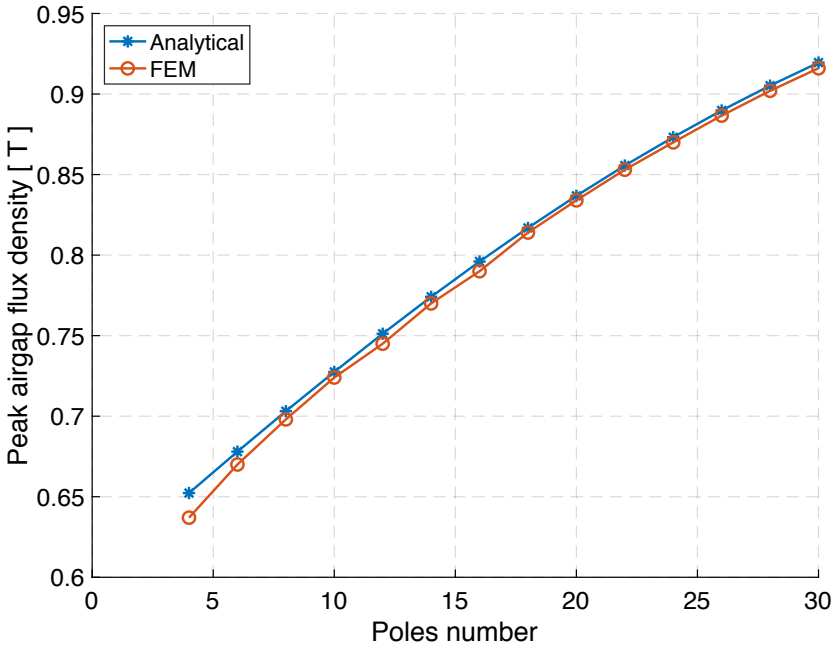

Figure 3.2: Variation of peak airgap flux density with number of poles. The figure also presents comparison between the peak airgap flux density calculated analytically and FEM model. The stator iron core and rotor back has $\mu_r \to \infty$, $\frac{R_i}{R_r} = 0.91, B_r = 0.6$ *T & airgap is 0.5 mm*

Figure 3.4 shows the impact of using non-linear iron material for both stator core and rotor back i.e. iron saturation. All dimensions were kept same in the FEM model and only iron permeability was changed in the two cases. A significant reduction in the airgap flux density can be seen for lower number of poles due to rotor back saturation. As the pole numbers were increased, the impact of saturation reduces. Therefore, to maximize utilization of Halbach magnet with thin rotor back it is good to choose large number of poles. However, high pole numbers also cause higher losses and hence, there should be a good trade-off between utilization and motor performance. Despite, saturation in rotor back the airgap flux density with iron-core rotor is higher than the air-core rotor. Hence, the motor with iron-core will always produce higher torque than the air-core rotor keeping other dimensions unchanged. However, the eddy loss in iron-core rotor is high both in magnets and the rotor back. Additionally, with iron-core the rotor weight will also increase. Therefore,

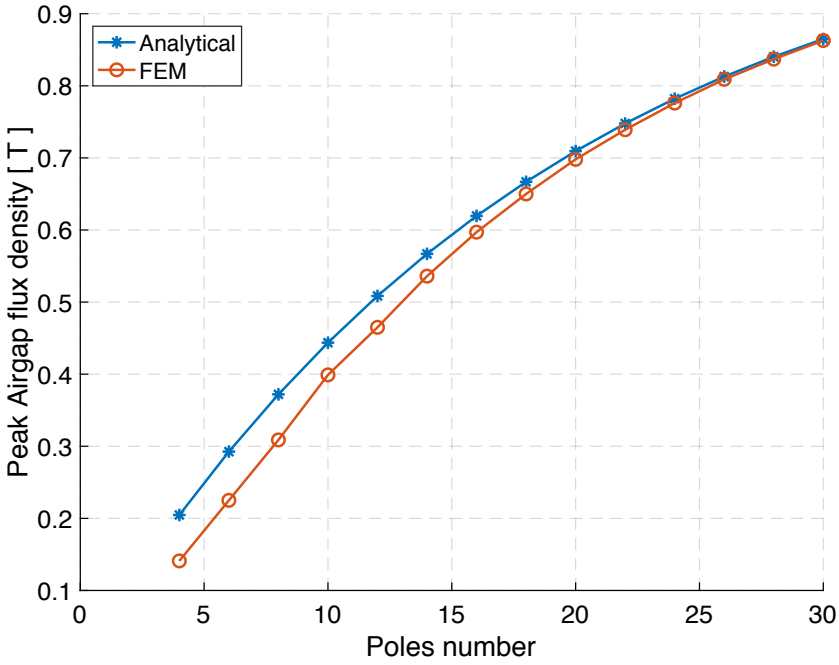

Figure 3.3: Variation of peak airgap flux density with number of poles without rotor back i.e. air cored rotor. The figure also presents comparison between the peak airgap flux density calculated analytically and FEM model. The stator iron core has $\mu_r \to \infty$, $\frac{R_i}{R_r} = 0.91, B_r = 0.6$ *T & airgap is 0.5 mm*

while designing these factors must be kept in consideration, specially eddy loss in magnets. The impact of rotor back is much larger at lesser number of poles. It can also be inferred that at a high number of poles, motor can be designed without rotor back or non-magnetic rotor back (for mechanical support) without degrading motor performance significantly. Another factor that needs to be considered while selecting number of poles is the maximum inverter switching frequency, with increase in pole number the maximum operating frequency will also increase.

3.1.2. Stator Winding

The stator winding used for the motor is FSTCW for the following reasons.

1. **Less axial space**: According to the specification for the motor the space available is large in radial direction and small in the axial direction. Therefore, to achieve compact design with minimum coil overhang, FSTCW is the obvious choice. Furthermore, FSTCW winding causes high leakage inductance and hence, the motor is expected to have wide constant power range [56].

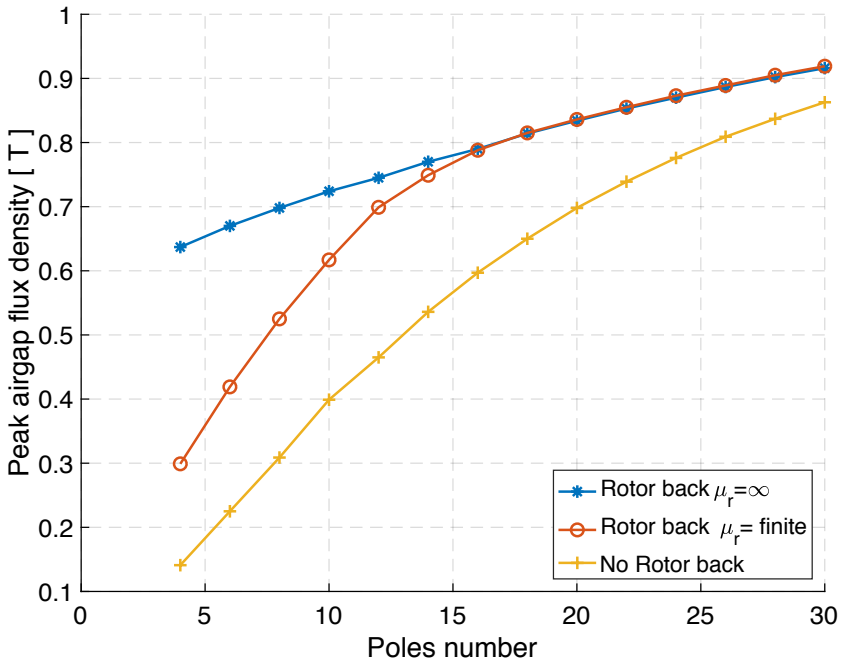

Figure 3.4: Impact of rotor back material on airgap flux density and its variation with number of poles, $\mu_r = finite$ represents non-linear iron material.

2. **Bonded Magnets**: The FSTCW causes excess harmonic loss in rotor however, that loss is expected to be low due to the use of high resistivity bonded magnets rotor.

3. **Halbach Rotor**: The motor has Halbach rotor and hence, the rotor back can be very thin or non magnetic. The magnetic field distribution is very sinusoidal. Hence, the rotor losses and other parasitic effects are expected to be minimal. Furthermore, with outer rotor arrangement the rotor cooling will be better.

The FSTCW has possibility to have single or double layer winding. In single layer winding, the coils are wound on alternate tooth whereas in double layer the windings are on each tooth. The fault tolerance and fill factor of single layer winding is higher than the double layer. On the other hand, the harmonic content, torque ripple and the eddy current loss in PM caused by single layer is much higher than that of the double layer. Therefore, for high frequency operation, double layer winding has advantage of lower losses. Moreover, the end winding of single layer is longer than the double layer. Furthermore, not all slot pole combinations of FSTCW can have single layer winding [34], [57], [58] and [59]. The advantages of double layer winding much better meets the requirements of the application and hence, double layer FSTCW was used for the motor design.

Slot Pole Combination

The performance of a motor with FSTCW depends on the slots poles combination. The study was done to calculate the impact of slots poles combination with Halbach magnet rotor on the motor's torque and inductance. 2D FEM model was used to calculate the inductance and torque. The maximum line current, line voltage, current density, magnet grade, magnet volume, airgap thickness and rotor dimensions were kept the same for all the calculations. The calculations were performed on the motor model with a non-magnetic rotor back to remove the impact of saturation in this part on torque or inductance. The inductance was calculated using frozen permeability method [60]. For comparison of inductance per unit (p.u.) system is used defined by the equations 3.3 - 3.4.

$$L_b = \frac{\psi_m}{I_{max}} \tag{3.3}$$

$$L_{p.u.} = \frac{L_d}{L_b} \tag{3.4}$$

where, ψ_m is the magnetic flux linkage, I_{max} is the maximum d-axis current, L_d is the d-axis inductance.

The first set of calculations were done using constant turns per phase for all the slots poles combination. As a current source was used for simulations instead of voltage source (to reduce simulation time), the current loading and density were same however, the line voltage was not. Table 3.1 presents the calculated parameters for different slots poles combinations. In SMPM motors the torque decreases with increase in pole numbers due to increase in magnetic flux leakage between the poles [54]. However, from the table it can be noted that with same slots, with increase in pole numbers the torque increases. This is due to the increase in the airgap flux density with poles in Halbach magnet. Furthermore, due to the impact of slots poles combination on fundamental winding factor it can also be seen that the torque increase 15% when pole numbers is changed from 14 to 16 whereas, the corresponding increase is only 1% for changing poles from 20 to 22. The winding factor increases as pole number approaches closer to slots number [34]. The torque for 18 slots/20 poles is higher than the 24 slots/20 poles whereas, torque for 18 slots/22 poles and 24 slots/22 poles are the same. This is due to the high saturation of stator core for 24 slots/20 poles at the maximum current.

The flux weakening capability of the motor depends on the p.u. inductance of the motor and to have a good flux weakening the desired p.u. inductance of the motor should be 1 [61], [56]. From the table 3.1 it can be seen that all the slots poles combination has p.u. inductance higher than 1 due to the high leakage inductance of the FSTCW [53], [62], [56]. The p.u. inductance increases with increase in pole numbers for a given slot number due to decrease in flux linkage and hence, lower base inductance, see equation 3.5 [63]. However, due to Halbach magnet rotor the

variation in flux linkage is also impacted by the pole numbers and hence, increase in the inductance is not very large. It can also be seen that the p.u. inductance decreases with increase in slot numbers because the magnetizing inductance is inversely proportional to the number of slots [64].

$$\psi_m = B_\delta \frac{2}{p} R_s \; L \; N_s \; k_{w1} \tag{3.5}$$

where B_δ is the fundamental airgap flux density, R_s is the stator inner (outer for outer rotor) radius, L is the motor active length, N_s is the number of turns per phase and k_{w1} is the fundamental winding factor.

Table 3.1: Impact of Slots Poles combination on Maximum Torque and Inductance. The maximum current, current density, airgap thickness, magnet volume and grade, rotor dimensions and turn per phase were kept the same.

Slots	Poles	Turns	Torque [p.u.]	Magnetic flux linkage [Wb]	L_d [p.u.]
18	14	50	0.72	4.05E-02	1.23
18	16	50	0.83	4.09E-02	1.31
18	20	50	0.96	3.79E-02	1.41
18	22	50	0.97	3.48E-02	1.41
24	20	50	0.90	3.63E-02	1.01
24	22	50	0.98	3.54E-02	1.09
24	26	50	1.07	3.27E-02	1.16
24	28	50	1.09	3.10E-02	1.16

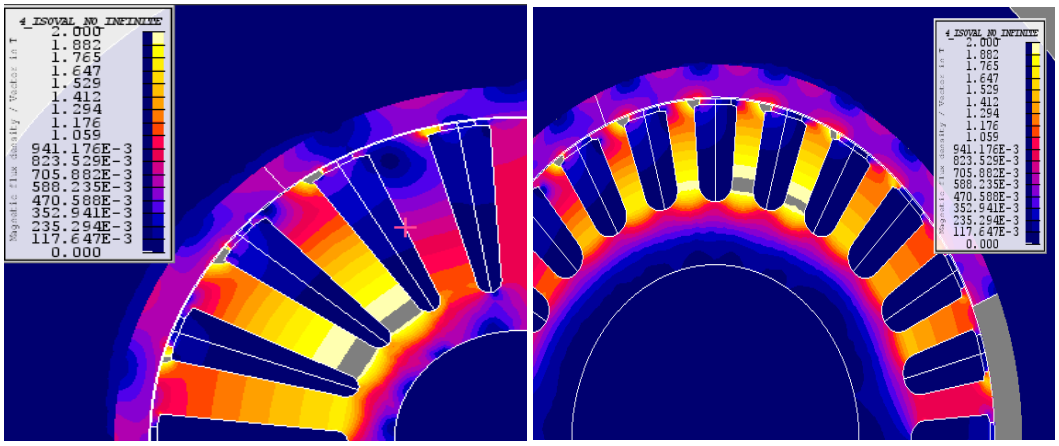

(a) 18 slots 14 poles *(b) 24 slots 26 poles*

Figure 3.5: Cross-section view of motor with different slots poles combinations.

The second set of calculations were performed by changing the turn numbers such that the motor terminal voltage at corner speed was the same for all the slot pole combinations. Fraction turn numbers were also used in the calculation to have a good comparison. The slots shapes were changed accordingly to the have maximum allowed current density of 13 A.mm^{-2}, as shown in figure 3.5. The calculated torque, flux linkage and p.u. inductance are given in Table 3.2. The torque increases with increase in the number of poles. However, the increase is not the same as it was in the case with constant turn numbers because of the higher saturation of the stator core, see figure 3.5. Furthermore, the p.u. inductance decreases with increase in either poles or slots number. The reduction in p.u. inductance with pole numbers is because the base inductance is increases more (because of higher increase in flux linkage) than the phase inductance. Therefore, with Halbach rotor it is advantageous to use higher number of poles both for torque and good flux weakening capability.

Table 3.2: Impact of Slots Poles combination on Torque and Inductance.The maximum current, current density, airgap thickness, magnet volume and grade, rotor dimensions and line voltage were kept same.

Slots	Poles	Turns	Torque [p.u.]	Magnetic flux linkage [Wb]	L_d [p.u.]
18	14	62	0.81	5.68E-02	1.71
18	16	54	0.88	4.90E-02	1.51
18	20	45.5	0.92	3.79E-02	1.37
18	22	45	0.93	3.40E-02	1.31
24	20	59.5	1.00	4.64E-02	1.18
24	22	54.5	1.01	4.13E-02	1.18
24	26	50	1.05	3.45E-02	1.11
24	28	49	1.07	3.17E-02	1.05

3.1.3. Eddy Current Loss in Magnets

As mentioned in section 3.1.2 one of the main drawbacks with FSTCW winding is the generation of many sub and higher order harmonics. For example, figure 3.6 shows the normalized MMF and the harmonics spectrum for 24 slots 26 poles configuration. It can be seen from that there are several sub-harmonics in addition to higher harmonics due to the winding arrangement and the harmonics spectrum varies a lot with different slots poles combination. These harmonics cause additional eddy loss in the rotor especially the magnet. In [65] a study on variation in rotor losses for an SMPM motor with different slots poles is presented. It can be seen that with higher number of poles with same slot number the rotor loss increases except some minima. Also, with increasing slot number while keeping number of poles constant, the eddy loss decreases. Furthermore, to reduce magnet eddy loss

different methods are used like magnet segmentation or skewing. Large number of magnet segments per pole implies higher volume of glue used for assembling. The use of glue makes extraction and recycling of the magnet difficult. Another way used to reduce magnet loss is the use of the bonded magnets instead of sintered magnets. However, the remanence of the bonded magnets is very low. It was decided in the project to use bonded Halbach magnet rotor due to easy manufacture, recycling and advantages in assembly/disassembly. Despite, bonded magnet the loss becomes critical with a single magnet cylindrical structure (ideal Halbach magnet). The magnitude of induced eddy current depends on the rate of change of flux density and the resistivity of the magnet. The bonded NdFeB magnets have resistivity in the order of 10-30 $\mu\Omega$.m [62]. Hence, 20 $\mu\Omega.m$ was used in calculations as magnet resistivity[1] [62].

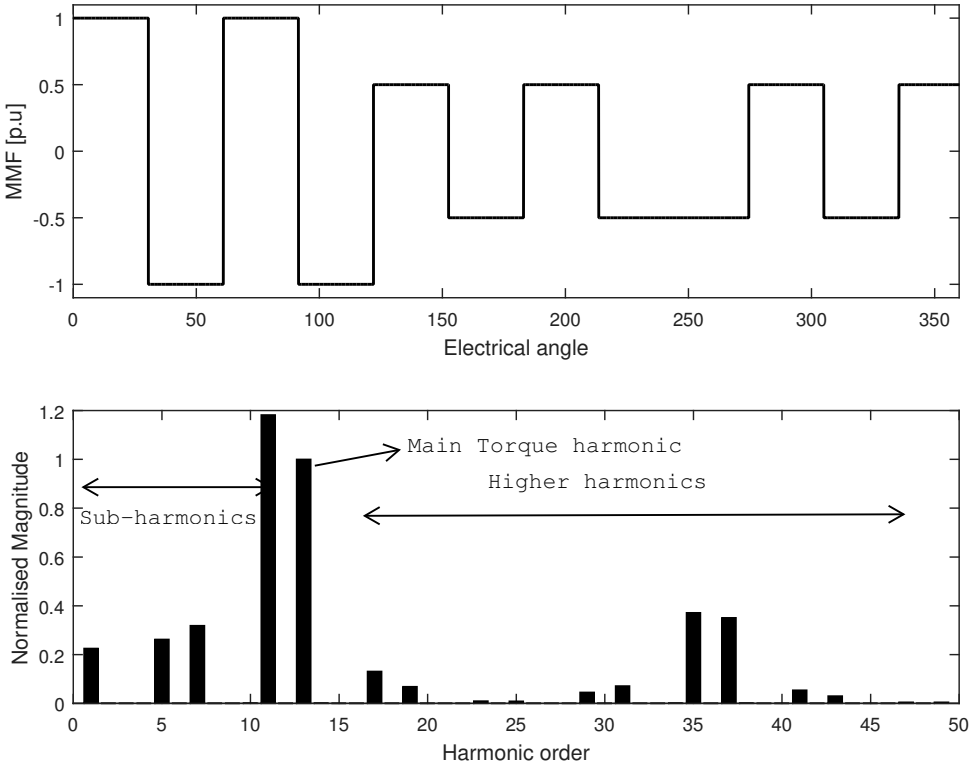

Figure 3.6: MMF of 24 slots 26 poles motor and the harmonic spectrum at t = 0, Ia = 1, Ib = -1/2 and Ic = -1/2

Table 3.3 presents the magnet loss in 24 slots 26 poles motor at various speed with magnetic and non-magnetic rotor back. The calculations were done using 2D FEM model. As expected the magnet loss increases with the square of the speed. There

[1] The calculations were done before magnet resistivity measurements were performed, presented in chapter 2. The lowest resistivity was in the range of 120 - 160 $\mu\Omega$.m

are two sources of eddy current magnet loss in the motor, first due to change of stator current and second due to variation of magnetic flux because of stator slotting. To further understand the loss distribution, simulations were performed once by setting remanence of magnet to 0 T with maximum stator current and again by setting remanence of the magnet to 0.6 T with 0 A stator current. The calculated loss is also given in table 3.3. It can be seen that in this motor design the magnet loss due to only stator current is almost 7 times higher than the loss due to only magnet. Furthermore, the total calculated loss (with both maximum current and Br =0.6) is difference of the loss due to only stator current and only magnet. The reason could be that the fields due to magnet and current will saturate the core and hence, reduce the change in flux.

Table 3.3: Contribution of stator current(max current,B_r=0) and slotting (B_r=0.6,I=0) in magnet eddy loss. Magnet resistivity used was 20 $\mu\Omega.m$

	Magnetic Rotor Back			Non-Magnetic Rotor Back		
Speed	Loss [W]	Loss [W], Br=0	Loss [W], I=0	Loss [W]	Loss [W], Br=0	Loss [W], I=0
1000	192	214	28	82	88	13.4
2284	920	1050	138	426	460	70.6
3000	1526	1746	236	736	792	60
4000	2596	2976	410	1298	1402	214
5000	3888	4436	626	2010	2168	332

The variation in magnet loss with speed is same for the motors designs, with magnetic or non-magnetic rotor back. However, with magnetic rotor back the magnet eddy loss is double as compared to non-magnetic rotor magnet loss over the speed range. Figure 3.7 and 3.8 show the normalized MMF and the harmonic spectrum due to stator current. It can be observed that with magnetic rotor back the MMF is higher than the non-magnetic rotor. Furthermore, from the harmonic analysis the sub harmonics for magnetic rotor back are much higher than the non-magnetic rotor and hence, the magnet loss is also high with magnetic rotor back. In section 3.1.1 it is shown that the magnetic rotor back increases the airgap flux density and hence, the torque of motor with magnetic rotor back is expected to be higher than the non-magnetic rotor back. The calculated torque for the 24 slots 26 poles motor with non-magnetic rotor back is 4% lower than the motor with magnetic rotor back. However, as discussed above, the magnet eddy loss is almost 50% lower. Therefore, motor with non-magnetic motor can be a very good choice to reduce eddy current loss without significant reduction in torque.

The impact of current on eddy loss was studied by applying different currents in d or q axis. With I_q applied I_d was kept 0 A and vice versa. Table 3.4 shows the variation of magnet loss with I_d and I_q. The calculated loss due to I_d is higher than due to the I_q. Furthermore, at lower current the eddy loss due to magnet is larger

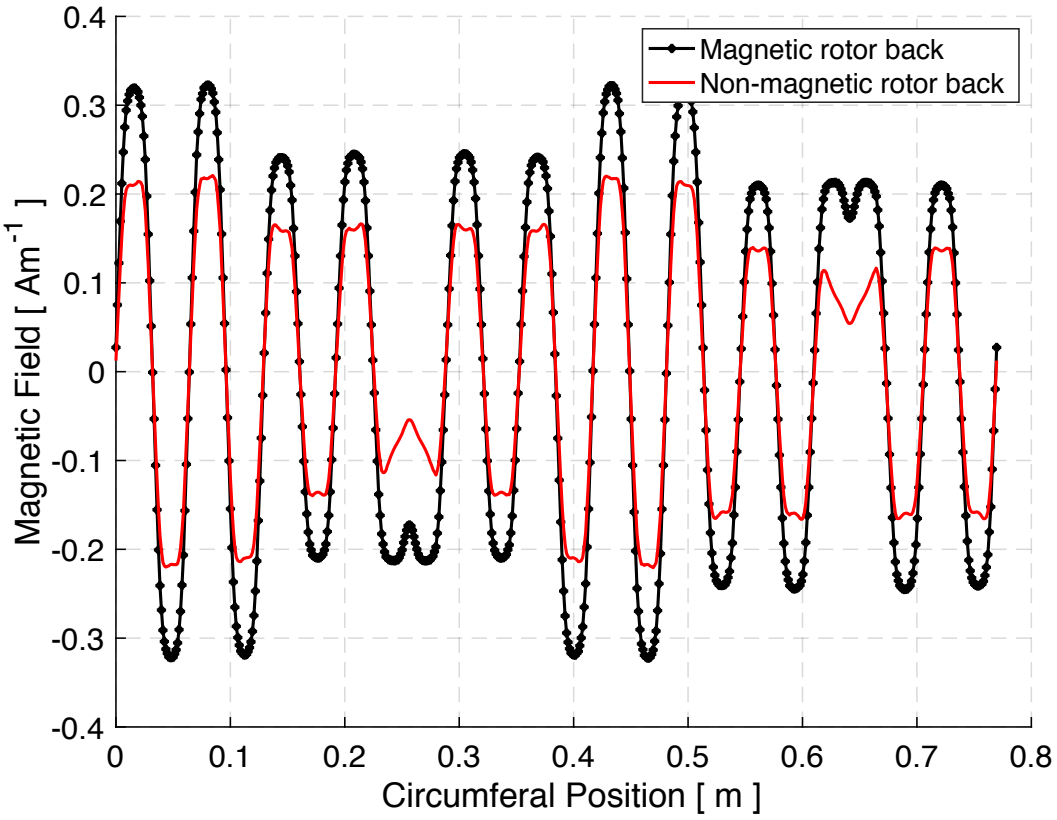

Figure 3.7: MMF of 24 slots 26 poles motor with magnetic and non-magnetic rotor back and at t = 0, Ia = 1, Ib = -1/2 and Ic = -1/2

Table 3.4: Variation of total and only due to current eddy loss at different I_d and I_q. Magnet resistivity used was 20 $\mu\Omega.m$

Iq [A]	Magnet Loss [W]	Magnet loss [W] @ Br=0	Id [A]	Magnet Loss [W]	Magnet loss [W] @ Br=0
0	136	0	0	136	0
50	154	24	50	244	24
150	302	214	150	514	216
250	572	578	250	822	582
350	924	1052	350	1144	1052
450	1320	1526	450	1474	1528

than that of current and both add up approximately. However, at higher current the total loss is the different from the sum of loss due to the current and the magnets. This could be due to the saturation of the core in presence of both stator current field and magnet field.

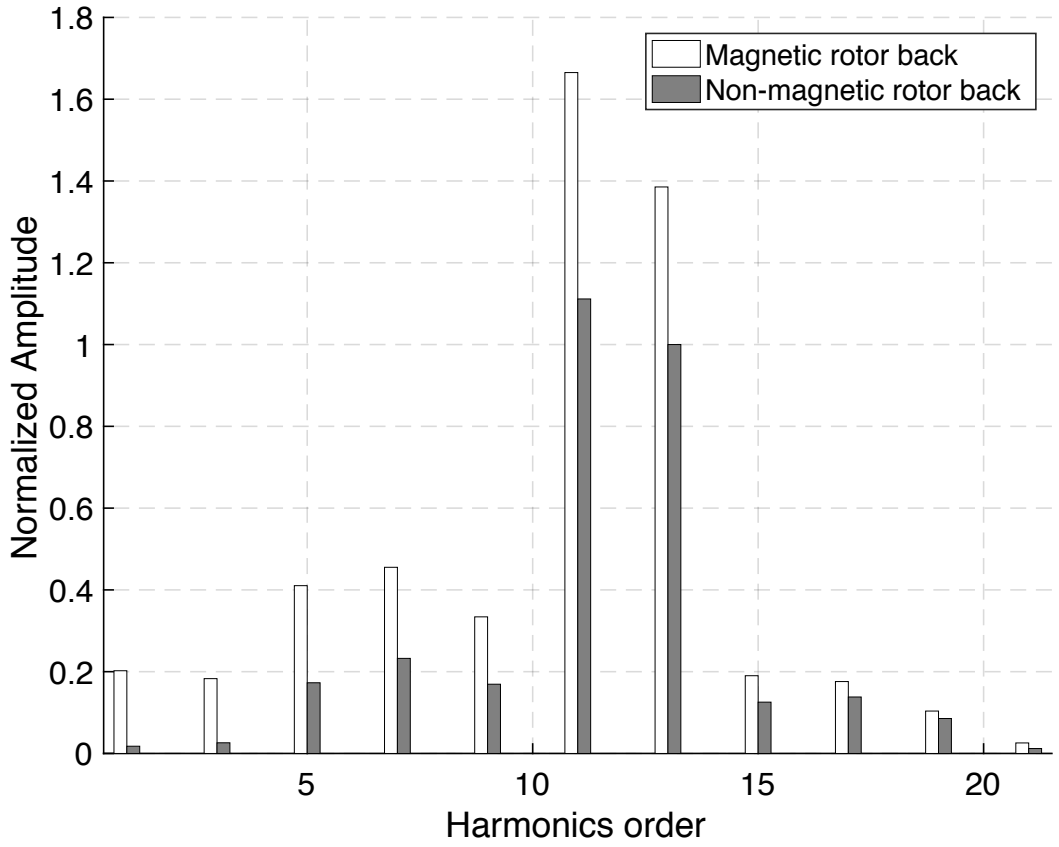

Figure 3.8: Harmonics spectrum of MMF of 24 slots 26 poles motor with magnetic and non-magnetic rotor back and at t = 0, Ia = 1, Ib = -1/2 and Ic = -1/2

An important requirement of motors in vehicle application is to withstand 3 phSC both electromagnetically as well as thermally (steady state). From the calculation it can be seen that I_d causes more eddy magnet loss which makes SC operation even worse for magnet. A study was performed to understand the impact of slots poles combination on magnet loss at 3 phSC steady state condition. The magnet loss is presented in % of the rated power for that particular slot pole combination. The magnet loss is increasing with increase in number of poles due to increase in operating frequency. Furthermore, the magnet loss has decreased with increase in slots number. The induced voltage depends on the rate of change of flux which is proportional to the product of flux density and area of cross section, see equation 3.6. The power loss due to eddy current varies with the square of voltage i.e. with square of the area. By increasing number of slots, the area of magnet per slot decreases and hence, the eddy loss also decreases with almost square ratio.

$$V_{eddy} = \frac{d\phi}{dt} \propto \frac{B.S}{dt} \tag{3.6}$$

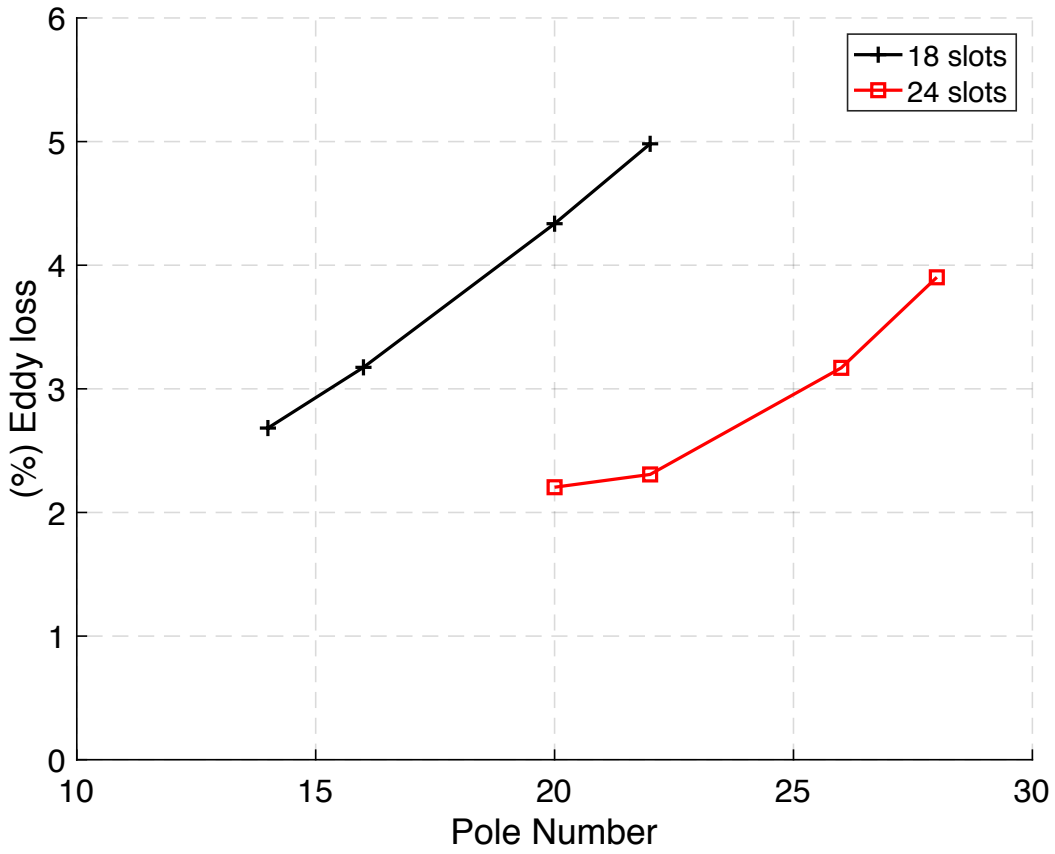

Figure 3.9: The impact of slot pole combination on magnet loss at 3phSC steady state operation.Magnet resistivity used was 20 $\mu\Omega.m$

$$P_{eddy} = \frac{V_{eddy}^2}{R_{mag}} \propto \left(\frac{B.S}{dt}\right)^2 \tag{3.7}$$

Impact of slot opening on magnet loss

Stator slot opening causes eddy currents in the magnet and it can be seen from the figure 3.10 that the maximum current density is at the edges of the slot openings. Table 3.5 presents the variation of the magnet loss and torque with slot opening width. It can be seen that increase in slot opening width causes higher magnet loss due to larger change in flux density in the magnet. However, the torque of the motor is increasing and then decreasing with increase in slot opening width. Small slot opening increases the flux leakage whereas, too wide slot opening reduces the fundamental airgap flux density.

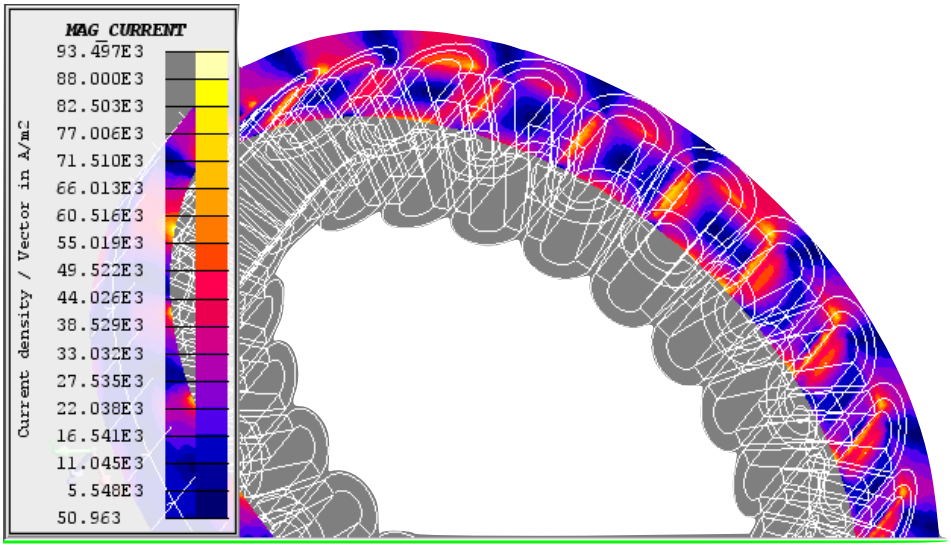

Figure 3.10: Current density in magnet at maximum load

Table 3.5: Impact of slot opening on Magnet loss and Torque. Magnet resistivity used was 20 $\mu\Omega.m$

Slot Opening [mm]	Magnet loss [W]	Torque [p.u.]
7	400	1.090
9	404	1.117
11	448	1.121
13	480	1.112
15	513	1.097

Comparison of 2D and 3D Magnet Loss

The magnet eddy loss calculated using 2D FEM model assumes eddy current flowing only in axial direction. The assumption is valid with small D_o/L ratio however, with high D_o/L (Diameter to length) the 2D FEM over calculates the magnet eddy loss. Therefore, magnet eddy loss was calculated with both 2D and 3D FEM model for corner speed at full load and 3 phSC steady state. Table 3.6 presents the calculated loss with different D_o/L ratios. It can be seen that 3D magnet loss is much lower than the 2D due to inclusion of current path perpendicular to the axial direction. Another reason for lower magnet loss in 3D calculation is the lower surface area due to the elliptical current path as shown in figure 3.11. Furthermore, from the table it can also been seen that as the ratio D_o/L is decreasing the ratio of 2D loss and 3D loss is also reducing because axial length is dominant as compared to the perpendicular path. Figure 3.11b shows the magnet loss density and the maximum density is close to slot openings.

Table 3.6: Magnet loss calculated using 2D and 3D FEM motor model

	Corner Speed at full load			3 ph SC at maximum speed		
D_o/L	9.4	4.7	2.4	9.4	4.7	2.4
3D Loss [W]	20	70.4	200	40	304	880
2D Loss [W]	86	174	346	528	1058	2116

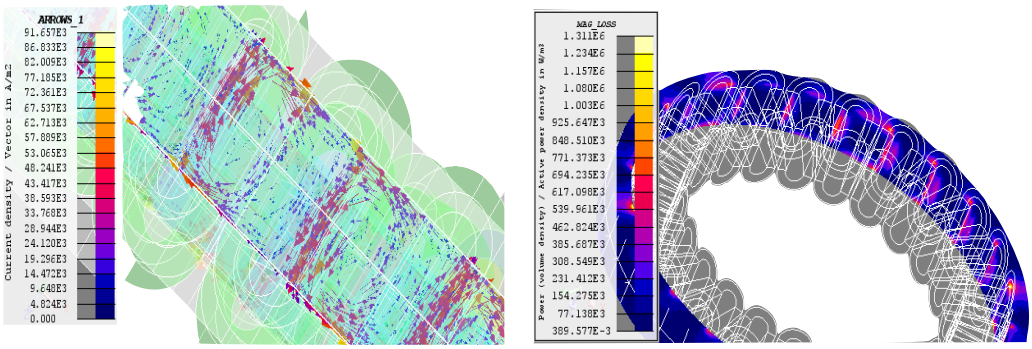

(a) Eddy Current density *(b) Magnet Eddy loss density*

Figure 3.11: Magnet eddy current and loss distribution

3.2. Motor Designs and Performance

Different motor simulations were performed to find optimal dimensions. At first, the motors were designed to meet the electromagnetic requirements by not considering any space constraints mentioned in the specification. The slots poles combination, maximum current, current density and line voltage were kept the same for all the designs. From the results discussed in section 3.1, 24 slots 26 poles is the best slots poles combination considering both motor losses and maximum required torque. Figure 3.12 shows the cross-section of different motor designs and figure 3.13 shows the calculated torque for all the designs over the speed range. The brief discussion of each designs are as following.

- **Design 1** : The motor design has large D_o/L ratio which makes it relatively easy to assemble. Furthermore, larger diameter implies larger airgap diameter and hence, the torque density is high. However, the design required thicker magnet to achieve the required torque with current and voltage limits. The thicker magnets makes difficult to realize the Halbach magnetization.

- **Design 2** : The motor design has lower D_o/L ratio along with thinner magnet compared to Design 1. The thinner magnets makes Halbach production easier. However, due to long axial length the motor assembly would be difficult.

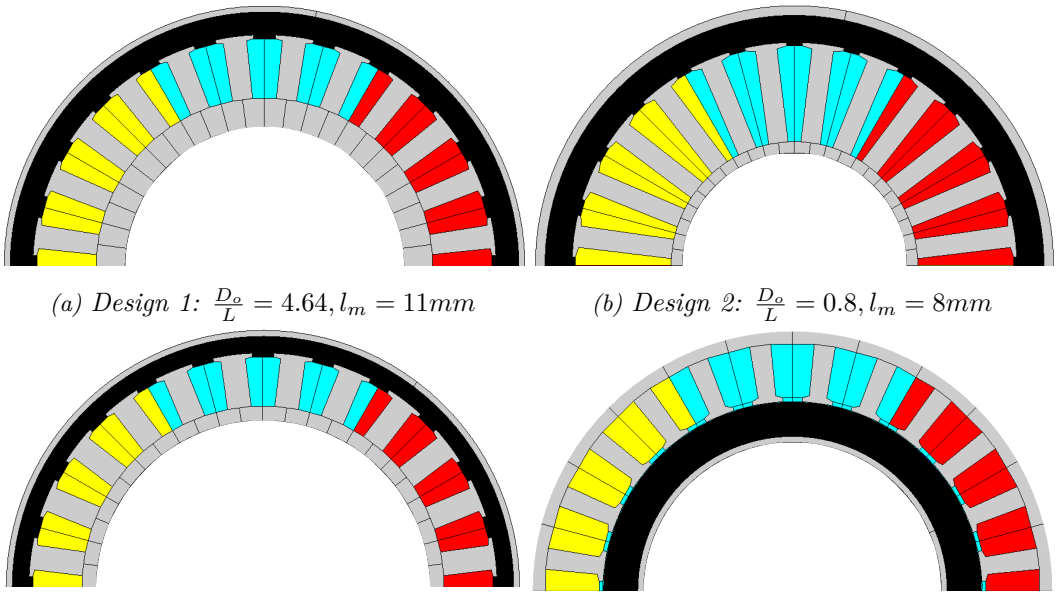

(a) Design 1: $\frac{D_o}{L} = 4.64, l_m = 11mm$ *(b) Design 2:* $\frac{D_o}{L} = 0.8, l_m = 8mm$

(c) Design 3: $\frac{D_o}{L} = 3.82, l_m = 8mm$ *(d) Design 4:* $\frac{D_o}{L} = 3.82, l_m = 17mm$

Figure 3.12: Cross-section of different motor design with 24 slots 26 poles delivering same motor torque, D_o is outer diameter, L is active length and l_m is magnet thickness

- **Design 3** : The motor design has same outer diameter as Design 1 however, the magnet thickness was reduced. As stated earlier also this will make magnet orientation and magnetization easy. To achieve same torque level the axial length of the motor was increased slightly.
- **Design 4** : Although, the project is defined for an outer rotor motor the inner rotor motor is also an interesting study. The biggest advantage with inner rotor is its conventional assembly process which is also good for recycling of motor. To attain the same level of torque thicker magnets were used. Like any inner rotor motor, the rotor cooling will be a challenge with FSTCW. It is important to note that cooling channels space was not considered while calculating motor torque which will take some space and hence, the active outer diameter will be lower.

Table 3.7 presents the weight of different parts of motor for different designs. The total motor as well as the magnet weights are lowest for Design 3 whose peak torque density is slightly lower than Design 1 because of its longer active length while its outer diameter is same. Design 2 is the heaviest motor and has least torque density also. The additional weight is due to the increase in the length because of reduction in the diameter and the magnet thickness is also large. The reduction in weight due to smaller diameter is lower than the weight increase due to the longer axial length. Another, drawback of the Design 2 compared to Design 1 and 3 is the lower cooling surface as it can be seen from the figure.

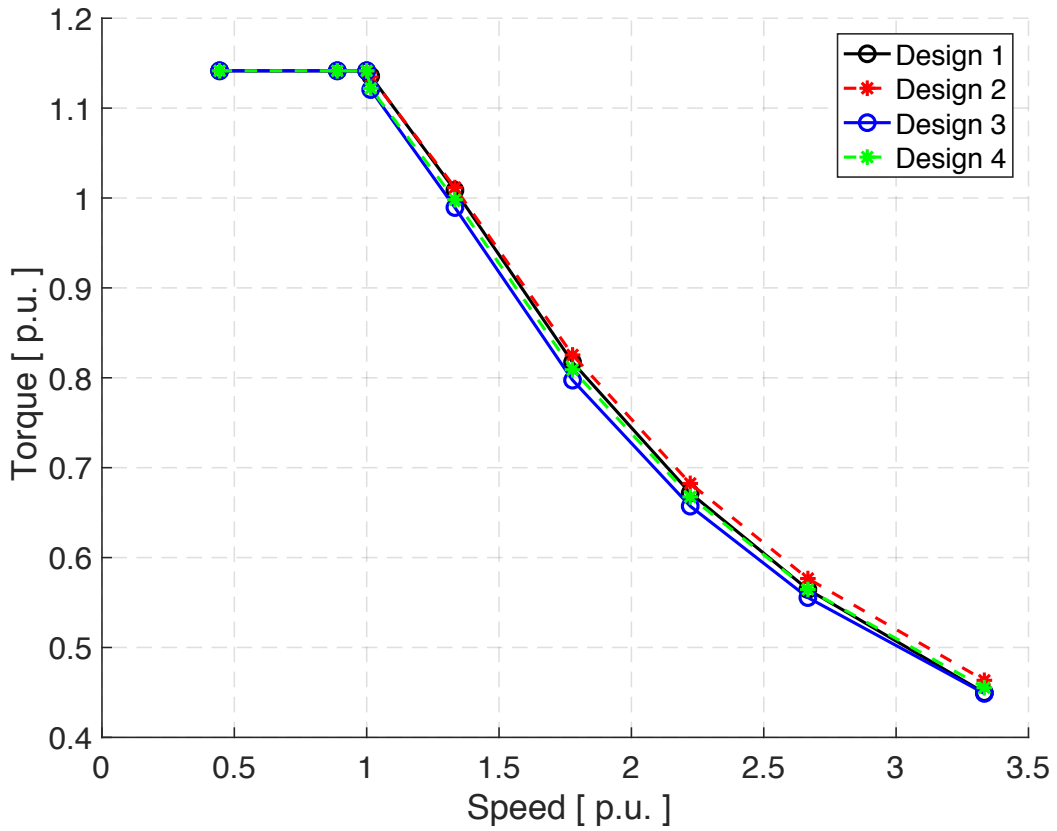

Figure 3.13: Torque Speed curve for different designs

Table 3.7: Motor parts weight for different designs

	Copper Weight [Kg]	Magnet Weight [kg]	Rotor Back [kg]	Stator Core [kg]	Total Weigh [kg]	Do/L [-]	Peak Torque Density [Nm/l]
Design 1	2.71	2.61	1.1	7.34	13.8	4.64	76
Design 2	4.6	3.89	2.29	8.88	19.7	0.80	59
Design 3	3.02	2.35	1.35	6.49	13.2	3.82	62
Design 4	3.85	3.46	0.79	6.81	14.9	3.82	63

Proposed Design

The final design proposed for the project is Design 1. Although, Design 3 has a lower weight with a high torque density the axial length is large which does not fit within the space specified for the motor. Figure 3.14 shows the arrangement of different parts of the motor for the stator and the rotor in Design 1. The motor assembly is same as assembly 2 discussed in section 1.3. The different features which make design easy for assembly/disassembly is discussed in chapter 4.

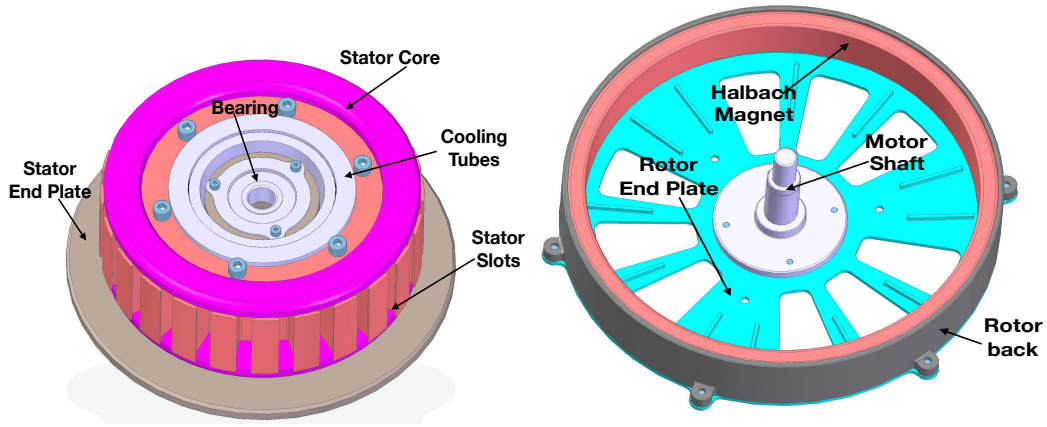

(a) Stator assembly *(b) Rotor assembly*

Figure 3.14: Stator and Rotor assembly for Design 1

Electromagnetic performance

The normalized voltage and back EMF waveform along with their harmonic spectrum at corner speed [2] is shown in figure 3.15. It can be seen that the back EMF waveform is very sinus in nature due to ideal Halbach magnet which causes sinusoidal airgap flux distribution. The current source FEM model was used for simulation to save time therefore, turn numbers were selected such that the motor reaches voltage limit at corner speed. The voltage waveform of the motor is also close to sinus and the harmonic spectrum does not have any significant sub/higher order harmonics. Figure 3.16 shows the peak torque at corner speed and the cogging torque of the motor. The calculated cogging torque of the motor is below 1 Nm. The cogging torque of motor with FSTCW depends on the slots poles combination. Smaller the difference between slots and poles number lower will be cogging torque [34]. The torque over a mechanical cycle shows torque ripple however, the ripple value is very small compared to the average torque. The smaller torque ripple was expected because of the slots poles combination and due to Halbach magnet.

Figure 3.17 shows the calculated torque of Design 1 over the whole speed range. The calculated torque fulfills the required torque both in constant torque and constant power region. The figure also presents the calculated torque for the SMPM motor with same slots poles combination. To have fair comparison the outer diameter, active length, current density, maximum current, line voltage, magnet grade and magnet volume were kept same for both the motors. The Halbach motor has approximately 22% higher torque than then SMPM motor. The higher torque is due to the higher airgap flux density as there is no flux leakage between the poles in Halbach compared to SMPM as shown in figure 3.18. Furthermore, it can be seen that, the motor with magnetic rotor back produces 5% higher torque compared to non-magnetic

[2] Corner speed is the speed where supply voltage reaches its limit

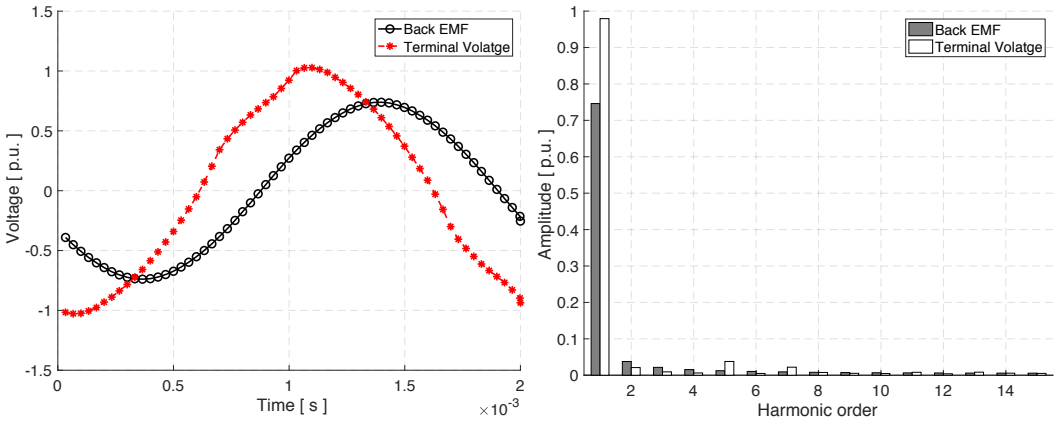

(a) Voltage waveform *(b) Harmonics Spectrum*

Figure 3.15: Voltage waveform and harmonics spectrum at 2250 rpm

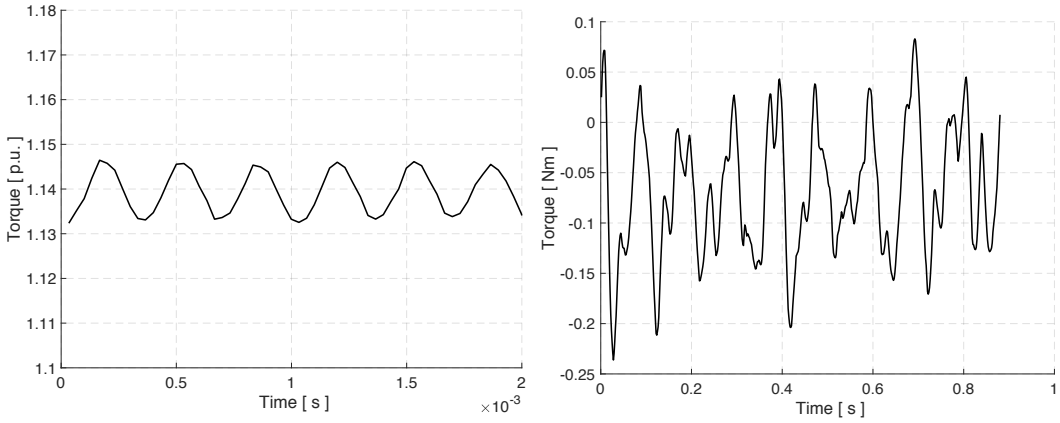

(a) Maximum Torque *(b) Cogging Torque*

Figure 3.16: Maximum torque and cogging torque for 24 slots 26 poles motor design

rotor core. The magnetic rotor core increases the airgap flux density, see section 3.1.1.

Thermal Performance

The temperature in different parts of the motor was calculated using lumped thermal model shown in figure 3.19. It was assumed that there is no heat transfer from stator to rotor through airgap (the cooling channel is inside the stator, see figure 3.14) and the temperature of the rotor back will be same as ambient because of the small thickness. The magnet loss (P_{mag}) for the motor was calculated using 3D FEM model whereas, stator copper loss(P_{cu}) and iron loss (P_{cu}) was calculated using 2D

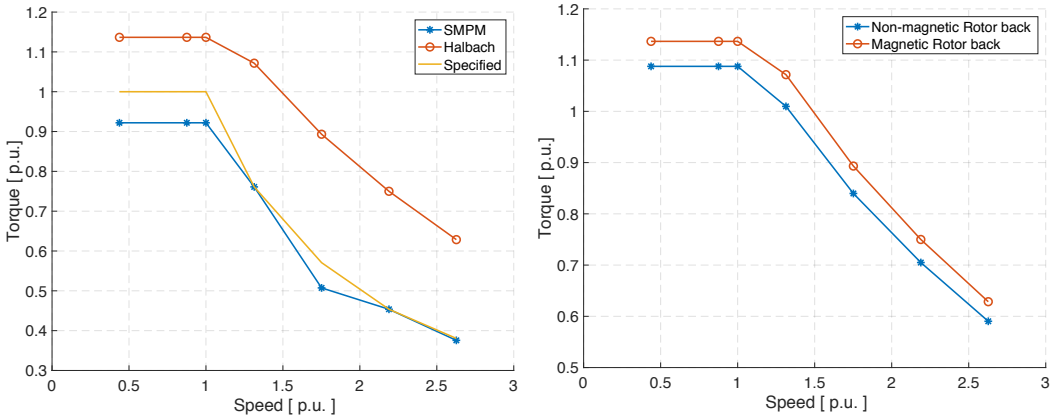

(a) Torque Vs Speed of Halbach and SMPM motor

(b) Torque Vs speed for magnetic and non-magnetic rotor core

Figure 3.17: Calculated torque over the speed range for Design 1 with magnetic and non-magnetic rotor back and SMPM

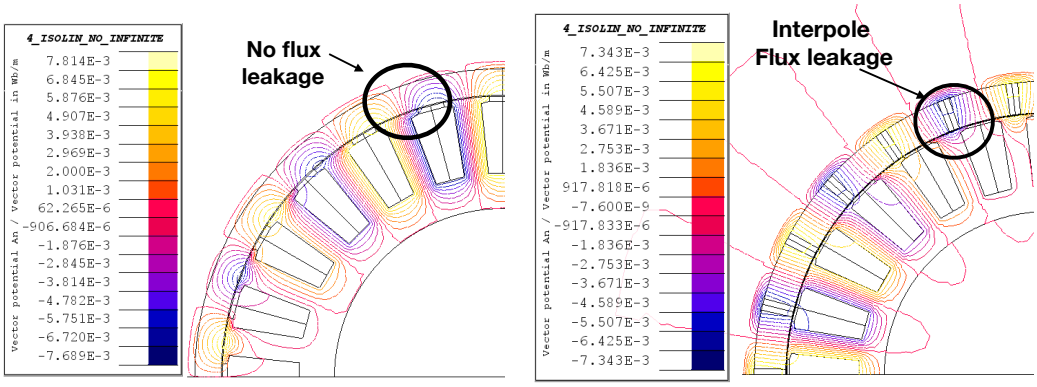

(a) Halbach Motor

(b) SMPM

Figure 3.18: Flux lines for Halbach and SMPM motor at no load

FEM. The temperature for cooling water (T_w) and ambient temperature (T_{amb}) used was 63°C. The values of R_{cu-i} and R_{i-w} were determined by experiments performed at Valeo. The thermal resistance of the magnet R_{mag} was 0.255 K.W^{-1}. Table 3.8 shows the calculated steady state temperature in different parts of the motor during continuous operation. The maximum temperature in the winding goes to 138 $°C$ which is much lower than the limit. For the magnet the worst scenario will be the SC operation and therefore, the magnet eddy loss was calculated only for 3 phSC steady state. Additionally, the magnet should be able to withstand 3 phSC steady state thermally. It can be seen that in 3 phSC at maximum speed, the copper and magnet temperature are 197 °C and 142 °C respectively. As per specification the copper insulation is class H and can easily withstand a temperature rise of 200 °C.

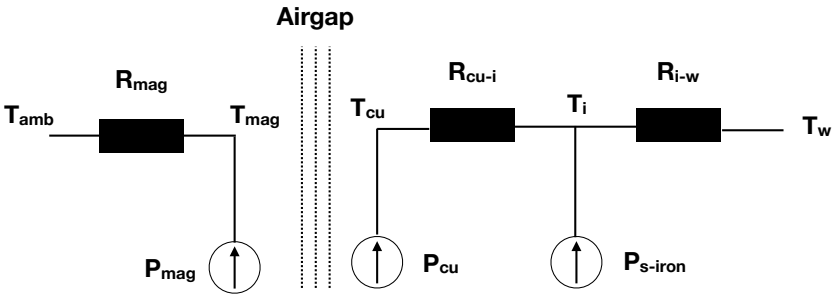

Figure 3.19: Lumped thermal model of the motor

Table 3.8: Temperatures in different parts of motor in continuous operation

Speed [p.u.]	Torque [p.u.]	Copper loss [p.u.]	Iron loss [p.u.]	Magnet Loss [p.u.]	T_i [$^\circ C$]	T_{cu} [$^\circ C$]	T_{mag} [$^\circ C$]
0.44	0.53	5.04E-03	1.95E-03	-	79	92	-
0.89	0.42	3.19E-03	5.82E-03	-	83	92	-
1.33	0.37	2.52E-03	1.04E-02	-	92	99	-
1.78	0.32	3.95E-03	1.16E-02	-	98	108	-
2.22	0.26	5.64E-03	1.31E-02	-	105	120	-
2.67	0.19	6.81E-03	1.49E-02	-	112	130	-
3.11	0.06	7.43E-03	1.71E-02	-	119	138	-
3 phSC maximum speed	-	2.07E-02	1.44E-02	6.08E-03	**143**	**197**	**142**
3 phSC Corner speed	-	2.07E-02	1.32E-03	1.60E-03	113	167	85

On the other hand, the magnet with PPS binder can withstand the high temperature mechanically, see section 2.3 however, the temperature can cause irreversible magnet demagnetization. Although, occurrence of 3 phSC at maximum speed is very unlikely, it should be considered during motor operation.

Magnet Demagnetization

Magnet has highest risk of demagnetization during SC in the motor especially, 2 phSC. So the demagnetization of the motor was studied for both 2 and 3 phSC using 2D FEM model. To study the transient SC, the motor was first run at a speed with full load and then SC was created using switches in the circuit. Figure 3.20 shows the electrical circuit and the motor mesh used to study the SC transient and the demagnetization in the motor. The time of closing of switch was selected such that the SC causes maximum transient stator current. Figure 3.21 and 3.22 show the transient stator current in the event of 2 phSC and 3 phSC at corner

speed and maximum speed. The calculated 2 phSC peak current is 2.2 p.u. and the 3 phSC current is 2.18 p.u. At corner speed the current is higher than at the maximum speed. The fact that at maximum speed the motor is running in flux weakening i.e. at lower load and hence, the SC does not cause high current. Therefore, for magnet demagnetization 2 phSC at corner speed was considered as the worst condition.

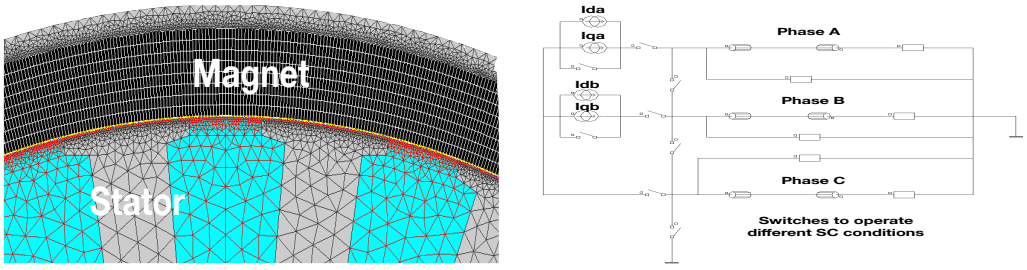

(a) Magnet Mesh *(b) Electric Circuit*

Figure 3.20: Magnet mesh and electrical circuit used to study demagnetization

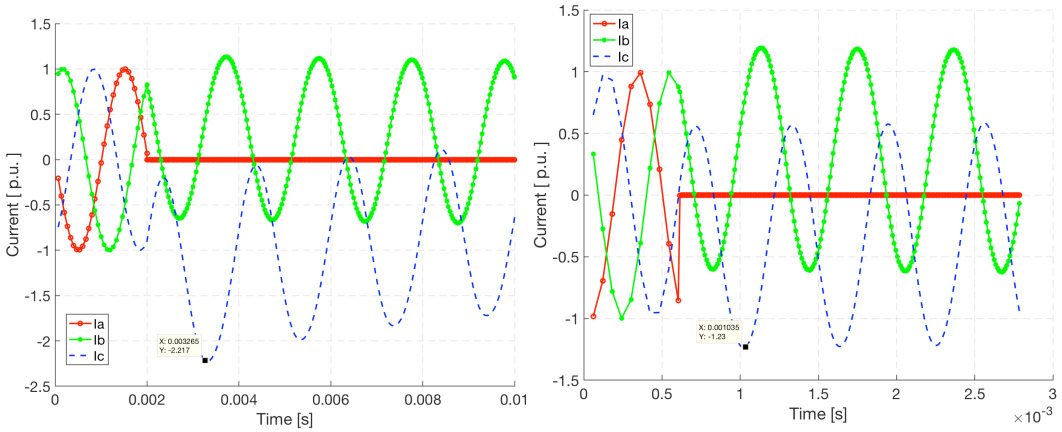

(a) 2 phSC current at corner speed *(b) 2 phSC current at maximum speed*

Figure 3.21: Transient current in 2 phase short circuit at different speed

The material used for bonded Halbach cylinder is MF18P from Aichi Steel. The demagnetization curve for the material is shown in figure 3.23a. Unlike, sintered magnets the bonded magnets knee is not very clear and it is close to origin i.e. low intrinsic coercivity that makes bonded magnets very prone to demagnetization especially at high temperatures. As knee is very close to origin partial demagnetization can happen easily and reduce the motor performance over time. It is also important to note that the recoil line of the magnet is very close, see 3.23b and therefore, the loss of remanence in negligible even after partial demagnetization.

Figure 3.24 and 3.25 show the distribution of the flux density and the magnetic field

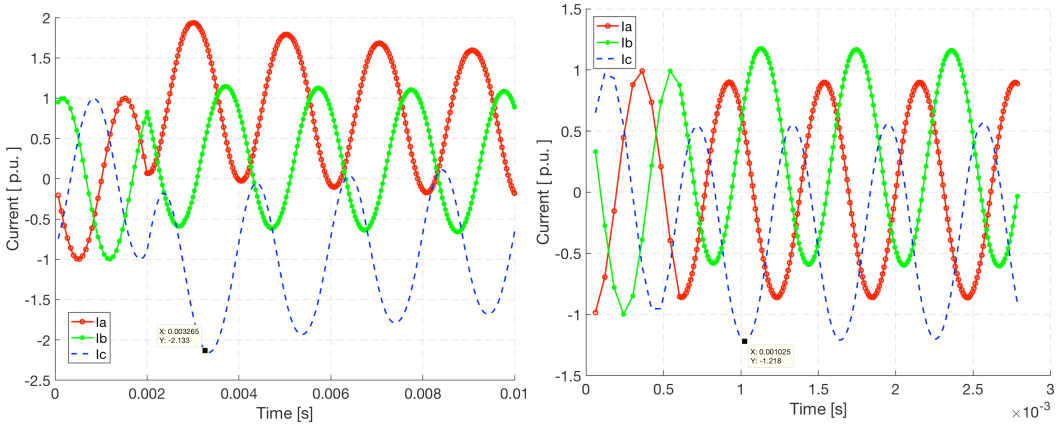

(a) 3 phSC current at corner speed *(b) 3 phSC current at maximum speed*

Figure 3.22: Transient current in 3 phase of short circuit at different speed

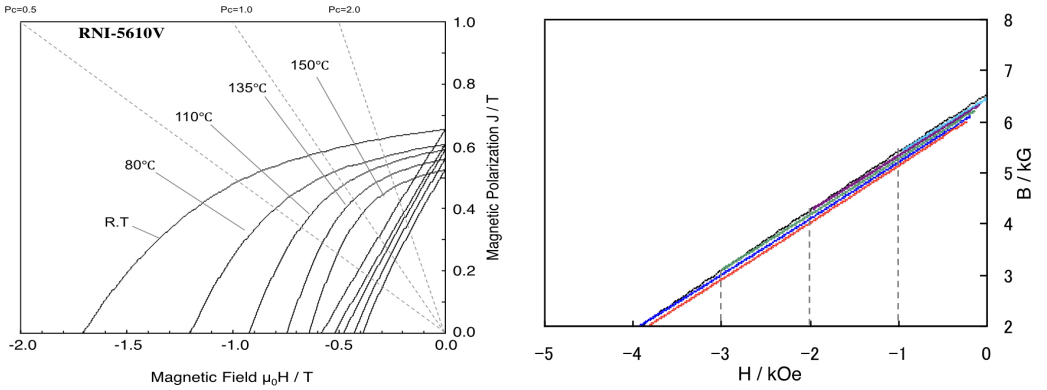

(a) BH & JH curves *(b) Recoil curves*

Figure 3.23: Hysteresis curve and recoil behaviour of Bonded magnet (MF18P, 2017)

in the magnet when transient SC current is at peak. Figure 3.25 shows the absolute of field, for easy presentation. It is expected to have a similar temperature during transient phase of SC as in continuous operation at that load point, which is in worst case expected to be in the range of approximately $85 - 100°C$. Figure 3.24 shows all the points in the magnets are above the knee of the BH curves. The low flux density distribution is similar for both 2 and 3 phSC as the transient peak current is also very close to 2.2 p.u. As per calculation, the temperature of the magnet reached its critical level during 3 phSC steady state however, the steady state SC current is less than 1 p.u. Therefore, the demagnetizing field during steady state operation will be much lower than transient state. The intrinsic coercivity of the material is 1.5 T and from the figure 3.25 it can be seen that the field in the magnet is much below 1 T in both 2 and 3 phSC. The method used overestimates the demagnetization because it considers the magnetization in radial direction. However, with different magnetization direction

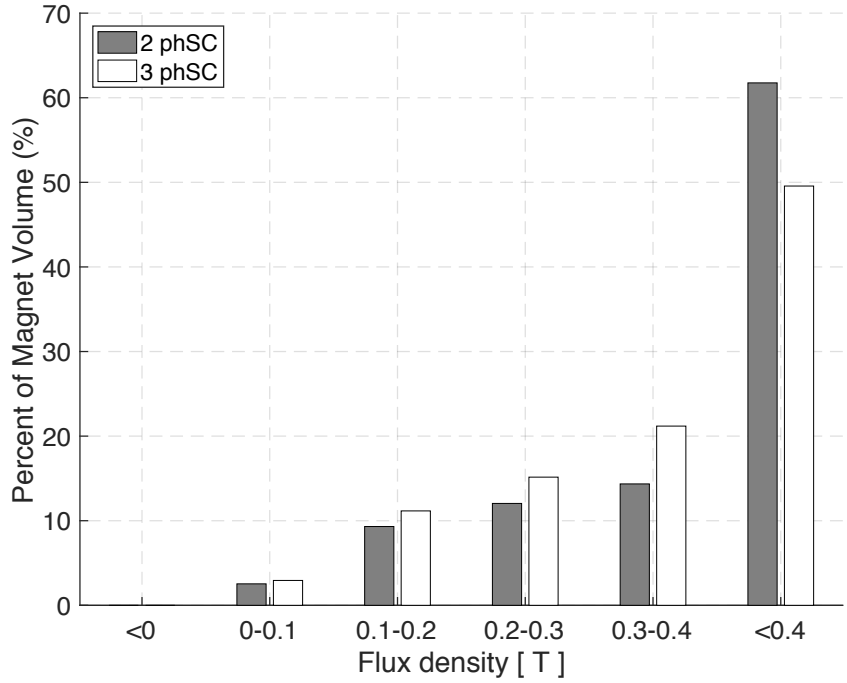

Figure 3.24: Percent distribution of flux density in the magnet at peak transient current in 2 & 3 phSC operating at corner speed

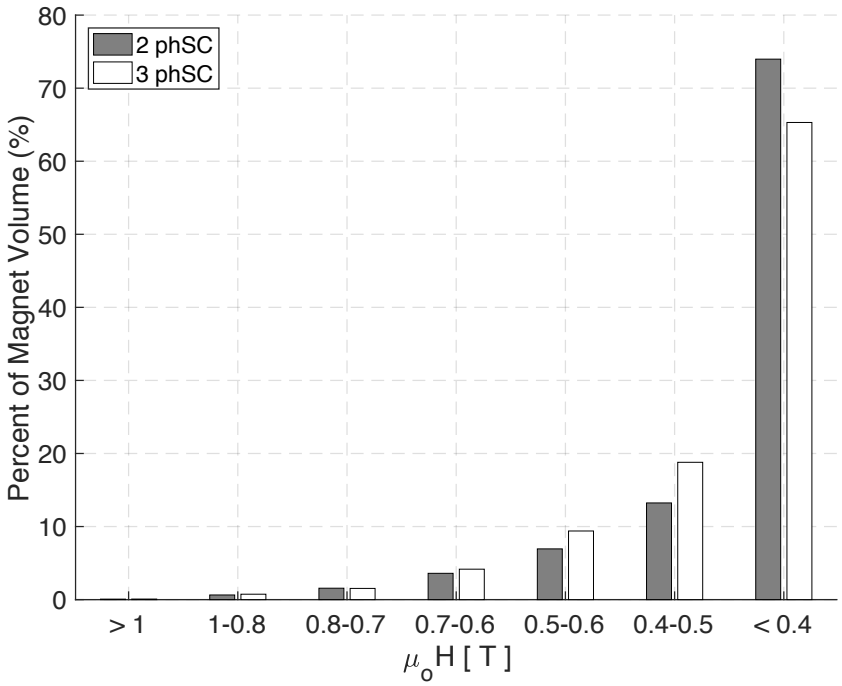

Figure 3.25: Percent distribution of absolute value of magnetic field (H) in the magnet at peak transient current in 2 & 3 phSC operating at corner speed

as with Halbach magnet the demagnetization model must consider angle between the field and the magnet orientation at that point [66]. Furthermore, increasing magnet segment per pole decreases the magnet demagnetization [43] and an ideal magnet can be approximated with very high number of segment. The analysis done represents the worst scenario for the magnet and in reality it is expected to have lower demagnetization during operation.

Motor Efficiency

The efficiency of the motor was calculated using equation 3.11, where P_{out} is calculated by equation 3.10. The electromagnetic torque calculated using FEM does not include iron loss and other mechanical losses. Therefore, to include the impact of stator loss the calculated torque was reduced by a torque equivalent to the iron loss, see equation 3.8 and 3.9. The rotor iron and magnet losses is almost negligible compared to the stator copper and iron loss and hence, not included in the torque calculation. The mechanical losses were also not included in the efficiency calculation.

$$T_{iron} = \frac{P_{s-iron}}{\omega_r} \tag{3.8}$$

$$T_{net} = T_{fem} - T_{iron} \tag{3.9}$$

$$P_{out} = T_{net} \; . \; \omega_r \tag{3.10}$$

$$\eta \; (\%) = \frac{P_{out}}{P_{out} + P_{s-iron} + P_{cu}} \times 100 \tag{3.11}$$

where, T_{iron} is the equivalent torque for stator iron loss, ω_r is the motor speed in radians per second, T_{net} is the final shaft torque, T_{fem} is the airgap torque calculated by FEM, P_{out} is the output power and η is the motor efficiency.

The iron loss of the motor was calculated using 2D FEM model. The FLUX software provides option of iron loss calculation using LS (Loss Surface) or Bertotti loss model. Losses were calculated using both the methods at different load points and the difference (Bertotti - LS loss) in calculated losses is shown in figure 3.26. It can be seen that this difference is mainly dependent on the speed and does not vary much with torque i.e. current. Furthermore, the difference in calculated loss increases with increase in the speed. The increase in difference is due to the extrapolation of iron loss at higher frequency for both the calculation methods. For the calculation of efficiency of the motor Bertotti iron loss is considered because it has higher value (Lowest efficiency).

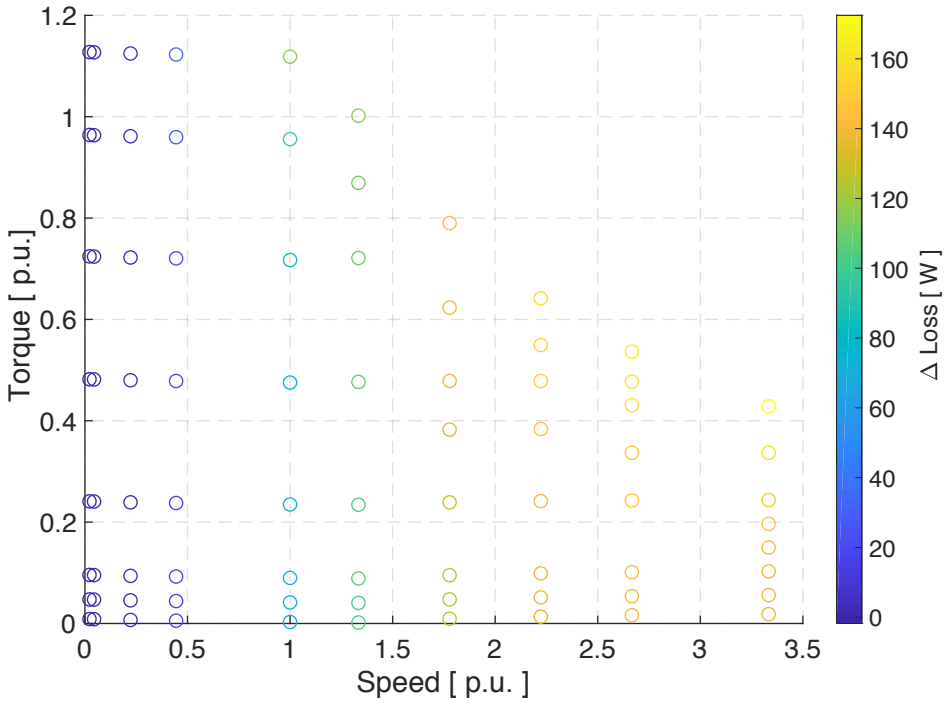

Figure 3.26: Difference in calculated loss using Bertotti and LS model (Bertotti - LS loss) by FEM

Figure 3.27 shows the efficiency of the motor at different regions. It can be seen that the motor has more than 90% efficiency in majority of region. The lower efficiency regions are low torque and high speed load points due to the increase in stator iron loss as shown in figure 3.28b. It can also be seen from the figure that iron loss is not vary much with increase in torque and is mainly dependent on the speed of the motor. On the other hand figure 3.28a shows the copper loss which is mainly varying with torque.

3.3. Motor Performance with Recycled Magnets

In last few years there has been many articles on recycling of sintered NdFeB magnets as summarised in [45]. It can be seen that the magnetic properties of recycled magnet are highly dependent on the method of recycling. The remanence (B_r) of the recycled magnet is varying in the range of 0 % to 20 % and so is the intrinsic coercivity. It is expected that with recycled magnets i.e. lower remanence the motor's torque capability will reduce. However, different strategies can be used to achieve same torque speed characteristic of the motor. In DEMTER project, the motor is designed for easy magnet recycling however, it is also imperative to understand the impact of recycled magnet on the motor's performance and how easy motor design can

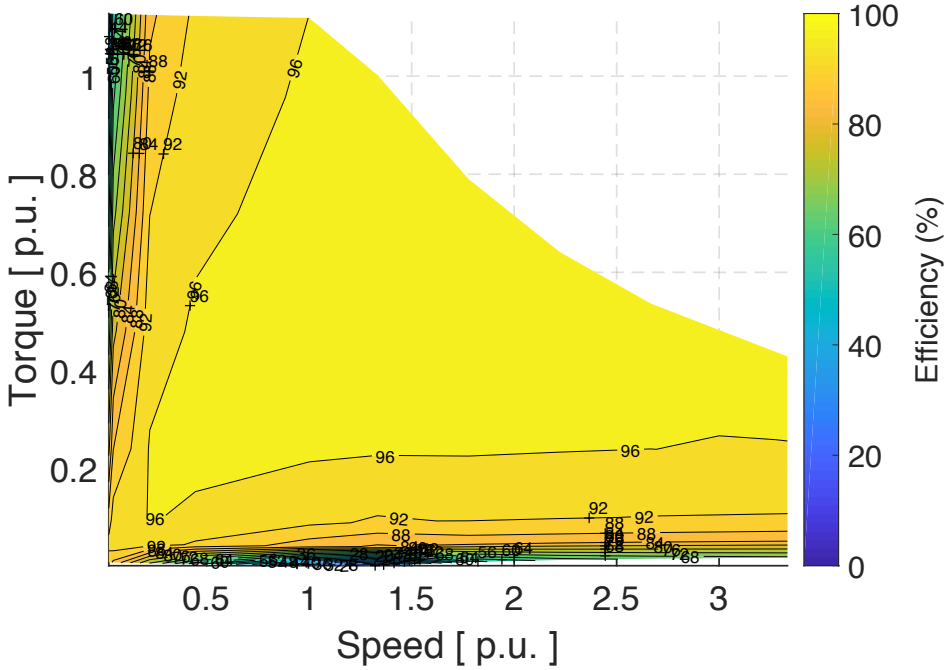

Figure 3.27: Efficiency map of the motor design 1

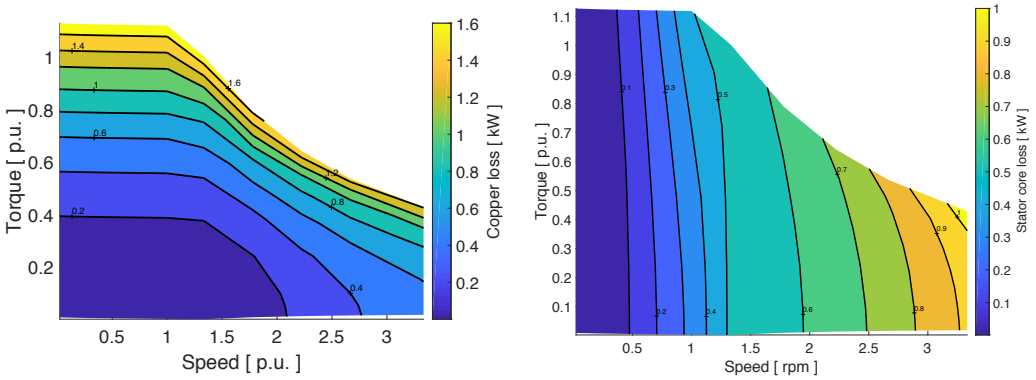

(a) Distribution of Copper loss *(b) Distribution of Iron loss*

Figure 3.28: Distribution of losses in the motor for the whole torque speed range

be adapted to use recycled magnet. In the chapter 2.4.2 the recycling methods of bonded magnet are discussed and shown that using proposed recycling process (70% virgin and 30% old magnet) the magnets can be produced without loss of remanence. However, the properties of the magnets are not known if the recycled magnet is produced using only old bonded magnets. Therefore, to study the adaptability of the motor for recycled magnet it was assumed that the variation in reduction of remanence, similar to sintered magnets, will be in the range 0 % - 20 % for bonded recycled NdFeB magnets. Furthermore, 4 different strategies that can be used to

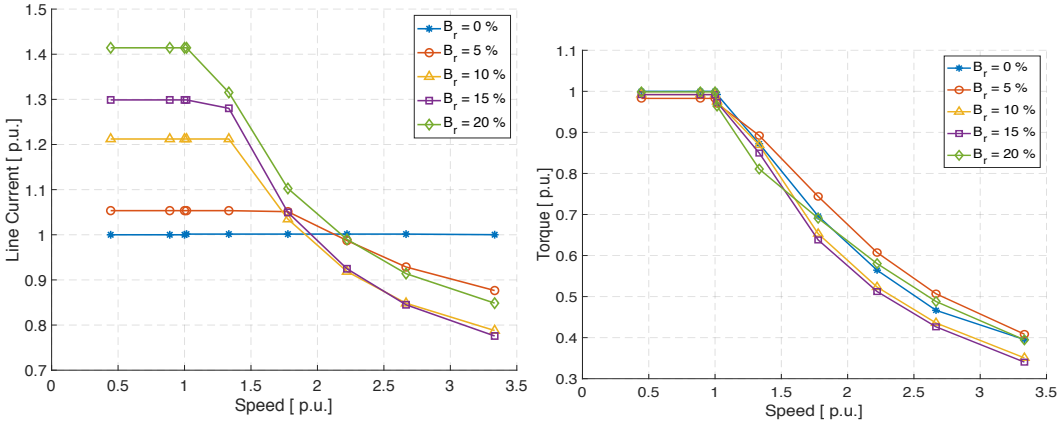

(a) Current Vs Speed *(b) Torque Vs Speed*

Figure 3.29: Torque and current over whole speed range for different % of remanence reduction in recycled magnets. B_r% is the remanence reduction compared to virgin magnet.

achieve similar torque speed characteristic with recycled magnets for the motor were studied. The evaluation of each strategy was performed with 5%, 10%, 15% and 20% lower remanence magnet using 2D FEM model. The thermal impact of different methods on motor used was not included in the investigation. Additionally, fractional number of turns per slot were also used for calculation purpose. The focus of the investigation was to understand the strategy that can be easily adopted in future to use recycled magnet without making big changes in motor design, considering different constraints. Therefore, the motor designs were not optimized for recycled magnets.

3.3.1. Converter Ratings

The first strategy studied was to modify the converter without making any change in the motor design except using recycled magnets. The lower magnetic remanence can be compensated by increasing the line current and voltage i.e. increasing the converter size. The current and voltage were increased such that the motor with recycled magnet has similar peak torque. The dimensions of the motor were kept same. Figure 3.29 shows the torque and current required to achieve similar performance using recycled magnet with different remanence. Almost 5% higher current is required for motor with 5% lower remanence magnet. However, the current required for 20 % lower remanence is around 40 % because of very high saturation. The current required by the motor with the recycled magnet in constant power region is much lower than the rating. With lower remanence the current required to achieve complete flux weakening is much lower i.e. the per unit inductance is high and hence, keeping same voltage limit current required is also less. This also explains the reduction

in maximum torque in constant power region compared to original design despite having similar peak torque.

3.3.2. Axial Length

The second strategy studied was to increase axial length of the motor with recycled magnet. This can be used in situations where changing converter ratings are not possible and some extra space is available. The torque produced in the motor is linearly proportional to the axial length of the motor, keeping other parameters constant. Therefore, by increasing axial length similar torque speed characteristic can be achieved with recycled magnets. The line current, voltage and dimensions of the motor except axial length were kept same for all the calculations. Additionally, the turn numbers per phase were changed such that the line voltage reaches its limit at corner speed. Figure 3.30 shows the current, torque versus speed curve with different remanence i.e. axial length. It can be seen that the torque speed characteristic for all the motors are very similar expect with 20 % lower remanence.

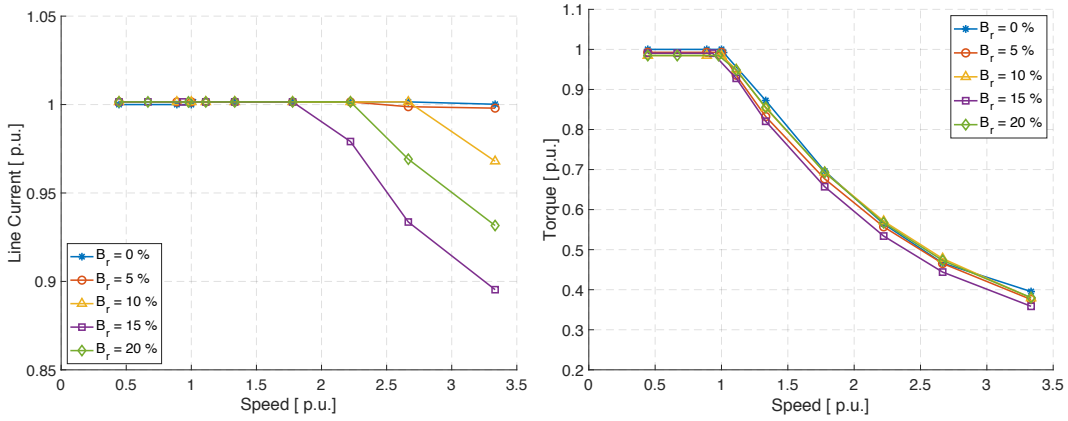

(a) Current Vs Speed *(b) Torque Vs Speed*

Figure 3.30: Torque and current over whole speed range for different % of remanence reduction in recycled magnets by increasing axial length. B_r% is the remanence reduction compared to virgin magnet.

In table 3.9 axial length of the motor required with recycled magnet to achieve same torque speed characteristic is presented. It is interesting to note that the percent increase in length is almost double of the % reduction in the remanence. The reason for this trend is the change in turn number which was decreased with increase in axial length as can be seen from the table. Increasing axial length causes increase in inductance and therefore, the voltage at corner speed will also increase. Hence, turn numbers were reduced such that the line voltage remains under its limit at the corner speed. Therefore, the torque of the motor with recycled magnet is not varying linearly with the axial length. The impact of different turns number can also be seen

Table 3.9: Different motor design parameters with recycled magnets i.e. lower remanence to achieve same peak torque

% Magnet Remanence Reduction	0	5%	10%	15%	20%
Axial Length [p.u.]	1	1.09	1.2	1.25	1.43
Corner speed [p.u.]	1	0.98	0.94	0.92	0.96
Inductance [p.u.]	1.09	1.08	1.12	1.20	1.18
Turns per phase	48	45	44	44	40

in the current versus speed curves. The motor with 15% lower remanence has highest p.u. inductance and hence, the complete flux weakening was achieved at lower speed compared to other designs.

3.3.3. Rotor Outer Diameter

The third method investigated of using recycled magnet in the motor with the same torque speed characteristic was increasing outer diameter. In this strategy also, the space required for motor with recycled magnet will be more without changing converter ratings. The airgap, outer and inner stator diameters of the motor were increased by the same value as outer diameter. Increasing magnet thickness increases complexity of Halbach magnetization. Hence, thickness of the magnet ring was kept same for all calculations with recycled magnets. Figure 3.31 shows the current and torque versus speed characteristic of the motor. It can be seen that almost same torque speed characteristic can be achieved with recycled magnet. The drop in current at high speed is due to the motor inductance. With large p.u. inductance full flux weakening can be achieved at current lower than rated current and the maximum torque developed at that speed depends on the voltage limit.

Table 3.10: Different motor design parameters with recycled magnets i.e. lower remanence to achieve same peak torque

% Magnet Remanence Reduction	0	5%	10%	15%	20%
Magnet Weight [p.u.]	1	1.12	1.16	1.24	1.30
Motor Weight [p.u.]	1	1.04	1.09	1.19	1.27
Inductance [p.u.]	1.09	1.07	1.13	1.14	1.20
Turns per phase	48	47	47	46	46

The turn numbers for different designs were modified such that the voltage limit can be maintained at corner speed. For 5% reduced remanence magnet motor the per unit inductance is almost 1 p.u., see 3.10 and hence, the rated current was used for the

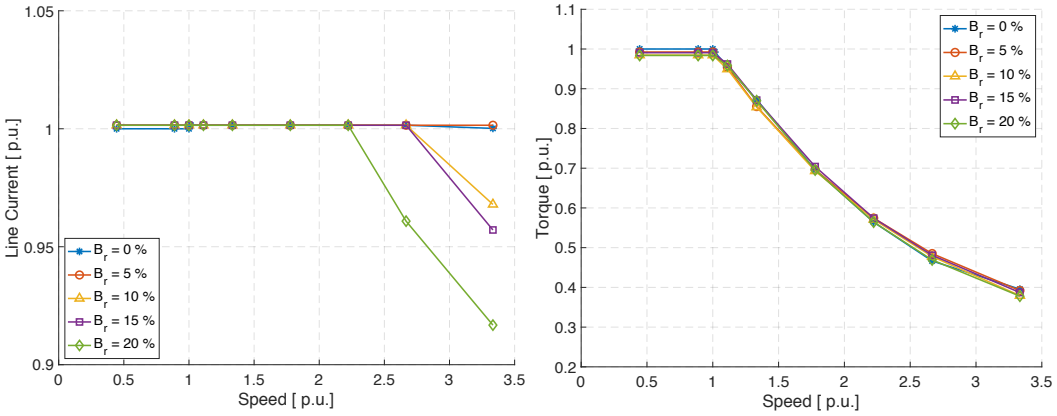

(a) Current Vs Speed *(b) Torque Vs Speed*

Figure 3.31: Torque and current over whole speed range for different % of remanence reduction in recycled magnets by increasing outer diameter. B_r% is the remanence reduction compared to virgin magnet.

whole speed range. On the other hand, for 15% lower remanence motor the per unit inductance is maximum i.e. magnetic flux linkage has reduced much more than the inductance and hence, the complete flux weakening happened at much lower speed. Table 3.10 also shows the impact of increased diameter on the magnet and total motor weight with recycled magnets. The increase in magnet weight is much higher than the increase in total motor weight. It is also important to note here that the increase in magnet weight is non-linear with reduction in magnet remanence. The reason for this trend could be the increase in airgap diameter with increase in outer diameter and hence, the developed torque. However, the % increase in total motor weight is much more in line with the % decrease in magnet remanence.

3.3.4. Rotor Inner Diameter

The last method studied to use recycled magnet was changing inner diameter of the rotor i.e. increasing magnet volume. The method can be used if changing converter or space available for the motor is not possible. Along with magnet diameter turns per phase were also increased such that the voltage and the current limits can be maintained with the peak torque. The current and torque versus speed curves for different designs are shown in figure 3.32. The calculated peak torque for all the designs are similar (within 3% of the reference). However, the maximum torque is varying significantly in constant power region. The torque of the motor with 15% and 20% lower remanence is much lower in constant power region compared to the original motor due to high p.u. inductance, seen table 3.11. Furthermore, the increase in the magnet volume for motor with 5% and 10% lower remanence is almost 60% and for 15% and 20% is almost 100% as shown in table 3.11. Despite, increase

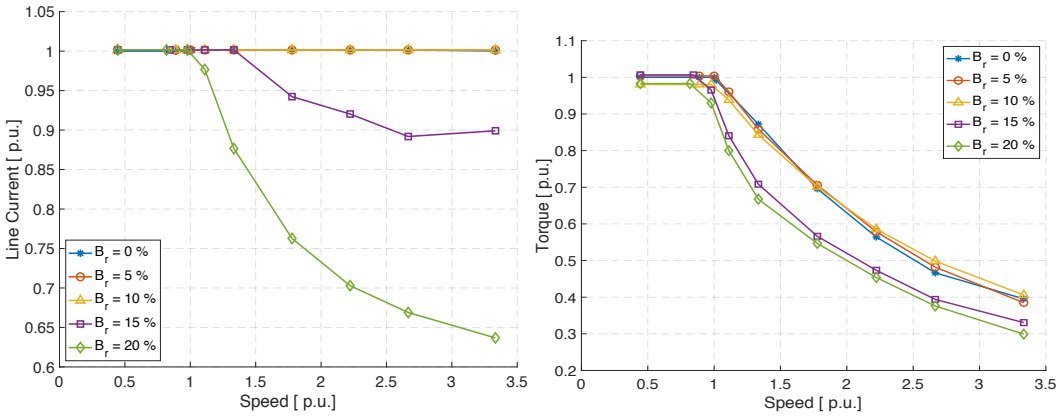

(a) Line Current Vs Speed *(b) Torque Vs speed*

Figure 3.32: Torque and current over whole speed range for different % of remanence reduction in recycled magnets by increasing inner diameter. B_r% is the remanence reduction compared to virgin magnet.

Table 3.11: Different motor design parameters with recycled magnets i.e. lower remanence to achieve same peak torque

% Magnet Remanence Reduction	0	5%	10%	15%	20%
Magnet Weight [p.u.]	1	1.59	1.59	1.99	1.99
Motor Weight [p.u.]	1	1.04	1.04	1.07	1.07
Corner speed [p.u.]	1	0.98	0.96	0.83	0.80
Inductance [p.u.]	1.09	0.87	0.99	1.1	1.17
Turns per phase	48	50	51	68	67

in the airgap flux density with increase in magnet thickness the developed torque has not increased by the same % due to decrease in airgap diameter. Additionally, with smaller airgap diameter i.e. stator outer diameter with the same number of slots the stator tooth becomes thinner and hence, cause higher saturation at the peak current. The high tooth saturation further decreases torque along with an increase in ripple. Furthermore, smaller the remanence of recycled magnet lower the corner speed of the motor to maintain the voltage limit. However, the reduction in corner speed is only significant for reduction higher than 15%. It is also important to note here that the turns per phase was increased with recycled magnet motor and hence, the slot current density will be much higher. This will have a significant impact on the thermal behaviour of the motor. Additionally, manufacturing and magnetisation of Halbach ring becomes highly complex and expensive with thicker magnet. Hence, manufacturing of ideal Halbach ring with 15 & 20% lower remanence magnet with desired performance will be very difficult to achieve.

3.4. Summary

The chapter presents the outer rotor motor design for full hybrid vehicle. The motor has an ideal Halbach magnet rotor manufactured using bonded NdFeB. It is shown that the airgap flux density of Halbach magnet, unlike SMPM, increases with number of poles and hence, the torque. The use of rotor back further increases the airgap flux density. Additionally, to achieve high torque density and compact motor design FSTCW is used for stator winding. The impact of slot pole combinations was also studied considering all the design constraints. The motor performance varied significantly with the combination and hence, selection of slot pole combination is critical for the motor. The eddy loss in magnet was also studied using 2D and 3D FEM models. Despite high electrical resistivity of bonded magnets, the eddy magnet loss is significant with FSTCW winding, especially at high speeds. It was also found that with the increase in slot numbers the magnet eddy loss decreases. Furthermore, with high D_o/L ratio the impact of eddy current path perpendicular to axial direction is very critical and is not considered in 2D calculations. Hence, a big difference was found between 3D and 2D loss calculation.

Based on the parametric investigation results, 24 slots and 26 poles were selected as the best slot pole combination for the motor. Different motor designs were studied by varying the axial length and magnet thickness such that they fulfil the torque speed specification. It was found that the motor with larger axial length has a lower magnetic mass and fulfils the torque speed requirement. However, the final design (Design 1) was selected based due to space available for the motor. The thermal calculation shows that the motor has no risk in continuous operation. However, for 3 phSC steady state at maximum speed the magnet and winding temperature reaches the critical limit. The probability of occurrence of this fault condition is expected to be less and hence, no design change was made. The demagnetization study of the magnet shows that the magnet should be safe against irreversible demagnetization during transient SC fault. The 3phSC steady state operation at maximum speed has high temperature which makes magnet very prone to demagnetization. However, in steady state the demagnetization field will be much smaller compared to the transient and hence, no irreversible demagnetization is expected. Additionally, the recoil curve of the magnet shows negligible loss of remanence for partial demagnetization and ideal Halbach arrangement is also good against demagnetization. The efficiency map of the motor shows a wide region of efficiency higher than 90%, which is a critical parameter for motors in (H)EVs.

The study on the impact of different strategies of using recycled magnets on motor torque speed characteristic was also done. The study assumed that the remanence of the magnets reduce by 20%. The first method is to increase the converter ratings, keeping the same motor design with recycled magnets, such that the motor has the same torque speed characteristic. The calculation showed that almost 5% higher supply current is required to achieve the torque speed characteristic with 5% lower

remanence. However, for further reduction in remanence the increase in current is not linear and is much higher. Therefore, the proposed motor design can be used easily for recycled magnet with upto 5% lower remanence without much loss in the performance. The other three investigated methods require change in motor design, instead of converter. In situations where space is not a constraint, the results showed that the axial length or outer diameter of the motor can be increased to achieve same torque speed characteristic with recycled magnets upto 20% lower remanence. However, considering manufacturing of cylindrical Halbach rotor with increased axial length would be much easier as compared to the increased outer diameter. In case of increasing axial length the diameter and thickness of the magnet ring does not change and hence, there is no need to modify the manufacturing process and tools. The assembly of motor with large axial length can be an issue and may require some modifications in non-active parts of the motor. On the other hand, increasing outer diameter of the rotor implies increases in the diameter (keeping magnet thickness same) of the Halbach cylinder which elevates the complexity of production and the cost. Therefore, motors with 20% lower remanence and increased diameter will be much harder and expensive to produce as compared to increased axial length. Finally, for situations where space as well as converter rating cannot be altered, recycled magnet can be used in the proposed motor by changing inner radius of the Halbach ring. The results show that the method can be used for recycled magnet up to 10% lower remanence without much change in torque speed characteristic. With further reduction in remanence the peak torque can be achieved however, the torque in constant power region is reduced significantly. Furthermore, in this method the thickness of the magnet is increased which will make magnetization of the Halbach ring very difficult and costly. From calculated results it can be concluded that for small change in remanence of recycled magnet, changing converter rating can be a good choice however, for large reduction increasing axial length of motor can be easily done.

Chapter 4

4 WIRE : Wighted Index of Recycling and Energy

As mentioned before, the demand of electrical motors for EVs and HEVs is growing every year and to maintain a sustainable supply the recycling of motors has become critical. The magnets used in the motors are predominantly NdFeB magnets which contain rare earth elements. In recent years projects like EREAN, RARE^3 etc are working on the recycling of extracted magnets. Another project called MORE was undertaken a few years ago which investigated the extraction and recycling of different components used in the drive train. One of the inferences from the project is that the motor designs present today are not designed for recycling i.e. extraction of magnet is very difficult [18] & [24]. Therefore, in DEMETER (H2020) project different ways of reuse/recycling path for magnets had been identified considering the environmental impact of each path. One of the objectives of the project was to design the motor for recycling. However, currently there is no method or tool available to benchmark recycling of motors and assist designers to achieve the motor with high recyclability specially easy extraction of magnet.

In this chapter a new method is presented to evaluate the recyclability of the designed motors for EVs and HEVs called **Weighted Index of Recyclability and Energy (WIRE)**. It was developed in close collaboration with the other 3 PhD involved in the DEMETER project work package 3. The method can be used during the design phase of the motor and considers both recyclability and its impact on energy consumption during the usage of the motor. The evaluation of recyclability of the motor is done considering standardization, assembly and disassembly of the motor. On the other hand, the evaluation of energy impact of the motor design is done on the basis of energy consumption over the complete life cycle and the cost of magnets.

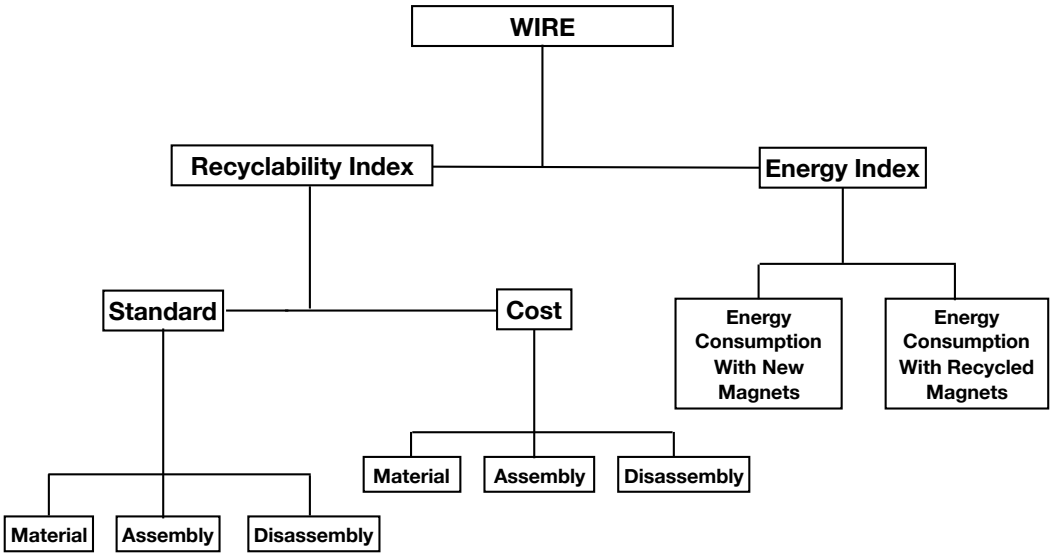

Figure 4.1: Flow chart of WIRE method

4.1. WIRE Method

As specified above, the WIRE approach consists of the recyclability index and the energy index. Figure 4.1 shows the flow chart of the methodology. The method considers both easy extraction of the magnet for recycling and the impact of the recycled magnet on the motor performance in terms of energy consumption. The methodology is detailed in the following sections.

4.1.1. Recyclability Index

The recyclability evaluation of the motor is done on the basis of standard and cost. Further each part is evaluated in three categories- assembly, disassembly and material of the motor. Each step or process is evaluated in two different ways one is called **Score (S)** and the other one is called **Importance (I)**. The **Score (S)** is scored on its relative scale in the respective category whereas, the **Importance (I)** depends on the relative criticality of material/processing in terms of recyclability of the materials. The product of the sub scores is the final score i.e. **(SxI)**. For each category, the scoring is done between 1-5, where 1 is the lowest and 5 the highest. It is important to note that the scoring is done on relative basis and hence, it is better to evaluate any motor design in focus groups consisting of personnel belonging to the domains of motor design and manufacturing. It is also important that one uses the same scoring rules to evaluate different motors to have a fair comparison. For example the figure 4.2 shows the evaluation sheet for motor materials for both standard and cost parts. For indexing different categories/process, guidelines and definitions were formulated

Scoring pattern	0-5	1 - Lowest score	5 - Highest score	
		1 - Lowest score	5 - Highest score	3 = neutral score

Assumption The motor developed is new and for the first time and manual disassembly with high volumes i.e. 50,000 per annum

MOTOR ID	Hub motor for in-wheel application										
Component/ Parts			Standard				Cost				Recyclability SCORE
		Remarks	S	I	SxI	Remarks	S	I	SxI	Remarks	
Materials											
- Stator											
	Lamination S	segmented stator	5	5	25	good for recycle not reuse	1	5	5		30
	Copper	AWG 24	5	5	25		2	1	2		27
- Rotor											
	Steel R	MS steel	5	5	25	good for recycle not reuse	1	4	4		29
	Magnets	NdFeB-rect shape	5	4	20	Because of shape	5	1	5	Because of coating	25
-Shaft											
	Shaft	Steel	4	5	20	shaft with hole for wires	1	2	2		22
-Endshileds											
	Drive Side	aluminium die cast	2	5	10	prepare new die	1	2	2		12
	Non-Drive side	aluminium die cast	2	5	10	prepare new die	1	2	2		12
				34	135			17	22		157
	section score				79.41 %				25.88 %		

Figure 4.2: Evaluation sheet of material for standardization and cost

in order to assist the designer during evaluation. This is further discussed in the following sections.

(a) Definitions of WIRE sheet

The evaluation of the motor is done in relative terms and hence, the definitions of different categories are very critical for accurate indexing. Following section presents the definition to evaluate each step / process in the motor. For simplicity of evaluation, many assembly/ disassembly processes are clubbed together while considering only primary material of the motor. The method is easily customizable according to the preference of the users.

- **Standard** : The category focuses on the use of standard material and processes. The evaluation of the Standard category is done with the view that the use of standard parts/process will simplify and encourage recycling. Furthermore, higher the number of standard components in the motor, the easier it will be for recycling which further improves the quality of the recycled output.

  a) Material

  – 'S' depends on the standardization of the material. The score is higher for materials which are easily available (off the shelf) and widely used. For example, random wound copper is more widely used and available than the rectangular strand cable of a certain dimension.

- 'I' depends on the materials' recyclability. For example, NdFeB magnet with and without coating is easily available however, in terms of recyclability the magnet, but without coating will be easier for recycling and hence the index shall be higher

b) Assembly

- 'S' depends on the process/activity standardization. While scoring it is important one should also consider the tools used. More non-standard tools or processes used in the assembly shall lower the score. For example, if special heat treatment/ or other special environment is needed for assembly, the process will be non-standard and thus the index shall be lower.

- 'I' depends on the criticality of the step/process for recycling of the material. For instance, if the assembly makes the recycling of the copper easier the index shall be high.

c) Disassembly

- 'S' depends on the process/activity standardization. While scoring it is also important to consider the tools used. More non-standard tools or process used in disassembly shall lower the index. For example, if some chemical is needed for extraction of certain components, the score shall be lower for the process.

- 'I' depends on the criticality of the step/process for recycling of the part. Similar to assembly, if disassembly of copper makes recycling easier, the index shall be high.

- **Cost** : The category focuses on the cost of material/processes and its impact on recycling. The evaluation of Cost category was done with the view that higher cost of any process will increase the overall recycling cost and hence, has a negative impact on recycling. On the other hand, higher material cost incentivises recycling of magnets and encourages recycling.

a) Material

- 'S' is directly correlated with the cost of the material. The processing cost of the component varies over a wide range. Therefore, to keep the tool simple and to avoid processing cost, only material cost is considered. Moreover, the non-standard design or the impact of processing will be taken care while scoring the standard category. For example, NdFeB magnet is roughly 10 times costlier than the laminations in the motor. Therefore, score of magnet will be higher than the laminations. The impact of different shapes of magnet should be considered while scoring the standard material category.

- 'I' depends on the impact of the material on recycling of the whole motor. For example, if the weight of the material is very low as compared to other materials, the material recovered will be very small. Therefore, the recovery in terms of economic value will be small, even with the high price of the material.

b) Assembly

- 'S' depends on the cost required to execute assembly processes. Higher the assembly cost, lower the score shall be since it impacts the recycling process negatively. For example, if there is a need of a special environment for assembly, it would lead to an increase in the process complexity and subsequently the cost.
- 'I' depends on the impact of the cost of the process on recycling process. For example, if a motor uses powder NdFeB magnet technology, the assembly cost is higher but it does not impact the recycling of the magnet at the end of life (EOL) of the motor. Therefore, the index shall be neutral.

c) Disassembly

- 'S' depends on cost required to execute the disassembly process/activity. Higher the disassembly cost lower the score shall be since it impacts the recycling process negatively. For example, a need of a special environment for disassembly, would lead to an increase in the complexity and subsequently the, cost which in turn discourages recyclability from a cost perspective.
- 'I' depends on the impact of cost of the process in recycling. For example, the cost of disassembly of the magnet is very critical its recycling. Therefore, the index shall be high for this process.

Calculation of Recyclability Index

The final weighted recyclability index (R) is calculated using equation 4.1 and 4.2. The R_w is in the scale of 1-5 and using equation (4.2) is expressed in percent, R.

$$R_w = \frac{S_1 * I_1 + S_2 * I_2 + \cdots + S_n * I_n}{\sum I_i} \tag{4.1}$$

$$R = \frac{R_w * 100}{5} \tag{4.2}$$

(b) General Guidelines for evaluation

This section provides some general guidelines, which can be used to score different sections of WIRE sheet. It is important to note here that the scores are relative and

can be varied on consensus or when the scenario changes. The authors decided the scores after considering various scenarios.

Scoring of materials for Standard category

Table 4.1 shows the scoring of material and its importance for recyclability with respect to their standardization. The table shows the scores for main components of the motor like lamination, magnet and copper. The materials are scored based on the definition given in section (**a**).

Table 4.1: Scoring of Material for Standard Category

Magnet Type	S	I	Magnet Type
Rectangular small pieces with/ without coating sintered, Bonded Magnet	5	5	Rectangular small pieces or powder without coating or binder
Sintered/bonded shape parallel/radially magnetized	4	4	Sintered with coating
Halbach bonded	3	3	Sintered any shape with coating/glue
Sintered or Bonded powder but magnetised in rotor	2	2	Bonded magnets
Sintered halbach multipole	1	1	Bonded magnets with glue

Lamination Type	S	I	Lamination Type
Silicone iron 0.35-0.6mm, Single solid rotor	5	5	Any silicone iron lamination or solid rotor or Aluminum
Silicone steel modular type	4	4	Cobalt steel
Cobalt Steel	3	3	Amorphous Steel
Amorphous , different shapes	2	2	Soft Magnet Composites (SMC)
SMC	1	1	Any new special handling material

Winding Type	S	I	Winding Type
Copper / aluminium strand circular	5	5	Copper any type
Copper rectangular standard, aluminium cast rotor	4	4	Aluminium wire/Cast aluminium /Copper rotor
Copper rectangular/circular non standard	3	2	Any new special handling material
Hollow circular copper wire	2		
Any thing special	1		

Assembly/Disassembly of the motor

The scoring guideline for individual components (stator, rotor, bearing etc) is shown in Table 4.2. However, there is one more critical step in assembly/disassembly, which is the separation of the rotor from the stator. The complexity of the process is even higher in PM motors. The ease of assembly / disassembly mainly depends on the force of extraction and the motor size. Therefore, to scale the process, the following method is used. The larger the volume and airgap flux density i.e. power of the motor, separation of rotor and stator will be more difficult and hence, the score shall be lower. Mathematically it can be presented by equation 4.3.

$$\mathbf{S} \propto \frac{1}{V * B_\delta} \tag{4.3}$$

where, V is volume of the motor and B_δ is the airgap flux density.

Assembly/Disassembly score for Cost

Table 4.2 gives the scoring guideline for assembly/disassembly in terms of cost. Simpler the process higher the score shall be.

Table 4.2: S of assembly/disassembly for Cost category

Assembly / Disassembly Cost	S
Easy assembly/disassembly without any tool	5
Easy assembly/disassembly with standard tools /process	4
Complex / Hard process with standard tools or more than one person required	3
Special pre/post treatment with special tools	2
New extra method to extract magnet from rotor	1

Scoring 'I' of material for Cost category

The scoring of 'I' depends on the weight of the material in the motor. Higher the weight of the material, higher will be the recovery of material from recycling. The proposed method to estimate I score is as follows. Let us assume, the motor has W_c kg of copper, W_s kg of stator steel, W_r kg of rotor steel and W_m weight of magnet and the weight (W_s) of stator steel is maximum. The I score for stator steel W_s is 5 and the rest is scaled in proportion to the W_s. The fractions are rounded off to the nearest integer.

$$\text{I for magnet is } \frac{W_m * 5}{W_s}$$

$$\text{I for copper is } \frac{W_c * 5}{W_s}$$

Table 4.3 shows the relative score of material used in the motors.

Table 4.3: Score of material cost in motor

Material Cost	S
Sintered Magnet	5
Bonded Magnet	4
SMC,Amorphous steel	3
Copper	2
Silicone Steel lamination	1

'I' of assembly/disassembly for Standard & Cost category

The criticality of each step during assembly and disassembly is shown in table 4.4. While indexing, the recycling of steel, copper and magnet was considered important and hence, the process affecting their recycling was indexed accordingly. If some step of assembly is very important for recycling of that material then it shall have a high index. For example, assembly of magnet and rotor is very significant for extraction of magnet and hence, has a high index.

Table 4.4: Importance of Assembly/Disassembly process

Process	Standard Importance	Cost Importance
Assembly of stator lamination	3	3
Assembly of copper winding	3	3
Assembly of rotor lamination	3	3
Assembly of magnet and rotor	5	3
Assembly of sensor wires	1	3
Assembly of rotor and stator	3	3
Assembly of end shields	3	3
Assembly of shaft	3	3
Disassembly of end shields	3	3
Separation of rotor and stator	4	4
Disassembly of copper	3	4
Disassembly of stator	3	3
Disassembly of magnets from rotor	5	5
Disassembly of rotor	3	3

Evaluation of Recyclability Index of a HUB motor

A commercially available motor was used to evaluate the WIRE method. The motor was disassembled manually using standard tools and the processes were observed with respect to ease of disassembly. Figure 4.3 shows the disassembly of hub motor. Based on the disassembly and assembly processes, the WIRE sheet was scored by the team. Figure 4.4 shows the recycling index for HUB motor for both standard and cost category. It can be seen that the scores of standard category are higher due to the fact that the motor has used all standard parts and standard process/tools for assembly/disassembly. The motor was an outer rotor PMSM motor and used rectangular sintered magnets glued to the rotor. This process of rotor assembly using pre-magnetized magnets and glue had lowered the score for assembly and to some extent disassembly. From the cost perspective, the index for material is much lower compared to assembly and disassembly which implies that the recovery of valuable material from the motor is very low. However, if scaled to thousands or millions, the values will be significant. Furthermore, the index is relative and in absolute terms

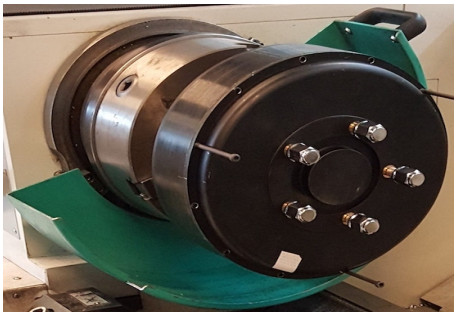

(a) Motor

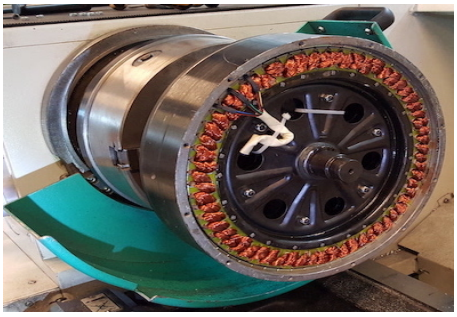

(b) Motor without End-shields

(c) Stator

(d) Rotor

Figure 4.3: HUB Motor Disassembly

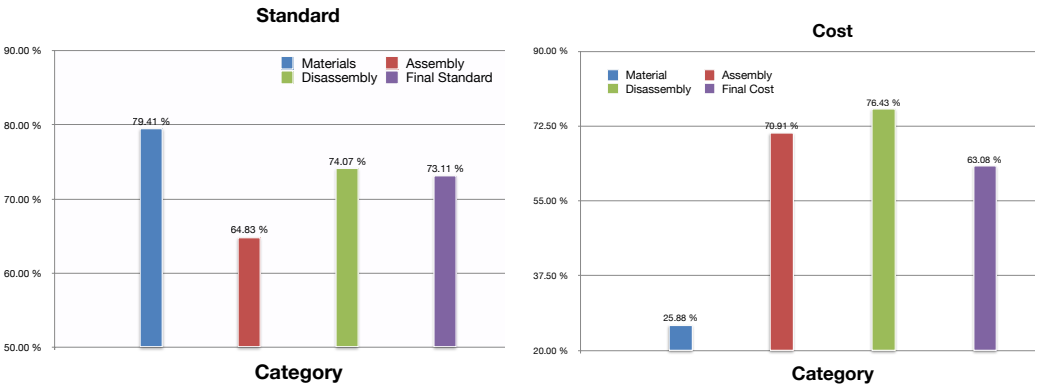

(a) Standard Distribution

(b) Cost Distribution

Figure 4.4: Distribution of Recycling index of the sample HUB motor

hence the cost of material can be higher than the cost of assembly and disassembly of the motor. The final recycling index (R) of the motor is 68.5%. The index is not low as compared to the other motors due to the use of standard parts and process however, as it was not designed for recycling it is not on the higher side either [27].

4.1.2. Energy Index

The second index of the WIRE method is Energy. The Energy index of the motor denotes the effectiveness of the motor to use recycled magnet during its operation phase i.e. life cycle. As shown in figure 4.1 the energy consumption of the motor is calculated with both new and recycled magnets for evaluating the index. Figure 4.5 shows the flow chart of the method used to calculate energy consumption of the motor over the whole life cycle and is presented in details in [12]. There can be different ways to achieve the same torque speed characteristic from the motor using recycled magnet as discussed in section 3.3. Any change in motor design to achieve same torque speed with recycled magnet shall reflect in its energy consumption. Therefore, energy cost is taken as the parameter to index different motor designs. Furthermore, one can choose any drive cycle for calculation of the index. Once energy consumption of motors with recycled and new magnets is calculated, the energy index is evaluated using equation 4.4. From the energy index it can be determined if the use of recycled magnet is beneficial in terms of cost during usage of the motor.

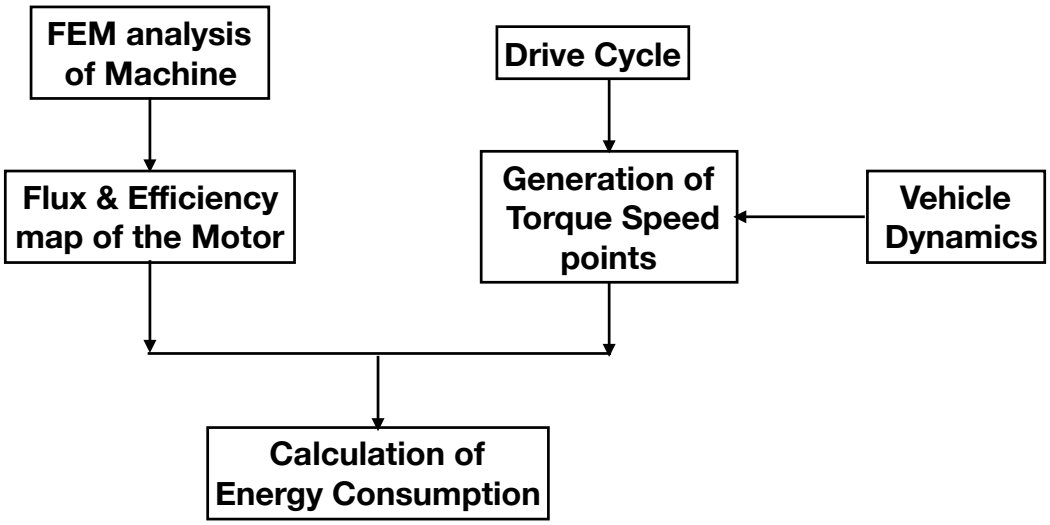

Figure 4.5: Flow chart to calculate energy consumption of the motor over life cycle

$$E_i = \left(\frac{E_c(r)}{E_c(n)}\right) \times \left(\frac{Mag_c(r)}{Mag_c(n)}\right) \tag{4.4}$$

where, E_i is the energy index, $E_c(r)$ *and* $E_c(n)$ is the energy cost for the motor with recycled and new magnets respectively and $Mag_c(r)$ *and* $Mag_c(n)$ is the magnet cost for recycled and new magnets respectively.

Evaluation of Energy Index of a HUB motor

To test the above method the energy index of a commercially available HUB motor, shown in figure 4.3, was calculated. The torque and different losses of the hub at

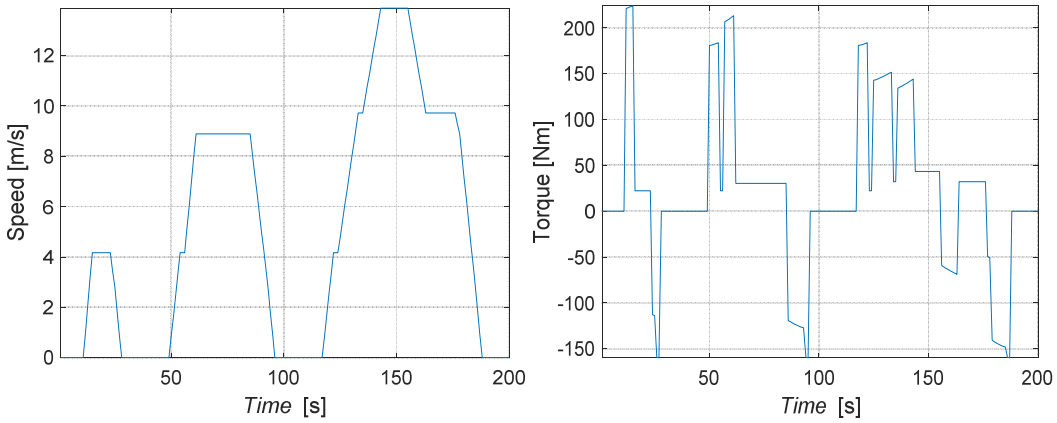

(a) Speed vs Time *(b) Torque vs Time*

Figure 4.6: Part of NEDC cycle used to calculate Energy Index of HUB motor

Table 4.5: Vehicle Parameters for HUB motor energy evaluation

Parameters	Value
Vehicle weight [kg]	920
Density of air [kg/m^3]	1.225
Frontal area [m^2]	1.85
Drag coefficient	0.4
Coefficient of rolling resistance	0.01
Tyre radius [mm]	210

various speeds were measured as described in the article [28]. Thereafter, FEM model results were validated against the measured values and the efficiency map of the motor was calculated. Then, using the same FEM model and replacing the magnets by recycled magnet i.e. reducing remanence by 20 %, the new efficiency map for recycled magnet motor was created. The axial length of the motor with recycled magnet was increased to achieve the same torque speed characteristics. The drive cycle used for evaluation is shown in figure 4.6. Only urban part of NEDC cycle was used for this evaluation because the motor was not designed for high speed operation. Furthermore, due to low peak torque of the motor it was assumed that the vehicle has 4 in-wheel motors without any gearbox to achieve the required torque. For the evaluation a compact city car with the vehicle parameters given in table 4.5 was considered.

As mentioned earlier, the efficiency of the hub motor was calculated with both the new and recycled magnets for the drive cycle and the efficiency with time is shown in figure 4.7. It was observed that the efficiency of recycled magnet motor at various points was higher than that of the new magnet motor. This happens mostly at high speed low torque points where iron loss is the main contributor of efficiency.

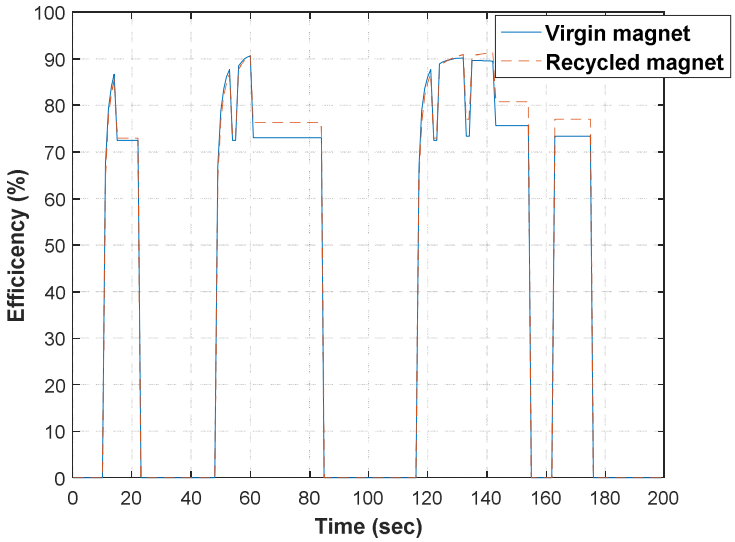

Figure 4.7: Efficiency of HUB motor with new and recycled magnets for NEDC cycle [12]

			VIRGIN MAGNETS					
	PM. mat. price(€/kg)		20	35	50	65	80	95
		PM. cost (€)	14.0	24.5	35.0	45.5	56.0	66.5
RECYCLED MAGNETS	5	4.05	0.282	0.161	0.113	0.087	0.071	0.059
	20	16.20	1.128	0.645	0.451	0.347	0.282	0.237
	35	28.35	1.974	1.128	0.790	0.607	0.494	0.416
	50	40.50	2.820	1.611	1.128	0.868	0.705	0.594
	65	52.65	3.666	2.095	1.466	1.128	0.917	0.772
	80	64.80	4.512	2.578	1.805	1.388	1.128	0.950
	95	76.95	5.358	3.062	2.143	1.649	1.340	1.128

Figure 4.8: Energy Index of HUB for NEDC cycle [12]

Because recycled magnets have lower remanence, the reduction in the iron loss is much more than the increase in copper loss of the motor. Therefore, as expected the total energy consumed by the motor for the drive cycle with new magnets is 3071 kWh which is slightly higher than with recycled magnets (2995 kWh). It is further assumed that the vehicle would operate for 2 hours daily for a period of 10 years in it's complete life time and the price for energy consumed would be 0.22 €/kWh. Hence, the total cost of electricity used by vehicle with new magnets and recycled magnets motor were expected to be 676 € and 659 € respectively. For calculation

purpose the price of the new sintered magnets was taken 45 €/kg. At present the price of the recycled magnet is uncertain and hence, different prices points were assumed to calculate the energy index using equation 4.4. Figure 4.8 shows the calculated energy index of the HUB motor for the NEDC drive cycle (urban part). Because the energy consumption with new or recycled magnet is almost same, the index is mainly varied with the magnet price. It can be seen that the index is higher than 1 if the recycled magnets price is equal or higher than the new magnets which is a logical and expected outcome. In other words, from an energy point of view, the use of recycled magnets becomes viable as soon as their price is lower than the new magnets. It would be fair to say that the method is sensitive to the parameters and reflects the changes. The absolute values do not significantly impact the final outcome. However, it is the ratio of the prices of both magnets along with energy consumption which are critical. Hence the method can be easily used to compare different motors used in the vehicle, contingent on the consistency of the criteria used for evaluation [12].

4.2. WIRE Evaluation for the Proposed Motor

4.2.1. Recyclability Index of the Motor

The proposed motor is designed with standard materials considering easy assembly and disassembly with the use of conventional tools and processes. The stator is made of standard silicone iron lamination of 0.35 mm thickness and the rotor is made of bonded NdFeB magnet with a steel sheet as rotor back. Figure 4.9 shows the stator and rotor assembly of the motor. The rotor and stator can be separated very easily without removing the end plates because of the absence of single motor frame as with the case of conventional inner rotor motors. Furthermore, the respective end plates are fixed with the rotor back and the stator using screws which makes it very easy to assemble/disassemble when required as shown in figure 4.10a. Due to the use of bonded Halbach magnet ring and steel sheet for rotor back there is almost no need of glue for the assembly. The outer rotor topology of the motor also helps in removal of glue from the assembly process. Also, as the magnetic field is on the inner side of the magnet ring, the assembly of rotor back and magnet becomes easier and safe. The simple rotor structure also makes disassembly very simple. The magnet ring can be extracted from the rotor back either by heating or cutting a small section of the back. The extraction by cutting was tested on the sample Halbach rotor prototype as shown in figure 4.11 and it can be seen that the magnet ring is not damaged and can be easily removed.

The separation of stator and rotor assembly is very critical step in the disassembly of the motor and more so for the magnets with the proposed motor design topology. The 3D FEM magneto static model was used to calculate the force required to pull out the rotor from motor. Figure 4.12 shows the extraction force required to pull the

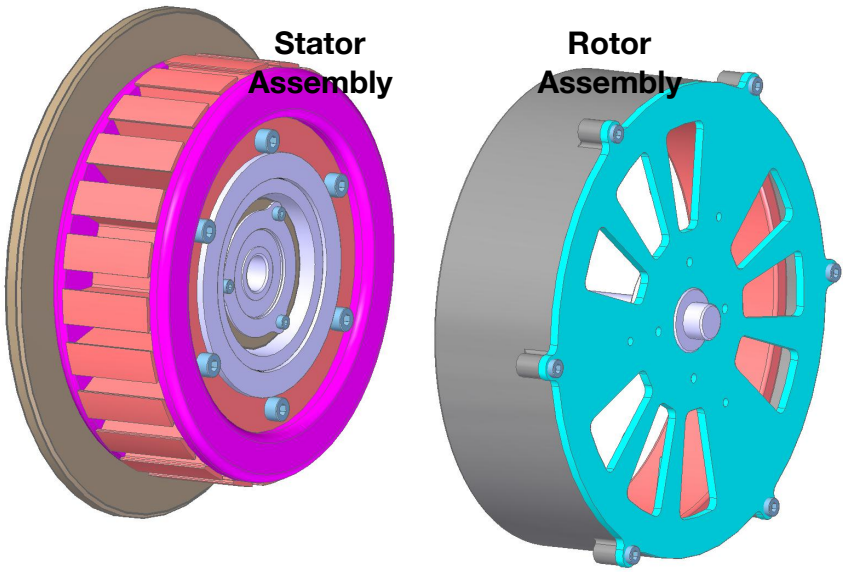

Figure 4.9: Stator and rotor assembly of the motor

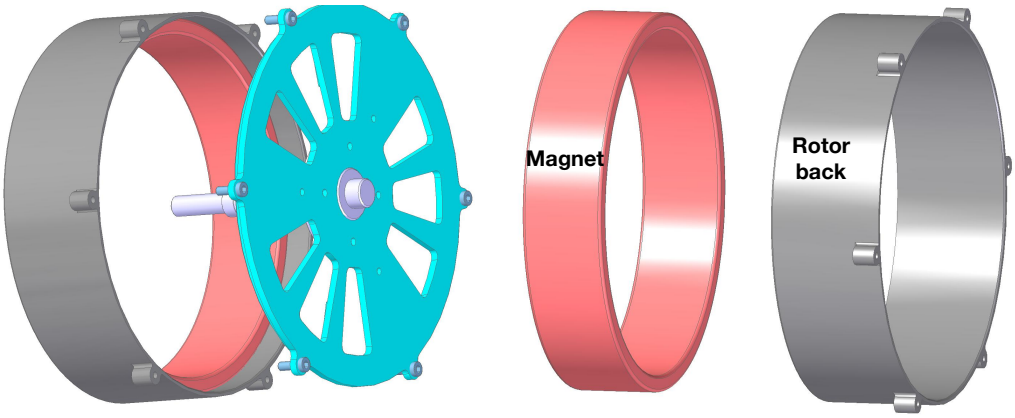

(a) Removal of rotor end plate from rotor assembly

(b) Separation of magnet and rotor back

Figure 4.10: Extraction of magnet from rotor assembly

rotor from the motor. The force varies with the position of the rotor with a maximum of 350N required for extraction. The extraction force depends on the volume and the airgap flux density of the motor as shown in equation 4.3. The extraction force is not very high and hence, it is expected that the rotor can be easily removed using standard tools.

The recyclability index of the proposed motor design was evaluated using WIRE. Figure 4.13 and figure 4.14 shows the scores for material, assembly and disassembly of the motor for both the standard and the cost category. The complete evaluation

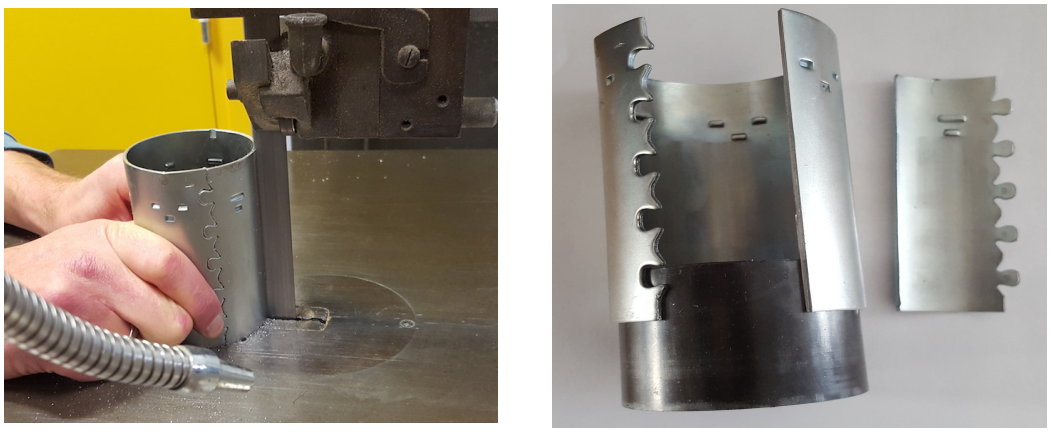

Figure 4.11: Extraction of magnet by cutting rotor back for a Halbach rotor sample

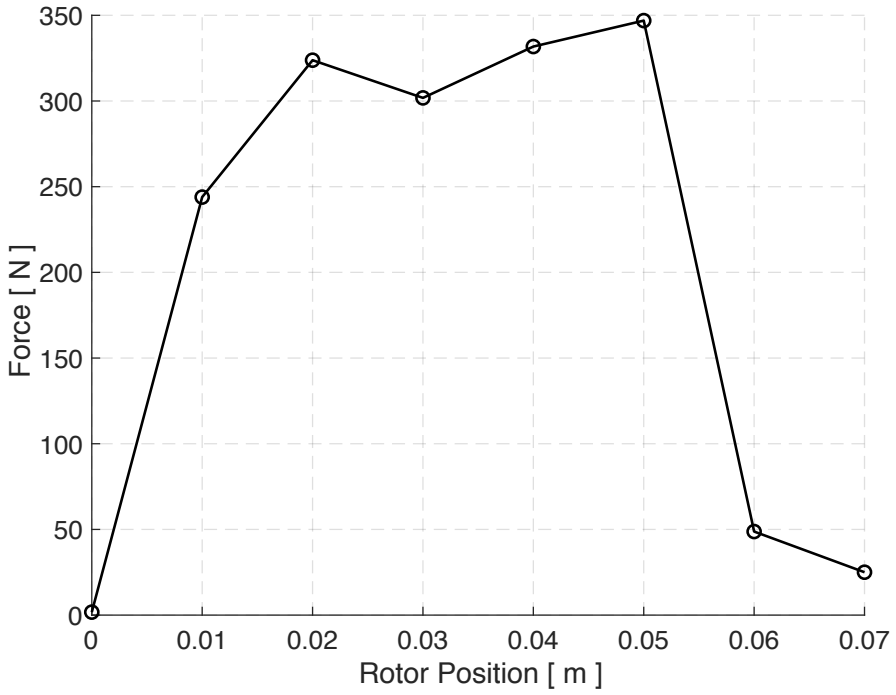

Figure 4.12: Force required to separate rotor and stator

scores for all the categories and sections is included in the Appendix A. From figure 4.14 it can be seen that material standard score is 75% as most of the components used are very standard and easily available. As discussed earlier the assembly process of the motor is easy due to the simple structure of the stator and the rotor hence, the assembly score is high. However, because the manufacturing process of Halbach magnet ring is complex and not standard, the score is slightly low. The disassembly score is higher than the assembly score because of no use of glue in

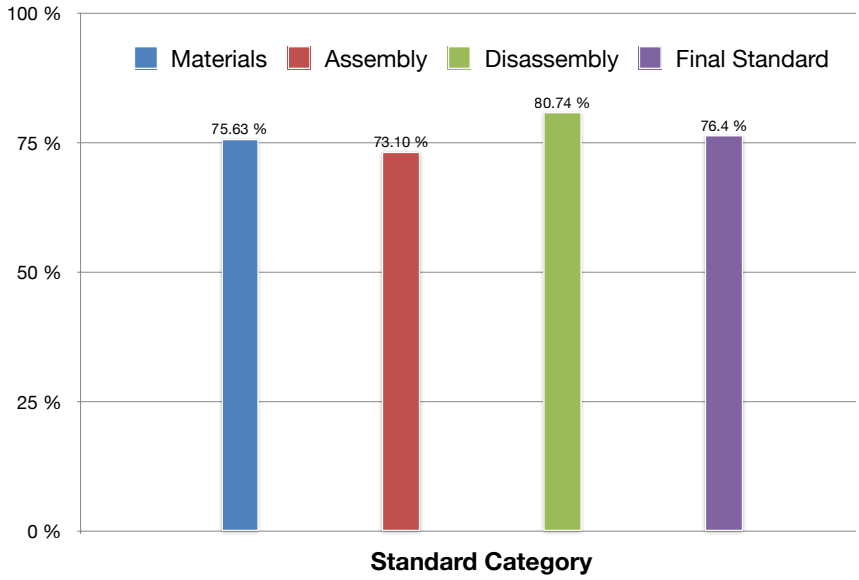

Figure 4.13: Scores of material, assembly and disassembly for standard category of recyclabiltiy index

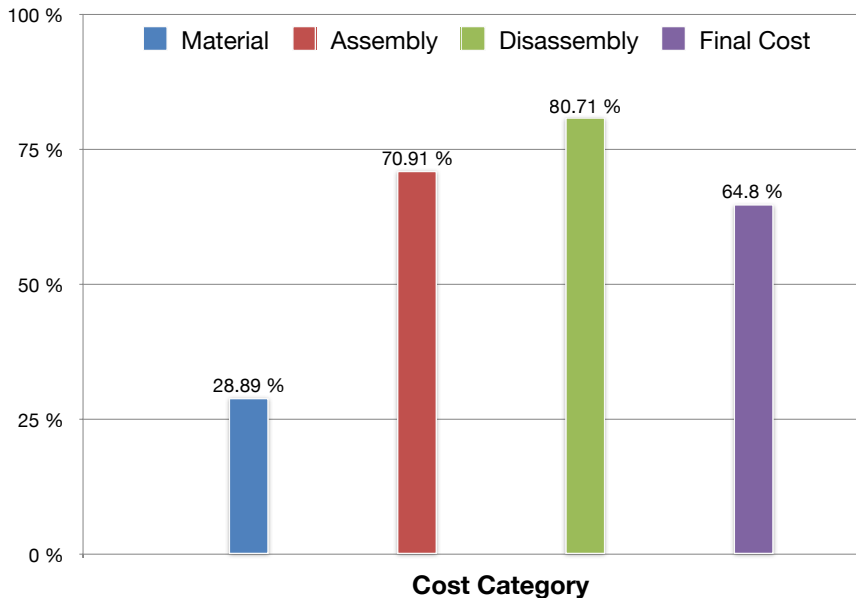

Figure 4.14: Scores of material, assembly and disassembly for cost category of recyclabiltiy index

rotor assembly and as discussed before no special tools are required for magnet extraction.

The cost score for the material is 28% , see figure 4.14 shows that the value of material recovery from the motor is not very high. While designing motor it was ensured that

use of magnet is optimal in order to achieve the required performance and magnet is the most valued component of this motor. The assembly cost of the motor is slightly lower than the disassembly because the manufacturing of Halbach magnet is currently expensive. The tooling and magnet orientation fixture makes the bonded Halbach manufacturing expensive and if this cost reduces in future, the overall recyclability of the motor would improve. The extraction of NdFeB powder from the bonded magnet is a complex and a tedious process while the proposed recycling process in chapter 2 utilizes maximum 30% of old magnets. Hence, the score I for bonded magnets recyclability is lower than the sintered magnets.

4.2.2. Energy Index of the Motor

The energy index of the motor was calculated for both Worldwide Harmonised Light Vehicle Test Procedure (WLTP) and New European Driving Cycle (NEDC) drive cycles, shown in figure 4.15. The vehicle was modelled as described in [5] and torque required from motor was calculated at different speeds. The main vehicle parameters are given in table 4.6, which are higher for a micro sized vehicle [67]. The required torque from the motor was calculated with different gear ratios considering that a majority of points remain in nominal operation of the motor. The load points for the motor with different gear ratios for the drive cycles are shown in figure 4.16- 4.17. With higher gear ratio the load points are shift towards higher speed with lower torque. Thereafter, efficiency of the motor at each point of the drive cycled was calculated using loss maps generated using FEM model of the motor. The efficiency of the motor does not consider mechanical and other stray losses.

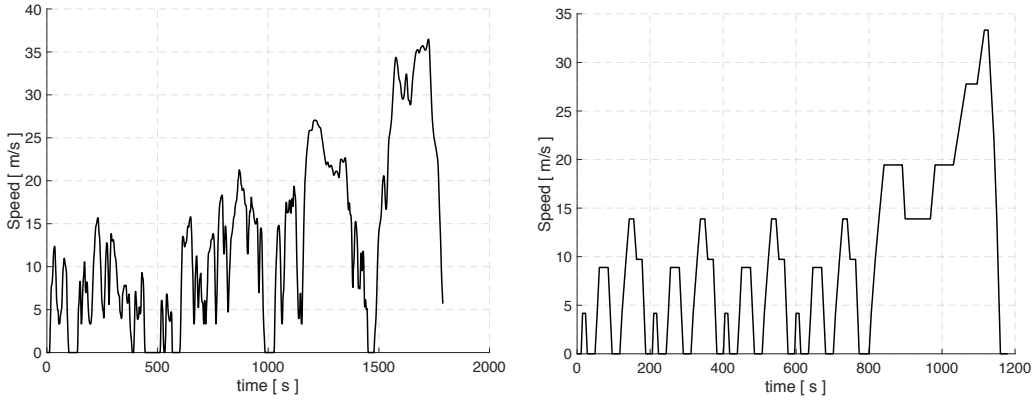

(a) WLTP drive cycle *(b) NEDC drive cycle*

Figure 4.15: Different drive cycles for EVs

As discussed in the section 3.3 the remanence of recycled magnets can vary in the range of 0 % - 20 %. A worst-case scenario of 20% lower remanence of the magnet was considered. Furthermore, energy consumption with recycled magnets was calculated

Table 4.6: Vehicle Parameters for modelling

Parameters	Value
Vehicle weight [kg]	500
Density of air [kg/m^3]	1.23
Frontal area [m^2]	1.85
Drag coefficient	0.4
Tyre radius [mm]	273

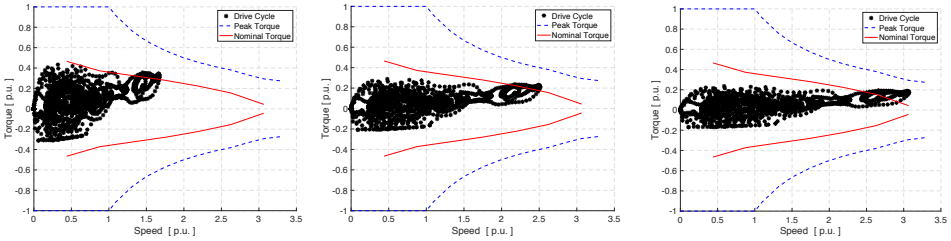

(a) Gear Ratio 3 *(b) Gear Ratio 4.5* *(c) Gear Ratio 5.5*

Figure 4.16: WLTP drive cycle load points with different gear ratio

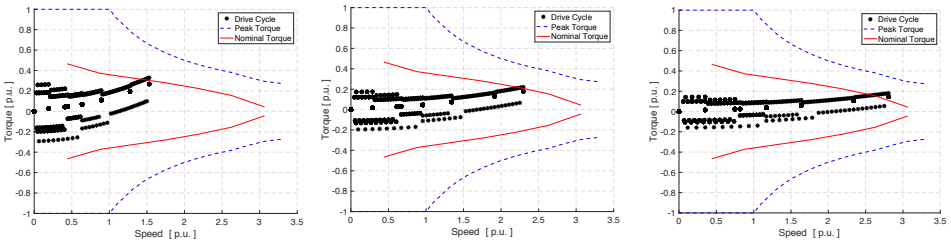

(a) Gear Ratio 3 *(b) Gear Ratio 4.5* *(c) Gear Ratio 5.5*

Figure 4.17: NEDC drive cycle load points with different gear ratio

for motor with an increased axial length of the motor or an increased current supply. The energy consumption was calculated by only considering the energy consumed by the motor over the whole life cycle and 100% regeneration was assumed during braking. The energy price used for calculation was 0.22 €/kWh.

Figure 4.18 and 4.18 show the cost of the energy consumed by the motor over the lifetime running in WLTP and NEDC drive cycle respectively. It can be seen that with the increase in gear ratio, the energy cost increases for virgin as well as for the recycled magnet motors. This is due to the much higher increase in the iron loss than the copper loss of the motor as with the increase in gear ratio the load point shifts to higher speed and low torque region, see figure 4.16, 4.17. The energy cost of the virgin magnet motor is slightly lower than the motor with increased length and recycled magnet. However, the cost of motor with increased current and recycled

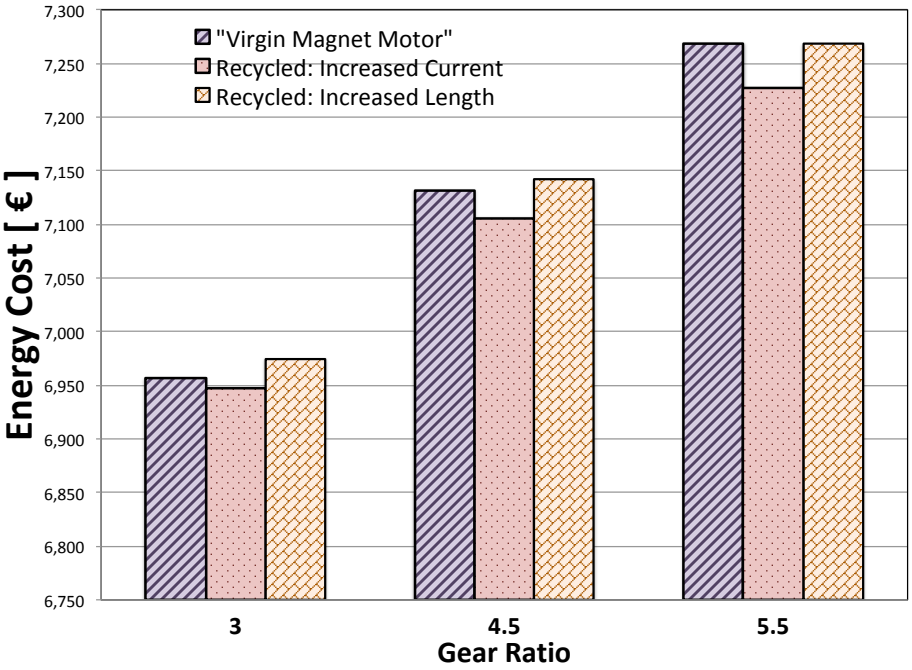

Figure 4.18: Calculated energy cost for WLTP drive cycle over life time

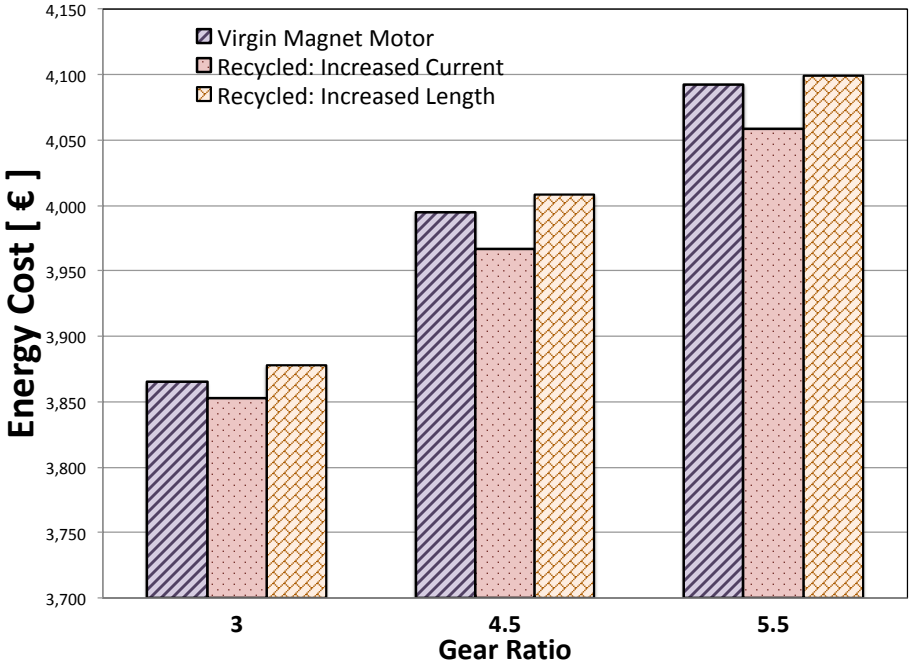

Figure 4.19: Calculated energy cost for NEDC drive cycle over life time

			NEW MAGNETS					
	PM. mat. Price(€/kg)		14	25	35	46	56	67
		PM. cost (€)	37	64	91	119	146	174
RECYCLED MAGNETS	4	9	0.250	0.143	0.100	0.077	0.062	0.053
	14	37	0.999	0.571	0.399	0.307	0.250	0.210
	25	64	1.747	0.999	0.699	0.538	0.437	0.368
	35	91	2.496	1.427	0.999	0.768	0.624	0.526
	46	119	3.245	1.854	1.298	0.999	0.811	0.683
	56	146	3.994	2.282	1.598	1.229	0.999	0.841
	67	174	4.743	2.710	1.897	1.459	1.186	0.999

(a) Energy Index for increased current strategy

			NEW MAGNETS					
	PM. mat. Price(€/kg)		14	25	35	46	56	67
		PM. cost (€)	37	64	91	119	146	174
RECYCLED MAGNETS	4	13	0.358	0.205	0.143	0.110	0.090	0.075
	14	52	1.434	0.819	0.573	0.441	0.358	0.302
	25	91	2.509	1.434	1.004	0.772	0.627	0.528
	35	131	3.584	2.048	1.434	1.103	0.896	0.755
	46	170	4.660	2.663	1.864	1.434	1.165	0.981
	56	209	5.735	3.277	2.294	1.765	1.434	1.207
	67	248	6.810	3.891	2.724	2.095	1.703	1.434

(b) Energy Index for increased length strategy

Figure 4.20: Energy index of recycled magnet motors for WLTP drive cycle. The values lower than 1 (green portion) shows recycling is better

			NEW MAGNETS					
	PM. mat. Price(€/kg)		14	25	35	46	56	67
		PM. cost (€)	37	64	91	119	146	174
RECYCLED MAGNETS	4	9	0.249	0.142	0.100	0.077	0.062	0.052
	14	37	0.997	0.570	0.399	0.307	0.249	0.210
	25	64	1.745	0.997	0.698	0.537	0.436	0.367
	35	91	2.492	1.424	0.997	0.767	0.623	0.525
	46	119	3.240	1.851	1.296	0.997	0.810	0.682
	56	146	3.988	2.279	1.595	1.227	0.997	0.839
	67	174	4.735	2.706	1.894	1.457	1.184	0.997

(a) Energy Index for increased current strategy

			NEW MAGNETS					
	PM. mat. Price(€/kg)		14	25	35	46	56	67
		PM. cost (€)	37	64	91	119	146	174
RECYCLED MAGNETS	4	13	0.359	0.205	0.143	0.110	0.090	0.076
	14	52	1.435	0.820	0.574	0.441	0.359	0.302
	25	91	2.511	1.435	1.004	0.773	0.628	0.529
	35	131	3.587	2.050	1.435	1.104	0.897	0.755
	46	170	4.663	2.665	1.865	1.435	1.166	0.982
	56	209	5.739	3.280	2.296	1.766	1.435	1.208
	67	248	6.815	3.894	2.726	2.097	1.704	1.435

(b) Energy Index for increased length strategy

Figure 4.21: Energy index of recycled magnet motors for NEDC drive cycle. The values lower than 1(green portion) shows recycling is better

magnet is lower than the virgin magnet motor. The iron volume is higher in the motor with increased length than the virgin magnet motor and hence, the iron loss is higher for the drive cycles. On the contrary, the motor with increased current has the same iron volume and smaller magnetic remanence which causes lower iron loss as compared to the virgin magnet motor.

Based on the energy cost of the virgin and recycled magnets motor, the energy index of both the strategies was calculated using the equation 4.4. The index depends on both the magnet price and the energy cost of virgin and recycled magnets. At present the price of recycled magnet is not known and hence, a range of price was assumed to calculate the index. Figure 4.20 and 4.21 presents the energy index of motors for WLTP and NEDC drive cycles for both the strategies used for recycled magnets. The values lower than 1 present scenarios which are feasible/better with recycled magnets. The energy indices of motors with the same strategy of using recycled magnets for different drives cycles are almost similar. However, the difference is significant between indices of different strategy. The motor with recycled magnets and increased axial length consume more energy and hence, it has higher index values for different magnet price as compared to the increased current strategy. It can also

be inferred from the indices that if the cost of recycled magnet is lower than the virgin magnet, the use of recycled magnets in the motor over the lifetime is better. Therefore, the strategy to use larger current with recycled magnet will be better from an energy efficiency perspective. However, one must keep in the consideration that the losses and cost on increased inverter ratings which are not considered in the method. Nevertheless, the method can be used to compare different strategies energy impact and is very sensitive to both magnet and energy price.

4.3. Summary

The chapter presents a new method called WIRE for evaluation of recyclability and its impact on motor performance. The evaluation outputs-Recyclability index and Energy index, should be considered while designing motor for recycling. The method considers standardization, assembly and disassembly of the motor for evaluation of the recyclability index. Many processes of assembly/disassembly were put together as one step and scored for simple evaluation. Also, only important materials of the motor were considered. However, the method is very simple to modify and any process can be expanded further and scored depending on the group evaluating the motor. The tool is very simple and easy to modify. However, it is important to use the same scoring rules to evaluate different motor index for comparison. The drawback is that the method scores less for new designs or methods that need special arrangement and the designer has to keep that in consideration during evaluation. The recycling evaluation of the proposed motor design is presented. The chapter outlines the features of motor design that enables an easy assembly and disassembly of the motor. The use of single Halbach ring enables a glue free rotor assembly and as demonstrated on a sample rotor the extraction of magnet is also very simple. Furthermore, the extracted magnet is of very good quality and can be directly reused or recycled. The motor has slightly lower score for assembly due the complex process of producing Halbach magnet cylinder compared to radially magnetized sintered magnets which are now industrialized. The score is also low due to the difficult recycling of bonded magnets into magnet powder. Moreover, the material cost of the motor is low compared to assembly and disassembly category which implies that the recovery of material from the motor in terms of their cost is not very high. In the framework of DEMETER project four different motors are designed and their recyclability indices are compared in [27].

Two different strategies to use recycled magnets were studied and their impact on energy was calculated. The motor with recycled magnet and increased current supply (higher converter ratings) consumed lower energy as compared to the motor with virgin magnet and the same results were reflected in the energy index of the motor. This implies that increasing the converter current and voltage ratings would be better for use in recycled magnet while lowering the lifetime energy .However, it is important to note here that the calculation does not consider any thermal impact

of increasing current which could be significant at higher values of current. The energy index for increasing the converter rating has a higher spread of values lower than 1, compared to increasing the axial length. However, if both the strategies are compared considering thermal impacts the motor with increased axial length has an advantage over increasing the converter rating. The calculation needs further investigation with better knowledge of the magnetic properties of the recycled magnet which are unfortunately not available at present. Nevertheless, it can be concluded that the method captures and reflects on the changes made in the design and can be used to compare different motors. The whole WIRE index can provide a good way to compare the motors recyclability and can be developed further to include more details as per the requirement.

Chapter 5
5 Motor Prototype and Measurement Results

The chapter presents the steps of assembly and measurement results of the prototype motor. The measurements were performed at Aalborg University, Aalborg, Denmark.

5.1. Motor Assembly

5.1.1. Rotor Assembly

Figure 5.1 shows the manufactured 26 poles bonded Halbach ring using Injection molding method described in chapter 2. The material used for manufacturing the ring was Magfine MF18P from Aichi Steel. The design proposed for the Halbach ring was with single ring. However, due to time constraints and large dimensions of ring 26 pieces were manufactured and glued to the rotor back. The use of magnet pieces do not impact the magnetization pattern which is same as the ideal Halbach magnet. Furthermore, use of 26 pieces (1 piece for 1 pole) ensures that the discontinuity is at the points where field is zero and hence, the impact of magnet joints would be negligible.

The flux density of the manufactured Halbach magnet was measured using the setup shown in figure 5.2. The Hall sensor probe was placed at 0.5 mm from the surface of the magnet and the jig was rotated mechanically 360°. The measured flux density in the air is shown in figure 5.3. It can be seen that the flux distribution is very close to an ideal sinusoidal. Furthermore, the calculated values of the flux density can also be seen in the figure. The measured and calculated values have good agreement. According to the datasheet the magnet remanence is in the range of 0.64 T to 0.69 T with PPS binder. From the measurement and calculated results it can be concluded that the final achieved remanence is 0.67 T at room temperature. From the figure it can be seen that at the intersection with X axis the measured value has a small

(a) (b)

Figure 5.1: Pictures of manufactured bonded NdFeB Halbach Ring [11]

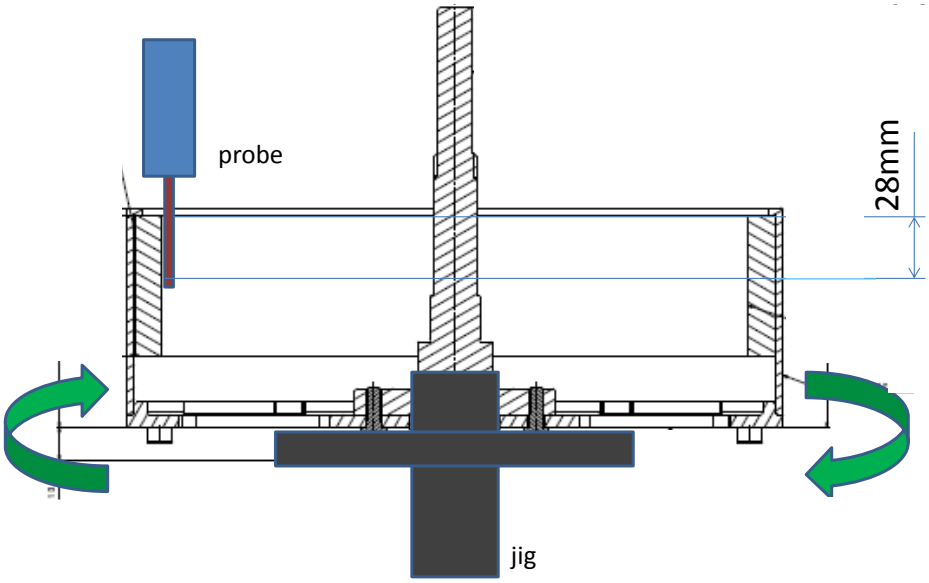

Figure 5.2: Schematic of measurement setup for magnetic flux density in air [11]

glitch due to the use of magnet pieces. Each magnet piece was reduced by certain angle to achieve the ring shape. However, as this size of ring was made for the first time, the gap between the pieces was slightly larger than expected which can be further reduced in the future. Furthermore, the resistivity of the magnet measured using 4 wire method is 177 $\mu\Omega$.m which is higher than the average values of sample measured earlier.

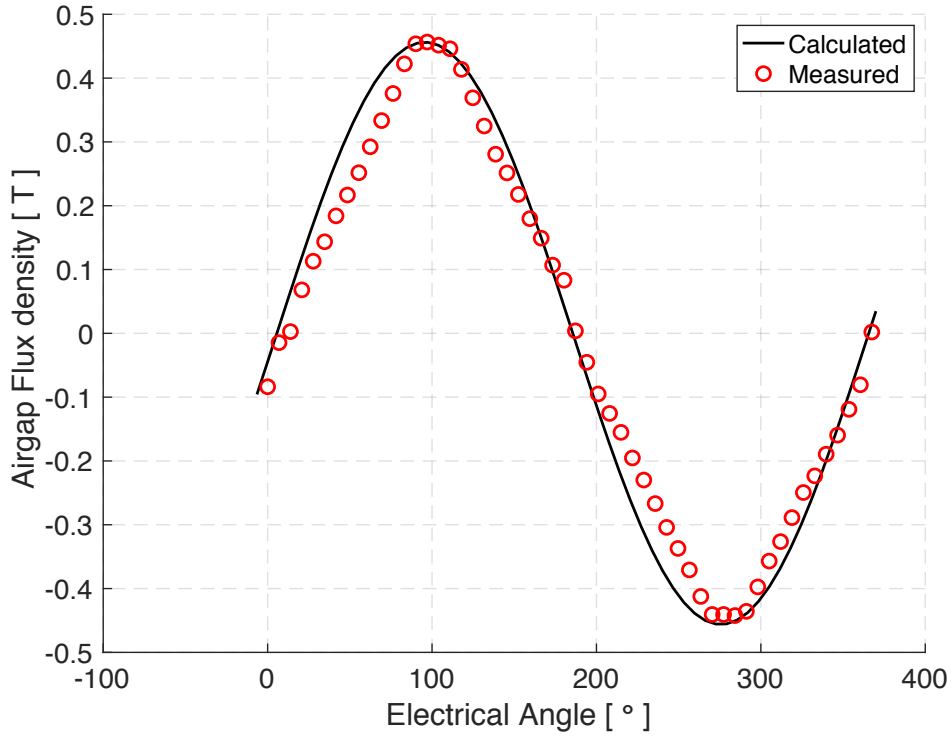

Figure 5.3: Comparison of measured and calculated magnetic flux density at 0.5 mm from magnet surface

5.1.2. Stator Assembly

Different steps in assembly of stator is shown in figure 5.4. The lamination used for stator core was M270-35A of a 0.35 mm thickness sheet. The diameter of the copper wire used for winding was 1 mm. The winding was done manually and the final slot fill factor achieved was 0.59 which is 18 % higher than the value assumed for calculation. The height of the end winding is roughly 25% of the active length of the motor. The average measured resistance of the one coil was 20 mΩ and the calculation showed that approximately a 50 % contribution comes from the end windings. The stator bracket was made of aluminium and fitted to the stator by press fit after machining. As can be seen from the figure the bracket also has water cooling chamber. Finally, the two bearings were fixed in the bracket using press fit. The whole stator assembly was done manually using standard tools.

5.1.3. Stator & Rotor Assembly

Figure 5.5 shows the assembly of the stator and the rotor. The assembly was done using a lathe machine. The final airgap of the motor was 0.4 mm, smaller than the

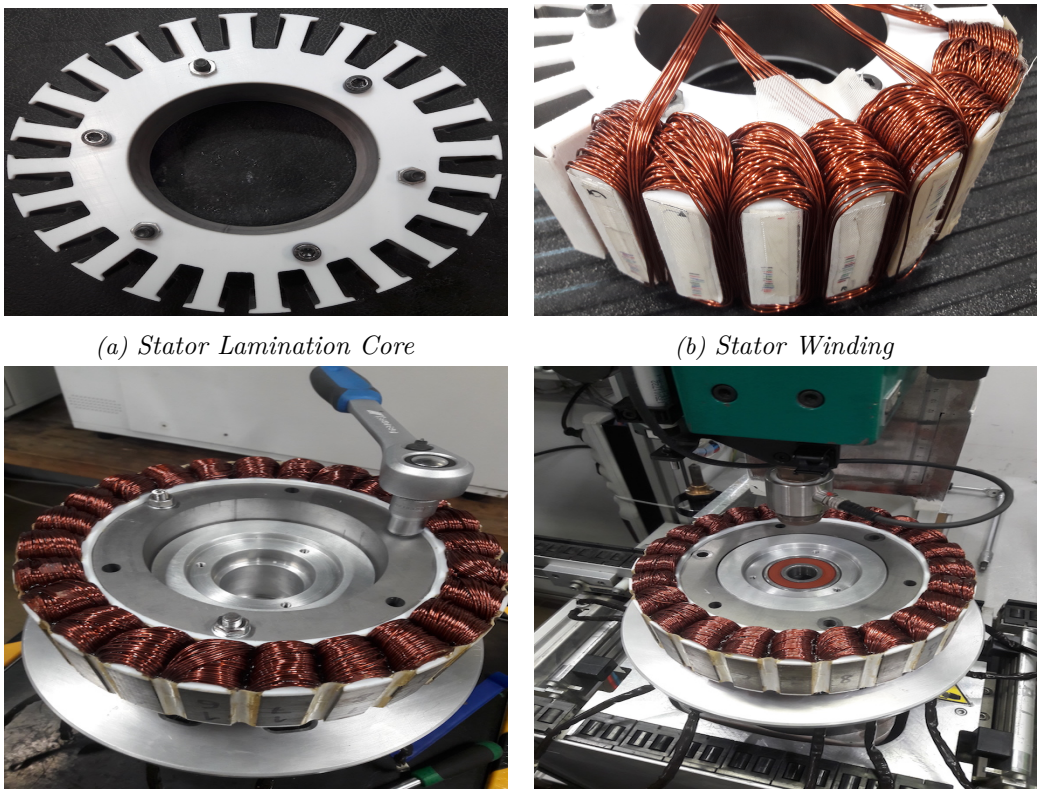

(a) Stator Lamination Core *(b) Stator Winding*

(c) Stator Bracket Assembly *(d) Bearing Assembly*

Figure 5.4: Different steps in stator complete assembly [13]

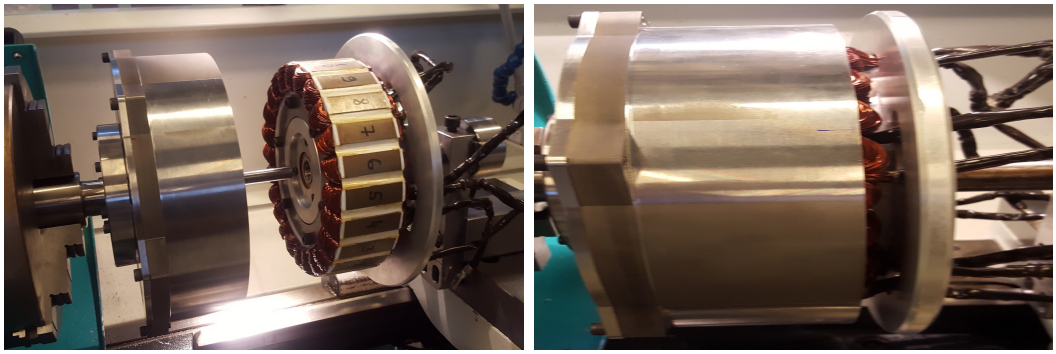

(a) *(b)*

Figure 5.5: Stator and Rotor Assembly

designed dimension due to the tolerances of different parts. The small airgap made the assembly of the stator and the rotor even more delicate. Furthermore, while assembling small vibrations were observed in the rotor. One of the reasons could be a thin rotor back and rotor plate.

5.2. Measurement Results

Measurement of the prototype motor was performed on the set up shown in figure 5.6. The external motor is a PM motor which can be controlled both in torque and speed mode using a suitable control interface. The set up has inbuilt Smart Torque by HBM torque transducer. The transducer can measure upto 500 Nm with ± 0.015 % accuracy.

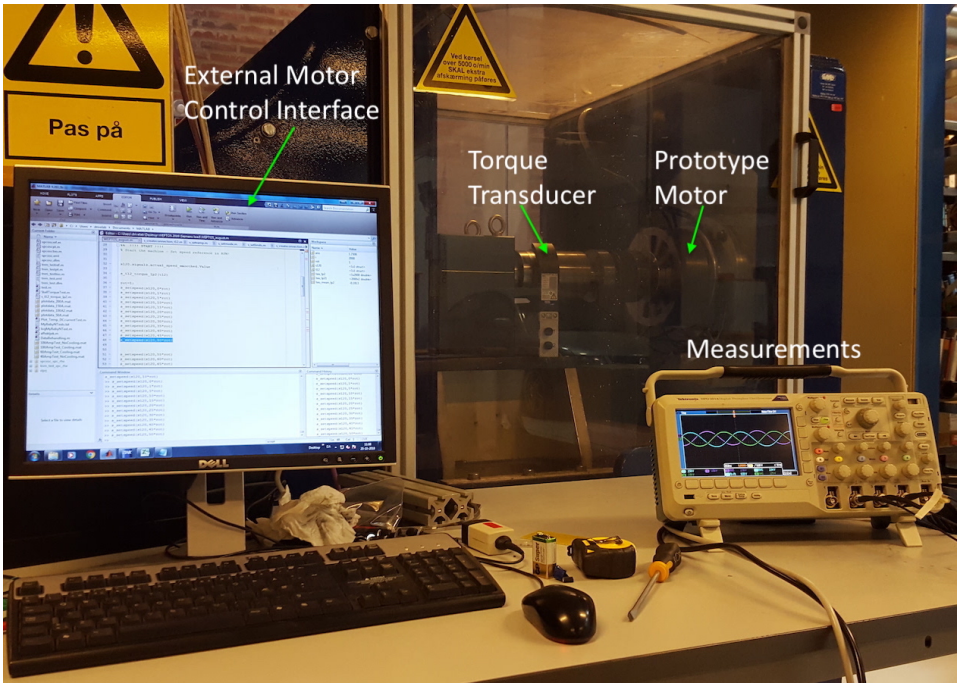

Figure 5.6: Measurement test bench

5.2.1. Winding and Insulation Resistance

Table 5.1 presents the resistance for both winding and insulation measured at room temperature, 25 °C. The winding resistance of each coil was measured using Sefelec MGR10. DC current was supplied and the resistance was calculated from the voltage across the coil. The slight difference between the measured coil resistance could be since the values include the resistance of the connecting wires and each coil had different lengths of connecting cable. The insulation resistance and insulation withstand voltage (Dielectric current) was measured between stack and the winding using Sefelec DXS50. A trapezoidal 500 V DC (10 s ramp up, 10 s steady and 10 s ramp down) was applied to measure the insulation resistance and the insulation dielectric current. The measured values show that the winding insulation and the

Table 5.1: Measured Resistance of winding and insulation of the prototype motor [13]

Coil	Winding Resistance [mΩ]	Insulation Resistance [MΩ]	Insulation Dielectric Current [mA]
A1	20.431	200000	0.13
C1	20.163	200000	0.12
B1	20.779	200000	0.11
A2	21.271	200000	0.08
C2	19.435	200000	0.11
B2	19.493	200000	0.11

creepage distances in the motor were good. No spark was observed during the measurement.

5.2.2. Back EMF (No-Load Test)

The back EMF test was performed by rotating the rotor at constant speed using external motor and measuring the voltage at the motor terminals in open load condition. The schematic of measurement set up at no load is shown in figure 5.7. Figure 5.8 shows the comparison between measured and calculated back EMF of the motor. As expected, the back EMF curves are very sinusoidal and match well with the calculated values. Furthermore, it can also be seen that all the three phases are well balanced.

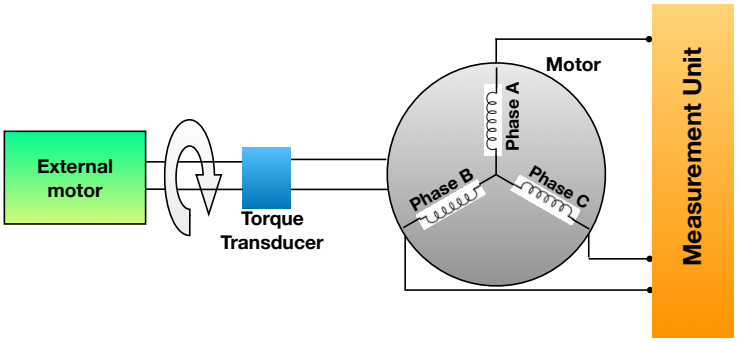

Figure 5.7: Schematic of measurement set up at no load operation

5.2.3. Cogging Torque

The rotor was rotated using an external load machine in no load condition at 1 rpm and the torque was measured. Figure 5.9 shows the measured cogging torque. The measured torque is slightly higher than the calculated value, probably due to the

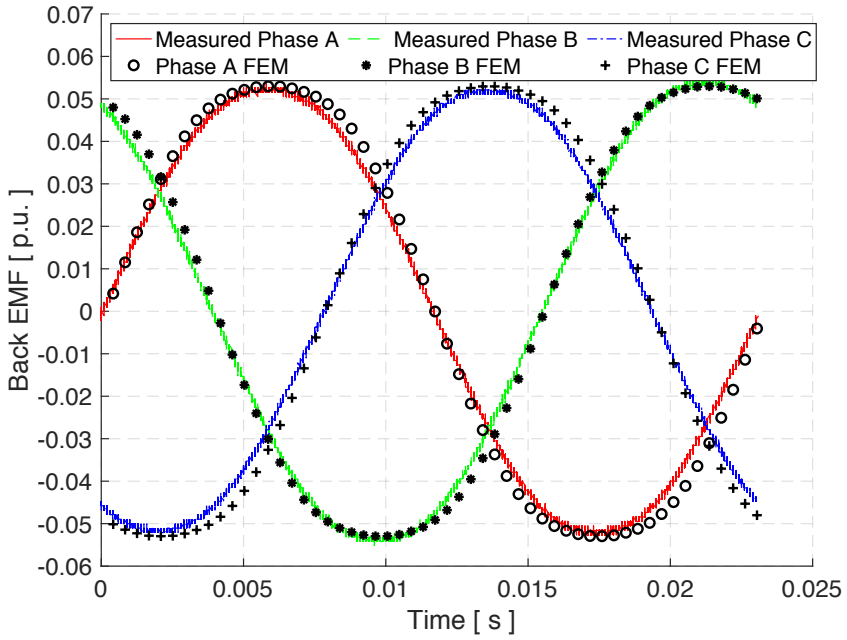

Figure 5.8: Comparison between measured and calculated phase Back EMF

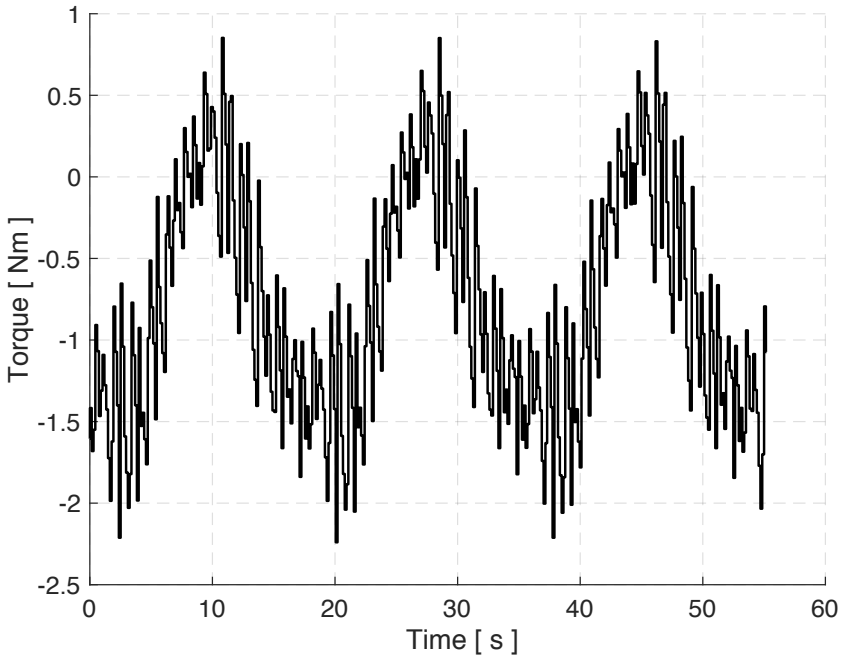

Figure 5.9: Measured cogging torque of the motor

bearing torque. Nevertheless, the torque is very small in magnitude compared to the rated torque of the motor.

5.2.4. Spin Down Test

The test is done to measure the no load losses (iron, magnet and mechanical losses) in the PM motor. The mechanical dynamics of PM motor is given by equation 5.1. The damping torque is caused by the core and other mechanical losses in the motor. Therefore, when electromagnetic and external mechanical torque is made 0, the damping torque can be calculated using equation 5.2 and the loss by equation 5.3.

$$T_{em} = J\frac{d\omega_r}{dt} + T_{damp} - T_{mech} \tag{5.1}$$

$$T_{damp} = -J\frac{d\omega_r}{dt} \tag{5.2}$$

$$P_{loss} = -J.\omega_r\frac{d\omega_r}{dt} \tag{5.3}$$

where, T_{em} is the electromagnetic torque, T_{damp} is the damping torque, T_{mech} is the external mechanical torque, J inertia of the rotating parts and ω_r is the mechanical speed.

Therefore, to measure the no load losses, the motor was spun using an external force in open circuit condition and then the external force was removed. The back EMF of the motor was measured while rotor is left to spin freely till the rotor eventually stops. Using the measured back EMF motor speed was calculated as EMF varies linearly with the speed. Figure 5.10 shows the measured EMF and the angular speed of the spin down test. Because of the vibration observed during the assembly of rotor and stator, the spin down test was done for only low speed.

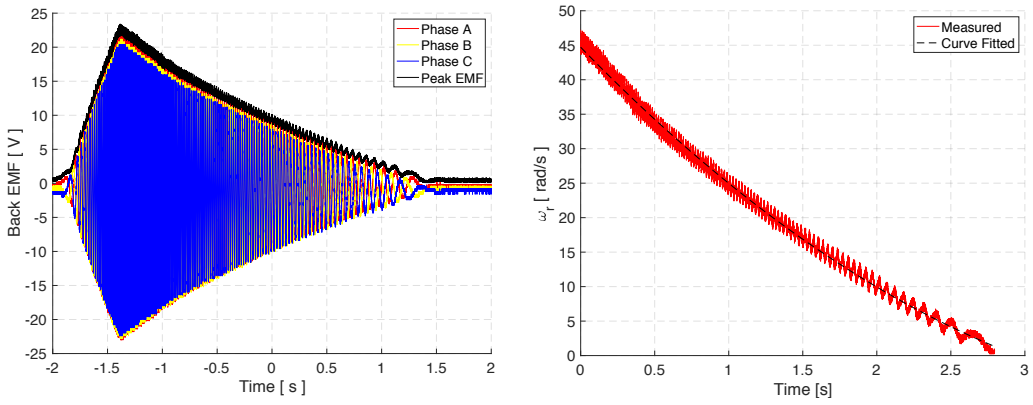

(a) Measured back EMF *(b) Angular speed*

Figure 5.10: Measured Back EMF and speed of the motor without any external torque

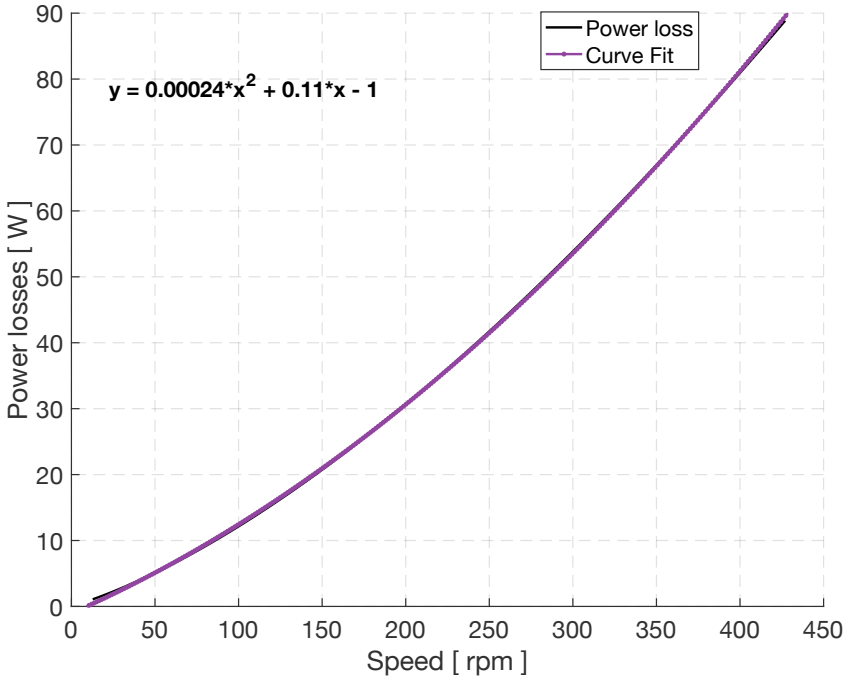

Figure 5.11: No load losses versus speed of the motor

5.2.5. Core and Mechanical Losses

To determine the core and mechanical losses (bearing and friction losses) of the motor, measurements were performed at no load and load (generator mode) conditions.

In no load measurement, the motor was rotated at different speeds using an external motor and the motor shaft torque was measured while motor terminals were open. Figure 5.7 shows the schematic of the measurement set up. The input power (Torque x speed) to the motor at no load should be equal to the losses in the motor i.e. core and mechanical losses. Figure 5.12 shows the power loss in the motor at no load condition and also the quadratic curve fit for the losses. It can be assumed that the core loss of the motor varies with square of the speed and the bearing and windage loss linearly. Therefore, quadratic curve fit match well with measured loss and gives a good motor loss equation (excluding copper loss).

In generator mode, the motor was rotated at different speeds using the external motor and a balanced three phase resistive load were connected to the motor terminal, as shown in the schematic figure 5.13. The power dissipation in the resistive load was measured using power analyser YOKOGAWA WT3000. Thereafter, the core and mechanical loss in the motor was calculated using 5.4.

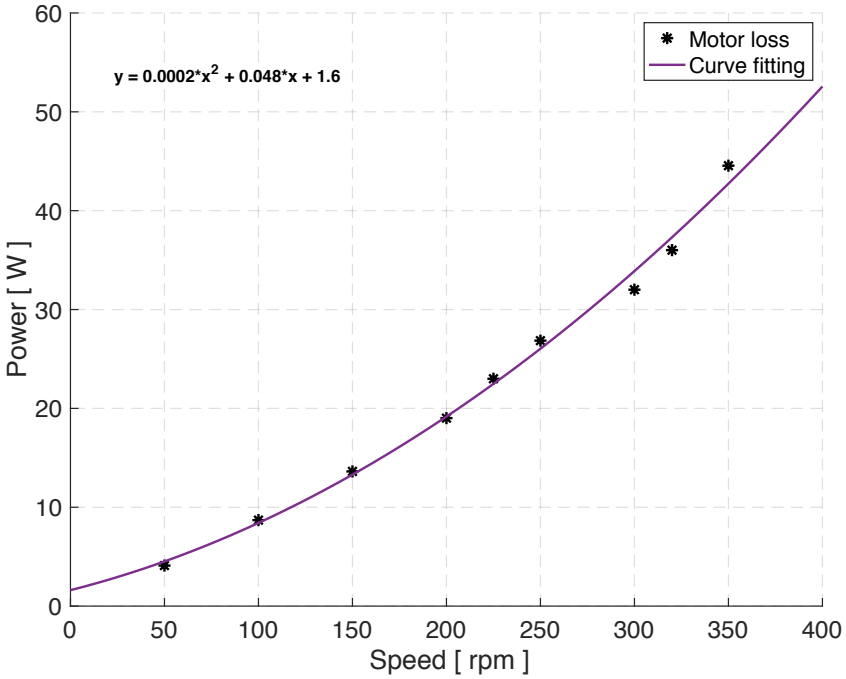

Figure 5.12: Motor loss (core+mechanical loss) in no-load condition at different speeds

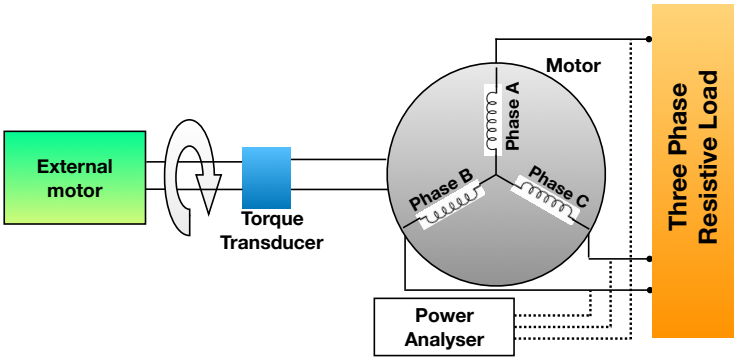

Figure 5.13: Schematic of measurement set up at load condition in generating mode

$$P_{loss} = P_{in} - P_{out} - P_{cu} \tag{5.4}$$

where, P_{loss} is core + mechanical loss, P_{in} is input power, P_{out} is output power and P_{cu} is copper loss in the motor.

Figure 5.14 shows the motor loss at different speeds with two different resistive loads i.e. 1.2 Ω and 5 Ω. The figure also shows the quadratic curve fit of the loss. Comparing the coefficients, it can be seen that the curve coefficients with smaller resistive load i.e. higher motor currents are slightly higher. However, the difference is not very large. Furthermore, the quadratic coefficient of the curve at no load,

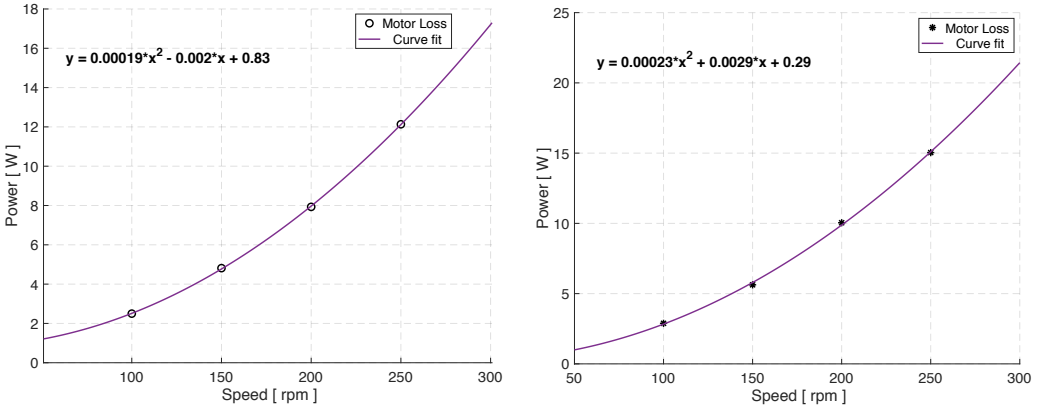

(a) Motor loss with resistive load 5 Ω *(b) Motor loss with resistive load 1.2 Ω*

Figure 5.14: Motor loss (core + mechanical) in generator mode at different speeds

is also similar to the curves at load. While, difference in the linear or constant coefficients are quite large. Similarly, the quadratic coefficient of curve from spin down test, see figure 5.11, is approximately the same and others coefficients have large difference. Based on the coefficients obtained from different measurements curve fit it can be inferred that the mechanical loss is varying in different test depending on the load and operating condition while the core loss variation with speed remains same.

5.2.6. Peak Motor Torque

The electromagnetic torque of a non-salient PM motor is given by equation 5.5. If current is fixed and rotor is rotated the instantaneous torque will depend on the angle α.

$$T_{em} = \frac{3}{2}\frac{p}{2}\left[I\psi_m sin(\alpha)\right] \tag{5.5}$$

where, I is stator current phasor, α is the angle between flux linkage and stator current vector.

Therefore, to fix the current, the motor was supplied with DC current and the windings were connected as shown in figure 5.15b, such that $I_a = I_{max}, I_b = -I_{max}/2, I_c = -I_{max}/2$, where I_a,I_b and I_c are the phase currents and I_{max} is the maximum current amplitude. Figure 5.15a shows the test bench set up for the measurement. The motor torque was measured by slowly rotating the rotor. The rotor was rotated manually using a lever because the external motor could not run lower than 1 rpm and the sampling time of torque transducer was not small enough to measure torque at every rotor position. Figure 5.16 shows the measured torque which is almost following the sinusoidal curve. The time interval is not equal because the rotor

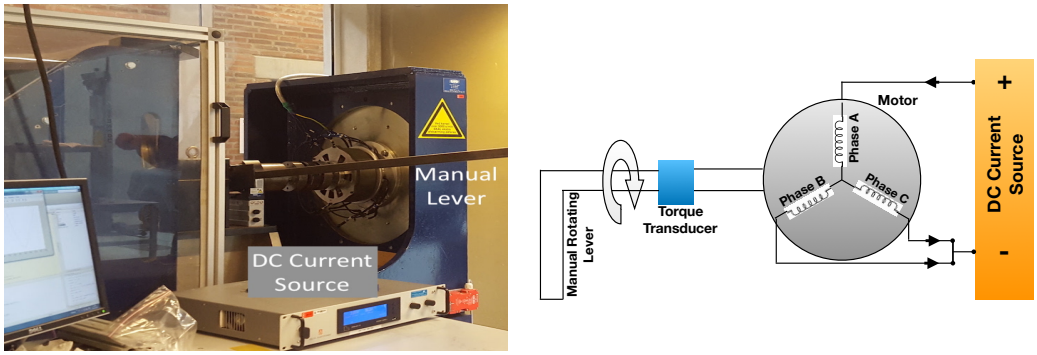

(a) Test bench set up *(b) Schematic of the measurement setup*

Figure 5.15: Test bench and schematic of set up for measurement of peak torque

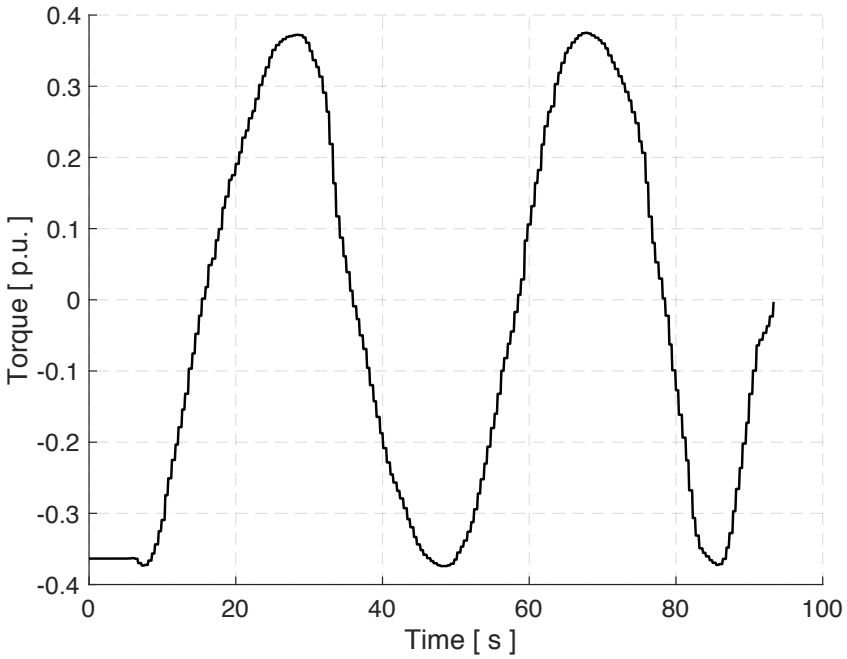

Figure 5.16: Measured peak torque with DC current

was rotated manually the speed of rotation was not constant for the whole cycle. Nonetheless, the peak torque can be measured using this method. Figure 5.17 shows the comparison between measured and calculated torque at different DC currents. The calculated torque values are slightly higher than the measured and one reason could be due to the absence of bearing static friction torque. At lower DC current up to 0.5 p.u. the difference in measured and calculated is lower than 5% as can be seen from the figure. The difference increased at higher currents. The increase in difference was due to two reasons. Firstly, the core was more saturated than in FEM model, which is also visible with the curve deviating slightly from straight line.

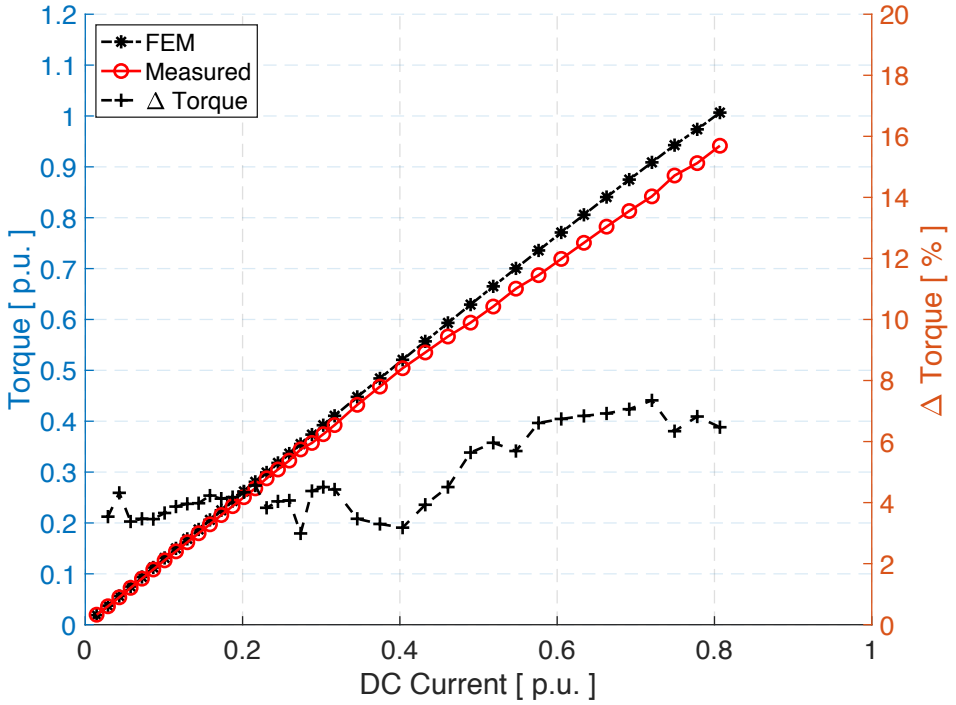

Figure 5.17: Comparison FEM vs Measured torque at different DC currents and % difference

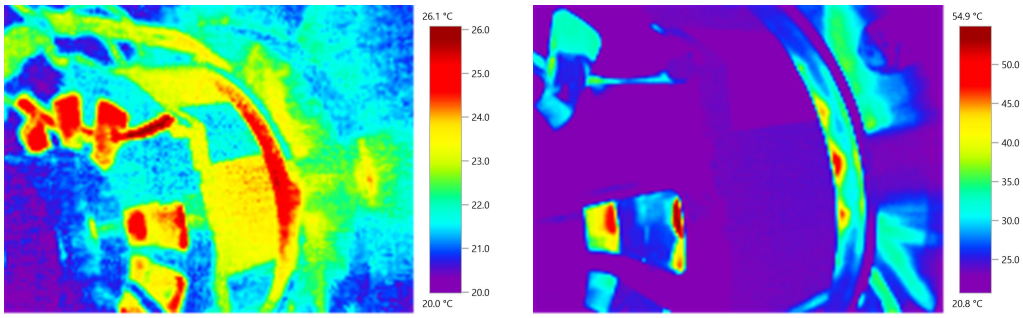

(a) Before *(b) After 30 s*

Figure 5.18: Thermal image of motor before and after 240 A DC current applied

Secondly, with higher currents the motor temperature increased rapidly as shown in figure 5.18 (without cooling). Over the time the magnet temperature also increased which in turn lowered the magnet remanence and hence, the torque. The torque measurement was again performed for 0.58, 0.63 and 0.69 DC p.u. current with cold motor. The measured torque increased to 0.70, 0.76 and 0.83 from 0.69, 0.75 and 0.81 respectively. The motor nominal required torque is around 0.5 p.u., see figure 1.10. From the measured values it can be seen that the torque is increasing linearly up to 0.6 p.u. and hence, no saturation or partial demagnetization should happen for nominal operation.

5.2.7. Motor Inductance

The inductance of the motor was measured using the methodology described in [68] and [34]. The schematic of the measurement set up is shown in figure 5.19a. The rotor was locked in Q position i.e. phase A current was aligned with the rotor Q axis. The single-phase AC voltage was applied and the current was measured. The relation between voltage and current electrical circuit is given by equation 5.6.

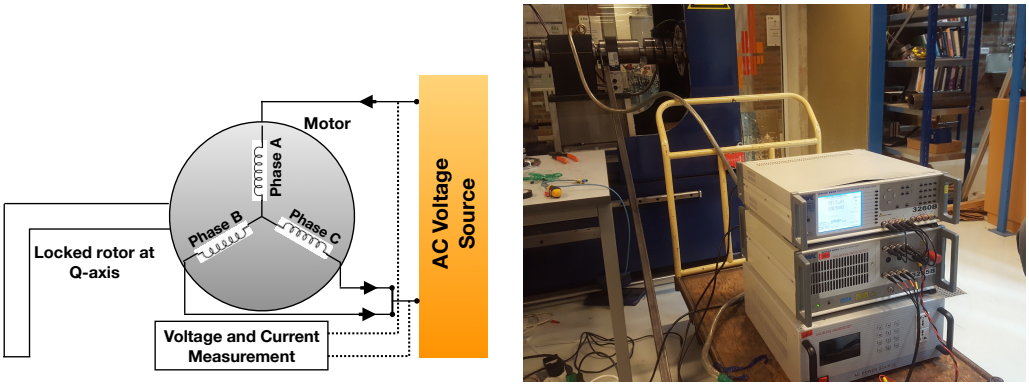

(a) Schematic of Set up 1 *(b) Set up 2*

Figure 5.19: Measurement set ups used to measure motor inductance

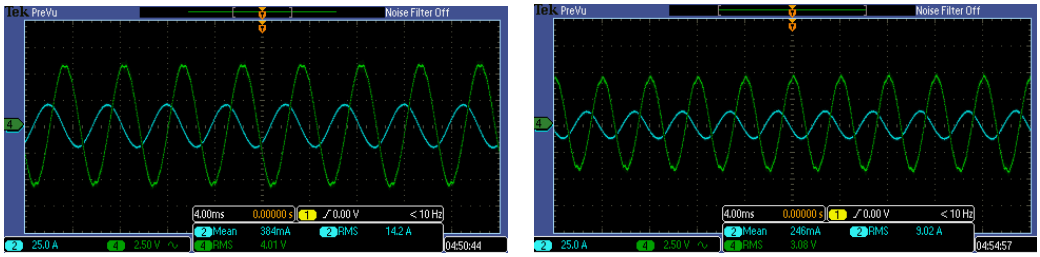

(a) Measurement 1 *(b) Measurement 2*

Figure 5.20: Measured voltage and current

$$V = \frac{3}{2}Ri + \frac{3}{2}L_q\frac{di}{dt} \tag{5.6}$$

where, V is the measured voltage, i is the measured current, L_q is q axis inductance and R is phase resistance.

The average value of the calculated L_q from measured voltage and current values using equation 5.6 is 0.121 mH which is 10% higher than the inductance value calculated using 2D FEM. The difference is due to the end winding inductance which was not included in 2D calculations. To validate the measurement the inductance

was also measured using Precision Magnetics Analyzer in the same set up as shown in the figure 5.19b. The measured value of inductance was 0.121 mH. The measured L_d inductance, by aligning rotor position to d axis, was 0.120 mH. The fact that motor is non-salient the L_q and L_d was expected to be equal.

5.2.8. Temperature Measurement

Temperature in different parts of the motor was measured by supplying constant DC current while connecting all the phases in series. The amplitude of DC current was selected such that it was equal to the maximum RMS current required during nominal operation of the motor. Figure 5.21 shows the measurement set up and the position of thermal sensors.

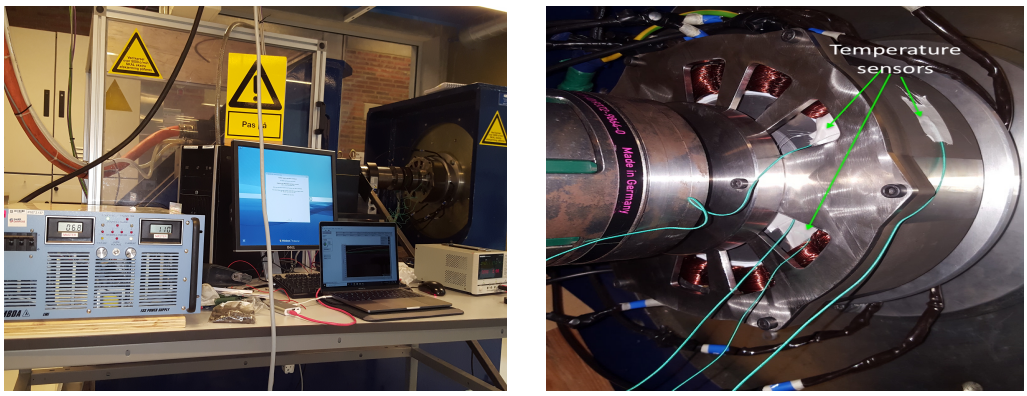

(a) Measurement set up *(b) Sensors position*

Figure 5.21: Temperature measurement set up and position of thermal sensors in the motor

The average temperature of the winding was calculated using equation 5.7 where, R_1 and R_2 were calculated from measured voltage and the current.

$$T_{avg} = \frac{R_2}{R_1}(235 + t_1) - 235 \tag{5.7}$$

where, t_1 is the initial winding temperature in °C, R_1 is the winding resistance at the temperature t_1, R_2 is the winding resistance at the end of the test, T_{avg} is the average winding temperature.

Figure 5.22 shows the measured temperature in different parts of the motor. The average temperature of the winding at the end of test was 136 °C and the temperature at the end winding was 143 °C. The temperature of the other end winding side was 131 °C. The temperature of core and stator bracket were almost equal which suggested that the parts were sufficiently in contact. The temperature of the rotor went up to 90 °C. It is important to note that the measurement was performed without any cooling. Furthermore, the core loss was also not there.

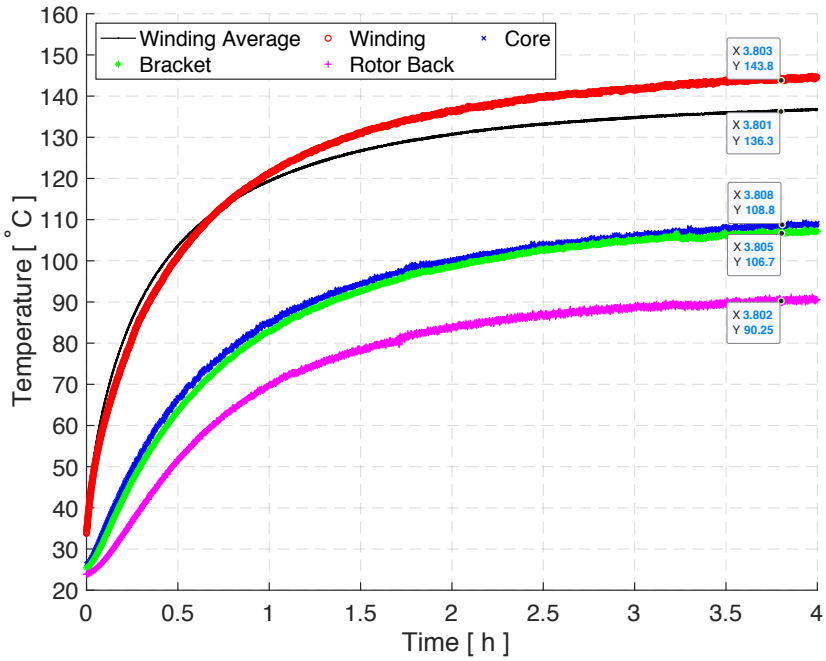

Figure 5.22: Measured temperature in different parts of motor with highest nominal current without cooling

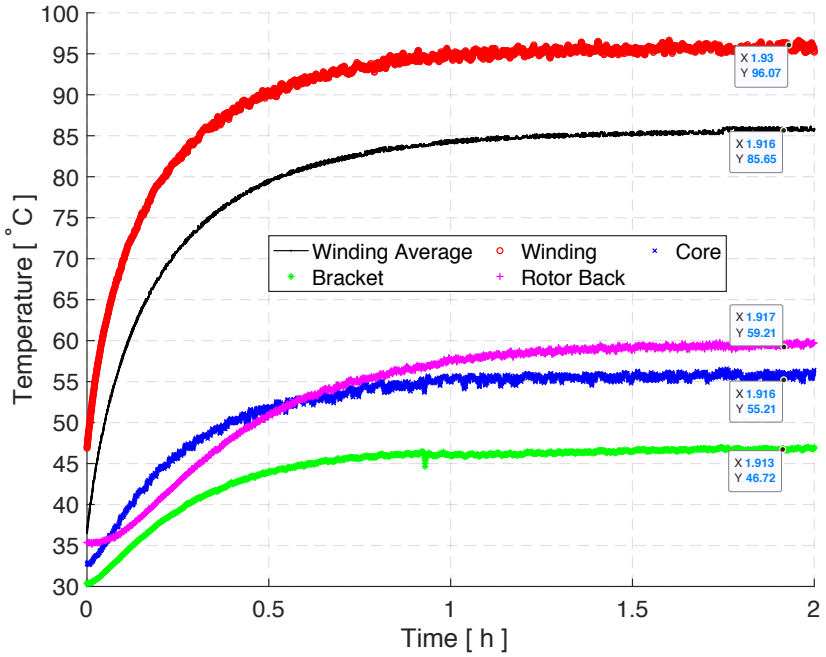

Figure 5.23: Measured temperature in different parts of motor with highest nominal current with water cooling, 2.7 $lmin^{-1}$

Another thermal measurement was performed with water cooling and the flow rate of water was 2.7 $lmin^{-1}$. Figure 5.23 shows the temperature in different parts of the motor with cooling. It can be seen with cooling the end winding temperature was 96 °C and the average winding temperature was 85 °C and the temperature on the other side of the end winding was 83.4 °C. A reduction of 56 °C compared to the temperature without cooling. . The other parts of motor also had similar reduction in steady state temperature. It is interesting to note a temperature difference of 13 °C in the core and the bracket with cooling which was only 2 °C without cooling. It suggests that the gap between bracket and core had increased after thermal measurement without cooling. The rise in temperature in the rotor back with cooling or without cooling was much higher than the expected. It was observed during the measurement that the temperature of the rotor back was different at different positions and the measured temperature was the hottest spot. However, further investigation should be done to understand the variation of temperature in the rotor back and reasons for such temperature increase. From the measured temperatures, heat conduction and convection coefficients were calculated using thermal model presented in section 3.2. The coefficient from the measurement are similar to the coefficients used at design stage.

5.3. Summary

A prototype was manufactured based on the proposed design. The remanence of the Halbach magnet produced using injection molding was higher than the expected value and the airgap flux density was also close to sinusoidal. A high winding fill factor, 0.59, was achieved for stator winding and the coil overhang height was also small. The assembly of all the motor parts was achieved using standard tools. It can be seen from the assembly steps that the process was very simple to achieve and can be done manually except assembly of stator and rotor. The disassembly was also done with defined process. Small vibrations in the rotor back were observed during the stator and rotor assembly. The vibration further amplified during measurements at high speeds. The reason could be thin rotor end plate or rotor back. Furthermore, the rotor assembly was not balanced and that could also aggravate vibration and the noise. Therefore, it is important to analyse motor design mechanically, specially stress and vibration calculations and most probably redesign some parts before performing high speed measurements.

Due to the issue of vibrations and noise at high speeds, the measurements were performed at only low speeds. The winding resistance of all the coils were almost the same and the insulation resistance showed that the motor insulation was suitable for the application. The back EMF measured for all the three phases were balanced and were in good agreement with the calculated values. The measured cogging torque of the motor was slightly higher than the calculated value however it is small as compared to the rated mean torque. Moreover, the measured cogging torque also

include static bearing friction. The no-load losses (iron and core loss) were calculated from spin down test. However, due to non-availability of proper set-up high speed spin down measurements was not done. Nevertheless, the no-load losses obtained from spin down test can be used for high speed (not very high) using extrapolating. The no load and generator mode load test were done to calculate the motor core and mechanical losses. The results showed that the core loss estimated from spin down test are in agreement to the calculated core loss from generator or no-load test. The difference in loss was due to the friction loss (bearing and windage). The fact that motor shaft was vertical during spin down test and horizontal for no-load and generator load test (on the test bench) could change the bearing behaviour. Nevertheless, it can be seen from the loss curves that the friction loss is the dominant part and the reason could be the mechanical issue. The peak torque of the motor was measured using DC current. The measured torque values are in good agreement with the calculated values. The motor has small saturation even at high currents (peak performance). Therefore, optimization of the core can be done and motor weight can be reduced. The inductance of the motor was measured by two different methods and the values are consistent. The measured inductance is 10% higher than the calculated using 2D FEM and the main reason of the difference is the end windings inductance which was not considered in 2D calculation. Finally, temperature measurements were done by supplying a DC current equal to the maximum nominal current with cooling and without cooling. The temperature in different parts were below the limit for both the cases. However, with 3phSC steady current the winding temperature needs to be validated because in real operation additional losses will be present. Some design changes can be made to improve cooling in winding which were not considered in the prototype motor for example using thermally conductive lamination end plates instead of PTFE insulator. The heat coefficients in different parts of the motor are very similar to the values used for design of the motor. Therefore, the lumped thermal model can be used to calculate temperature in different operating conditions.

Chapter 6
6 Conclusion and Future Work

6.1. Conclusion

Permanent magnet motors are the most preferred motors for (H)EVs application due to their high efficiency, low weight and compact design. The primary factor driving the adoption of PM motors is the use of strong magnets like NdFeB or SmCo. The magnetic properties of these magnet are further improved by using heavy REE. The availability of heavy REEs is limited. Hence, recycling is important to maintain a sustainable supply of magnets. Another, challenge in the process of recycling is the extraction of magnet from the motor. Currently, the motors used in vehicles are not designed for easy assembly and disassembly, which not only makes extraction process difficult, but also lowers the quality and yield of the extracted magnet. Therefore, the primary focus of the thesis was to design an outer rotor Halbach motor for (H)EV with easy assembly and disassembly.

The manufacturing of Halbach magnet is complex however, it is shown that Halbach magnet manufactured using bonded NdFeB magnet had almost the ideal sinusoidal field distribution. The magnetic material used for Halbach magnet was Dy free anisotropic bonded NdFeB (MagFine18P) with PPS binder. The characterization of the magnet showed very stable magnetic properties across varying levels of temperature. Further, no mechanical deformation was observed in the magnet sample at high temperatures and it maintained similar magnetic properties at room temperature after cooling. The measured average resistivity of the magnet was around 135 $\mu\Omega$.m which is much higher than the sintered magnet. Additionally, the thermal conductivity of the magnet was 1 $W.m^{-1}.K^{-1}$. The field distribution of sample Halbach magnet was very close to sinusoidal distribution and also matched well with the calculated values. The recycling methods for both sintered and bonded magnet are discussed. It can be inferred that the recycling process of bonded magnets is much shorter and simpler. Furthermore, the results from Aichi Steel for the proposed recycling route of bonded magnet showed that with 70% virgin magnet and 30% old magnet, the new recycled magnet would not lose any significant magnetic

properties. The recycling method is much easier to implement and is environment friendly.

Various parametric studies were performed to finalize the motor design which would meet the specification. It was shown that it was better to use a higher pole number for Halbach magnet rotor. However, the pole number was selected considering converter switching frequency, magnet eddy loss and iron loss in the motor. Furthermore, it was also shown that slot pole combination had a significant impact on the motor torque and loss. The magnet eddy loss reduced with an increase in slot number. To include end winding effect in eddy loss calculation 3D FEM model was used and the results differed significantly as compared to the 2D loss calculation. Higher the D_o/L ratio, higher was the difference between 2D and 3D eddy loss results. The calculated performance of the final proposed design fulfils both electromagnetic as well as mechanical requirements of the motor. The Halbach magnet motor had approximately 22% higher torque than the conventional SMPM motor with same slot pole combination, magnet volume and grade. In addition, due to the use of an ideal Halbach magnet rotor, the motor had very low cogging torque and higher order harmonic content. The thermal calculation using lumped model showed that the temperature in different parts of the motor was within the defined limits during continuous operation. However, the temperature of magnet as well as the windings reached a critical limit for the steady state 3phSC operation at maximum speed. Since, the occurrence of this event is very unlikely it was decided to proceed without any design modification. The demagnetization study of the motor showed negligible irreversible demagnetization. The knee of the magnetic curve is not very distinct for the magnet. However, the recoil curves are very close and hence, for partial demagnetization, the magnet should not lose remanence when the field is removed. Motor torque speed characteristic with recycled magnet was also investigated. At present, the remanence of recycled magnet reported in literature is varying from 0 - 20% and hence, 4 different recycled magnet i.e 5%, 10%, 15% and 20% lower remanence were studied. It was found that when the recycled magnet has upto 5% lower remanence the supply current could be increased to achieve the same torque speed characteristic of the motor. However, for even lower remanence the increase in current is much higher and would have severe thermal impact on the motor. For such cases, similar motor performance could be achieved with change in design like increasing axial length or increasing the outer diameter of the motor. Implementing either of the changes will not degrade (rather increase) the thermal performance of the motor. However, increasing axial length is more apt considering manufacturing of Halbach magnet as neither thickness nor diameter of the ring would change, provided space is not a constraint. In situations where space as well as converter rating change is not possible, inner diameter of the magnet could be changed by using a thicker magnet. The results showed that this method could be used for up to 10% lower remanence and for a higher reduction the motor would not be able to fulfil the torque requirement at higher speeds.

In the thesis, a method called WIRE was developed to benchmark different motor

designs based on their recyclability and energy cost. The method could be used during the design phase of the motor. The evaluation of the proposed design was done using the WIRE approach. It was demonstrated that the rotor assembly of the proposed design could be done without the use of glue. The absence of glue also made the extraction of magnet very easy. Furthermore, the impact of the recycled magnet on the energy cost of the motor was calculated. It was shown that the index mainly depended on the price of both the recycled and virgin magnets due to the fact that energy consumption is almost the same for both magnets. The index also showed the situations where it would be viable to use recycled magnets considering the energy cost of the motor during its life time.

Finally, based on the designed motor a prototype was built and measurements were performed to characterise the motor. The assembly and disassembly was done manually using standard tools with ease. The winding resistance of the motor was well balanced and no failure was observed in the insulation. The back EMF of the motor is in very good agreement with the calculated values. Moreover, the measured EMF was balance and sinusoidal for all the three phases. The peak torque measurements were also done using DC current. The difference in calculated and measured peak torque of the motor is below 5 % for all the currents. Furthermore, it can be deduced that the level of saturation in the iron core is small and hence, there is a good scope for the optimization. The thermal measurements showed that the motor can easily withstand the nominal operation with or without cooling. Therefore, the electromagnetic performance of the prototype is in expected range compared to the calculated design. However, some mechanical issues were observed while assembling and testing of the motor which limited the measurements speed up to only 400 rpm. The mechanical design of the motor needs further investigation. Additionally, the cooling of the motor can also be improved by making some changes in the material used which will further improve the motor performance.

6.2. Future Work

Following are the suggestions for the future work that can be performed.

- The primary cost incurred in the manufacturing of bonded Halbach magnet is tooling cost for new mold and fixture. A further investigation could be made to make this process more adaptable to different designs and to optimize cost. Additionally, due to time constraint and complex manufacturing of large size Halbach cylinder, the prototype was made with 26 pieces (26 poles). The single piece cylinder could make the rotor assembly glue free hence, it would be worth investigating the challenges in terms of technology and production costs of large magnet Halbach rings.
- Recycling methods for bonded magnets require some experimental validation. Furthermore, it would be interesting to know the ratio of new to old magnets

which would make the resultant recycled magnet unsuitable for motors and analyse the trends in magnet properties across varying levels of the mix ratio. Other routes of recycling also need further investigation.

- The motor was designed using Design of Experiments method by FEM tool. It would be interesting to run other optimization algorithms on the motor and compare the resulting designs.
- The motor was mainly designed with a double layer to avoid a higher magnetic eddy loss. However, since the magnet prototype resistivity was much higher, single layer could be used in the stator which would make the winding easy and improve the fill factor. Additionally, 24 slot 26 poles can have a single layer winding and therefore, the measurements could be performed on the motor after stator rewinding. This would be economical as the production of a new rotor is not required.
- The motor design was finalised based on the electromagnetic calculations. However, during assembly and measurements mechanical issues, mostly related to assembly of the motor, were observed. Therefore, a detailed mechanical design study must be done.
- The WIRE methodology developed in the project is at a very early stage and requires further development. The scoring guideline can be made more objective by taking feedback from different organizations, both motor as well as magnet manufactures, on different processes. Further, once recycled magnets are available, using the proposed design changes in the motor like increasing axial length or increasing supply current, energy consumption can be measured for the prototype. It would be very interesting to see the impact of recycled magnet on the overall energy consumption for the drive cycle. The measurement results can be further used to improve calculation of both the indices of the WIRE method.

Bibliography

[1] Internaltion Energy Agency, Ed., *Global EV Outlook 2017*, 2017.

[2] EURARE. http://www.eurare.eu/about.html.

[3] European Training Network for the Design and Recycling of Rare-Earth Permanent Magnet Motors and Generators in Hybrid and Full Electric Vehicles (DEMETER). https://etn-demeter.eu.

[4] LE VEHICULE ELECTRIQUE PAR CEUX QUI LE CONCOIVENT. http://www.vedecom.fr.

[5] J. Larminie and J. Lowry, *Electric Vehicle Technology Explained.* Wiley, 2004, https://books.google.fr/books?id=bEOZL8f1NacC.

[6] M. Rilla, "Design of salient pole pm synchronous machines for a vehicle traction application – analysis and implementation," Ph.D. dissertation, Acta Universitatis,Lappeenranta University of Technology, 2012.

[7] J. de Santiago, H. Bernhoff, B. Ekergård, S. Eriksson, S. Ferhatovic, R. Waters, and M. Leijon, "Electrical Motor Drivelines in Commercial All-Electric Vehicles: A Review," *IEEE Transactions on Vehicular Technology*, vol. 61, no. 2, pp. 475–484, Feb 2012.

[8] Bonded Magnet Materials and Processing Options. http://www.magnetapplications.com/tech-center/tech-briefs/view/34/bonded-magnet-materials-and-processing-options.

[9] F. Mandil and S. Rivoirard, "Aichi bonded magnets Bulk and Halbach cylinder," Neel Institute,Grenoble, France. Internal communication.

[10] A. Walton. Recycling of rare earth earth materials. https://ec.europa.eu.

[11] "Internal Communication with Aichi Steel ," https://www.aichi-steel.co.jp.

[12] P. Upadhayay, A. Garcia, Z. Li, A. K. Jha, P. O. Rasmussen, A. Kedous-Lebouc, and J.-C. Mipo, "Evaluation of Energy Cost Index for an Electric Vehicle Motor over a particular Drive Cycle with Recycled Magnet Concept," in *XXIII rd International Conference on Electrical Machines (ICEM'2018)*, September 2018, pp. 1–7.

[13] "Internal Communication with Valeo Electrical, Creteil, France ," https://www.valeo.com/en/.

[14] Top 10 best-selling electric vehicles in 2017. http://www.chinadaily.com.cn/a/201802/08.

[15] C. C. Chan, "The State of the Art of Electric, Hybrid, and Fuel Cell Vehicles," *Proceedings of the IEEE*, vol. 95, no. 4, pp. 704–718, April 2007.

[16] K. Chau and W. Li, "Overview of electric machines for electric and hybrid vehicles," *International Journal of Vehicle Design*, vol. 64, no. 1, pp. 46–71, January 2014.

[17] Countries are announcing plans to phase out petrol and diesel cars. Is yours on the list? https://www.weforum.org/agenda/2017/09/countries-are-announcing-plans-to-phase-out-petrol-and-diesel-cars-is-yours-on-the-list/.

[18] T. Elwert, D. Goldmann, F. Römer, M. Buchert, C. Merz, D. Schueler, and J. Sutter, "Current Developments and Challenges in the Recycling of Key Components of (Hybrid) Electric Vehicles," *Recycling*, vol. 1, no. 1, pp. 25–60, 2015, http://www.mdpi.com/2313-4321/1/1/25.

[19] L. Kumar and S. Jain, "Electric propulsion system for electric vehicular technology: A review," *Renewable and Sustainable Energy Reviews*, vol. 29, no. Supplement C, pp. 924 – 940, 2014, http://www.sciencedirect.com/science/article/pii/S1364032113006734.

[20] EUROPEAN RARE EARTHS COMPETENCY NETWORK (ERECON), Ed., *Strenghthening of the European Rare Earths Supply Chain*, 2015.

[21] Magnet Materials Comparison Guide. https://www.duramag.com/techtalk/tech-briefs.

[22] Neodymium Iron Boron vs. Samarium Cobalt. http://www.mceproducts.com/Knowledge_Base/Articles.

[23] K. Binnemans, P. T. Jones, T. Müller, and L. Yurramendi, "Rare Earths and the Balance Problem: How to Deal with Changing Markets?" *Journal of Sustainable Metallurgy*, vol. 4, no. 1, pp. 126–146, Mar 2018, https://doi.org/10.1007/s40831-018-0162-8.

[24] U. Bast, R. Blank, M. Buchert, T. Elwert, F. Finsterwalder, G. Hornig, T. Klier, S. Langkau, F. Marscheider-Weidemann, J.-O. Muller, C. Thurigen, F. Treffer, and T. Walter, "Recycling von Komponenten und strategischen Metallen aus elektrischen Fahrantrieben," Aug-2014.

[25] A. K. Jha, L. Garbuio, A. Kedous-Lebouc, J. P. Yonnet, and J. M. Dubus, "Design and comparison of outer rotor bonded magnets Halbach motor with different topologies," in *2017 15th International Conference on Electrical Machines, Drives and Power Systems (ELMA)*, June 2017, pp. 6–10.

[26] A. K. Jha, A. Kedous-Lebouc, L. Garbuio, J. P. Yonnet, and J. M. Dubus, "FEA based analysis on effect of slot pole combination on motor torque and magnet eddy current loss with bonded NdFeB Halbach rotor," in *2017 20th International Conference on Electrical Machines and Systems (ICEMS)*, Aug 2017, pp. 1–5.

[27] A. K. Jha, Z. Li, A. Garcia, P. Upadhayay, P. O. Rasmussen, A. Kedous-Lebouc, and L. Garbuio, "Weighted Index of Recycling and Energy (WIRE) Cost for Motors in Electric Vehicles," in *2018 International Symposium on Power Electronics, Electrical Drives, Automation and Motion (SPEEDAM)*, June 2018, pp. 1–5.

[28] A. Garcia, A. K. Jha, Z. Li, , P. Upadhayay, and P. O. Rasmussen, "Validation of Efficiency Maps of an Outer Rotor Surface Mounted Permanent Magnet Machine for Evaluation of Recyclability of Magnets," in *Intermag 2018*, April 2018.

[29] A. K. Jha, A. Kedous-Lebouc, L. Garbuio, J. P. Yonnet, and J. M. Dubus, "Electric Vehicle Motor Designed for Recycling with High Torque Density And Efficiency," *IEEE Transactions on Vehicular Technology,(Submitted)*.

[30] S. M. Lukic and A. Emadi, "Effects of drivetrain hybridization on fuel economy and dynamic performance of parallel hybrid electric vehicles," *IEEE Transactions on Vehicular Technology*, vol. 53, no. 2, pp. 385–389, March 2004.

[31] Z. Rahman, K. L. Butler, and M. Ehsani, "A Comparison Study Between Two Parallel Hybrid Control Concepts," in *SAE Technical Paper*. SAE International, 03 2000, https://doi.org/10.4271/2000-01-0994.

[32] D. Richard and Y. Dubel, "Valeo StARS Technology: A Competitive Solution for Hybridization," in *2007 Power Conversion Conference - Nagoya*, April 2007, pp. 1601–1605.

[33] World's Top 10 Best-Selling Electric Vehicles. https://autowise.com/worlds-top-10-best-selling-electric-vehicles/.

[34] F. Meier, "Permanent-Magnet Synchronous Machines with Non-Overlapping Concentrated Windings for Low-Speed Direct-Drive Applications," Ph.D. dissertation, KTH, Electrical Machines and Power Electronics, 2008, qC 20100826.

[35] K. Halbach, "Design of permanent multipole magnets with oriented rare earth cobalt material," *Nuclear Instruments and Methods*, vol. 169, pp. 1–10, Feb. 1980, http://adsabs.harvard.edu/abs/1980NucIM.169....1H.

[36] E. Potenziani, II, H. A. Leupold, and D. J. Basarab, "A novel self-shielding permanent-magnet rotor assembly," *Journal of Applied Physics*, vol. 64, p. 5986, Nov. 1988, http://adsabs.harvard.edu/abs/1988JAP....64.5986P.

[37] K. Atallah and D. Howe, "The application of Halbach cylinders to brushless AC servo motors," *IEEE Transactions on Magnetics*, vol. 34, no. 4, pp. 2060–2062, Jul 1998.

[38] Z. Q. Zhu, Z. P. Xia, K. Atallah, G. W. Jewell, and D. Howe, "Integrated design of magnet powder aligning system and brushless motor using anisotropic Halbach cylinders," in *1999. Ninth International Conference on Electrical Machines and Drives (Conf. Publ. No. 468)*, 1999, pp. 123–127.

[39] Z. Q. Zhu and D. Howe, "Halbach permanent magnet machines and applications: a review," *IEE Proceedings - Electric Power Applications*, vol. 148, no. 4, pp. 299–308, Jul 2001.

[40] Z. Q. Zhu, "Recent Development of Halbach Permanent Magnet Machines and Applications," in *2007 Power Conversion Conference - Nagoya*, April 2007, pp. K–9–K–16.

[41] J. Ofori-Tenkorrang and J. H. Lang, "A comparative analysis of torque production in Halbach and conventional surface-mounted permanent-magnet synchronous motors," in *Industry Applications Conference, 1995. Thirtieth IAS Annual Meeting, IAS '95., Conference Record of the 1995 IEEE*, vol. 1, Oct 1995, pp. 657–663 vol.1.

[42] M. Marinescu and N. Marinescu, "New concept of permanent magnet excitation for electrical machines: analytical and numerical computation," *IEEE Transactions on Magnetics*, vol. 28, no. 2, pp. 1390–1393, Mar 1992.

[43] M. Galea, L. Papini, H. Zhang, C. Gerada, and T. Hamiti, "Demagnetization Analysis for Halbach Array Configurations in Electrical Machines," *IEEE Transactions on Magnetics*, vol. 51, no. 9, pp. 1–9, Sept 2015.

[44] Z.Q.Zhu, Z. P. Xia, K. Atallah, G. W. Jewell, and D. Howe, "Powder alignment system for anisotropic bonded NdFeB Halbach cylinders," *IEEE Transactions on Magnetics*, vol. 36, no. 5, pp. 3349–3352, Sep 2000.

[45] S. Hogberg, "Design for Direct Reuse of Rare Earth Permanent Magnets," Ph.D. dissertation, Department of Electrical Engineering,Center for Electric Power and Energy (CEE), 2016-10-31.

[46] E. A. Perigo, S. C. da Silva, R. V. Martin, H. Takiishi, and F. J. G. Landgraf, "Properties of hydrogenation-disproportionation-desorption-recombination NdFeB powders prepared from recycled sintered magnets," *Journal of Applied Physics*, vol. 111, no. 7, p. 07A725, 2012, https://doi.org/10.1063/1.3677761.

[47] S. Högberg, J. Holbøll, N. Mijatovic, B. B. Jensen, and F. B. Bendixen, "Direct Reuse of Rare Earth Permanent Magnets Coating Integrity," *IEEE Transactions on Magnetics*, vol. 53, no. 4, pp. 1–9, April 2017.

[48] O. Diehl, E. Brouwer, A. Buckow, R. Gauß, and O. Gutfleisch, "Efficient Recycling of Rare Earth Permanent Magnets," *Laboratory Journal – Business Web for Users in Science and Industry*, January 2016, https://www.laboratory-journal.com.

[49] T. Elwert, D. Goldmann, F. Roemer, and S. Schwarz, "Recycling of ndfeb magnets from electric drive motors of (hybrid) electric vehicles," *Journal of Sustainable Metallurgy*, vol. 3, no. 1, pp. 108–121, Mar 2017.

[50] Y. Yang, A. Walton, R. Sheridan, K. Güth, R. Gauß, O. Gutfleisch, M. Buchert, B.-M. Steenari, T. Van Gerven, P. T. Jones, and K. Binnemans, "Ree recovery from end-of-life ndfeb permanent magnet scrap: A critical review," *Journal of Sustainable Metallurgy*, vol. 3, no. 1, pp. 122–149, Mar 2017, https://doi.org/10.1007/s40831-016-0090-4.

[51] Y. Yamagata and F. Yamashita, "Method of recovering and recycling magnetic powder from rare earth bond magnet," Mar. 18 2003, http://www.google.com/patents/US6533837.

[52] T. Terada, H. Onishi, Y. Yamagata, and F. Yamashita, "Method of producing recycled raw material powder for use in bonded magnet and method of recycling bonded magnet," Jul. 29 2003, http://www.google.com/patents/US6599450.

[53] A. M. EL-Refaie, "Fractional-Slot Concentrated-Windings Synchronous Permanent Magnet Machines: Opportunities and Challenges," *IEEE Transactions on Industrial Electronics*, vol. 57, no. 1, pp. 107–121, Jan 2010.

[54] P. Salminen, "Fractional slot permanent magnet synchronous motors for low speed applications," Ph.D. dissertation, Lappeenranta University of Technology, Electrical Engineering, Physics, 2004.

[55] Z. P. Xia, Z. Q. Zhu, and D. Howe, "Analytical magnetic field analysis of Halbach magnetized permanent-magnet machines," *IEEE Transactions on Magnetics*, vol. 40, no. 4, pp. 1864–1872, July 2004.

[56] A. M. El-Refaie, T. M. Jahns, and D. W. Novotny, "Analysis of surface permanent magnet machines with fractional-slot concentrated windings," *IEEE Transactions on Energy Conversion*, vol. 21, no. 1, pp. 34–43, March 2006.

[57] N. Bianchi, S. Bolognani, M. D. Pre, and G. Grezzani, "Design considerations for fractional-slot winding configurations of synchronous machines," *IEEE Transactions on Industry Applications*, vol. 42, no. 4, pp. 997–1006, July 2006.

[58] D. Ishak, Z. Q. Zhu, and D. Howe, "Eddy-current loss in the rotor magnets of permanent-magnet brushless machines having a fractional number of slots per pole," *IEEE Transactions on Magnetics*, vol. 41, no. 9, pp. 2462–2469, Sept 2005.

[59] D.Ishak, Z. Q. Zhu, and D. Howe, "Comparison of PM brushless motors, having either all teeth or alternate teeth wound," *IEEE Transactions on Energy Conversion*, vol. 21, no. 1, pp. 95–103, March 2006.

[60] J. A. Walker, D. G. Dorrell, and C. Cossar, "Flux-linkage calculation in permanent-magnet motors using the frozen permeabilities method," *IEEE Transactions on Magnetics*, vol. 41, no. 10, pp. 3946–3948, Oct 2005.

[61] W. L. Soong and T. J. E. Miller, "Practical field-weakening performance of the five classes of brushless synchronous AC motor drive," in *1993 Fifth European Conference on Power Electronics and Applications*, Sept 1993, pp. 303–310 vol.5.

[62] A. M. El-Refaie, T. M. Jahns, P. J. McCleer, and J. W. McKeever, "Experimental verification of optimal flux weakening in surface PM Machines using concentrated windings," *IEEE Transactions on Industry Applications*, vol. 42, no. 2, pp. 443–453, March 2006.

[63] C. Sadarangani, *Electrical Machines: Design and Analysis of Induction and Permanent Magnet Motors*. Division of Electrical Machines and Power Electronics, School of Electrical Engineering, Royal Inst. of Technology, 2006, https://books.google.fr/books?id=FZsGcgAACAAJ.

[64] P. Ponomarev, "Tooth-Coil Permanent Magnet Synchronous Machine Design for Special Applications," Ph.D. dissertation, Lappeenranta University of Technology, Electrical Engineering, Physics, 2013-10-24.

[65] N. Bianchi, S. Bolognani, and E. Fomasiero, "A General Approach to Determine the Rotor Losses in Three-Phase Fractional-Slot PM Machines," in *2007 IEEE International Electric Machines Drives Conference*, vol. 1, May 2007, pp. 634–641.

[66] S. Ruoho, "Modeling demagnetization of sintered NdFeB magnet material in time-discretized finite element analysis," Ph.D. dissertation, Aalto University, Electrical engineering, 2011.

[67] P. Lazari, J. Wang, and L. Chen, "A Computationally Efficient Design Technique for Electric-Vehicle Traction Machines," *IEEE Transactions on Industry Applications*, vol. 50, no. 5, pp. 3203–3213, Sept 2014.

[68] K. Lu, M. Vetuschi, P. O. Rasmussen, and A. E. Ritchie, "Determination of high-frequency$d$- and$q$-axis inductances for surface-mounted permanent-magnet synchronous machines," *IEEE Transactions on Instrumentation and Measurement*, vol. 59, no. 9, pp. 2376–2382, Sept 2010.

Appendix A

A WIRE Evaluation Sheets

The appendix presents the evaluation sheet of the proposed motor design in the thesis for material, assembly and disassembly. As mentioned in the chapter 4 many process are clubbed together to simplify the evaluation. However, if required the process can be expanded easily.

MOTOR ID	Halbach motor										
Component/ Parts			Standard				Cost				Recyclability SCORE
		Remarks	S	I	SxI	Remarks	S	I	SxI	Remarks	
Materials											
- Stator											
	Lamination S	segmented stator	5	5	25	good for recycle not reuse	1	5	5		30
	Copper	AWG 24	5	5	25		2	2	4		29
- Rotor											0
	Steel R	MS steel	5	5	25	good for recycle not reuse	1	3	3		28
	Magnets	NdFeB-halbach	3	2	6	Halbach cylinder	4	2	8	bonded magnet	14
-Shaft											0
	Shaft	Steel	4	5	20	standard shaft	1	2	2	same for all motors	22
-Endshileds											0
	Drive Side	aluminium die cast	2	5	10	prepare new die	1	2	2	same for all motors	12
	Non-Drive side	aluminium die cast	2	5	10	prepare new die	1	2	2	same for all motors	12
				32	121			18	26		147
	section score				75.63 %				28.89 %		

Figure A.1: Recyclability index for Material of Halbach Motor

Component/ Parts			Standard				Cost				Recyclability SCORE
		Remarks	Score	Imp.	F.S.	Remarks	Score	Imp.	F.S.	Remarks	
Assembly											
- Stator											0
	Lamination S	standard lamination	5	3	15	standard lamination assembly	4	3	12	standard	27
	Copper winding	Standard circular strand	4	3	12	semi automatic winding process	4	3	12	semi automatic winding process	24
- Rotor											0
	Steel R	MS steel	5	3	15	solid rotor	4	3	12	standard	27
	Magnets with glue	NdFeB-full halbach ring	2	5	10	highly magnetized magnetswith high	3	3	9	injection mold magnet	19
-Shaft											0
	Shaft	Steel	5	3	15	single solid piece	4	3	12	standard no holes	27
-Endshileds											0
	Drive Side	aluminium die cast	4	3	12	For assembly okay	4	3	12		24
	Non-Drive side	aluminium die cast	4	3	12		4	3	12		24
- Assembly of rotor and stator			2	3	6	Stong forces and outer rotor so complex	3	3	9	need extra tool to proper aligning of the stator and rotor	15
											0
Wires	Wires		3	1	3	neutral score for all 4 motors	3	3	9	same for all motors	12
	Sensor wires		3	1	3	neutral score for all 4 motors	3	3	9		12
Sensing assembly	Sensors	Linear latch type	3	1	3	neutral score for all 4 motors	3	3	9		12
				29	106			33	117		223
	section score				73.10 %				70.91 %		

Figure A.2: Recyclability index for Assembly of Halbach Motor

Component/ Parts			Standard				Cost				Recyclability SCORE
		Remarks	Score	Imp.	F.S.	Remarks	Score	Imp.	F.S.	Remarks	
Disassembly											
- End shields											
	Drive side Bearing		5	3	15	Only unscrewing is needed	4	3	12	first one hard to take	27
	Non-Drive side bearing		4	3	12	other little okay to disassemble	4	3	12	second one little easy	24
- Separation of rotor and stator			2	4	8	High forces	3	4	12		20
											0
- Stator											0
	Lamination S	standard lamination	4	3	12	unscrew stator from end-shields	4	3	12	rivet and way to assenmle the 2 plates, welding unknown	24
	Copper winding	AWG 24	4	3	12	Low varnish	4	4	16		28
- Rotor											0
	Steel R	MS steel	5	3	15	solid hollow rotor	4	3	12		27
	Magnets	NdFeB-rect shape	4	5	20	Ring structure it is easy	5	5	25	Process-magnet difficult	45
-Shaft											0
	Shaft	Steel	5	3	15		4	3	12		27
				27	109			28	113		222
	section score				80.74 %				80.71 %		
				88	3.818			79	3.241		3.5
					76.4 %				64.8 %		
										Final Recyclability Score	70.90 %

Figure A.3: Recyclability index for Disassembly of Halbach Motor

B Appendix B

Temperature Measurements

The appendix presents the temperature measurement curves of bonded NdFeB magnet for different input power. The setup of the measurement is shown in chapter 2, section 2.3.4.

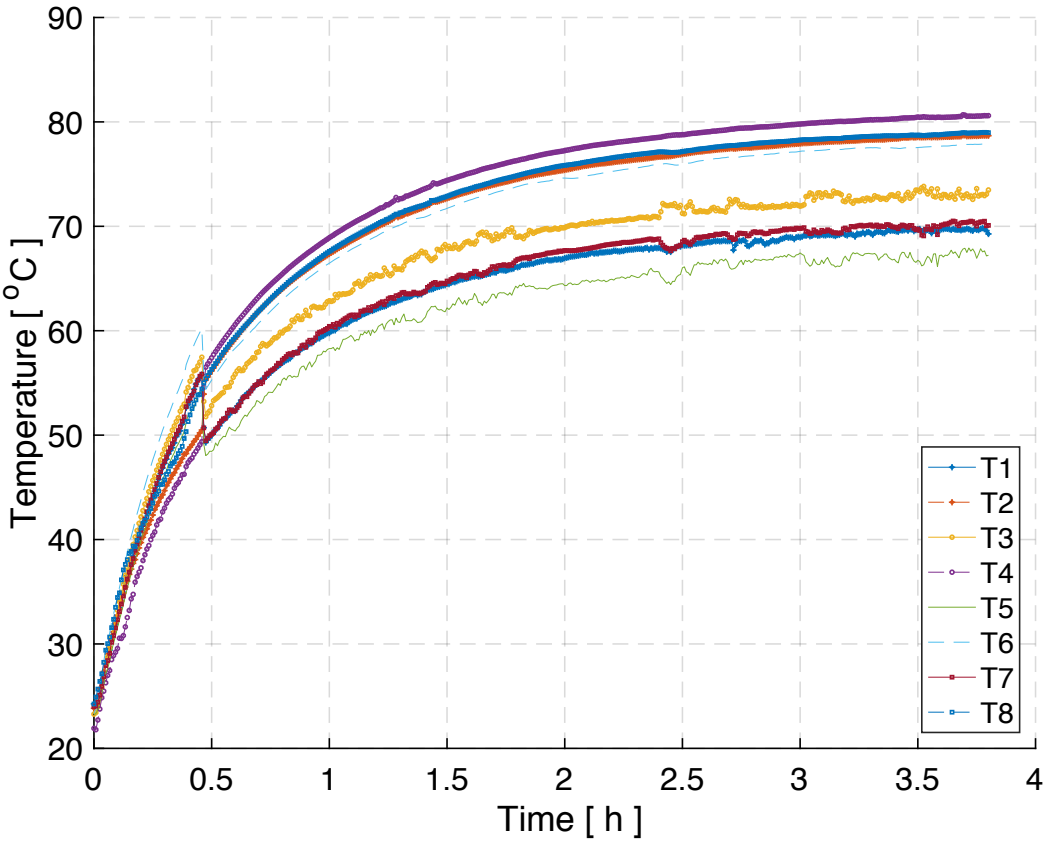

Figure B.1: Temperature at 13 W

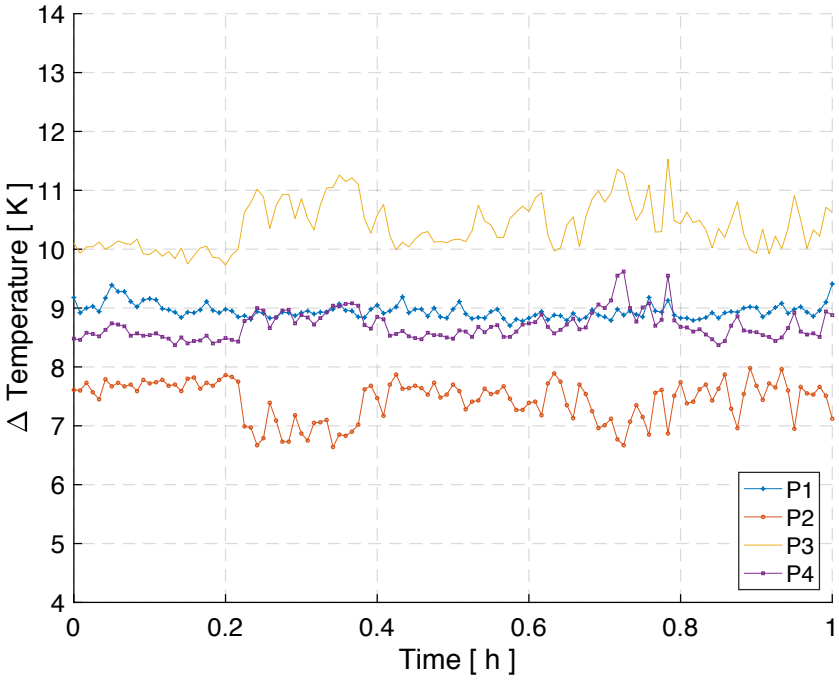

Figure B.2: Temperature difference at 13 W

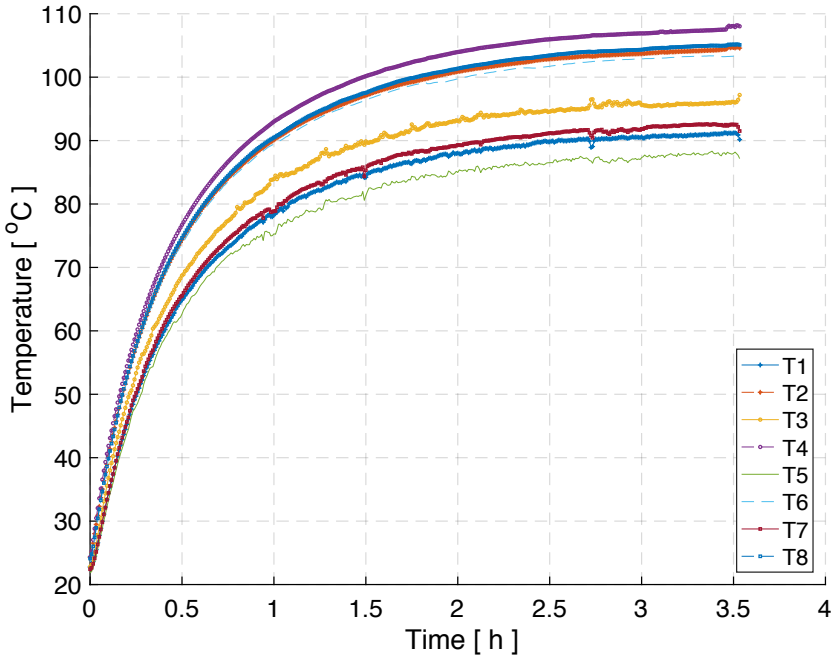

Figure B.3: Temperature at 20 W

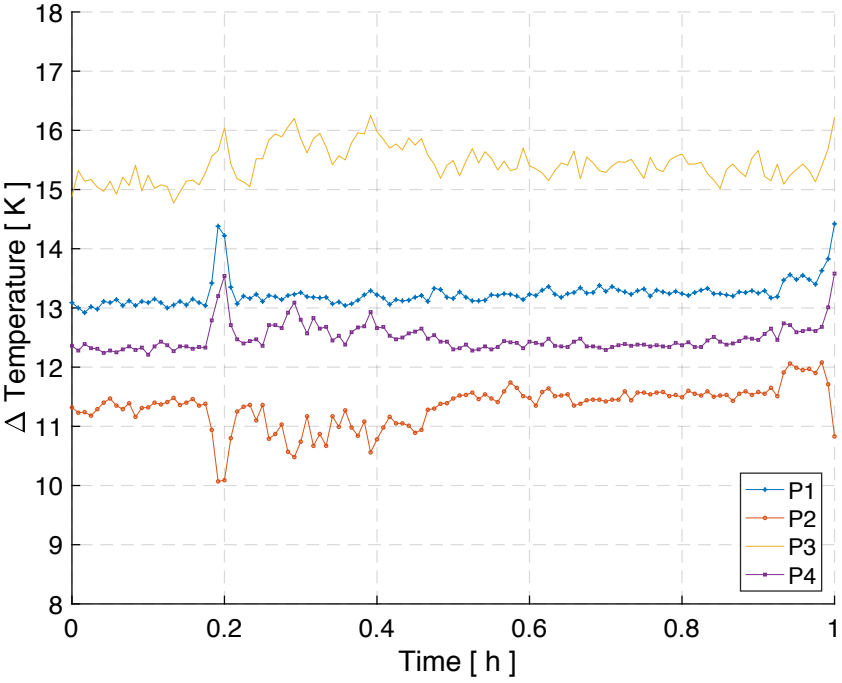

Figure B.4: Temperature difference at 20 W

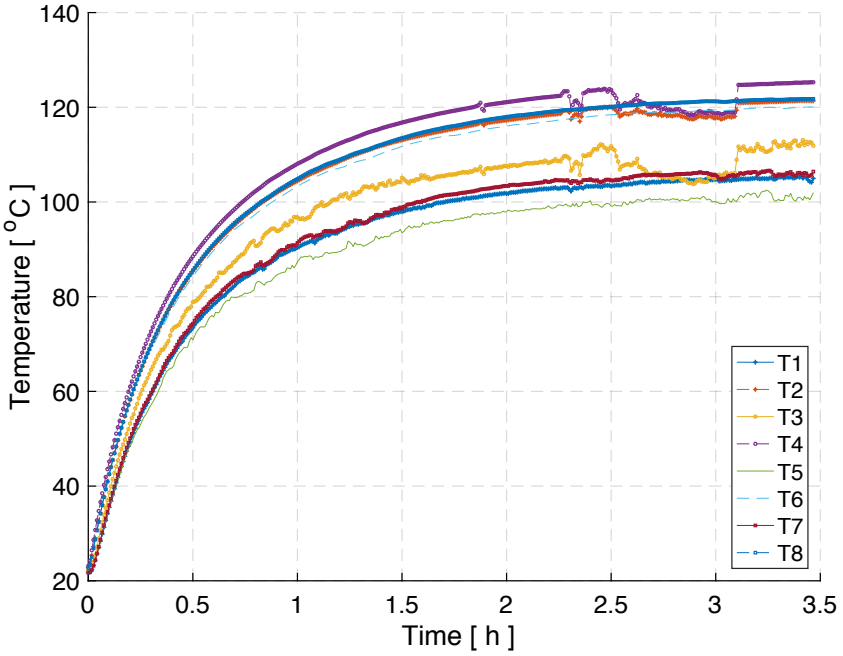

Figure B.5: Temperature at 25 W

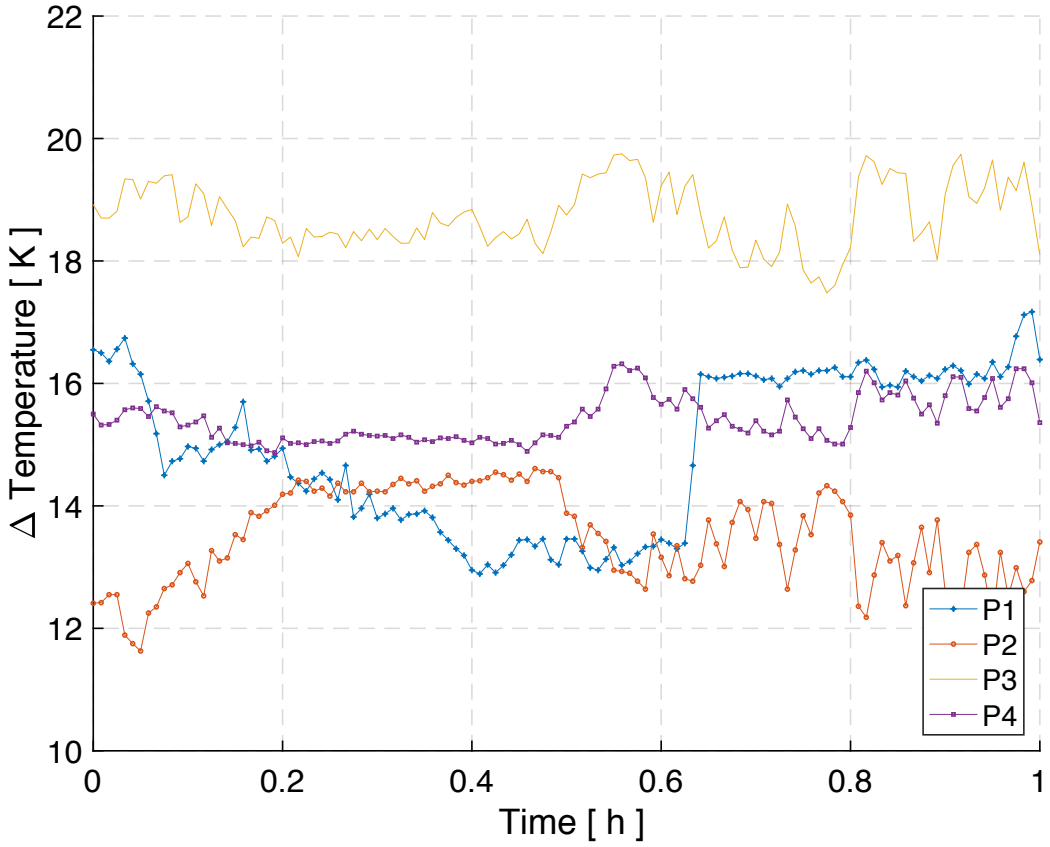

Figure B.6: Temperature difference at 25 W

Appendix C

C Modelling of Halbach Magnet in Flux 2D & 3D

As described in 2 the Halbach magnets can be represented mathematically by equation 2.1 - 2.5. Following are the steps used to create a Halbach magnet model in FLUX 12.3 version based on the equations mentioned above.

Step 1: After building the geometry for Halbach magnet,three spatial variables are defined Ax, Ay and theta as shown in figure C.1. There is no variable for z direction as the there will not be any flux (ideally).

Step 2: Define all three variables following equation. An example shown in figure C.2.

Step 3: Export the values of remenance at each node of magnet region in file mag_exp, as shown in figure C.3.

Step 4: Import the values of remenance at each node of magnet region into a new spatial variable mag_imp from the file mag_exp, as shown in figure C.4.

Step 5: Create a new magnet material using the spatial quantity created in previous step (mag_imp) , as shown in figure C.5.

Step 6: Assign the new magnet material created in previous step to the magnet region in the model , as shown in figure C.6.

Step 7: Finally, the Halbach magnet orientations and flux lines for 6 pole motor should be as shown in figure C.7.

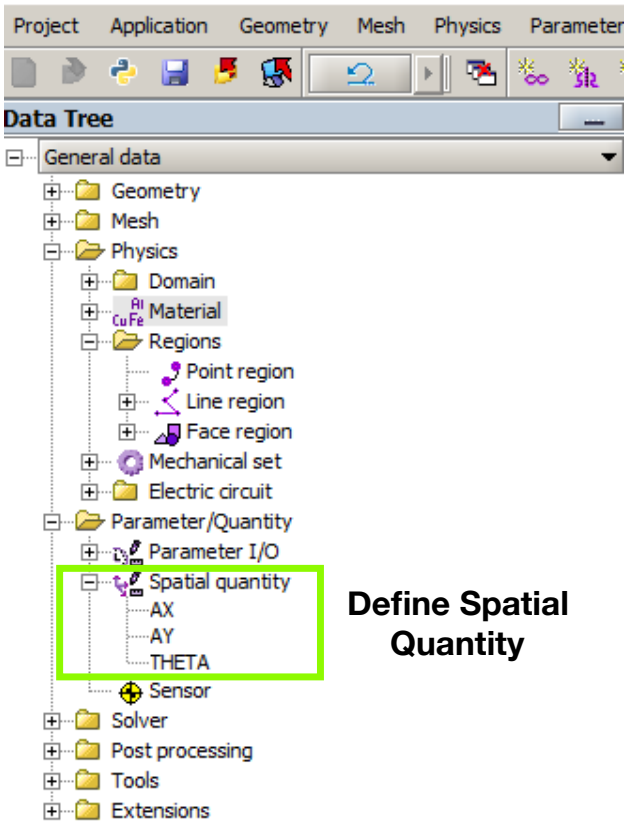

Figure C.1: Step1: Creating three spatial variables

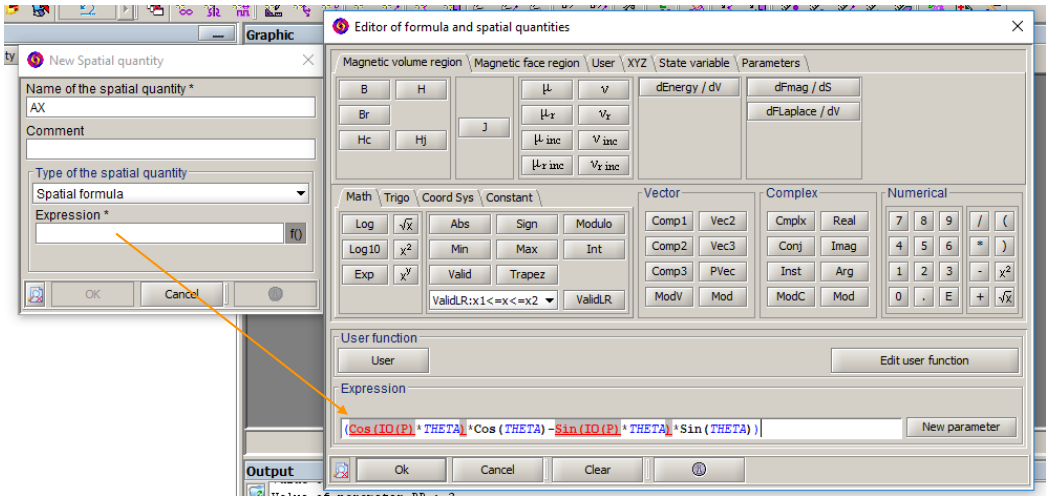

Figure C.2: Step2: Defining spatial variables

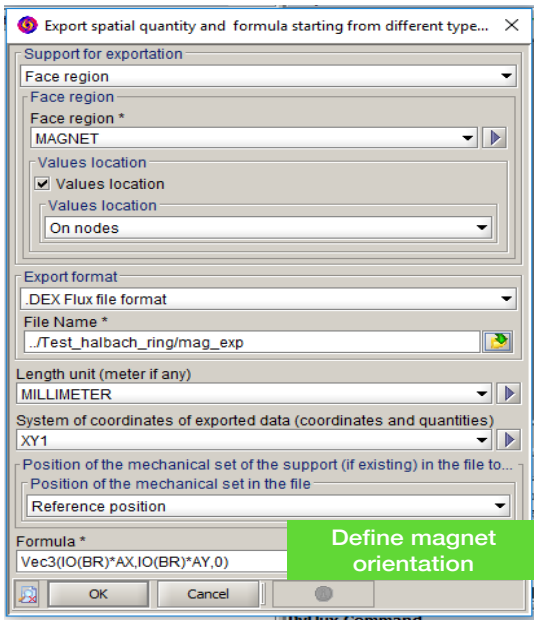

Figure C.3: Step3: Exporting magnetic remenance values of each node of magnet volume

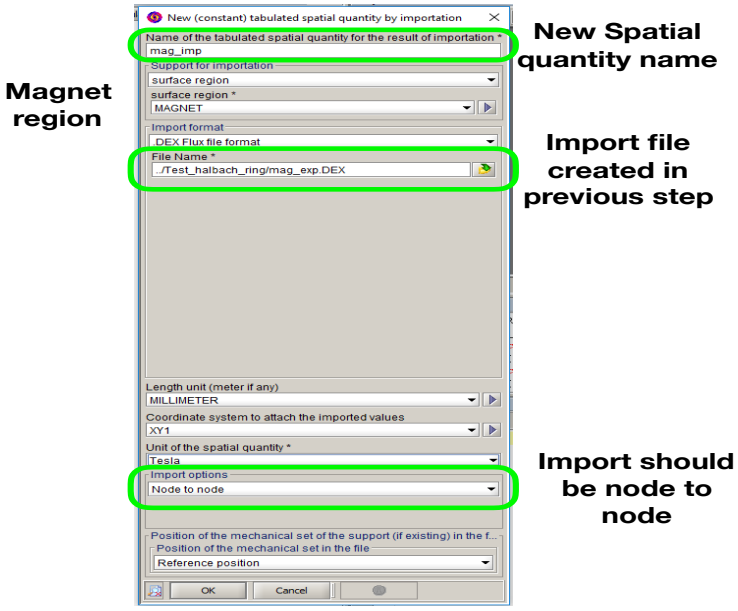

Figure C.4: Step4: Importing magnetic remenance values of each node of magnet volume to a spatial quantity variable

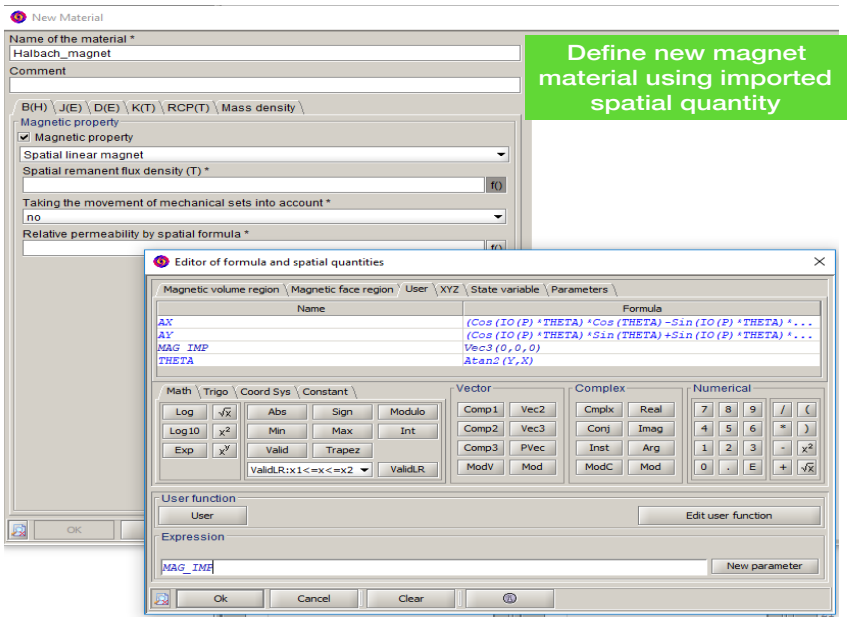

Figure C.5: Step5: Creating new spatial linear magnetic material

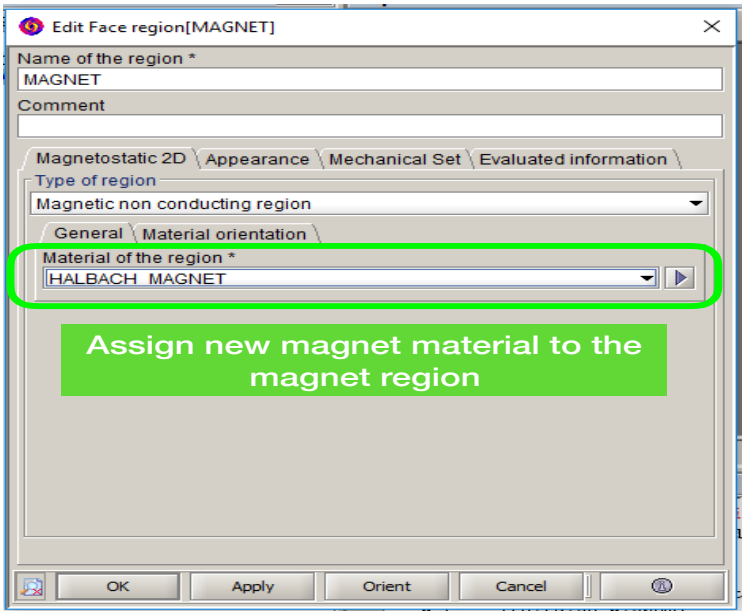

Figure C.6: Step6: Assign new magnet material to the magnet region

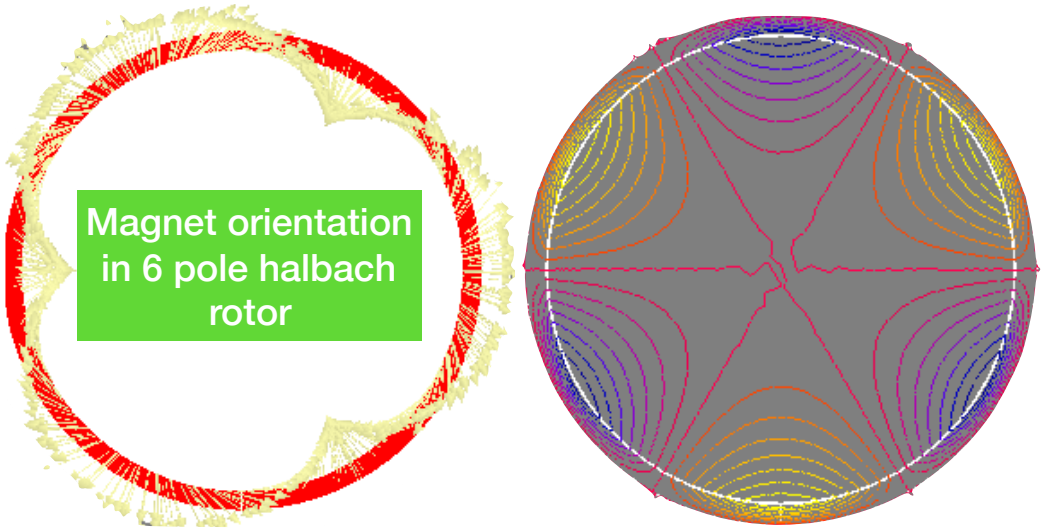

(a) Series Hybrid Vehicle *(b) Flux line*

Figure C.7: Final Halbach model for 6 poles

Publications

Design and Comparison of Outer Rotor Bonded Magnets Halbach Motor With Different Topologies

Amit Kumar Jha[1], Lauric Garbuio[1], Afef Kedous-Lebouc[1], Jean-Paul Yonnet[1], Jean-Marc Dubus[2]
[1] Univ. Grenoble Alpes, CNRS, Grenoble INP G2Elab, 38000 Grenoble, France, e-mail: Amit-kumar.jha@g2elab.grenoble-inp.fr
[2] Valeo Electrical Systems, 2 Rue Andre Boulle F 94000 Creteil, France

***Abstract*— The outer rotor Halbach cylinder motor is designed for hybrid electric vehicle application. The Halbach cylinder is made of bonded magnet and hence the design presented is high torque density motor with low remanence magnet. Different slots poles combinations for double layer tooth coil winding is also evaluated to find the best combination. The Halbach cylinder motor is also compared with different other motor topologies. The outer rotor Halbach motor has the highest torque compared to other topologies over the whole speed range. Variations of inductance and flux linkage of different topologies are also studied and are presented in the article.**

Keywords—Bonded Halbach cylinder; (H) EV motor; slot pole combination

I. INTRODUCTION

The demand for environment friendly sustainable mode of transportation is increasing globally. It is desired that the traction motor used in automotive application should have high efficiency; high power density and can operate at high speed (good flux weakening capability). With increasing number of permanent magnet (PM) motors, it is also very important that the motor should be very easy to assemble and disassemble enabling easy extraction and recycling of the magnets. Most of the motors designed for automotive applications use either inset or surface mounted PM (SMPM). The PM motors by their design are complex and the extraction of the magnets is very tough. Furthermore, to achieve high torque density, sintered magnets are used in the motors causing very high rotor iron losses especially eddy current loss in the magnets at high frequency. Moreover, to improve the flux weakening capability of PM motors, concentrated tooth coil winding is used [1]. The later further increases the eddy current loss in the magnet [1], [2].

Halbach cylinder by its construction creates sinus airgap magnetic flux density waveform and the flux is also concentrated only on one side of the cylinder [3]. Therefore, use of Halbach cylinder in rotor reduces its iron losses compared to conventional PM motors. However, to achieve high torque density, the designs presented in literature use sintered magnets to form the Halbach rotor. Like conventional PM motors, the Halbach cylinder made of sintered magnets also have very high eddy current loss in magnets at high speed and the airgap flux waveform is not very sinus. Furthermore, the manufacturing of Halbach cylinder from pre-magnetized sintered magnets is very difficult and complex process, which makes the motor very expensive. Therefore, in this paper, a design of outer rotor Halbach array magnet motor is presented using bonded NdFeB. The use of bonded magnets ensures low eddy current loss in magnets even at very high operating frequency. Furthermore, low magnet losses give flexibility to use high pole number, which is desired for Halbach cylinder rotor. Unlike, sintered magnets, the Halbach cylinder with bonded magnets do not require any adhesive agent which enables easy extraction of magnets from rotor and is also mechanically robust. Different topologies of Halbach array motor have been studied and their performances in term of torque were compared over the whole speed range. Furthermore, comparison with conventional SMPM motor has also been done and the results are presented in the following sections.

II. DESIGN OF OUTER ROTOR HALBACH CYLINDER MOTOR USIGN FINITE ELEMENT METHOD

A. Motor Design and Specification

The main focus of the design was to fulfill the torque over the speed range of [1000 - 6000 rpm] while keeping the design simple and easy for recycling with minimum volume of magnet. The magnet used for Halbach cylinder was bonded NdFeB with remanence (Br) of 0.6 T. Due to bonded magnet no extra adhesive agent is required without compromising on the mechanical strength of the rotor. Furthermore, the outer rotor arrangement also adds to the mechanical robustness of the rotor. Another advantage of using outer rotor is larger airgap diameter. Figure 1 shows the cross section view of the motor. The design specification is mentioned in Table 1.Double layer concentrated winding was used for the stator winding to decrease the end winding length. The motor is water cooled and the current density is maintained accordingly. The motor model was realized and performance was calculated using finite element (FEM) FLUX™ 2D software.

Halbach cylinder is a special arrangement of many magnets having different magnetization orientation such that the resultant field distribution is sinusoidal concentrated only on one side of magnet as shown in Figure 2. To achieve Halbach cylinder either pre-magnetized segments having required magnetization orientation or bonded magnets can be used. Halbach cylinder using pre-magnetized magnets are more difficult to make compared to bonded magnets. Furthermore, to hold the segmented magnets adhesive agents are required which makes disassembly and recycling process of the magnets very difficult. Figure 2 shows a 4 pole internal field Halbach cylinder. As can be seen at different points on the cylinder the orientation of the magnet is different. The

picture on the left shows the flux lines and it can be seen that due to orientation of the magnet the field is only concentrated on one side of the magnet ring and there is almost no field on the outer side of the ring.

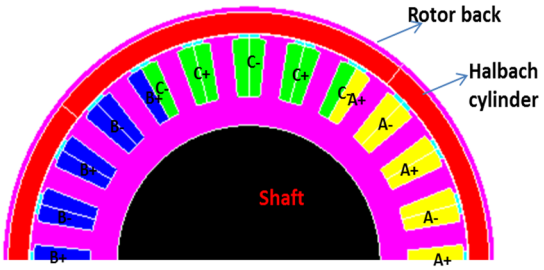

Figure 1:Cross-section of 24 slots / 26 poles outer rotor motor

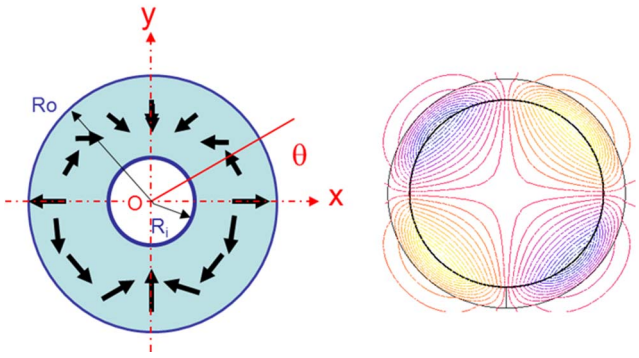

Figure 2: 4 pole internal field Halbach Cylinder (left) Showing magnetic orientation (right) resulting field distribution

The magnetization of Halbach cylinder can be described mathematically in *xyz* coordinate using (1) - (5).

$$\vec{M} = M_x\vec{x} + M_y\vec{y} + M_z\vec{z} \quad (1)$$

where

$$M_x = B_r[\cos(p\theta)\cos(\theta) - \sin(p\theta)\sin(\theta)] \quad (2)$$

$$M_y = B_r\,[\cos(p\theta)\sin(\theta) + \sin(p\theta)\cos(\theta)] \quad (3)$$

$$M_z = 0 \quad (4)$$

$$\theta = \tan^{-1}\left(\frac{y}{x}\right) \quad (5)$$

p is the number of pole-pairs, B_r is magnet remanence and *x,y* are the coordinate of the point on the magnet ring.

B. Slots Poles combination

The motor performance largely depends on the slots poles combination of the tooth coil winding. Due to concentrated tooth coil there are limited slots poles combinations available with good winding factor. For Halbach array motor, the airgap flux density increases with the number of poles up to certain number [3] for a given airgap length. Unlike conventional PM motors, it is advantageous for the motor with Halbach cylinder rotor to have higher number of poles. Therefore, it is a compromise between higher iron loss and torque. Moreover, the pole number is also limited by inverter switching frequency. Figure 4 shows the variation of D-axis inductance with different poles slots numbers.

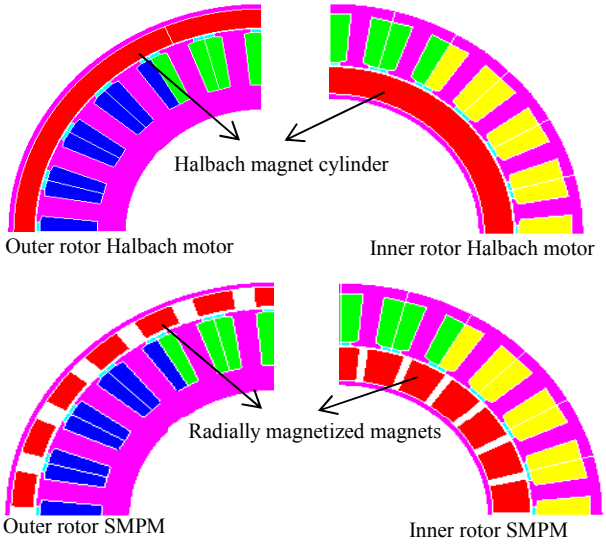

Figure 3: Cross-Section of different motor topologies

Table 1: Design specification for the motor

DC link Voltage	300 V	Axial length	76 mm
RMS Current	245 A	Maximum output power	50 kW
Outer Diameter	262 mm	Maximum torque	205 Nm

The number of turns and the slot shape for tooth coil winding were kept same in different combinations of slots and poles while calculating inductance. This was performed using the technique of frozen permeability [4]. The end winding effects are not considered in the calculation. It can be seen that the inductance is increasing with the increase in pole number for a given slot number. This is can be explained by the increase in the airgap harmonic leakage flux [5]. The d-axis inductance is higher for the lower slot number because with decrease in slot number the magnetizing inductance increases [5].

In literature, it is demonstrated that the criterion for good flux weakening capability for the motor is to have 1 per unit (p.u.) inductance [1], [6]. Using (6) and (7), the p.u. inductance of the motor can be calculated. Therefore, by definition a motor with 1 p.u. inductance can achieve 100% flux weakening at maximum current.

$$L_b = \psi_m / I \quad (6)$$

$$L_{(p.u)} = L_d / L_b \quad (7)$$

where ψ_m is the magnetic flux linkage, I is the maximum allowed current and L_d is the d-axis inductance.

Considering the criterion, all the slots poles combinations shown in Figure 4 have very good flux weakening capability. The pole combination with 24 slots has lower inductance closer to 1 p.u. than with 18 slots. The selection of poles was made as per torque requirement and considering the limitations of converter at high speed. Hence, motor with 24 slots 26 poles was selected, because it fulfills the specified torque speed requirement, as the design for further study.

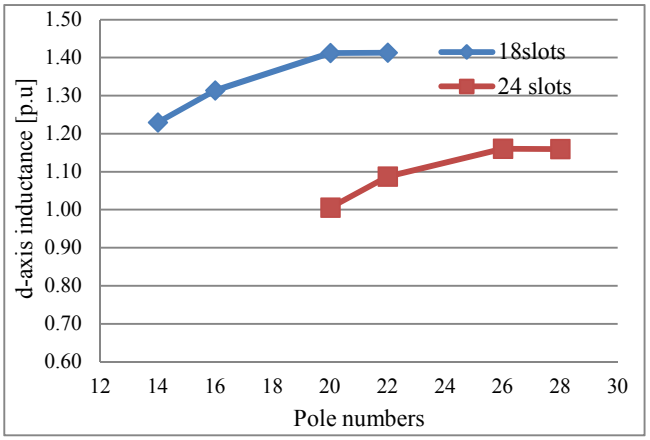

Figure 4: Variation of per unit (p.u.) inductance with different pole numbers.

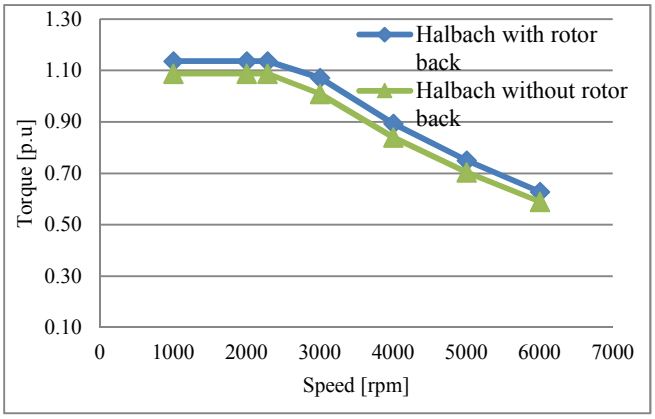

Figure 5: Torque comparison of different motor topologies with Halbach cylinder rotor

III. COMPARISON OF DIFFERENT MOTOR TOPOLOGIES

For each topology, the FEM model was made and torque was evaluated from 1000 rpm to 6000 rpm. Figure 3 shows cross-section of different topologies studied. The phase-phase voltage, airgap length, outer diameter, active length, maximum current, current density, slot/pole combination, total magnet volume and the magnet grade were kept same for all the studied topologies. The aim of the study was to compare electromagnetic performance of different topologies and therefore, to remove the effect of material properties from comparison, same materials were used in every motor model i.e. same lamination and magnets. In the study made, thermal and end winding effects were not considered for different topologies. Unlike, conventional PM motors, Halbach cylinder motor can be designed without rotor back due to shielding effect. Figure 5 shows the comparison of the maximum torque over whole speed range for the motor with and without rotor back with the same airgap diameter. The fundamental airgap flux density and the torque of motor with a rotor back are respectively 5.6 % and 5% higher than without a rotor back which is due to increase in flux linkage as can be seen from Figure 5 and Figure 7.

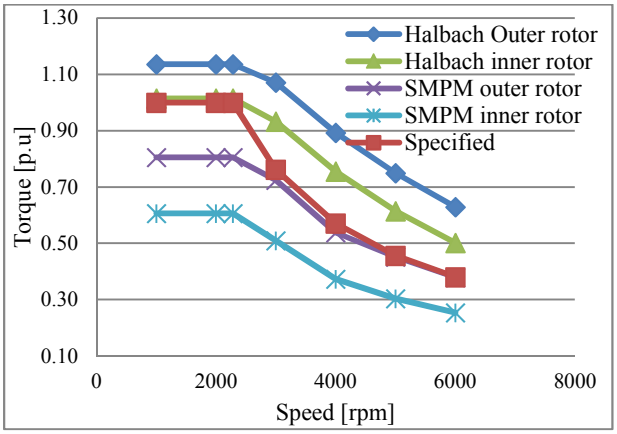

Figure 6: Torque comparison of motors with Halbach cylinder and SMPM rotor

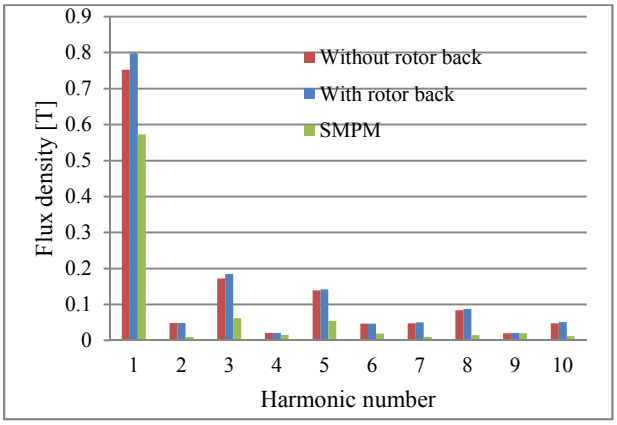

Figure 7: Harmonic analysis of airgap flux density of different Halbach and SMPM motor

The conventional SMPM motor was evaluated and compared with motor with Halbach considering the whole speed range. Figure 6 shows the torque-speed curve over the whole speed range. The outer rotor motor has higher torque than the inner rotor because of larger airgap diameter. It can also be seen that the outer rotor Halbach motor produces 41% higher torque than the outer rotor SMPM motor. Figure 7 and Figure 9 shows that the fundamental flux density and the flux linkage of the outer rotor Halbach motor is 39% and 42% higher than the SMPM motor respectively. The higher flux density in Halbach motor is due to two reasons. Firstly, there is no flux leakage between poles in Halbach rotor compared to SMPM as shown in Figure 8. Secondly, increasing the pole

numbers also increases the airgap flux density of Halbach cylinder [3]. The thickness of the magnet in SMPM motor is larger than the Halbach motor to have same amount of magnet volume. Hence, the airgap diameter of SMPM motor is smaller than the Halbach by 4 %. Due to this difference in airgap diameter the difference in flux density is lower than the difference in flux linkage. The effect of saturation on both the motor design is almost same as can be inferred from the decrease in flux linkage with increase in current

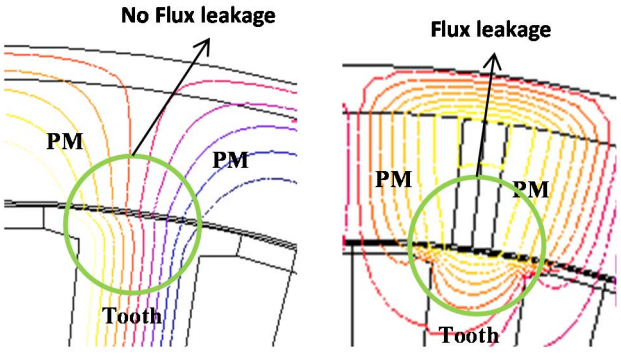

Figure 8: Flux lines in motor with Halbach cylinder (left) and SMPM (right) at no load showing flux leakage between poles

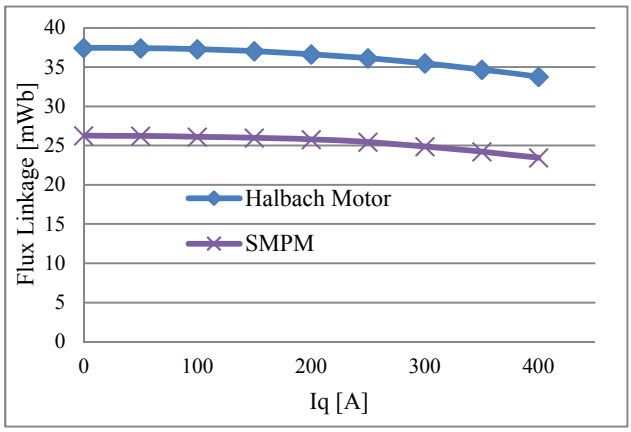

Figure 9: Variation of flux linkage with q-axis current for Halbach

Figure 10 shows the cogging torque of SMPM and Halbach motor. The Halbach motor has lower cogging torque than SMPM due to sinus magnetic field distribution. It is worth noting here that, due to the tooth coil winding, the absolute value of the cogging torque for both the designs is very small (less than 1% of the average rated torque).

Flux weakening capability of the motors used in automotive application is very important factor for the design. A good trade-off between torque and wide flux weakening range is achieved by having 1 p.u. inductance. Figure 11 shows the variation of per unit inductance of Halbach and SMPM motor. The absolute value of inductance of both the motors is approximately the same however, due to lower flux linkage in SMPM motor the base inductance is low. Hence, the p.u. inductance of the SMPM is higher than the Halbach motor. The SMPM has around 1.69 p.u. inductance and therefore, the motor has very good flux weakening capability as can be seen from Figure 6. However, high p.u. inductance is also a reason for lower torque of SMPM compared to Halbach motor.

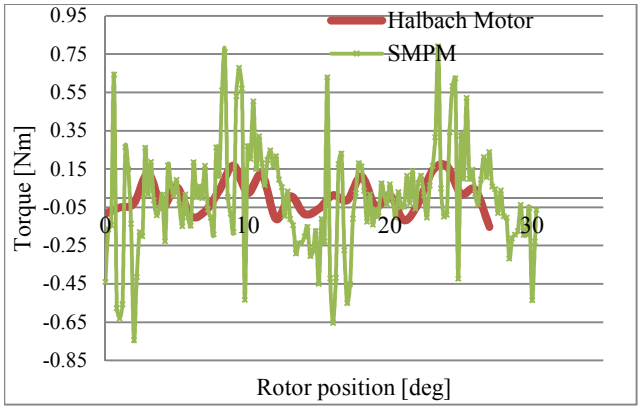

Figure 10: Cogging torque of Halbach motor and SMPM motor

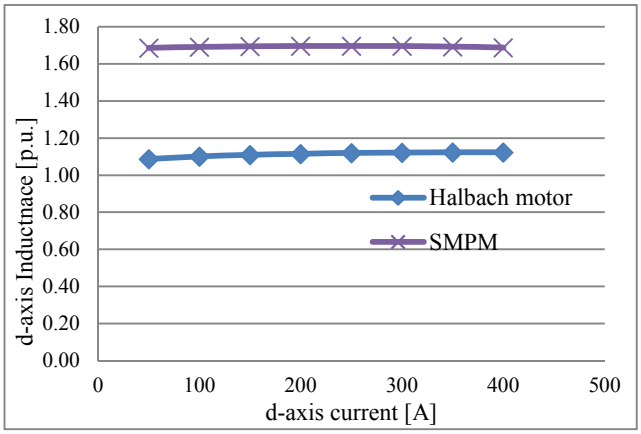

Figure 11: Per unit d-axis Inductance variation with d- axis current of SMPM and Halbach motor

III. CONCLUSION

The motor design with bonded magnet Halbach cylinder rotor presented in the article fulfills the torque speed requirement and can be used in high torque density applications. The motor has good flux weakening capability with around 1p.u. inductance. The bonded magnet due to its high resistivity, i.e. low eddy current loss, gives flexibility to use high pole numbers which is desirable for motor with Halbach cylinder.

The outer rotor Halbach cylinder with rotor back produces 5% higher torque than the motor without rotor back. The

Halbach cylinder gives a possibility to use cylinder with non-magnetic rotor back which will reduce the rotor loss furthermore. Therefore, it is a good choice for very high speed applications. The magnetic flux leakage in Halbach motor is negligible compared to SMPM. Hence, Halbach cylinder also has better utilizations of magnets used in the motor. The outer rotor Halbach motor produces 41 % and 87 % higher torque than the conventional outer and inner rotor SMPM motor respectively with the same current density, line voltage, current, outer diameter, magnet volume and grade. Due to sinus magnetic flux distribution of Halbach cylinder, the cogging torque is also lower than the SMPM motor. The use of concentrated tooth coil winding gives very good flux weakening capability for both the motors. However, the Halbach motor has good balance between flux weakening and torque compared to SMPM.

ACKNOWLEDEGEMENTS

The research leading to these results has received funding from European Community's Horizon 2020 Programme ([H2010/2014-2019]) under Grant Agreement no. 674973 (MSCA-ETN DEMETER). This publication reflects only the author's view, exempting the Community from any liability. Project website http://etn-demeter.eu/

REFERENCES

[1] Ayman M.EL-Refaie, Thomeas M. Jahns. Donald W. Novotny, "Analysis of Surface Permanent Magnet Machine With Fractional -Slot Concentrated Winding," *IEEE Trans on Energy Conversion,* vol. 21, no. 1, pp. 34-43, March,2006.

[2] Ayman M.El-Refaie,Thomas M.Jamns, Patrick J. McCleer, John W. McKeever, "Experimental Verification of Optimal Flux Weakening in Surface PM Machine Using Concetrated windings," *IEEE,* vol. 42, no. 2, pp. 1050-1057, March/April 2006.

[3] Zhu.Z.Q,Xia.Z.P,Shi.Y.F,Howe.D,Pride.A,Chen.X.J, "Performance of Halbach magnetized Brushless AC motor," *IEEE Trans on Magnetics,* vol. 39, no. 5, pp. 2992-2994, September,2003.

[4] Jill Alison Walker,David G. Dorrell,Calum Cossar, "Flux-linkage calculation in permanent-magnet motors using the frozen permeabilities method," *IEEE TRANSACTIONS ON MAGNETICS,* vol. 41, no. 10, pp. 3946-3948, October,2005.

[5] P. Ponomarev, "Tooth-Coil Permanent Magnet Synchronous Machine Design for specail applications," PhD Thesis,Acta Universitatis Lappeenrantaensis, Lappeenranta, 2013.

[6] W.L.Soong, T.J.E.Miller, "Field-weakening performance of brushless synchronous AC motor drives," *IEE Proc-Electr. Power Appl,* vol. 141, no. 6, pp. 331-340, November 1994.

[7] D.Howe, Zhu.Z.Q, "Halbach permanent magnet machines and applications: a review," *IEE Proc. Electr. Power Appl,* vol. 148, no. 4, pp. 299-308, July,2001.

[8] F. Meire, "Permanent-Magnet Synchronous Machines with Non - Overlaping Concentrated winding for low speed Direct Driven drive Applications," PhD Thesis, Royal Institute of Technology, School of Electrical Engineering, Stockholm, 2008.

FEA Based Analysis on Effect of Slot Pole Combination on Motor Torque and Magnet Eddy Current Loss With Bonded NdFeB Halbach Rotor

Amit Kumar Jha[1], Afef Kedous-Lebouc[1], Lauric Garbuio[1], Jean-Paul Yonnet[1], and Jean-Marc Dubus[2]
[1]Univ. Grenoble Alpes, CNRS, Grenoble INP G2Elab, 38000 Grenoble, France
[2]Valeo Electrical Systems, 2 Rue Andre Boulle F, 94000
Email: Amit-kumar.jha@g2elab.grenoble-inp.fr

***Abstract*—The effect of slots poles combination on inductance and torque was investigated on the motor with outer rotor bonded NdFeB Halbach cylinder designed for automotive application. Motor with Halbach rotor has better performance with higher number of slots and poles combination. The magnet eddy loss was calculated and analyzed with different slots poles. The impact of rotor back on the eddy current was also investigated. The eddy loss calculated using 3D FEA models were also compared with 2D and shows a big difference between the two.**

***Index Terms*—Bonded Halbach cylinder, Eddy current loss, Slots Poles combination,Tooth coil winding**

I. Introduction

In recent years many studies has been done on using concentrated tooth coil winding (TCW) in permanent magnet (PM) motors. The TCW has many advantages over distributed winding especially the short end-windings and better flux weakening capability [1] which makes it apt for automotive application motors. The selection of slots poles combination is critical for motor performance with TCW. In [4] the effect of slots poles on motor performance with surface mounted magnet (SMPM) rotor is presented. However, the investigation does not include the impact of number for turns on torque and inductance and therefore, the performance of motor with different slot pole will not be same taking voltage into consideration. Furthermore, the TCW arrangement inherently increases both the higher order harmonics and sub-harmonics compared to distributed windings, which increase the rotor losses. The magnets performance is very much dependent on the operating temperature and very high magnet loss i.e. high temperature not only decreases motor performance but can also cause partial irreversible demagnetization of the magnets. The different motor designs presented in literature for vehicle application use predominantly sintered NdFeB magnets, because of high remanence value, to achieve high torque density. However, with TCW winding eddy current loss is a design issue for high speed motor, which is further increased due to the low resistivity of the sintered magnets. The most common method to reduce the eddy currents loss is to use small segments of magnets. The drawbacks of using small segments are that the magnets need high volume of glue to stay together and also the performance drops slightly due to lower magnet density. Another method to overcome the high eddy magnet loss is to use bonded magnets which has resistivity at least 10-20 times higher than the sintered magnets [2]. However, the torque density of conventional SMPM with bonded magnets is low because of lower remanence. Furthermore, the bonded magnets have very low thermal conductivity and the operating temperature range is also low. Hence, even low eddy current loss can cause high temperature rise in magnet and can be critical for the motor operation.

In this paper, a motor design with outer rotor bonded Halbach cylinder motor for electric vehicle application is studied. In [9] it is presented that high torque density motor, higher than SMPM, can be designed using bonded NdFeB magnet by using Halbach rotor structure. Therefore, a detailed 2D finite element analysis (FEA) study has been done to investigate the effect of slots poles combination on the motor inductance and torque including the impact of number of turns. In [7] a general approach for eddy loss estimation with different slots poles for SMPM is given. However, when compared with Halbach, the SMPM motor has different geometry especially the magnet arrangement. The Halbach rotor has continuous magnet region and also the rotor back is very thin. Therefore, the variation of eddy current loss in magnet with different slots poles was calculated and presented in this article. The magnet eddy loss for motor with magnetic and non-magnetic rotor back is also presented. Finally, to estimate more accurate eddy loss 3D model was simulated for 24 slots 26 poles motor and the comparison of 2D and 3D calculation is presented.

II. Motor Description

Figure 1 shows the cross-section of a 24 slots 26 poles outer rotor motor with winding arrangement. The magnet in the rotor is a bonded NdFeB magnet with Halbach arrangement. It is single magnet structure which eliminates the use of glue. Furthermore, because of outer rotor the need of glue/bandage for rotor back and magnet is not required to have mechanical strength. Therefore, the design is not only easy to manufacture, the use of bonded Halbach rotor reduces the complexity involved in rotor (magnet) assembly/disassembly and makes it reuse/recycle friendly. Moreover, outer rotor also makes cooling of rotor slightly easy compared inner rotor. Motor design parameters are given in Table I.

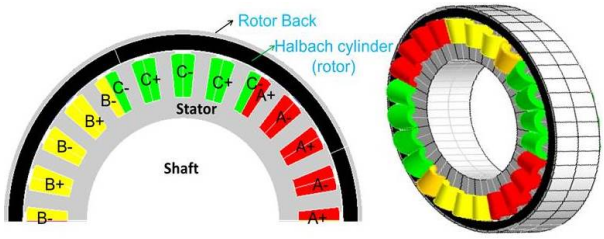

Fig. 1. Cross-section of 24 slots 26 poles outer rotor Halbach cylinder motor with phase windings arrangement, A,B,C are different phase windings

TABLE I
MAIN SPECIFICATION FOR MOTOR DESIGN

DC link Voltage	300 V	Axial length	76 mm
RMS Current	245 A	Maximum output power	50 kW
Outer Diameter	262 mm	Maximum torque	205 Nm

A. Halbach cylinder

Mathematically, the magnetization of the outer rotor magnet i.e. inner field can be defined by equation (1)-(5). Figure 2 shows the magnetization direction around the magnet and the resultant field distribution. It can be seen that the field is concentrated on only one side of the cylinder which gives a possibility to have a rotor with very thin or non-magnetic rotor back to support mechanically. The concentration of flux on one side of the ring also improves the performance and reduces losses in rotor back.

$$\mathbf{M} = M_x\mathbf{x} + M_y\mathbf{y} + M_z\mathbf{z} \tag{1}$$

where,

$$M_x = B_r[\cos(p\theta)\cos(\theta) - \sin(p\theta)\sin(\theta)] \tag{2}$$

$$M_y = B_r[\cos(p\theta)\sin(\theta) + \sin(p\theta)\cos(\theta)] \tag{3}$$

$$M_z = 0 \tag{4}$$

$$\theta = \arctan(\frac{y}{x}) \tag{5}$$

where, p is the number of pole-pairs, B_r is magnet remanence and x,y are the coordinates of the point on the magnet

B. Methodology

The 2D and 3D electromagnetic transient model was made using finite element (FEM) FLUX^{TM} software. The d-axis inductance and flux linkage at different d&q currents was calculated using frozen permeability technique [3]. To compare between different designs per unit (p.u.) was used and the values were calculated using equation (6)-(8). The calculation of inductance and torque is done using 2D model and does not include end-windings effect. The line voltage, line current, current density, slot-fill factor, air-gap length, outer diameter,

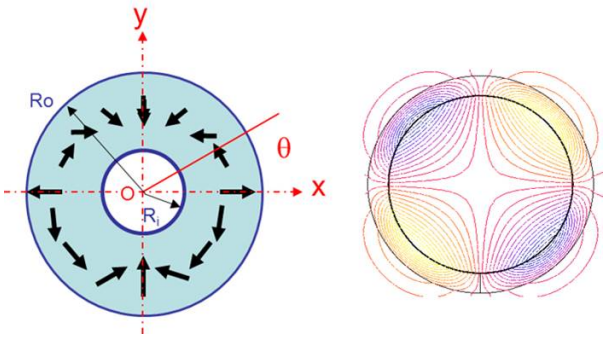

Fig. 2. (left) Magnetization of 4 pole Halbach cylinder, (right) Field distribution due to Halbach cylinder

magnet volume and magnet grade were kept same for all the calculations.

$$L_b = \frac{\psi_m}{I_{max}} \tag{6}$$

$$L_{p.u} = \frac{L_d}{L_b} \tag{7}$$

$$T_{p.u} = \frac{T}{T_{rated}} \tag{8}$$

where, ψ_m is the magnetic flux linkage, I_{max} is the maximum d-axis current, L_d is the d-axis inductance, T is the calculated torque and T_{rated} is the specified torque at base speed.

2D models were used to study the variation of magnet loss with different parameters to save simulation time. Although, 2D models overestimates loss especially for motor with shorter axial length compared to the diameter. However, the trend of variation of loss with different parameters should remain same (ignoring radial impact) in both 2D and 3D and hence, 2D calculations is good enough to compare losses in different designs. Thereafter, to attain more accurate value performance was calculated using 3D model and compared with 2D.

III. IMPACT OF SLOTS POLES COMBINATION ON MOTOR PERFORMANCE

The motor performance varies significantly with the slots poles combination with TCW. 2D FEM transient model was used to study the impact of slots poles combination on the inductance and torque. The models used for calculation have a non-magnetic rotor back. The current source was used for modeling and the number of turns were changed with pole numbers to keep same line voltage. Figure 3 shows the variation of inductance with different slot and pole numbers. The p.u. inductance is reducing with increase in pole numbers. The number of turns were reduced with increase in poles number to keep the same line voltage. Therefore, despite increase in the air-gap harmonic leakage inductance with pole number [4] the total d-axis inductance is decreasing due to reduction in turn number. Furthermore, with same pole number the d-axis inductance is lower for higher slot number because of reduction in magnetization inductance [4].

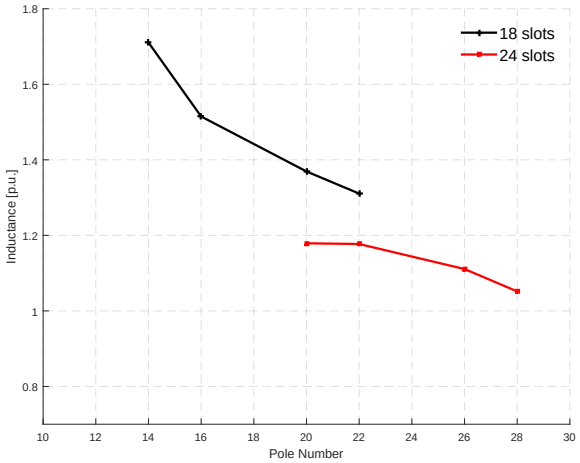

Fig. 3. Variation of d-axis inductance(p.u) with different slots and poles number

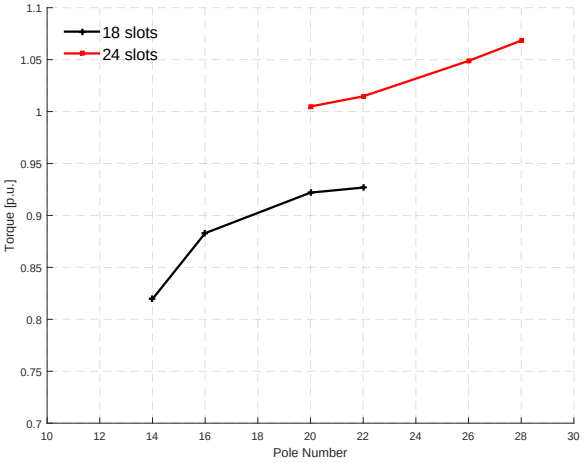

Fig. 4. Variation of torque(p.u.) with different slots and poles number

The maximum calculated torque with different slots and poles combination is shown in figure 4. The torque is increasing with increase in pole numbers and the increase is non-linear. There are three reasons for this behavior. Firstly, the non-linearity is due to the higher saturation at lower pole number compared to higher poles with given dimensions. Secondly, the air-gap flux density increases with increase in pole number [6]. Thirdly, unlike SMPM, due to Halbach arrangement the magnetic flux leakage with increase in pole number is negligible [9]. Therefore, it is desired to design motor with higher slot and pole numbers however, the pole numbers are limited due to eddy current loss and inverter switching frequency.

IV. Magnet Eddy current loss

Figure 5 shows the normalized MMF and the harmonics spectrum for 24 slots 26 poles configuration. It can be seen from the figure 5 there are several sub-harmonics in addition

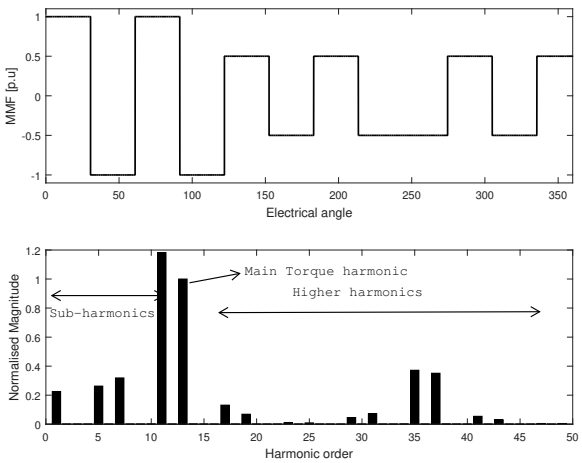

Fig. 5. MMF of 24 slots 26 poles motor and the harmonic spectrum at t = 0, Ia = 1, Ib = -1/2 and Ic = -1/2

to higher harmonics due to tooth coil winding arrangement. These harmonics cause additional eddy loss in magnet. The magnitude of induced eddy current depends on the rate of change of flux density and the resistivity of the magnet. The bonded NdFeB magnets have resistivity in the order of 10-30 $\mu\Omega.m$. Hence, 20 $\mu\Omega.m$ was used in calculations as magnet resistivity [2]. In vehicle operation the motor shall be able to operate continuously with 3 phase short circuit (3phSC) keeping temperature rise within allowed limit and also in terms of eddy loss is the worst case scenario. Therefore, eddy current loss during 3phSC in magnets were calculated and compared.

A. 2D Analysis of Magnet Eddy loss

The Halbach cylinder rotor unlike SMPM, due to the shielding effect as shown in figure 2 can be designed without rotor back or with thin non-magnetic rotor back. Figure 6 and 7 shows the comparison of the magnetic field in the middle of magnet and the harmonic spectrum for the motor with magnetic and non-magnetic rotor back. The simulation model in both the cases has same motor dimensions and the magnet was turned off i.e. the $Br = 0$. It can be seen from the figure that the magnetic rotor back increases the induction in the motor and also has higher sub-harmonics. This is due to the fact that the ratio of the slot opening and magnet thickness is around 1 and hence, it reduces the reluctance seen by stator current MMF. The increase in induction cause increase in torque along with the eddy loss. The calculated eddy current loss during 3phSC for the motor with non-magnetic rotor back is around 50% lower than the motor with magnetic rotor back whereas the reduction in torque or power is only 4% at rated speed.

The eddy current magnet loss is caused by change of field due to stator current and by magnetic flux while crossing slot openings i.e. due to stator slotting. In table II the magnet eddy loss due to stator current, slotting and the total is presented. As expected the loss is varying squarely with speed over the

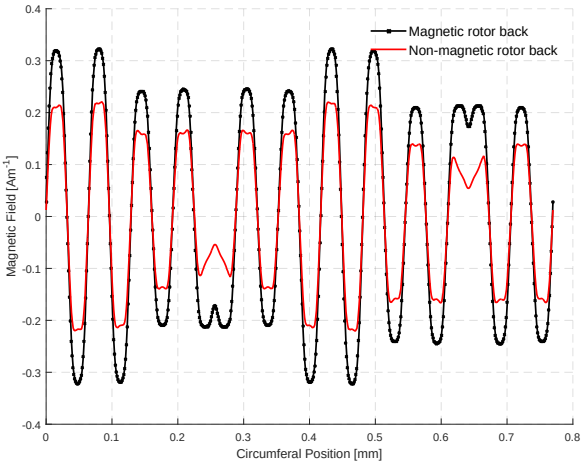

Fig. 6. Magnetic field due to stator current in middle of magnet with magnetic and non-magnetic rotor back

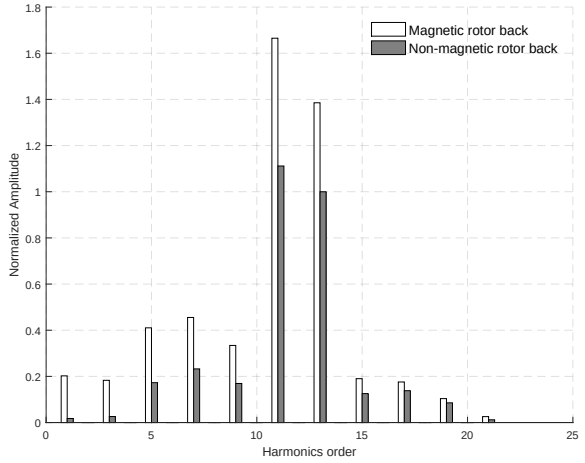

Fig. 7. Normalized harmonic spectrum of magnetic field with rotor back and without rotor back. The 13th order with non-magnetic rotor back is considered as base harmonic. value

whole speed range (frequency). The eddy loss with magnetic rotor back is almost double due to non-magnetic rotor on all investigated speeds. The eddy current loss due to slotting is around 13% of the total loss and it is interesting to note that the total loss is lower than the loss only due to current. Moreover, the eddy loss only due to slotting is slightly higher with non-magnetic rotor back than with magnetic rotor back. In table III the total magnet eddy loss and due to I_d and I_q current is given. It can be seen that the magnet eddy loss only due to current increases approximately squarely with increase in current. Notably, at lower current the total loss is higher than the loss only due to current however, at higher current loading the total loss in lower than the loss only due to current. Therefore, it can be inferred that at lower current loading slotting increases total loss whereas, at higher current loading the loss due to slotting lowers the total loss due to saturation

TABLE II
CONTRIBUTION OF STATOR CURRENT(MAX CURRENT,B_r=0) AND SLOTTING(B_r=0.6,I=0) IN MAGNET EDDY LOSS

	Magnetic Rotor Back			**Non-Magnetic Rotor Back**		
Speed	Loss [W]	Loss [W], B_r = 0	Loss [W], I = 0	Loss [W]	Loss [W], B_r = 0	Loss [W], I = 0
1000	192	214	28	82	88	14
2284	920	1050	138	426	460	70
3000	1526	1746	236	736	792	60
4000	2596	2976	410	1289	1402	214
5000	3888	4436	626	2010	2168	332

TABLE III
VARIATION OF TOTAL AND ONLY DUE TO CURRENT EDDY LOSS AT DIFFERENT I_d AND I_q

Iq [A]	Magnet loss [W]	Magnet loss due to stator current B_r = 0 [W]	Id [A]	Magnet loss [W]	Magnet loss due to stator current B_r = 0 [W]
0	136	0	0	136	0
50	154	24	50	244	24
150	302	214	150	514	216
250	572	578	250	822	582
350	924	1052	350	1144	1052
450	1320	1526	450	1474	1528

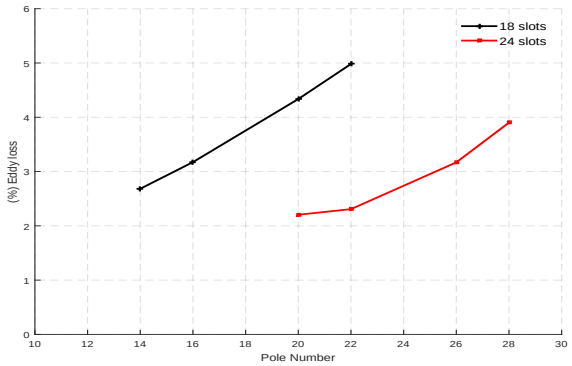

Fig. 8. Variation of eddy loss with different slots poles at 3phSC. The eddy loss is % of output power at rated speed

of stator tooth. In table III the eddy loss is also presented when current is only in d-axis or only in q-axis. The eddy loss is higher when current is in d-axis then the current in q-axis. The eddy loss due to current is similar irrespective of I_d or I_q. Hence, the difference is due to the slotting. The loss due to slotting is higher when current is in d-axis.

Figure 8 shows the variation of eddy current loss with different slots poles at 3phSC steady state condition. The magnet loss is increasing with the pole number due to increase in operating frequency. The loss is also higher as the SC current increased because of lower inductance as shown in figure 3. The motor with higher slot number has lower eddy current loss due to the fact that with increase in slot numbers the cross-section area of induced eddy current decreases.

B. Comparison of 2D and 3D loss calculation for 24 slots 26 poles motor

The axial length is 57% of the outer rotor radius of the motor, shown in figrue 1 and table I and with this dimension the end-winding effects are significant. Therefore, to study the impact of end-windings on eddy loss 3D model for 24 slots

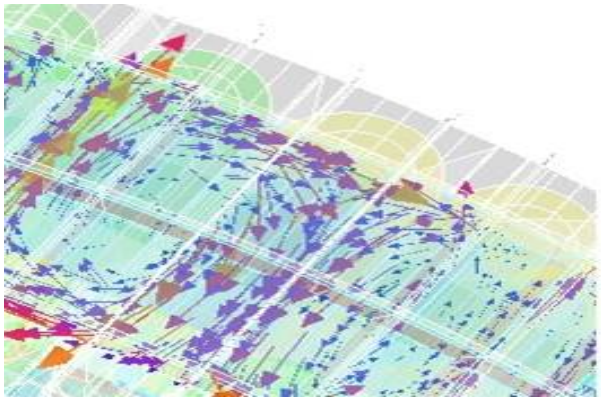

Fig. 9. Induced Eddy currents in the magnet

26 poles outer rotor motor was modeled and the eddy current loss in the magnet was calculated. The calculated magnet loss from 3D is 53% and 73% lower than the 2D calculation with magnetic and non-magnetic rotor back respectively. The reduction in torque due to end-winding effect is around 7%. Figure 9 shows the induced eddy current in the magnets with 3phSC. The ratio of slot pitch and active length is around 1 therefore, the circumferential resistance is non-negligible compared to axial resistance. Taking circumferential resistance into calculation the magnet loss is expected to be half. The further reduction of loss can be explained due to the elliptical path of eddy current which reduces the area for induced eddy current and hence, eddy loss. It is also important to note that the induced current paths are not uniform and one reason could be continuous magnet region with isotropic resistivity. Moreover, the high magnet loss even with bonded magnets could be due to single magnet cylinder structure.This phenomenon can cause some hotspots in the magnet. The ratio of eddy loss with magnetic and non-magnetic rotor back in 2D and 3D is approximately 2 and 3 respectively. The trend between 2D and 3D is same but the difference has increased and therefore, to have realistic values 3D calculation is very important.

V. Conclusion

The impact of slots poles for TCW winding on the motor performance is investigated. The p.u. inductance of the motor reduces with increase in pole number with maximum allowed voltage and current. Moreover, the inductance is lower with higher slot number. The torque of the motor increases with increase in pole numbers. Therefore, the motor with Halbach cylinder and TCW should have higher slots poles combination to achieve good performance.

The magnet loss with non-magnetic rotor back is around 50% lower than the magnetic rotor back whereas the power or torque is only 4%. Therefore, the non-magnetic rotor back Halbach cylinder is very good option for motors in very high speed operation like automotive application. The main magnet loss is due to the stator current and the stator slotting lowers the total magnet eddy loss at high current loading. The eddy loss increases with increase in pole number but decreases with increase in slot number. The eddy loss calculated with magnetic rotor back in 3D model is almost 53% lower than the respective 2D model. The end-windings effect is very pronounced due to dimensions of the motor and the effect is very high for eddy loss compared to torque. Therefore, to have realistic eddy loss calculation 3D simulation is needed. The magnet loss calculated using 3D is around 4% of the output power. The loss is very high for bonded magnet and can cause thermal demagnetization. Therefore, appropriate design modification is requried to lower the eddy loss. Furthermore, the range of resistivity of bonded magnets is very wide and hence in future study the resistivity and magnet eddy loss will be validated by measurements.

Acknowledgment

The research leading to these results has received funding from European Communitys Horizon 2020 Programme ([H2010/2014-2019]) under Grant Agreement no. 674973 (MSCA-ETN DEMETER). This publication reflects only the authors view, exempting the Community from any liability. Project website http://etn-demeter.eu/

References

[1] Ayman. M.EL-Refaie, Thomeas M. Jahns and Donald W. Novotny, "Analysis of Surface Permanent Magnet Machine With Fractional -Slot Concentrated Winding," *IEEE Trans on Energy Conversion*, vol. 21, no.1, pp. 34-43, March, 2006.

[2] Ayman. M.EL-Refaie, Thomeas M. Jahns, Patrick J. McCleer and John W. McKeever, "Experimental Verification of Optimal Flux Weakening in Surface PM Machines Using Concentrated Windings," *IEEE Transactions on Industry Applications*, vol. 42, no.2, pp. 443-453, March/April, 2006.

[3] Jill Alison Walker, David G. Dorrell, Calum Cossar, "Flux-linkage calculation in permanent-magnet motors using the frozen permeabilities method," *IEEE Transactions on Magnetics*, vol. 41, no. 10, pp. 3946-3948, October, 2005.

[4] P. Ponomarev, "Tooth-Coil Permanent Magnet Synchronous Machine Design for specail applications,"*PhD Thesis*, Universitatis Lappeenrantaensis, Lappeenranta, 2013.

[5] F. Meire, "Permanent-Magnet Synchronous Machines with Non - Overlaping Concentrated winding for low speed Direct Driven drive Applications," *PhD Thesis*, Royal Institute of Technology, School of Electrical Engineering, Stockholm, 2008.

[6] D.Howe, and Zhu.Z.Q, "Halbach permanent magnet machines and applications: a review," *IEE Proc. Electr. Power Appl,* vol. 148, no. 4, pp. 299-308, July, 2001.

[7] Nicola Bianchi, Silverio Bolognaniand and Emanuele Fomasiero, "A General Approach to Determine the Rotor Losses in Three-Phase Fractional-Slot Machines PM," *IEEE International Electric Machines & Drives Conference,* vol. 1, pp. 634-641, July, 2007.

[8] Sreeju S. Nair, Jiabin Wang, Liang Chen, Robert Chin, Iakovos Manolas and Dmitry Svechkarenko, "Prediction of 3-D High-Frequency Eddy Current Loss in Rotor Magnets of SPM Machines," *IEEE Transactions on Magnetics,* vol. 52, no. 9, pp. 634-641, Sept, 2016.

[9] Amit kumar Jha, Afef Kedous-Lebouc, Lauric Garbuio, Jean-Paul Yonnet and Jean-Marc Dubus, "Design and Comparison of Outer Rotor Bonded Magnets Halbach Motor with Different Topologies," *International Conference on Electrical Machines, Drives and Power Systems (ELMA),* Sofia, Bulgaria, June, 2017.

[10] Dahaman Ishak, Zhu.Z.Q and David Howe, "Eddy-Current Loss in the Rotor Magnets of Permanent-Magnet Brushless Machines Having a Fractional Number of Slots Per Pole," *IEEE Transactions on Magnetics,* vol. 41, no. 9, pp. 2462-2469, September, 2005

Weighted Index of Recycling and Energy (WIRE) Cost for Motors in Electric Vehicles

Amit Kumar Jha[1+], Ziwei Li[1,2+], Adolfo Garcia [3+], Pranshu Upadhayay [1,2+], Peter Omand Rasmussen[3], Afef Kedous-Lebouc[1] and Lauric Garbuio[1]
[1]Univ. Grenoble Alpes, CNRS, Grenoble INP G2Elab, 38000 Grenoble, France
[2]Valeo - Equipements Electriques Moteur, 2 rue Andre Boulle, 94000 Creteil, France
[3]Deaprtment of Energy Technology,Aalborg University, Pontopidanstrade 111, Aalborg East 9220
[+]These four authors contributed equally to this work
Email: Amit-kumar.jha@g2elab.grenoble-inp.fr

***Abstract*—With increasing demand of electric vehicles it is very important to recycle critical rare earth materials used in the permanent magnet motors such as Neodymium (Nd), Dysprosium (Dy) and Cobalt (Co) etc. To achieve easy recycling, focus of the motor design shall shift to design for recycling. The article presents a methodology (WIRE) to evaluate and benchmark the motor in terms of their recyclability. The method can be used to compare different motors. The method was used for evaluation of a commercial permanent magnet based HUB motor and the results are presented. A comparison between recyclability index of four different motors topology is also presented.**

***Index Terms*—Motor Recycling, Magnet Recycling, Motor Benchmarking**

I. Introduction

The demand for cleaner mode of urban transport is increasing and many countries like UK, France, Norway, Sweden etc have already announced the phasing out of diesel and petrol cars from their streets in couple of decades and likely more countries will join soon [1]. The sales of electric vehicle (EV) and hybrid electric vehicle (HEV) in recent years is growing every year and is projected to continue at higher rate in coming years [2]. At present, almost all automobile manufacturers are using permanent magnet (PM) motors to achieve high efficient vehicles [3]- [4]. The amount and quality of PM is critical for high performance motors. Therefore, to maintain the vehicle growth it is very important to have sufficient and sustainable supply of magnets. At present, Neodymium Iron Boron (NdFeB) magnets are the strongest magnets. The magnet contains critical rare earth materials like Nd and Dy. Due to limited availability of these materials it is very crucial to recycle them and use again in motors. In recent years, there has been some focus from industry and researchers on recycling of magnets. The projects like EREAN, RARE^3 etc are focusing on developing methods to recycle extracted magnets. The extraction of magnets from the existing electric motor design has been investigated in the project called MORE. The motor designs present today are not designed for recycling i.e. extraction of magnet is very difficult [3] & [5]. In Demeter (H2020) project one of the goals is to design motor for recycling. However, the challenge for the motor designers is to evaluate motors with respect to the recyclability and comparison of different designs. At present there is no tool to analyze the motors design for the recycling and benchmark them. In this article a method is presented to analyze and evaluate the recycling of the motors for EVs and HEVs. The method is divided in two parts. The first part evaluates recyclability of the motor considering standardization, assembly and disassembly of the motor. The second part evaluates the impact of the motor design on the performance of the motor considering energy consumption over the complete life cycle. In this article only first part is presented and discussed. The method was used to evaluate the recycling index of a commercial hub motor and the results are presented. The evaluation of four different motors designed for DEMETER project were carried out by using WIRE method. The comparison of scores are also presented and analysed.

II. Methodology

The first part of the WIRE methodology is to evaluate the ease of assembly/disassembly of electric motors. The evaluation process is divided in two parts - Standard and Cost. Each part has three categories Material, Assembly and Disassembly. Moreover, the evaluation of each material or process in each category is done in two parts. The first is **Score (S)** which depends on its relative scale in respective section. The second is **Importance (I)** which depends on material/process relative criticality in terms of recyclability of materials. The final score is the product of both i.e. **(SxI)**. The score for each activity is in the range of 1-5. For evaluation of WIRE it is recommended to have a group of 5-6 people from different fields, involved in design and manufacturing process of the motor. Figure 1 shows the evaluation sheet for the different materials of the motor for both the parts-standard and cost. Although, the evaluation largely depends on the mutual agreement of the group formed for evaluation i.e. standard and cost, certain guidelines are formed to evaluate different sections. Furthermore, the process/ materials in different sections are different depending on the criticality of the material/process. For example, the wires of sensor is important while assembling however, their importance is negligible while disassembly.

Scoring pattern	0-5	1 - Lowest score	5 - Highest score	
		1 - Lowest score	5 - Highest score	3 = neutral score
Assumption	The motor developed is new and for the first time and manual disassembly with high volumes i.e. 50,00			

MOTOR ID	Hub motor for in-wheel application							
Component/ Parts		Standard			Cost			Recyclability SCORE
		S	I	SxI	S	I	SxI	
Materials								
- Stator								
	Lamination S	5	5	25	1	5	5	30
	Copper	5	5	25	2	1	2	27
- Rotor								0
	Steel R	5	5	25	1	4	4	29
	Magnets	5	4	20	5	1	5	25
-Shaft								0
	Shaft	4	5	20	1	2	2	22
-Endshileds								0
	Drive Side	2	5	10	1	2	2	12
	Non-Drive side	2	5	10	1	2	2	12
			34	135		17	22	157
	section score			79.41 %			25.88 %	

Fig. 1: Evaluation sheet of material for standardization and cost

A. *Definitions of WIRE sheet*

As mentioned earlier, the WIRE evaluation is relative and hence, the accuracy of the method largely depends on the definitions of different sections. Different process/materials has different significance in the final recycling of the motor. It is important to note that the scoring is relative and hence the tool is good for comparing two motors evaluated keeping same scaling in consideration. In the following section definitions of different terms used for the evaluation are given.

- **Standard** : The category focuses on the use of standard material/processes. The evaluation for Standard category is done with the view that use of standard parts/process will simplify and encourage the recycling. Furthermore, higher the number of standard component in the motor easier it will be for recycling and further improves the quality of the recycled output.
  1) Material
     - 'S' depends on the standardization of the material. The score is higher for material, which are easily available (off the shelf) and widely used. For example, random wound copper winding are more used and widely available then rectangular strand cable of certain dimension.
     - 'I' depends on materials recyclability. For example, NdFeB magnet with and without coating is easily available however, in terms of recyclability the magnet without coating will be easier for recycling and hence its index shall be higher.
  2) Assembly
     - 'S' depends on the process/activity standardization. While scoring it is also important to consider the tools used. More non-standard tools or process used in assembly shall lower the score. For example, if special heat treatment/ or other special environment is needed for assembly, process will be non-standard and thus the index shall be lower.
     - 'I' depends on the criticality of the step/process for recycling of the part. For example, if the assembly of the copper affects the recycling of the copper. Therefore, the index shall be high.
  3) Disassembly
     - 'S' depends on the process/activity standardization. While scoring it is also important to consider the tools used. More non-standard tools or process used in disassembly shall lower the index. For example, if some chemical is needed for extraction of certain component the score shall be lower for the process.
     - 'I' depends on the criticality of the step/process for recycling of the part. Same as assembly, if disassembly process of copper make recycling easier the index shall be high.
- **Cost** : The category focuses on the cost of material/processes and its impact on recycling. The evaluation for Cost category is done with the view that higher cost of any process will increase the overall recycling cost and hence, has negative impact on the recycling. On the other hand, higher material cost incentives the recycling of that particular material like magnets and encourages recycling.
  1) Material
     - 'S' depends on the cost of the material. Higher the material cost higher the score. The processing cost of the component varies over a wide range. Therefore, to keep the tool simple and to avoid processing cost variation of the component only material cost is considered. Moreover, the non-standard design or the impact of processing will be taken care while scoring standard category. For example, NdFeB magnet is roughly 10 times costlier than the laminations in the motor. Therefore, score of magnet will be higher than the laminations. The impact of different shapes of magnet should be considered while scoring standard material category.
     - 'I' depends on the impact of the material on recycling of the whole motor. For example, if the weight of the material is very low comparing to other materials, the material recovered will be very small. Therefore, the recovery in terms of economic value will be small, even with high price of the material.
  2) Assembly
     - 'S' depends on cost required to execute the assembly process/activity. Higher the assembly cost lower the score shall be as it impacts the recycling process negatively. For example, if there

TABLE I: Scoring of Material for Standard Category

Magnet Type	S
Rectangular small pieces with/ without coating sintered, Bonded Magnet	5
Sintered/bonded shape parallel/radially magnetized	4
Halbach bonded	3
Sintered or Bonded powder but magnetised in rotor	2
Sintered halbach multipole	1
Lamination Type	**S**
Silicone iron 0.35-0.6mm, Single solid rotor	5
Silicone steel modular type	4
Cobalt Steel	3
Amorphous, different shapes	2
SMC	1
Winding Type	**S**
Copper / aluminium strand circular	5
Copper rectangular standard, aluminium cast rotor	4
Copper rectangular/cricular non standard	3
Hollow circular copper wire	2
Any thing special	1

I	Magnet Type
5	Rectangular small pieces or powder without coating or binder
4	Sintered with coating
3	Sintered any shape with coating/glue
2	Bonded magnets
1	Bonded magnets with glue
I	**Lamination Type**
5	Any silicone iron lamination or solid rotor or Aluminum
4	Cobalt steel
3	Amorphous Steel
2	Soft Magnet Composites (SMC)
1	Any new special handling material
I	**Winding Type**
5	Copper any type
4	Aluminium wire/Cast aluminium /Copper rotor
2	Any new special handling material

is a need of special environment for assembly, it increases the complexity and hence cost.

- 'I' depends on the impact of cost of the process in recycling. For example, if a motor uses powder NdFeB magnet technology. The assembly cost is higher but this cost does not impact the recycling of the magnet at the end of life (EOL) of the motor. Therefore, the index shall be neutral.

3) Disassembly

- 'S' depends on cost required to execute the disassembly process/activity. Higher the disassembly cost lower the score shall be as it impacts the recycling process negatively. For example, if there is a need of special environment for disassembly, it increases the complexity and hence, cost which in turn discourages recyclability economically.
- 'I' depends on the impact of cost of the process in recycling. For example, the cost of disassembly of the magnet is very critical for the recycling of the magnet. Therefore, the index shall be high for that process.

B. Calculation of Recyclability Index

The final weighted recyclability index (R) is calculated using equation 1 and 2. The R_w is in the scale of 1-5 and using equation (2) is expressed in percent, R.

$$R_w = \frac{S_1 * I_1 + S_2 * I_2 + \cdots + S_n * I_n}{\sum I} \tag{1}$$

TABLE II: S of assembly/disassembly for Cost category

Assembly / Disassembly Cost	S
Easy assembly/disassembly without any tool	5
Easy assembly/disassembly with standard tools /process	4
Complex / Hard process with standard tools or more than one person required	3
Special pre/post treatment with special tools	2
New extra method to extract magnet from rotor	1

$$R = \frac{R_w * 100}{5} \tag{2}$$

C. General Guidelines for scoring

The section provides some general guidelines, which can be used to score different sections of WIRE sheet. It is important to note here that the scores are relative and can be varied on general consensus or when scenario changes. The authors decided the scores after discussing different scenarios.

1) Scoring of materials for Standard category: Table I shows the scoring of material and its importance for recyclability with respect to their standardization. The table shows the scores for main components of the motor like lamination, magnet and copper. The materials are scored based on the definition given in section II-A.

2) Assembly/Disassembly score for Cost: Table II gives the scoring guideline for assembly/disassembly in terms of cost. Simpler the process higher the score shall be.

3) Assembly/Disassembly of stator and rotor: The scoring guideline for individual components (stator, rotor, bearing etc)

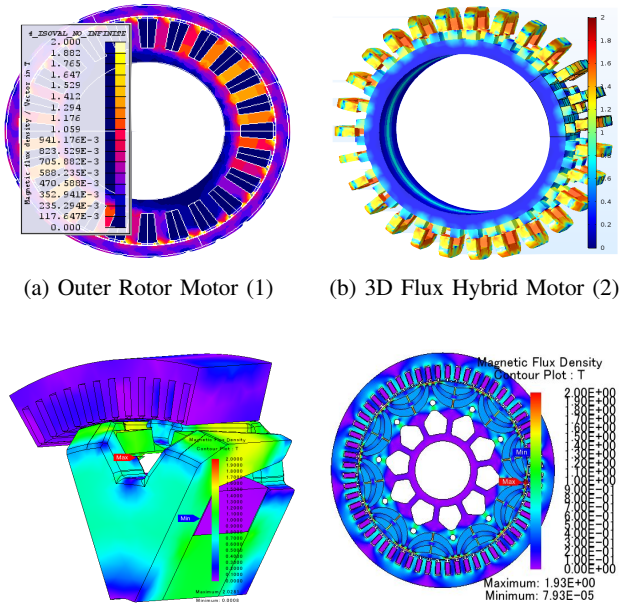

(a) Outer Rotor Motor (1) (b) 3D Flux Hybrid Motor (2)

(c) Claw Pole Motor (3) (d) Radial IPM Motor (4)

Fig. 2: Flux density distribution in different motors

TABLE III: Score of material cost in motor

Material Cost	**S**
Sintered Magnet	5
Bonded Magnet	4
SMC,Amorphous steel	3
Copper	2
Silicone Steel lamination	1

TABLE IV: Importance of Assembly/Disassembly process

Process	**Standard Importance**	**Cost Importance**
Assembly of stator lamination	3	3
Assembly of copper winding	3	3
Assembly of rotor lamination	3	3
Assembly of magnet and rotor	5	3
Assembly of sensor wires	1	3
Assembly of rotor and stator	3	3
Assembly of end shields	3	3
Assembly of shaft	3	3
Disassembly of end shields	3	3
Separation of rotor and stator	4	4
Disassembly of copper	3	4
Disassembly of stator	3	3
Disassembly of magnets from rotor	5	5
Disassembly of rotor	3	3

is shown in Table II. However, there is one more critical step in assembly/disassembly, which is separation of a rotor from a stator. The complexity of the process is even higher in PM motors. The ease of assembly / disassembly mainly depends on the force of extraction and its size. Therefore, to scale the process following method is used. Larger the volume and airgap flux density i.e. power of the motor, separation of rotor and stator will be difficult and hence, the score shall be lower. Mathematically it can be presented by equation 3. Figure 2 shows the flux density distribution in motor for 4 different topologies designed in framework of DEMETER project. Motor 3 has lowest flux density and hence, disassembly will be much easier compared to other motors.

$$\mathbf{S} \propto \frac{1}{V * B_{\delta}^{2}} \tag{3}$$

where, V is volume of the motor and B_{δ} is the airgap flux density.

4) Scoring 'I' of material for Cost category: The scoring of 'I' depends on the weight of the material in the motor. Higher the weight of the material higher will be the recovery of material from recycling. The proposed method to estimate that is as follows. Lets assume, the motor has W_c kg of Copper, W_s kg of Stator steel, W_r kg of rotor steel and W_m weight of Magnet and the weight (W_s) of stator steel is maximum. The I score for stator steel W_s is 5 and the rest is scaled in proportion to the W_s. The fraction numbers are rounded to nearest integer.

$$\text{I for magnet is } \frac{W_m * 5}{W_s}$$

$$\text{I for copper is } \frac{W_c * 5}{W_s}$$

Table III shows the relative score of material used in the motors.

5) 'I' of assembly/disassembly for Standard & Cost category: The criticality of each step during assembly and disassembly is shown in table IV. While indexing, the recycling of steel, copper and magnet was considered important and hence, the process affecting their recycling was index accordingly. If some step of assembly is very important for recycling of that material then it shall have high indexed. For example, assembly of magnet and rotor is very significant for extraction of magnet and hence, has high index.

III. WIRE EVALUATION FOR HUB MOTOR

The developed methodology was used for evaluating commercial permanent magnet based HUB motor. The motor was disassembled manually with standard tools and the process was observed keeping in mind the recycling of the parts. Figure 3 shows the different stages while disassembly of the motor. After complete disassembly of the motor the WIRE sheet, was filled by the authors. For simplicity many assembly/disassembly steps are clubbed together and score and importance were given. The scores of standard and cost of the WIRE evaluation is shown in figure 4. The final cost index is lower than the final standard index. The motor is a commercial motor and has used more standard parts and processes. The index for cost of the material is lower compared to assembly and disassembly. It is important to note here that the index is relative and in absolute terms cost of material can be higher than the assembly and disassembly of the motor. As mentioned earlier the method is developed to compare different motors recyclability. The final recycling index (R) of the motor is

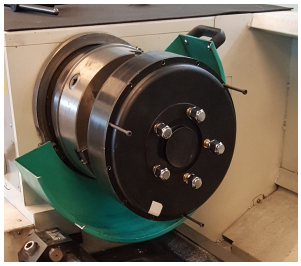

(a) Motor

(b) Motor without End-shields

(c) Stator

(d) Rotor

Fig. 3: HUB Motor Diassembly

68.5%. The low index was expected as motor is not designed for recycling.

IV. Comparison of Recyclability Index of four motors

Figure 4 shows the four different motors designed for (H)EVs with ease of recycling in the framework of DEMETER project. Motor 1 is an outer rotor topology motor with an ideal Halbach magnet manufactured using bonded magnet. Motor 2 is a 3D flux hybrid motor using modular amorphous steel stator core and the rotor has sintered magnet placed between rotor laminations. Motor 3 is a permanent magnet based claw pole motor topology designed for easy extraction of magnet for mild hybrid vehicle. Motor 4 is an interior PM(IPM) motor using thermoplastic type bonded magnets and can be magnetized inside a rotor core. The motors were evaluated using WIRE method to compare the recyclability index. Figure 6 presents the index of all 4 motors in standard and cost category for assembly, disassembly and material. It can be seen that motor 3 has highest score in assembly subcategory because the process for the claw pole is highly industrialized and the design change made for easy recycling is minor. On the other side motor 2 has lowest score because the 3D flux machine has U core laminations for stator which requires special process to assemble. Moreover, due to the magnets position and glue that used for magnet fixing, the rotor assembly is also more complicated than the rest. The disassembly of motor 1 has maximum score because of simple rotor structure and no glue is used for magnet assembly, whereas motor 2 has the lowest because to extract magnet special processing is required. The material used in all 4 motors are standard and hence, have similar scores. The material cost of motor 2 has the highest

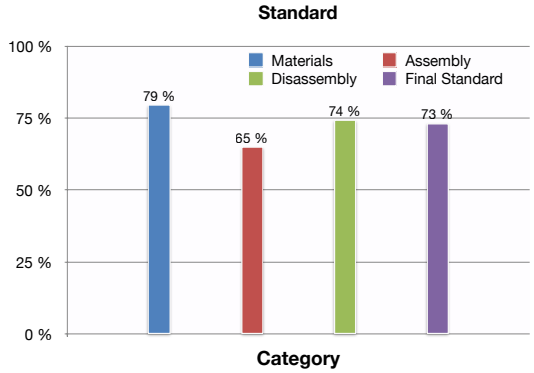

(a) Standard Distribution

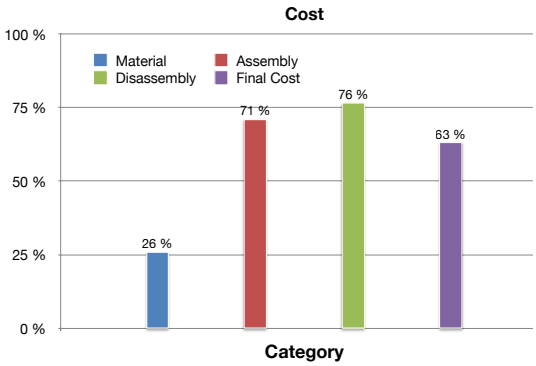

(b) Cost Distribution

Fig. 4: Distribution of Recycling index of the sample motor

score shows that the recovery of high valued material from motor 2 is maximum compared to others. For assembly and disassembly in terms of cost the trend is same for all the motors. Motor 1 has the highest score because of simple structure. Thus, the disassembly process does not need any special treatment of magnets before extraction. Whereas, some pretreatments are required for other motors to extract magnet, which contributes to lower indexes. The final recyclability index of four motors are 71%, 63%, 71% and 64% respectively

V. Conclusion and Discussion

The WIRE method is developed for indexing the recyclability (R) and energy impact of the motors. In this article recyclability part of the method is presented. The method is simple to use and can be modified as per the requirement. The methodology takes standardization and cost into consideration for determining the recyclability of the motor. The recycling of any motor depends on the materials used, assembly and disassembly. The evaluation is relative in nature and hence, will be effective in comparison of motors done keeping the scaling same. To make method evaluation objective, different scoring guidelines is also presented and can be modified if the evaluating team finds suitable. The motor designed for recycling should have higher standard components with easy assembly and disassembly process.

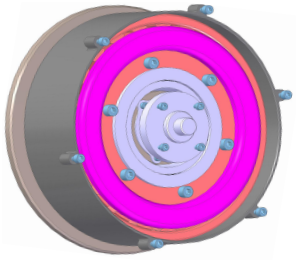

(a) Outer Rotor Motor (1)

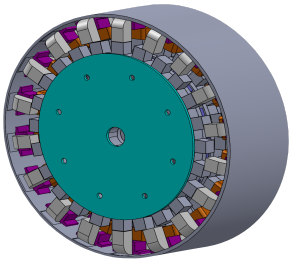

(b) 3D Flux Hybrid Motor (2)

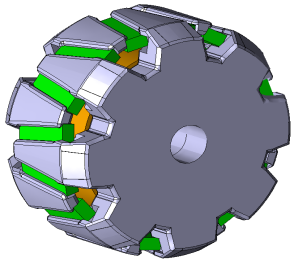

(c) Claw Pole Motor (3)

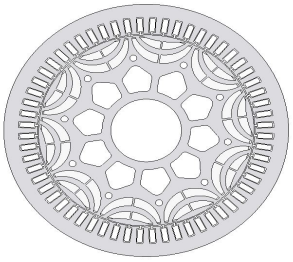

(d) Radial IPM Motor (4)

Fig. 5: Four Different Motors Designed in DEMETER project

The evaluation was done for a commercial hub motor and the scores are presented. Many processes in assembly/disassembly were clubbed together to keep the evaluation simple due to lack of certain information. The recycling index for the motor is 68.5%, which is low as motor is not designed for the recycling and the index can be improved by modifying small design changes.

The final recyclability index of four motors are 71%, 63%, 71% and 64% respectively. The scores obtained reflect that the method is able to distinguish the features of motor for easy recyclability. The WIRE score comparison of the 4 motors show that the recyclability increases with the high utilization of standard materials. It further improves if machine design is such that it can be assembled and disassembled using conventional process and tools. The use of glue for magnet assembly makes recovery of magnet from motor difficult and lowers the recyclability index. Furthermore, use of complicated motor structure also lowers the recyclability index. However, one has to keep in mind the method by its nature scores lower for new / innovative designs / method as can be seen in the case of motor 2. Therefore, the designers must strive to use conventional/ standard method of assembly and disassembly with magnet assembly without any glue to make motor easier for recycling.

ACKNOWLEDGMENT

The research leading to these results has received funding from European Communitys Horizon 2020 Programme ([H2010/2014-2019]) under Grant Agreement no. 674973 (MSCA-ETN DEMETER). This publication reflects only the authors view, exempting the Community from any liability. Project website http://etn-demeter.eu/

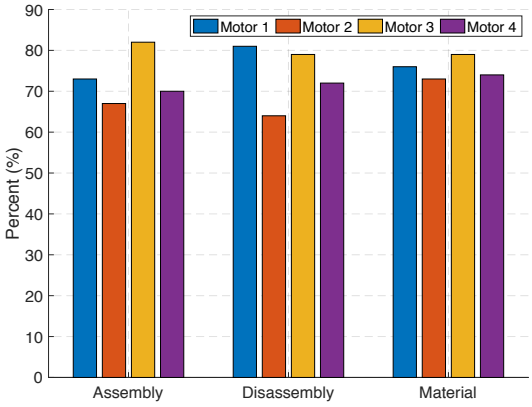

(a) Score of Standard category for 4 motors

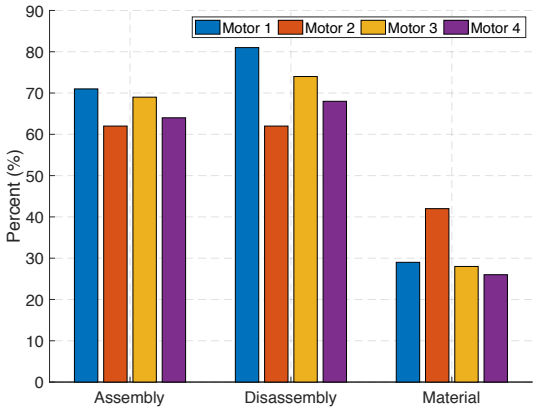

(b) Score of cost category for 4 motors

Fig. 6: WIRE evaluation scores for all four motors

REFERENCES

[1] Countries are announcing plans to phase out petrol and diesel cars. is yours on the list? [Online]. Available: https://www.weforum.org/agenda/2017/09/countries-are-announcing-plans-to-phase-out-petrol-and-diesel-cars-is-yours-on-the-list/

[2] Internaltion Energy Agency, Ed., *Global EV Outlook 2017*.

[3] T. Elwert, D. Goldmann, F. Rmer, M. Buchert, C. Merz, D. Schueler, and J. Sutter, "Current developments and challenges in the recycling of key components of (hybrid) electric vehicles," *Recycling*, vol. 1, no. 1, pp. 25–60, 2015. [Online]. Available: http://www.mdpi.com/2313-4321/1/1/25

[4] L. Kumar and S. Jain, "Electric propulsion system for electric vehicular technology: A review," *Renewable and Sustainable Energy Reviews*, vol. 29, no. Supplement C, pp. 924 – 940, 2014. [Online]. Available: http://www.sciencedirect.com/science/article/pii/S1364032113006734

[5] U. Bast, R. Blank, M. Buchert, T. Elwert, F. Finsterwalder, G. Hornig, T. Klier, S. Langkau, F. Marscheider-Weidemann, J.-O. Muller, C. Thurigen, F. Treffer, and T. Walter, "Recycling von komponenten und strategischen metallen aus elektrischen fahrantrieben," Aug-2014.

Validation of Efficiency Maps of an Outer Rotor Surface Mounted Permanent Magnet Machine for Evaluation of Recyclability of Magnets

Adolfo Garcia Gonzalez[1], Amit Kumar Jha[2], Ziwei Li[3], Pranshu Upadhayay[3], and Peter Rasmussen[1]
[1]Department of Energy Technology, Aalborg University, Aalborg 9220 Denmark
[2]G2Elab Grenoble INP, Grenoble 38031 France
[3]VALEO Electrical Systems, Creteil 94000 France

The goal of this paper is proposing a methodology for the evaluation of the recyclability criterion of permanent magnets (PMs) in electrical machines for Hybrid and Electric Vehicles ((H)EVs). Such methodology was validated with measurements performed to a PM machine of the hub type. In addition, the methodology proposed here is approached in terms of energy consumption. Hence, measurements of torque and speed were taken at various working points. This study comprises the disassembly of one unit in order to determine the main dimensions of the machine for modelling in 2D Finite Element Method (FEM). Additionally, samples of the magnets in the rotor were taken for characterization of their properties. The results of simulations were contrasted with the measurements for the validation of the efficiency maps. Finally, a study case was selected, in which the use of recycled magnet material was simulated and the reduction of efficiency was quantified.

***Index Terms*—Efficiency maps, 2D-FEM, driving cycle, energy consumption, magnet recyclability.**

I. Introduction

THE global trend towards the implementation of (H)EVs is challenging from the perspective of energy supply and the use of materials with high fluctuation of prices in the international market such as Rare Earth Elements (REEs). Recycling of REEs has been proposed as an alternative for counteracting this situation. Furthermore, work has been carried out in the design of electrical machines with recycled materials [1], [2], [3]. However, there is a lack of tools allowing to determine the feasibility of the recycling of PMs in electrical machines. Hence, this article attempts to set the base for a methodology for evaluating of the recyclability of their PMs [4]. In this regard, two approaches might be adopted. One from the perspective of the disassembling process [5], [6]. The second one from the perspective of the energy consumption in the life cycle of the machine. The evaluation of the energy consumption of a machine used in (H)EVs may be done under any of the defined driving cycles [7]. Therefore, it is required to determine the efficiency of the machine at any given working point. In this sense, the methodology proposed here is validated with measurements performed to an outer rotor surface mounted PM machine of the hub type commercially available and used in both electrical scooters and small city cars.

Efficiency maps have shown to be useful at representing the performance of electrical machines in propulsion applications [8]. In addition, work has been carried out with efficiency maps as optimization tool [9]. Furthermore, the analysis of different machines under various driving cycles have been addressed in earlier studies [10]. However, the work presented here is aimed to validate a methodology for the evaluation of the recyclability criterion from an economic perspective (i.e. energy consumption).

Experimental results focused on the determination of efficiency of the machine are presented in Section II. In section III results of simulations are included, as well as, the elaboration of the efficiency maps. Section IV is devoted to the determination of the efficiency maps in a study case assuming the use of recycled magnets. The analysis of the results obtained are shown in section V. Lastly, conclusions are drawn and future work is proposed.

Corresponding author: A Garcia Gonzalez. (email: agg@et.aau.dk). A. Garcia Gonzalez, A. Kumar Jha, Z. Li, P. Upadhayay and P. Rasmussen contributed equally.

II. Experimental set-up

Measurements were performed on an outer rotor surface mounted PM which is generally used in electrical scooters or small city cars [11]. The set-up is shown in figure 1. A resistive load was connected to the machine operating as generator, and values of input and output power were measured. The results of efficiency at different values of torque and speed are illustrated in figure 2.

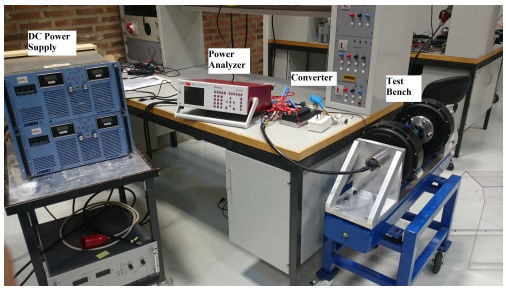

Fig. 1: Experimental set-up.

A. Disassembly

The disassembly of the machine was carried out in order to obtain the main dimensions for the elaboration of the 2D

978-1-5386-6425-4/18/$31.00

FEM model. Samples of the magnets were taken and analysed with the Physical Property Measurement System (PPMS) from Quantum Design®.

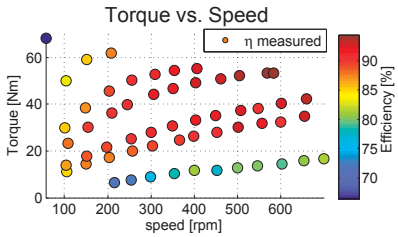

Fig. 2: Measured efficiency at different values of torque and speed.

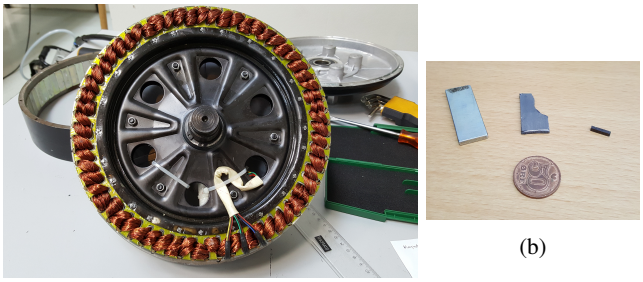

(a) (b)

Fig. 3: (a) Disassembly process, (b) Magnet samples.

B. Main dimensions

The main dimensions of the outer rotor machine analysed in this study are shown in table I.

TABLE I: Main machine dimensions.

Parameters	Value
Stack length L_{stack} [mm]	40
Maximum speed [rpm]	700
Air-gap length [mm]	0.6
Magnet axial length [mm]	40
Magnet thickness [mm]	3
Magnet width [mm]	14
Stator radius [mm]	126.5
Number of poles	56
Number of slots	63
Winding type: concentrated	

III. Elaboration of Efficiency Maps

Figure 4 illustrates the model implemented in 2D FEM. In addition to the dimensions in table I, the properties of the materials were required as inputs. The test performed to the magnet with PPMS yielded a value of remanence of approximately $B_r = 1.2$ T. On the other hand, the quality of the material of the stator laminations was unknown. Nevertheless, the properties of a standard SiFe lamination with similar thickness were modelled. Hence, the lamination M400-50 was selected. Simulations were run applying the measured current. The efficiency of the measured working points was estimated with the calculated no-load losses (i.e. stator and rotor iron losses and PM losses) and copper losses. The effect of harmonics induced by the modulation of the inverter were disregarded in the simulations. The results are shown in figure 5. Most of the results follow the trend of the measurements illustrated in figure 2.

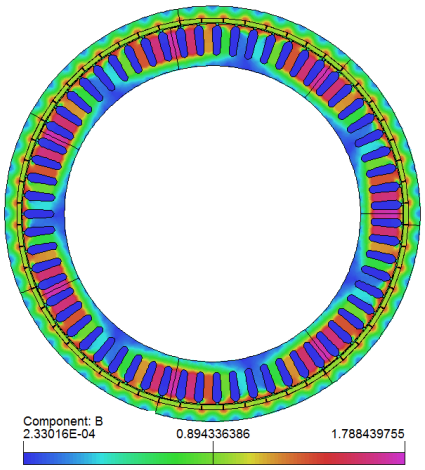

Fig. 4: Geometry modelled in FEM and magnetic flux density distribution at T=11.6 Nm and n=105 rpm.

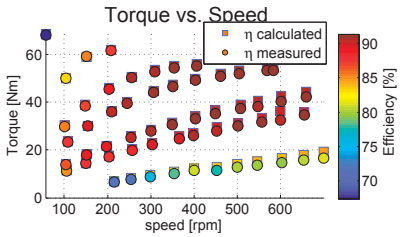

Fig. 5: Measured and calculated efficiency at different values of torque and speed.

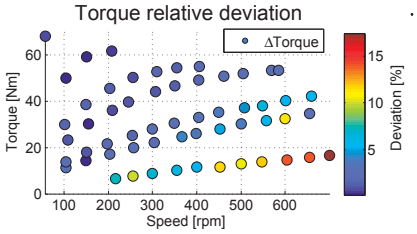

Fig. 6: Deviation in measured and calculated torque at different values of torque and speed.

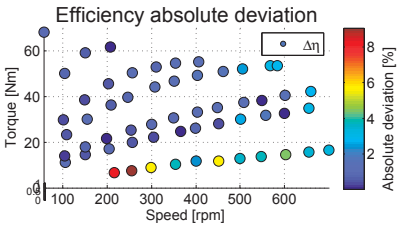

Fig. 7: Deviation in measured and calculated efficiency at different values of torque and speed.

Figure 6 shows the deviation in the calculation of the torque compared with measurements. The maximum deviation was

estimated of approximately 17 %. In addition, the deviation in the calculation of the efficiency is illustrated in figure 7, with a maximum value of approximately 9 %. Various factors might be the source of such differences. In the case of the torque, the quality of the lamination might influence the performance of the machine regarding torque production. The deviations in the efficiency calculations are due to the absence of the mechanical losses in the simulation results. In addition, simulations do not account for processes such as cutting, stacking, etc. that might diminish the quality of the laminations, thus increasing the losses. Additionally, errors in the measurements may influence the deviations between measured and simulated efficiencies. Further analysis in this regard is presented in section V.

After contrasting the simulated values with the measurements, the magnet flux linked with the stator windings Ψ_m was determined and the torque was obtained analytically with the expression:

$$T = \frac{3}{2}(\Psi_m \cdot I_q \cdot p) \tag{1}$$

Where I_q is the current applied in the *q-axis* and p is the pole-pairs number. This expression allows having torque values at currents that were not measured, enhancing the resolution for the elaboration of the efficiency maps. The copper losses p_{cu} were obtained with the DC resistance of the windings R_w and the measured current I_m as:

$$p_{cu} = 3 \cdot I_m^2 \cdot R_w \tag{2}$$

For obtaining the stator and rotor iron losses and PM losses at any speed, quadratic fitting was applied to the losses calculated with 2D FEM simulations. Consequently, the efficiency was determined at any working point of the machine. The resulting efficiency map is presented in figure 8. This efficiency map agrees with the efficiency map of a Surface Mounted PM machine, which values of efficiency are higher as the machine is at its highest performance. In addition, it shows the incremental behaviour of the iron losses with the speed, and the increment of the copper losses with the increment of the torque.

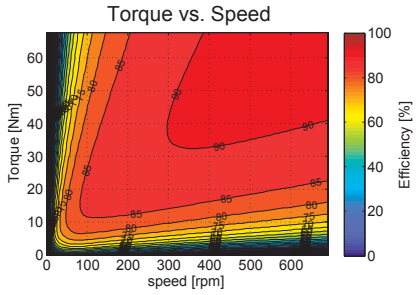

Fig. 8: Efficiency map of the original machine.

IV. Study Case

The main goal of DEMETER project [12] is the study of the recyclability and reuse of magnets in (H)EVs. Therefore, a study case was defined in order to verify the methodology followed so far. Magnets manufactured with recycled material are expected to have lower remanence [13]. Hence, the remanence adopted for this study case was assumed to be 20 % lower, that is, $B_r = 0.96$ T. In order to perform a fair comparison, some assumptions were adopted for the study case presented here:

- Same geometry as in figure 4 was analysed. That is, similar values of current were applied to a new set of simulations with PMs of lower remanence.
- For performing a valid comparison, same performance in terms of torque production was required. Consequently, the axial length of the machine was increased by 15 %, that is, the new stack length was $L_{stack} = 46$ mm.
- The thermal aspects of having higher copper losses were disregarded for the analysis.

The procedure described previously was followed for the elaboration of the efficiency maps for this study case. Figure 9, illustrates the efficiency maps resulting from the use of assumed recycled magnets. Here it is observed the reduction of the efficiency in the region at low speed and high torque, where the copper losses are dominant. In the region at high speed low torque, where the no-load losses are dominant, the variation is less noticeable.

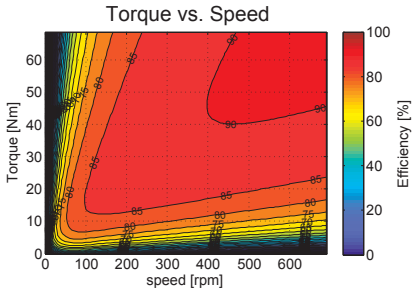

Fig. 9: Efficiency map of the machine for the study case.

A. Comparison of efficiency maps

Figure 10 shows the deviations between the efficiency map for the original machine and the efficiency map obtained for the study case. The differences are more noticeable in the regions at high torque and low speed. That is, where the copper losses are dominant due to the higher current. In contrast, in regions at low torque and high speed, the deviations are lower. In this region the iron losses are dominant due to the higher frequency. However, the reduction of the iron losses due to the reduction of the remanence of the PMs is compensated by the increment of the length of the machine.

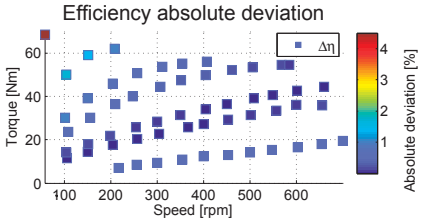

Fig. 10: Absolute error of efficiencies between efficiency map of original machine and machine with magnets of lower remanence.

V. Results Analysis

This section is intended to enhance the understanding of the results in the presence of deviations between measurements and calculations. Furthermore, the analyses reported in this section were carried out on the original machine for similar values of torque and speed as for measurements. Hence, a decay test was performed on the original machine. It consisted in running the machine solely by pulling the shaft and recording the back-emf waveforms in an oscilloscope. A time decaying back-emf wave-form was obtained, and the no-load losses p_{decay} (i.e. core losses, PM losses and mechanical losses) were obtained with the expression [14]:

$$p_{decay}(\omega_m) = -\omega_m J \frac{d\omega_m}{dt} \tag{3}$$

Where J is the inertia of the machine and ω_m is the mechanical angular speed. The inertia J was estimated with the main dimensions of the machine. The no-load losses as function of the speed of the machine were approximated by quadratic curve fitting. Figure 11 shows the decay test results, the calculated losses performed with 2D FEM and the measured no-load losses.

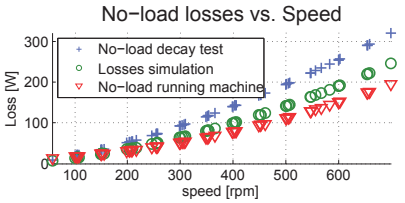

Fig. 11: Measured and calculated no-load losses in the original machine.

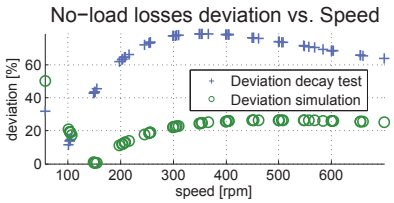

Fig. 12: Deviations in the no-load losses.

The deviations between measured and simulated results are shown in figure 12. The maximum deviation was estimated in approximately 50 %. The main source for this deviation would correspond to the portion of the mechanical and stray losses that are not included in the 2D FEM model. Additionally, the specific losses of the laminations in the actual machine remain unknown. Furthermore, as mentioned in section III the processing of the laminations (i.e. cutting, stacking, etc.) is not accounted in the simulations. Regarding the decay test results, figure 12 shows the largest deviations of approximately 79 %. The no-load losses p_0 with the machine running were determined with the following expression:

$$p_0 = P_m - P_o - p_{cu} \tag{4}$$

Where P_m is the input power measured with the power analyser and P_o is the output power obtained with the measurements of torque and speed in the torque transducer. Note that p_0 contains the mechanical losses, core losses and PM losses.

A. Effect of the calculation of J

In order to evaluate the sensitivity of the value of inertia J in the losses calculated with the decay test, J was modified by ± 10 %. The results are shown in figure 13.

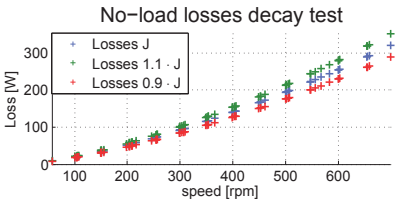

Fig. 13: Comparison of no-load losses with various values of inertia J.

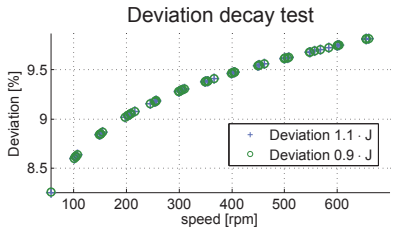

Fig. 14: Deviation of losses calculation with changing J.

As shown in figure 14 the maximum deviation was estimated in 10 %. In this work, the calculation of J was performed both analytically and with the help of CAD software. The relative error between the two methods was approximately 3 %. The inertia calculated analytically was $J_{ana} = 0.0899$ kg·m^2. With CAD software, this value was estimated in $J_{cad} = 0.0905$ kg·m^2. The maximum calculated deviation due to the variation of the value of J was estimated in 3 %.

B. Effect of the measurement of torque

During the test with load in the machine, oscillations in the reading of torque were observed. In addition, an offset value was present in the interface used to read the values of torque. Such offset was identified having a value of approximately 0.35 Nm. The goal in this section is to identify the behaviour of the measured losses accounting for such deviations of the torque measurements. Hence, expression 4 was evaluated for the calculation of the no-load losses, accounting for the torque offset, by subtracting its value from the measurements. The results after applying quadratic curve fitting to the data are shown in figure 15 together with the decay test results and the values obtained with simulations.

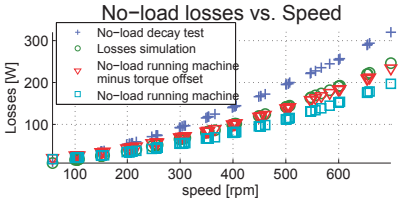

Fig. 15: No-load losses in the machine with torque offset.

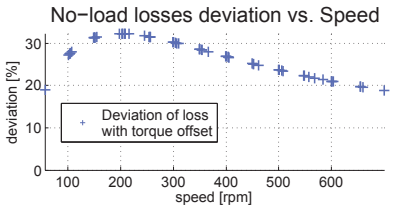

Fig. 16: Deviation in the no-load losses accounting for torque offset.

As it can be observed in figure 16, the subtraction of the torque offset from the measured values leads to the increment of the no-load losses. The maximum deviation between the decay test results and the measured values is of approximately 32 %. Which shows that the calibration of the torque transducer might have a significant impact in the estimation of the no-load losses as in equation 4. In addition, the losses calculated in 2D FEM are still close or even higher than the measured values. This might be the indication that in the original machine, an electrical lamination of lower specific losses was used. As future work, it would be interesting to determine the type of lamination that is being used by the manufacturer of this product.

VI. Conclusions

A reduction of efficiency when recycled magnets are used was quantified at 4.5%. This maximum value was obtained in the region at low speed and high torque in figure 10. Such deviation in the efficiency has its source in the increment of the stack length for obtaining the same torque as in the original machine. In addition, the increment of the resistance of the windings with increased stack length, had a significant impact in the copper losses. On the other hand, in the region at high speed and low torque the reduction in efficiency was estimated in 1%. This is consistent with having a reduced remanence of the magnets compensated with the increment of the stack length of the machine.

In general, a larger consumption of energy is expected if magnets manufactured with recycled materials and with lower remanence are used for electrical machines in (H)EVs. However, for future work it has been defined the study of the energy consumption of the machine analysed here under various driving cycles, including the European urban driving cycle ECE-15. Additionally, the prices of both energy and magnet materials will be evaluated for establishing a recycling index [15]. Furthermore, the methodology proposed here is expected to facilitate the comparison of diverse types of PM machines (e.g. surface mounted PM, inset PM, Halbach rotor, etc.) from an early design stage.

Acknowledgement

The research leading to the results presented in this article has been funded by the European Communitys Horizon 2020 Programme ([H2010/2014-2019]) under Grant Agreement no. 674973 (MSCA-ETN DEMETER). This publication reflects only the authors view, exempting the Community from any liability. Project website http://etn-demeter.eu/. Special thanks to professors Sylvie Hebert and Antoine Maignan for helping in the characterization of the magnets at the Laboratory of Cristallography and Material Sciences CRISMAT at ENSI-CAEN.

References

[1] M. Kimiabeigi, R. S. Sheridan, J. D. Widmer, A. Walton, M. Farr, B. Scholes, and I. R. Harris, "Production and application of hpms recycled bonded permanent magnets for a traction motor application," *IEEE Transactions on Industrial Electronics*, vol. 65, no. 5, pp. 3795–3804, May 2018.

[2] S. Högberg, J. Holbøll, N. Mijatovic, B. B. Jensen, and F. B. Bendixen, "Direct reuse of rare earth permanent magnets - coating integrity," *IEEE Transactions on Magnetics*, vol. 53, no. 4, pp. 1–9, April 2017.

[3] S. Högberg, F. B. Bendixen, N. Mijatovic, B. B. Jensen, and J. Holbøll, "Influence of demagnetization-temperature on magnetic performance of recycled nd-fe-b magnets," in *2015 IEEE International Electric Machines Drives Conference (IEMDC)*, May 2015, pp. 1242–1246.

[4] Y. Yang, A. Walton, R. Sheridan, K. Güth, R. Gauß, O. Gutfleisch, M. Buchert, B.-M. Steenari, T. Van Gerven, P. T. Jones, and K. Binnemans, "Ree recovery from end-of-life ndfeb permanent magnet scrap: A critical review," *Journal of Sustainable Metallurgy*, vol. 3, no. 1, pp. 122–149, Mar 2017. [Online]. Available: https://doi.org/10.1007/s40831-016-0090-4

[5] T. Elwert, D. Goldmann, F. Roemer, and S. Schwarz, "Recycling of ndfeb magnets from electric drive motors of (hybrid) electric vehicles," *Journal of Sustainable Metallurgy*, vol. 3, no. 1, pp. 108–121, Mar 2017. [Online]. Available: https://doi.org/10.1007/s40831-016-0085-1

[6] A. Kumar Jha, Z. Li, A. Garcia Gonzalez, P. Upadhayay, and P. Rasmussen, "Weighted index of recycling and energy (WIRE) cost for Motors in electric vehicles," in *SPEEDAM 2018, Accepted*, 2017.

[7] T. Barlow, "A reference book of driving cycles for use in the measurement of road vehicle emissions: Version 3," 2009. [Online]. Available: https://books.google.dk/books?id=jnowMwEACAAJ

[8] S. M. Lukic and A. Emado, "Modeling of electric machines for automotive applications using efficiency maps," in *Proceedings: Electrical Insulation Conference and Electrical Manufacturing and Coil Winding Technology Conference (Cat. No.03CH37480)*, Sept 2003, pp. 543–550.

[9] P. Lazari, J. Wang, and L. Chen, "A computationally efficient design technique for electric-vehicle traction machines," *IEEE Transactions on Industry Applications*, vol. 50, no. 5, pp. 3203–3213, Sept 2014.

[10] K. Kiyota, H. Sugimoto, and A. Chiba, "Comparing electric motors: An analysis using four standard driving schedules," *IEEE Industry Applications Magazine*, vol. 20, no. 4, pp. 12–20, July 2014.

[11] "Wuxi lingming electric drive technology co., ltd," Internet: http://www.lingmingmotor.com, 2015, [Nov. 22, 2017].

[12] "European training network for the design and recycling of rare-earth permanent magnets," Internet: http://etn-demeter.eu, 2015, [Nov. 22, 2017].

[13] R. Sheridan, A. Williams, I. Harris, and A. Walton, "Improved hddr processing route for production of anisotropic powder from sintered ndfeb type magnets," *Journal of Magnetism and Magnetic Materials*, vol. 350, pp. 114 – 118, 2014. [Online]. Available: http://www.sciencedirect.com/science/article/pii/S0304885313007014

[14] A. Fitzgerald, C. Kingsley, and S. Umans, "Parameter determination from no-load and block-rotor tests," in *Electric Machinery*, 6th ed. New York, US: McGraw-Hill, 2003, ch. 6.

[15] P. Upadhayay, A. Garcia Gonzalez, Z. Li, A. Kumar Jha, P. Rasmussen, A. Kedous-Lebouc, and J.-C. Mipo, "Evaluation of energy cost index for an electric vehicle motor over a particular drive cycle with recycled magnet concept," in *ICEM 2018, Submitted to*, 2018.

VII. BIOGRAPHIES

Adolfo Garcia Gonzalez received his M.Sc. degree in Electrical Engineering from KTH Royal Institute of Technology, Sweden, in 2015. He is currently working toward a Ph.D. degree at the Section of Electrical Machines of the Department of Energy Technology at Aalborg University. His research interests include modelling and design of electrical machines with 3D-Flux and non-traditional materials for traction applications.

Amit Kumar Jha received B.E degree (2008) in Electrical and Electronics Engineering from Birla Institute of Engineering, Mesra, India and M.Sc. degree (2012) in Electrical Power Engineering from Royal Institute of Technology, Stockholm, Sweden. He is currently working as Ph.D. researcher at G2Elab, Grenoble, France focusing on design of electrical motor with easy recycling for electric vehicles. Prior to PhD, he has worked in different companies like Bombardier Transportation AB, Vasteras, Sweden, Xylem water solutions, Stockholm, Sweden and Schneider Electric Pvt. Ltd, India. His fields of interest are design of electric motor and its drives for different motor applications and study system performance.

Ziwei Li received his M.Sc. degree in Electrical Engineering from KTH Royal Institute of Technology, Sweden, in 2015. He is currently working towards a Ph.D degree at the laboratory of G2Elab, Grenoble INP, Grenoble and Valeo - Equipements Electriques Moteur, Crteil, France. His research interests include modeling and optimization of radial flux electrical machines with rare earth magnets recycling concepts for electrical vehicle applications.

Pranshu Upadhayay was born in Jorhat, Assam, India in 1986. Following a B. Tech degree (2007) in Electrical Engineering from Nirma University, India, he received M. S. (Research) in Electrical Engineering (2015) from the Indian Institute of Technology Delhi, India. He is currently working towards his Ph.D. degree from G2Elab, Grenoble INP, Universit Grenoble Alpes, and is also associated with Valeo - Equipements Electriques Moteur, Crteil, France. From 2007 to 2015 he was associated with multinational companies like Schneider Electric India Pvt. Ltd., and Crompton Greaves Ltd., at Mumbai, India. He has published 8 papers in International conference proceedings. His fields of interest include electrical machines and drives, design and FE analysis of special electrical machines, 3D flux claw-pole machines and rare earth magnet reuse and recycling concept in EV and HEV applications.

Peter Omand Rasmussen was born in Aarhus, Denmark, in 1971. He received the M.Sc.E.E. and Ph.D. degrees from Aalborg University, Aalborg, Denmark, in 1995 and 2001, respectively. In 1998, he became an Assistant Professor, and in 2002, he became an Associate Professor at Aalborg University. His research areas are the design and control of switched reluctance, permanent-magnet machines, and magnetic gears.

Evaluation of Energy Cost Index for an Electric Vehicle Motor over a particular Drive Cycle with Recycled Magnet Concept

Pranshu Upadhayay, Adolfo G. Garcia, Ziwei Li, Amit K. Jha, Peter O. Rasmussen, Afef Kedous-Lebouc, Jean-Claude Mipo

***Abstract* – Nowadays, in automotive applications, the electric vehicle motors generally utilize permanent magnet motors due to their various advantages like high torque density, high efficiency, compactness and ease of control. In this paper emphasis is given to the evaluation of energy cost index for an EV motor over a particular drive cycle during motors operational lifetime. Performance evaluation over the entire drive cycle, instead of at rated conditions, provides a better idea of the efficiency and energy consumption of an electric motor. Therefore, energy cost evaluation for the urban part of New European Driving Cycle i.e. ECE-15 is selected in this study and the energy cost index is evaluated for an EV motor for virgin and recycled magnets utilized in the machine. The comparison shows that utilizing recycled magnets can provide economical advantage over using virgin magnets albeit under certain assumptions.**

***Index Terms*—automotive, cost, driving cycle, electric motors, electric vehicles, energy, finite element analysis, permanent magnets, recycle, reuse.**

I. Introduction

THE electric vehicles (EV) and hybrid electric vehicles (HEV) are the new key developments in the automotive industry with the implementation of new regulations and norms in various countries around the world. Generally, the EV machines used in automotive applications are permanent magnet (PM) machines due to various advantages like high torque density, high efficiency, compactness and ease of control [1]. The PMs deployed in these EV motors are commonly rare earth (RE) magnets i.e. Neodymium Iron Boron (NdFeB) magnets. However, due to price fluctuations and supply-demand issues of RE materials utilized in NdFeB magnets, lot of research is being undertaken to reduce or utilize RE free magnets in PM machines. In recent years, numerous studies are being carried out in recycling of critical materials, and NdFeB magnets contain a few of these critical materials i.e. Neodymium (Nd) and Dysprosium (Dy) [2]. Due to the use of NdFeB magnets in PM machines, reuse and recycle of PMs in electric motors is being re-analyzed in some of the applications around the world [3]-[4]. Nevertheless, there are challenges in developing methodologies for reuse or recycle of magnets in electric motors due to varying motor topologies, technologies, material characteristics, proper disposal at end-of-life (EoL) and economic/environmental implications.

In this regard a methodology is being developed to analyze the recyclability of PM motors with two main aspects. First, recyclability of the motor considering standardization, assembly and disassembly of the motor and second, considering energy consumption by the electric motor during its complete lifetime with variation in permanent magnet compositions [5]-[6]. In this paper a commercial PM based HUB motor is used to evaluate the second part of above methodology development. In Section II benchmarking of sample HUB motor is done by dis-assembly, experimentation and finite element (FE) analysis. Then in Section III efficiency map and energy consumption of sample HUB motor with virgin magnets for urban part of New European Driving Cycle (NEDC) i.e. ECE-15 [7] is evaluated. Similarly, machine performance and energy consumption with recycled magnets for the same ECE-15 drive cycle is evaluated in Section IV. Finally in Section V, comparison in energy consumption between virgin magnets and recycled magnets for sample HUB motor is done to obtain the energy cost index. Finally, conclusion is presented in the last section.

II. Benchmarking of Sample Electric Vehicle Motor

The sample EV motor is a commercial PM based HUB motor with outer rotor topology. The sample motor is utilized in medium speed electric 2-wheeler or small compact low speed city cars. Fig. 1 shows the sample HUB motor. The DC bus voltage for the sample motor is 72 V, maximum speed of 700 rpm and output power upto 3.5 kW. The motor

The research leading to these results has received funding from European Community's Horizon 2020 Programme ([H2020/2014-2019)] under Grant Agreement no. 674973 (MSCA-ETN DEMETER). This publication reflects only the author's view, exempting the Community from any liability. Project website: http://etn-demeter.eu/.

First four authors contributed equally to this work.

P. Upadhayay is with Valeo - Equipements Electriques Moteur, 2 rue André Boulle, 94000 Créteil, France & also with Univ. Grenoble Alpes, CNRS, Grenoble INP, G2Elab, 38000 Grenoble, France (e-mail: pranshulink@gmail.com).

A. G. Gonzalez is with the Department of Energy Technology, Aalborg University, Aalborg 9220, Denmark (e-mail: agg@et.aau.dk).

Ziwei Li is with Valeo - Equipements Electriques Moteur, 2 rue André Boulle, 94000 Créteil, France & also with Univ. Grenoble Alpes, CNRS, Grenoble INP, G2Elab, 38000 Grenoble, France (e-mail: ziwei.li@valeo.com).

A. K. Jha is with Univ. Grenoble Alpes, CNRS, Grenoble INP, G2Elab, 38000 Grenoble, France (e-mail: amit-kumar.jha@grenoble-inp.fr).

P. O. Rasmussen is with the Department of Energy Technology, Aalborg University, Aalborg 9220, Denmark (e-mail: por@et.aau.dk).

A. Kedous-Lebouc is with Univ. Grenoble Alpes, CNRS, Grenoble INP, G2Elab, 38000 Grenoble, France (e-mail: afef.lebouc@grenoble-inp.fr).

J. C. Mipo is with Valeo - Equipements Electriques Moteur, 2 rue André Boulle, 94000 Créteil, France (e-mail: jean-claude.mipo@valeo.com).

controller is a standard three-phase power electronic inverter with hall sensor inputs used for position sensing.

Fig. 1. A commercial PM based HUB motor

A. *Experimental measurements*

The motor was assembled on a test bench with high precision torque transducer connected to the shaft. The input power measurements were recorded using an industrial grade power analyzer so as to limit the uncertainties in measurement. Fig. 2 shows the experimental test setup utilized for the measurements and performance evaluation.

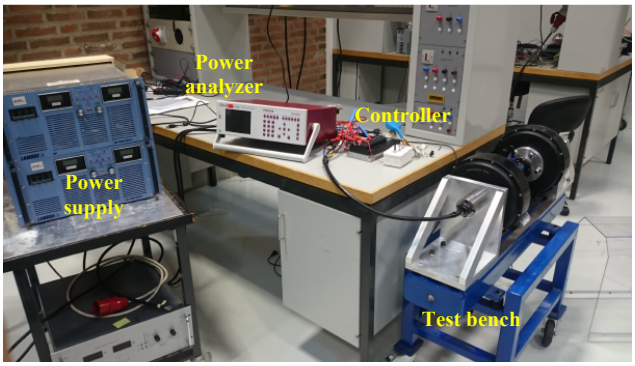

Fig. 2. Experimental test setup for performance evaluation

Two machines were assembled back to back and a resistive load was connected to the machine which would operate as a generator and load the test machine. Different resistance values were used with a set of speed variations to get the torque, speed, voltage, output power and input power of the test machine. Fig. 3 depicts the experimental torque vs. speed with the corresponding efficiency values.

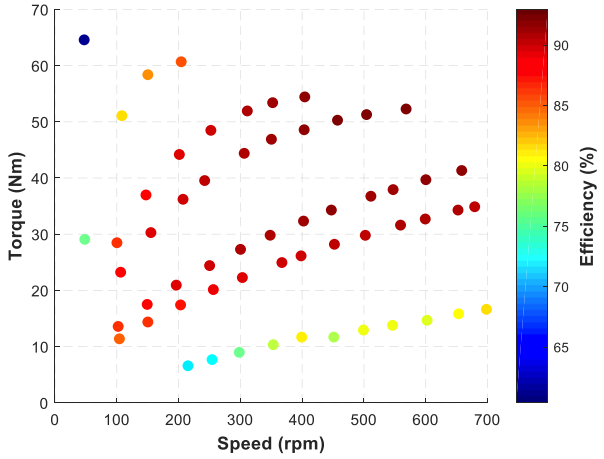

Fig. 3. Experimental torque vs. speed with corresponding efficiency values by virgin magnets

B. *Disassembly and dimensions*

The major dimensions, weight and materials were identified by disassembling the machine in step by step process. Fig. 4 shows the disassembled machine and the magnets. Table I depicts the main machine dimensions which would be utilized later on for 2-dimensional (2D) FE analysis so as to obtain simulated performance of the machine.

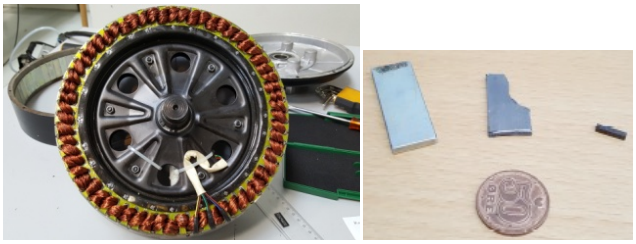

Fig. 4. Disassembled machine and permanent magnets

TABLE I
MAIN DIMENSIONS OF THE MACHINE

Parameters	Value
Stack length [mm]	40
Maximum speed [rpm]	700
Air-gap length [mm]	0.6
Magnet axial length [mm]	40
Magnet thickness [mm]	3
Magnet width [mm]	14
Stator outer diameter [mm]	253
Number of poles	56
Number of slots	63

The PMs were shaped in appropriate sizes so as to be analyzed for their magnetic properties. They were put to test in Magnetic Property Measurement System (MPMS®) from Quantum Design. It was observed that the magnetization (M) at 0 Oe applied field (H) of the magnet is around 130 emu/g which corresponds to around 1.2 T as remanence flux density (B_r) at temperature of 300 K i.e. approximately 27 °C.

C. *Finite element analysis & comparison with test results*

The machine was modeled in commercially available FE analysis software by using the dimensional details obtained earlier in Section II (B). The magnet properties were utilized from the MPMS measurements with 1.2 T as the B_r value. The stator lamination was a standard silicon iron soft magnetic material with loss of around 5 W/kg at 1.5 T, 50 Hz. Time-stepping 2D motion analysis was carried out to get the various performance parameters like back electromotive force (EMF), cogging torque, electromagnetic torque, iron losses, copper losses and winding voltages. Fig. 5 shows the 2D model along with the flux density plot at no-load by FE analysis.

The experimental winding current values were fed as an input in the FE analysis at various speed points to get the developed torque and losses of the machine. Finally the input power, output power, voltage and efficiency were evaluated by simulation results. In Fig. 6 it can be noticed that the comparison of simulated and experimental results for torque vs. speed with corresponding efficiency values of the machine.

It can be observed that the simulated and experimental results match fairly well and there is a maximum percentage error of 9% in torque and 5% in efficiency values.

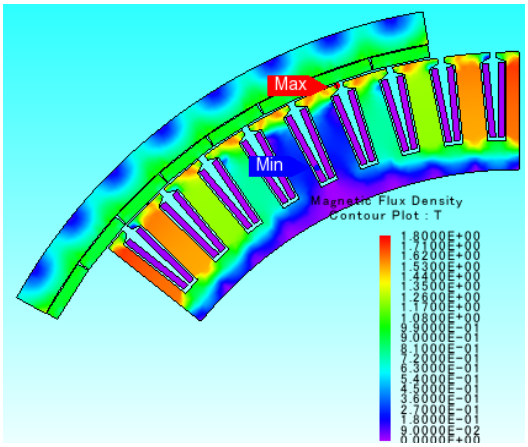

Fig. 5. Flux density plot of the sample HUB motor with virgin magnets

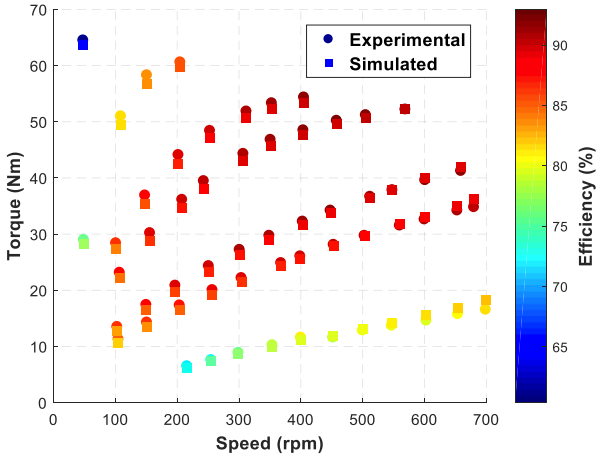

Fig. 6. Comparison of experimental & simulated torque vs. speed with corresponding efficiency values by virgin magnets

III. Efficiency Map and Energy Evaluation of the Sample HUB Motor with Virgin Magnets

Energy consumption for a reference drive cycle requires performance parameters of the machine for the complete torque vs. speed envelope. As a result, efficiency map of the motor needs to be evaluated so as to acquire the precise torque and efficiency points for the corresponding speed values in the reference drive cycle.

A. Methodology for energy consumption evaluation

A methodology has been developed to evaluate the energy consumed by the machine for a particular drive cycle. Various literatures depict the importance of evaluating the energy consumption of a machine for different drive cycles with diverse vehicle dynamics [8]-[17]. Fig. 7 shows the flow diagram of the developed methodology. In this, the machine performance is evaluated using FE analysis and utilizing the flux map of the machine, efficiency map is generated. Along with this, vehicle parameters like wheel radius, vehicle weight, rolling resistance, air density, drag coefficient and frontal area are used as input for deriving torque vs. time curve from speed vs. time of drive cycle. Now, these are used as input to the efficiency map and energy consumption for one cycle of the drive cycle is evaluated. Finally, total energy consumed in the lifetime of the machine is estimated by assuming that the motor operates for 2 hours daily for 10 years.

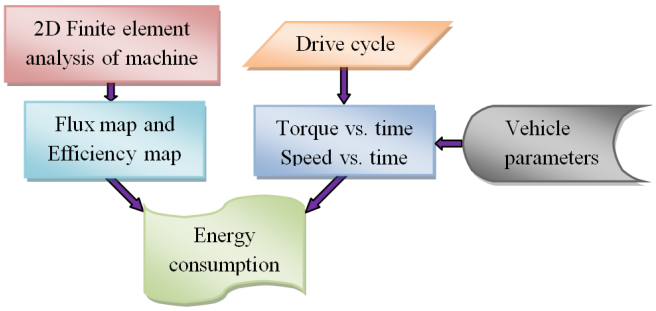

Fig. 7. Flow diagram for energy evaluation methodology

In this study it is assumed that the vehicle is a compact city car with the vehicle parameters as listed in Table II.

TABLE II
Vehicle Parameters

Parameters	Value
Vehicle weight [kg]	920
Density of air [kg/m^3]	1.225
Frontal area [m^2]	1.85
Drag coefficient	0.4
Coefficient of rolling resistance	0.01
Tyre radius [m]	0.21

B. Efficiency map and energy consumption

The efficiency mapping of the machine is evaluated by utilizing the flux map with different values of direct axis current (I_d) and quadrature axis current (I_q). Similarly, iron loss mapping is also required for various values of machine flux induction and current levels. Therefore, by utilizing optimization algorithm, the efficiency mapping is obtained for the sample motor. Fig. 8 illustrates the efficiency map of the sample motor with virgin magnets.

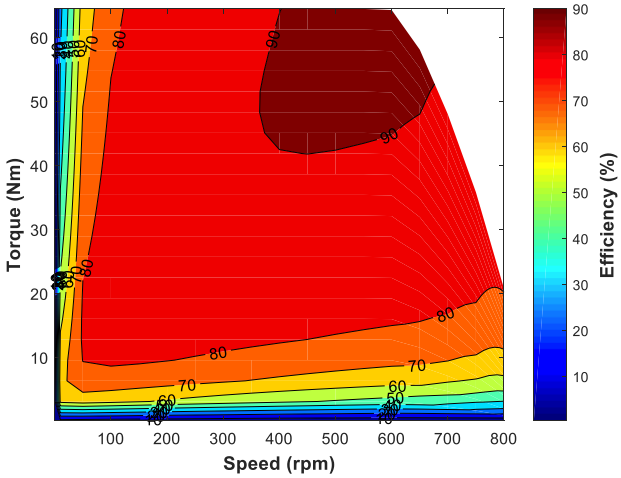

Fig. 8. Efficiency map of the sample HUB motor with virgin magnets

The drive cycle selected for this study is the urban part of the NEDC i.e. ECE-15 [7]. Fig. 9 shows the speed vs. time profile of the ECE-15 drive cycle.

The instantaneous wheel torque can be derived by using

the following equation [8]-[17]:

$$T_w = \left(ma + mgC_r + \frac{1}{2}\rho_a C_d A_f v^2\right) r_w \quad (1)$$

where, T_w is wheel torque, m is mass of vehicle, a is acceleration, g is gravity, C_r is coefficient of rolling resistance, ρ_a is density of air, C_d is coefficient of drag, A_f is vehicle frontal area, v is velocity of vehicle and r_w is radius of the wheel. Hence, using Eq. (1), vehicle parameters as in Table II and ECE-15 drive cycle, the wheel torque vs. time profile can be obtained. Fig. 10 shows the wheel torque vs. time profile for the selected vehicle and ECE-15 drive cycle.

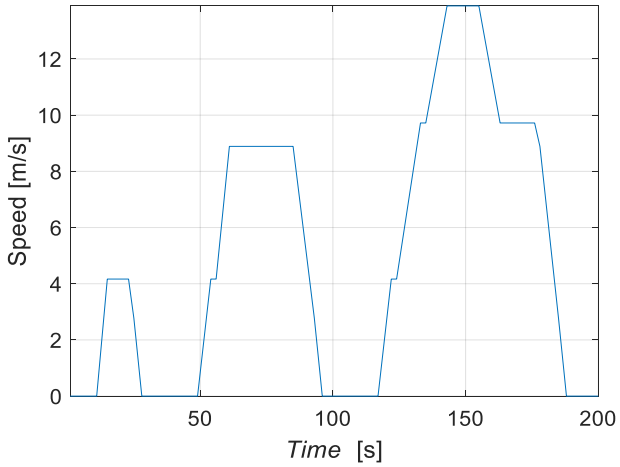

Fig. 9. Speed vs. time profile of the ECE-15 drive cycle

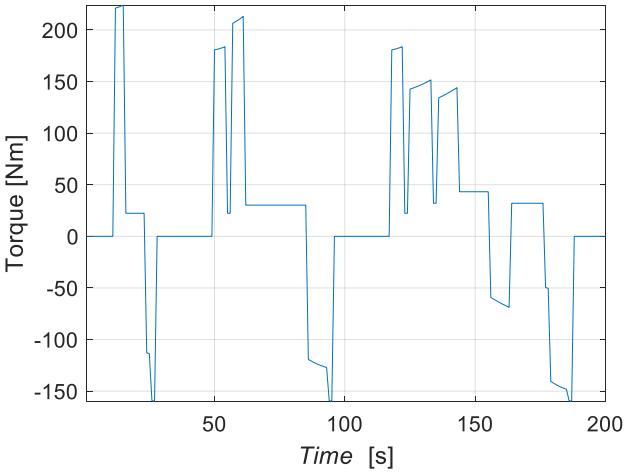

Fig. 10. Wheel torque vs. time profile for the specified vehicle and ECE-15

In typical EVs, the electrical machine is coupled to the wheels via transmission hence they have high speeds and high efficiencies. But here, it can be observed that maximum torque required at wheel is around 220 Nm. The maximum motor torque which can be delivered is around 65 Nm. Hence, it is assumed that four motors would be used in the vehicle with direct drive in-wheel configuration to achieve required vehicle wheel torque.

As per the flow diagram in Fig. 7, this torque vs. speed profile and efficiency map are employed together to get the energy consumed by one motor during the lifetime of 10 years with 2 hours of daily operation. The energy consumption can be calculated as:

$$E_c = \int_0^t E(t)dt \quad (2)$$

where, E_c is total energy consumed, $E(t)$ is energy input as function of time and t is time. The regenerative braking and negative torque values are assumed to be zero in the energy calculations. As a result, for the sample HUB motor with virgin magnets, the total energy consumed for the complete lifetime is 3071 kWh from Eq. (2). The harmonized electricity price for Europe region is considered as 0.22 €/kWh [18]. Therefore, the energy cost for one motor with virgin magnets is € 676 for the entire assumed lifetime. The weight of total magnet in the motor is 0.7 kg, and NdFeB material price considered is 45 €/kg [19], consequently the total magnet price is € 31.5 in one motor.

The study has utilized ECE-15, but the methodology can be used to assess any drive cycle like NEDC, Urban Dynamometer Driving Schedule, Worldwide Harmonized Light Vehicles Test Procedure etc & this is considered as future work.

IV. Machine Performance with Recycled Magnets

It has been observed for past many years that rare earth material price fluctuates a lot due to regulatory factors, supply-demand issues, political and economical factors. It is for this reason recycling and reuse of rare earth materials from electronic components, computer hard drives and automotive components, have garnered a lot of interest [2]. Research is been carried out in recycling the PM scrap from various sources and fabricate recycled magnets by hydrogen decrepitation (HD) and hydrogenation, disproportionation, desorption, recombination (HDDR) [20]-[22].

In this study, magnetic property of recycled magnet considered is around 0.96 T as B_r. This is as per reference [20], where new magnet material has 1.36 T as B_r and recycled magnet has 1.08 T as B_r, hence 20% reduction in the B_r. In this study virgin magnet has 1.2 T as B_r, and taking 20% reduction for recycled magnet, the B_r evaluated is 0.96 T.

A. Performance characteristics

For the evaluation of machine performance with recycled magnets in sample motor, the methodology utilized is similar to performance calculated with virgin magnets as in Section II (C). The sample motor's dimensional parameters are kept same as that with virgin magnets; only magnet properties are altered with recycled magnet properties i.e. having 0.96 T as B_r and increased length of the motor to achieve same torque as obtained with virgin magnets. The length of stator, rotor and magnets is increased from 40mm to 46mm. Henceforth, 2D time-stepping FE analysis is carried out to get the performance characteristics like back EMF, cogging torque, electromagnetic torque, iron losses, copper losses and winding voltages. Performance has been evaluated with similar current values as used in test and simulations during the study with virgin magnets in Section II (C). Fig. 11 shows simulated torque vs. speed with corresponding efficiency values by virgin and recycled magnets. It can be observed that torque values match fairly well for virgin and recycled magnets. But the efficiency at certain points has increased with recycled magnets due to cumulative decrease of total losses, as iron losses has reduced but copper losses has increased.

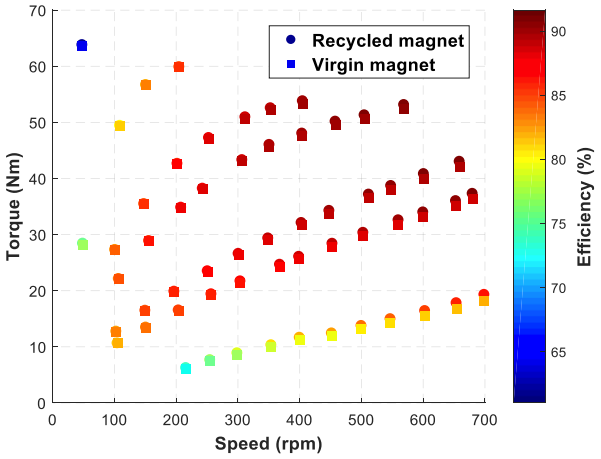

Fig. 11. Simulated torque vs. speed with corresponding efficiency values by virgin and recycled magnets

B. *Efficiency map and energy consumption*

The efficiency map and energy consumption of the sample motor with recycled magnets is evaluated similarly as done while using virgin magnets in Section III (B). By utilizing the flux map with different values of I_d and I_q and iron loss map for various values of machine flux induction and current levels, the efficiency map is generated for the motor with recycled magnets. Fig. 12 illustrates the efficiency map of the sample motor with recycled magnets.

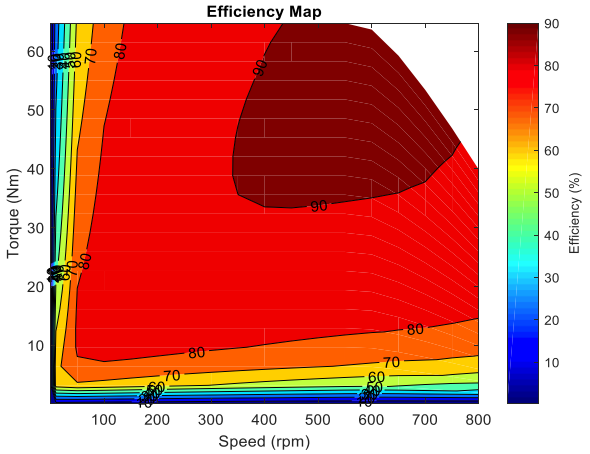

Fig. 12. Efficiency map of the sample HUB motor with recycled magnets

Hereafter employing the flow diagram in Fig. 7, torque vs. speed profile and efficiency map together can provide energy consumed by one motor during the lifetime of 10 years with 2 hours of daily operation with recycled magnets. Consequently, for sample motor with recycled magnets, total energy consumed for complete lifetime is calculated as 2995 kWh from Eq. (2). Similarly, assuming the harmonized electricity price for Europe region as 0.22 €/kWh [18], the energy cost for one motor with recycled magnets is € 659 for the assumed lifetime.

It is difficult to comment on the price of recycled magnets as it is subject to ongoing research studies. But as it is assumed to be prepared from scrap PMs the price is assumed to be lower compared to virgin PMs. Due to increased length the PM weight increases from 0.7 kg to 0.81 kg with recycled magnets. Therefore, assuming the price of recycled magnet material as half of virgin magnets i.e. 22.5 €/kg with certain estimates, the total PM price calculated would be € 18.23 since motor contains 0.81 kg of magnets.

V. Energy Cost Index and Comparison between Virgin and Recycled Magnets

Energy cost evaluation considering the machine performance on a particular drive cycle or duty cycle gives more insights than evaluating machine performance at rated loads. Since machine performance could be optimized for rated conditions but their operation may not be subjected to rated conditions during a specific duty cycle. Therefore, comparing machine performance at a particular drive cycle with different magnet scenarios would provide information about the importance of energy and magnet cost.

For this purpose, an index has been proposed to compare the energy cost in relation to magnet cost. The temperature for both the machines has been assumed the same. For instance, in this study energy consumption cost with virgin magnets is € 676 and magnet cost is € 31.5 for the sample motor. Considering this as the base scenario and naming it as Scenario 1 and/or Scenario base. The energy cost computed with recycled magnets is € 659 and magnet cost is € 18.23 for the sample motor; and naming it as Scenario 2. The energy cost index is defined as follows:

$$EC_i = \left(\frac{E_c(j)}{E_c(b)}\right).\left(\frac{Mag_c(j)}{Mag_c(b)}\right) \quad (3)$$

where, EC_i is the energy cost index, $E_c(j)$ is energy cost for Scenario j, $Mag_c(j)$ is magnet cost for Scenario j, $E_c(b)$ is energy cost for Scenario base and $Mag_c(b)$ is magnet cost for Scenario base. As a result, energy cost index for Scenario 2 as per Eq. (3) is evaluated as 0.564. From Fig. 13 it can been observed that the design with recycled magnets has low efficiency in low speed high torque region and high efficiency in high speed low torque region as compared to efficiencies with virgin magnets. However, the drive cycle has most of the points in high speed low torque region; hence energy consumption is low with recycled magnets for this drive cycle. Hence, it can be deduced that energy consumption depends on both drive cycle and machine design.

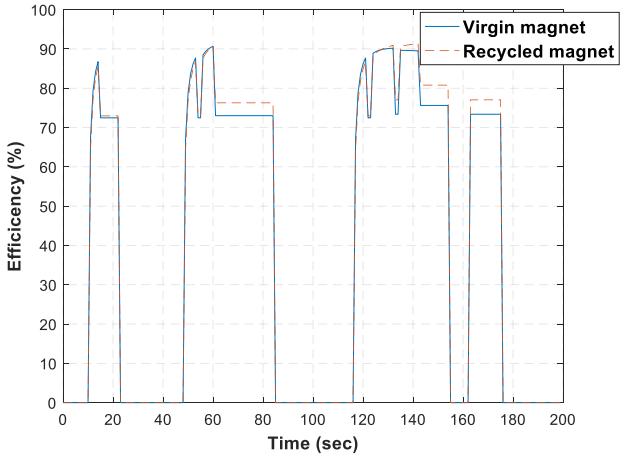

Fig. 13. Efficiency vs. time profile for virgin and recycled magnets

For analysis purpose, few more scenarios are assumed, for example, Scenario 3 where energy cost is € 676 (energy

cost for virgin magnets) and magnet cost is € 18.23 (magnet cost for recycled magnets) and Scenario 4 where energy cost is € 659 (energy cost for recycled magnets) and magnet cost is € 31.50 (magnet cost for virgin magnets). Table III represents the comparison of energy cost index for different scenarios, computed using Eq. (3).

TABLE III
COMPARISON OF ENERGY COST INDEX FOR DIFFERENT SCENARIOS

	Energy cost (€)	PM material price (€/kg)	Magnet cost (€)	Energy cost index
Scenario 1	676	45.0	31.50	1.000
Scenario 2	659	22.5	18.23	0.564
Scenario 3	676	22.5	18.23	0.579
Scenario 4	659	45.0	31.50	0.975
Scenario 5	700	37.6	30.46	1.000

Hence, it can be observed that the energy cost index for Scenario 3 is 0.579 and Scenario 4 is 0.975. This indicates that lower the energy cost index, better is the machine in economic aspects and is advantageous as compared to base scenario. Considering one more hypothetical scenario (Scenario 5), where the recycled magnet cost is approximately equal to virgin magnets i.e. € 30.46 and energy cost is € 700; the energy cost index computed is 1.000, as shown in Table III. This is equal to energy cost index of base scenario, indicating that even if the price of recycled magnet are similar to virgin magnet and have higher energy consumption, the economic impact is same. Other than the above cited advantages, with recycled magnets one can observe one more advantage which is that, they have low environmental impact as compared to virgin magnets. The mining of rare earth materials have negative repercussions in terms of environmental and human conditions. The preparation of recycled magnets has lower implications on human labour aspects as no mining is required. Additionally they have environmental benefits like reduction in air and water pollution. It can be argued that even for the preparation of recycled magnets a number of environmental hazards are possible like storage of hydrogen gas and its use in HD and HDDR process, and use of certain chemicals for separation of materials. But if both the circumstances are weighed together, the authors assume that mining would have higher negative impact than producing recycled magnets from scrap [23]. The authors recommend future studies and research into economic-environmental comparison between virgin and recycled magnet production and usage phase.

A general representation of the index is tabulated in Table IV, where energy cost index varies with the cost of virgin and recycled magnets. In this the E_c virgin magnet is € 676, E_c recycled magnet is € 659 and weight of virgin magnet is 0.7 kg and weight of recycled magnet is 0.81 kg. Hence, it can be observed that as the PM material price varies for virgin and recycled magnets the index varies accordingly. The greener the index it is better economically when compared to red coloured cells in Table IV. Similar, hypothesis can be generated with variable energy costs for different grades of magnets and the index would indicate the cases which are economically more advantageous.

TABLE IV
ENERGY COST INDEX WITH VARYING MAGNET COSTS

			VIRGIN MAGNETS					
	PM. mat. price(€/kg)		20	35	50	65	80	95
		PM. cost (€)	14.0	24.5	35.0	45.5	56.0	66.5
RECYCLED MAGNETS	5	4.05	0.282	0.161	0.113	0.087	0.071	0.059
	20	16.20	1.128	0.645	0.451	0.347	0.282	0.237
	35	28.35	1.974	1.128	0.790	0.607	0.494	0.416
	50	40.50	2.820	1.611	1.128	0.868	0.705	0.594
	65	52.65	3.666	2.095	1.466	1.128	0.917	0.772
	80	64.80	4.512	2.578	1.805	1.388	1.128	0.950
	95	76.95	5.358	3.062	2.143	1.649	1.340	1.128

VI. CONCLUSION

In this paper, the energy cost index evaluation methodology over ECE-15 drive cycle for an EV motor with PMs has been presented. The methodology is utilized to present different scenarios where virgin magnets and recycled magnets were employed and energy cost index was computed. It has been observed that the recycled magnets can provide better economical advantage than virgin magnets as it is assumed that the cost of recycled magnets would be lower than virgin magnets in this case study. Lower the energy cost index, the machine is better in terms of economic evaluation as compared to base scenario. The recycled magnets also provide benefits in terms of environmental aspects as they would be less polluting in their production than virgin magnet materials mined from various sources around the world. The methodology for energy cost index evaluation is a comparative tool and can be adjusted as per the individuals' needs and calculations. The scenarios can vary from motor design and different drive cycles, which can provide varied results and conclusions. Thus, generating an index for comparison provides reasonably good inspiration on using recycled magnets in electrical machines. Future work is planned with experimental utilization of recycled PMs in electrical machine designs.

VII. ACKNOWLEDGMENT

The research leading to these results has received funding from European Community's Horizon 2020 Programme ([H2020/2014-2019)] under Grant Agreement no. 674973 (MSCA-ETN DEMETER). This publication reflects only the author's view, exempting the Community from any liability. Project website: http://etn-demeter.eu/.

Special thanks to Prof. Sylvie Hebert and Prof. Antoine Maignan for helping in the characterization of the magnets at CRISMAT lab of ENSICAEN.

VIII. REFERENCES

[1] T. Elwert, D. Goldmann, F. Romer, M. Buchert, C. Merz, D. Schueler, and J. Sutter, "Current developments and challenges in the recycling of key components of (hybrid) electric vehicles," *Recycling Journal*, vol. 1, no. 1, pp. 25– 60, October 2015.

[2] Y. Yang, A. Walton, R. Sheridan, K. Guth, R. Gauß, O. Gutfleisch, M. Buchert, B. M. Steenari, T. V. Gerven, P. T. Jones, and K. Binnemans, "REE recovery from end-of-life NdFeB permanent magnet scrap: A critical review," *Journal of Sustainable Metallurgy*, vol. 3, no. 1, pp. 122–149, Mar 2017.

[3] M. Kimiabeigi, R. S. Sheridan, J. D. Widmer, A. Walton, M. Farr, B. Scholes, and I. R. Harris, "Production and Application of HPMS Recycled Bonded Permanent Magnets for a Traction Motor Application," *IEEE Trans. on Industrial Electronics*, vol. 65, no. 5, pp. 3795-3804, May 2018.

[4] U. Bast, R. Blank, M. Buchert, T. Elwert, F. Finsterwalder, G. Hornig, T. Klier, S. Langkau, F. Marscheider-Weidemann, J.-O. Muller, C. Thurigen, F. Treffer, and T. Walter, "Recycling von komponenten und strategischen metallen aus elektrischen fahrantrieben," MORE Project report, Aug 2014.

[5] A. K. Jha, Z. Li, A. Garcia, P. Upadhayay, P. O. Rasmussen, A. Kedous-Lebouc, and L. Garbuio, "Weighted index of recycling and energy (WIRE) cost for Motors in electric vehicles," International *Symposium on Power Electronics, Electrical Drives, Automation and Motion (SPEEDAM)* 2018, pp. 1-6, June 2018.

[6] A. G. Gonzalez, A. K. Jha, Z. Li, P. Upadhayay, and P. Rasmussen, "Validation of Efficiency Maps of an Outer Rotor Surface Mounted Permanent Magnet Machine for Evaluation of Recyclability of Magnets," *INTERMAG 2018*, pp. 1-4, April 2018.

[7] T. J. Barlow, S. Latham, I. S. McCrae, P. G. Boulter, *A reference book of driving cycles for use in the measurement of road vehicle emissions*, version. 3, United Kingdom: IHS, 2009, pp. 21.

[8] P. Lazari, J. Wang, and L. Chen, "A Computationally Efficient Design Technique for Electric-Vehicle Traction Machines," *IEEE Trans. on Industry Applications*, vol. 50, no. 5, pp. 3203-3213, Sep.-Oct. 2014.

[9] K. Kiyota, H. Sugimoto, and A. Chiba, "Comparing Electric Motors: An Analysis Using Four Standard Driving Schedules," *IEEE Industry Applications Magazine*, vol. 20, no. 4, pp. 12-20, July-Aug. 2014.

[10] Qi Li, Tao Fan, Ye Li, Z. Wang, X. Wen, and Jing Guo, "Optimization of external rotor surface permanent magnet machines based on efficiency map over a target driving cycle," *20th International Conference on Electrical Machines and Systems (ICEMS) 2017*, pp. 1-5, Aug. 2017.

[11] P. D. Walker, and H. M. Roser, "Energy consumption and cost analysis of hybrid electric powertrain configurations for two wheelers," *Applied Energy Journal*, vol. 146, pp. 279-287, May 2015.

[12] C. Krasopoulos, M. Beniakar, and A. G. Kladas, "Comparison of Three Different In-Wheel SMPM Motor Configurations Based on the Urban NEDC," *Materials Science Forum*, vol. 856, pp. 233-238, May 2016.

[13] Ganji B., Kouzani A. Z., Trinh H. M., "Drive Cycle Analysis of the Performance of Hybrid Electric Vehicles," In: Li K., Fei M., Jia L., Irwin G.W. (eds) *Life System Modeling and Intelligent Computing. Lecture Notes in Computer Science*, vol. 6328, pp. 434-444, Springer, Berlin, Heidelberg, 2010.

[14] J. O. Estima, and A. J. M. Cardoso, "Efficiency Analysis of Drive Train Topologies Applied to Electric/Hybrid Vehicles," *IEEE Trans. on Vehicular Technology*, vol. 61, no. 3, pp. 1021-1031, Mar. 2012.

[15] E. Carraro, M. Morandin, and N. Bianchi, "Traction PMASR Motor Optimization According to a Given Driving Cycle," *IEEE Trans. on Industry Applications*, vol. 52, no. 1, pp. 209-216, Jan.-Feb.. 2016.

[16] O. Karabasoglu, and J. Michalek, "Influence of driving patterns on life cycle cost and emissions of hybrid and plug-in electric vehicle powertrains," *Energy Policy Journal*, vol. 60, pp. 445-461, Sep. 2013.

[17] M. Novak, J. Novak, and Z. Novak, "Methodology for Efficiency Mapping of Permanent Magnet Synchronous Motors," *19th International Conference on Electrical Drives and Power Electronics (EDPE) 2017*, pp. 205-210, Oct. 2017.

[18] Electricity price statistics, http://ec.europa.eu/eurostat/statistics-explained/index.php/Electricity_price_statistics

[19] Alliance LLC, Commodity prices. http://www.allianceorg.com/magnetandmaterialcosts.html

[20] R .S. Sheridan, A. J. Williams, I. R. Harris, and A. Walton, "Improved HDDR processing route for production of anisotropic powder from sintered NdFeB type magnets," *Journal of Magnetism and Magnetic Materials*, vol. 350, pp. 114-118, Jan. 2014.

[21] R. S. Sheridan, R. Sillitoe, M. Zakotnik, I. R. Harris, and A. J. Williams, "Anisotropic powder from sintered NdFeB magnets by the HDDR processing route," *Journal of Magnetism and Magnetic Materials*, vol. 324, no. 1, pp. 63-67, Jan. 2012.

[22] M. Zakotnik, I. R. Harris, and A. J. Williams, "Multiple recycling of NdFeB-type sintered magnets," *Journal of Alloys and Compounds*, vol. 469, no. 1-2, pp. 314-321, Feb. 2009.

[23] H. Jin, P. Afiuny, S. Dove, G. Furlan, M. Zakotnik, Y. Yih, and J. W. Sutherland, "Life Cycle Assessment of Neodymium-Iron-Boron Magnet-to-Magnet Recycling for Electric Vehicle Motors," Environ. Sci. Technol. Journal, 52 (6), pp 3796–3802, 2018.

IX. BIOGRAPHIES

Pranshu Upadhayay was born in Jorhat, Assam, India in 1986. Following a B. Tech degree (2007) in Electrical Engineering from Nirma University, India, he received M. S. (Research) in Electrical Engineering (2015) from the Indian Institute of Technology Delhi, India. He is currently working towards his Ph.D. degree from G2Elab, Grenoble INP, Université Grenoble Alpes, and is also associated with Valeo - Equipements Electriques Moteur, Créteil, France.

From 2007 to 2015 he was associated with multinational companies like Schneider Electric India Pvt. Ltd., and Crompton Greaves Ltd., at Mumbai, India. He has published 8 papers in International conference proceedings. His fields of interest include electrical machines and drives, design & FE analysis of special electrical machines, 3D flux claw-pole machines and rare earth magnet reuse and recycling concept in EV and HEV applications.

Adolfo Garcia Gonzalez received his M.Sc. degree in Electrical Engineering from KTH Royal Institute of Technology, Sweden, in 2015. He is currently working toward a Ph.D. degree at the Section of Electrical Machines of the Department of Energy Technology at Aalborg University.

His research interests include modelling and design of electrical machines with 3D-Flux and non-traditional materials for traction applications.

Ziwei Li received his M.Sc. degree in Electrical Engineering from KTH Royal Institute of Technology, Sweden, in 2015. He is currently working towards a Ph.D degree at the laboratory of G2Elab, Grenoble INP, Grenoble and Valeo - Equipements Electriques Moteur, Créteil, France.

His research interests include modeling and optimization of radial flux electrical machines with rare earth magnets recycling concepts for electrical vehicle applications.

Amit Kumar Jha, received B.E degree (2008) in Electrical and Electronics Engineering from Birla Institute of Engineering, Mesra, India and M.Sc. degree (2012) in Electrical Power Engineering from Royal Institute of Technology, Stockholm, Sweden. He is currently working as Ph.D. researcher at G2Elab, Grenoble, France focusing on design of electrical motor with easy recycling for electric vehicles.

Prior to PhD, he has worked in different companies like Bombardier Transportation AB, Vasteras, Sweden, Xylem water solutions, Stockholm, Sweden and Schneider Electric Pvt. Ltd, India. His fields of interest are design of electric motor and its drives for different motor applications and study system performance.

Peter Omand Rasmussen was born in Aarhus, Denmark, in 1971. He received the M.Sc.E.E. and Ph.D. degrees from Aalborg University, Aalborg, Denmark, in 1995 and 2001, respectively.

In 1998, he became an Assistant Professor, and in 2002, he became an Associate Professor at Aalborg University. His research areas are the design and control of switched reluctance, permanent-magnet machines, and magnetic gears.

Afef Kedous-Lebouc has received her Electrical Engineering and Ph.D. degrees from Grenoble Institute of Technology (former Institut National Polytechnique de Grenoble) in 1982 and 1985. She is a Senior CNRS Researcher at Grenoble Electrical Engineering Laboratory G2Elab.

She managed its MADEA Team "Advanced Materials and electromagnetic devices" from 2004 to 2012. She is expert in magnetism, magnetic materials and application in electrical engineering devices. She managed more than 35 industrial projects and participated in many international research programs. She is expert within the International Electrotechnical Commission (IEC TC 68). She has more than 250 publications (80 international journals and 28 invited conferences). She has a large experience in PhD training (35 PhD, 30 already defended).

Jean-Claude Mipo received the Ph.D. degree in electrical engineering from the University "Pierre et Marie Curie", France. Since 1998, he has been with Valeo - Equipements Electriques Moteur, where he is currently Advanced Technical Manager.

Electric Vehicle Motor Designed for Recycling with High Torque Density And Efficiency

Amit Kumar Jha[1], Afef Kedous-Lebouc[1] Lauric Garbuio[1], Jean-Paul Yonnet[1], and Jean-Marc Dubus[2]
[1]Univ. Grenoble Alpes, CNRS, Grenoble INP G2Elab, 38000 Grenoble, France
[2]Valeo Electrical Systems, 2 Rue Andre Boulle F 94000
Email: Amit-kumar.jha@g2elab.grenoble-inp.fr

***Abstract*—The article presents a design of outer rotor Halbach magnet electric motor enabling easy assembly and disassembly. With proposed design a glue free permanent magnet rotor can be manufactured and the extraction of magnets can be done using standard tools. The magnet used for Halbach cylinder is bonded NdFeB magnet. The measured characteristic of the magnet material is also presented. The results shows that the motor fulfills the torque speed characteristic of hybrid electric vehicle with very good efficiency.**

***Index Terms*—Motor Recycling, Magnet Recycling, Motor Benchmarking**

I. Introduction

More and more countries are looking electric vehicle as an alternative to control pollution due to conventional cars and moving very aggressively towards that. Many countries like UK, France, Norway, Sweden etc have already moved forward and set targets to use electric vehicles in place of present cars [1]. The sales of electric vehicle is increasing and expected to increase further with more and more countries start promoting electric vehicle [2]. The vehicle is driven by high efficient electric motors, majority of them are permanent magnet (PM) motors [3]- [4]. The PM motors provide high efficient due to strong magnets, NdFeB. Majority of car manufactures use PM motors and hence, the demand of strong magnets, which are made of critical rare elements, are very high and will increase with increase in demand for electric cars. Therefore, it is very critical to have sufficient and sustainable supply of magnets for the motors to support growth of electric vehicle. These strong magnets contains critical rare earth materials like Nd and Dy. In addition to limited availability of these materials it is very important to recycle them for environment. Many projects has been started to investigate recycling and reuse of magnets. The projects like EREAN, RARE^3 etc are focusing on developing methods to recycle extracted magnets. The project MORE [5] has looked into recycling of all components of vehicle. The PM motors used in electric vehicles are, either inset (IPM) or surface mounted PM (SMPM) motors. The present motor designs possesses three challenges for recycling. Firstly, The extraction of magnets is very difficult and needs complex process that makes the extraction expensive [3]- [5]. Secondly, the use of glue/band-aid to fix magnet on rotor in SMPM or in magnet slots in IMP and to remove these adhesives chemical or heat treatment done which not environment friendly. Thirdly, designs are very non-standard both in terms of material and process. Moreover, for NdFeB sintered magnets coating is also required that has to be removed before starting recycling process. The quality of recycled magnet largely depends on the status of extracted magnet from used motor. Therefore, to achieve good recycling of magnets consideration must be put at the design phase of the motor. In Demeter, H2020, project the main goal is to design motor keeping recycling as main criteria without loosing its performance.

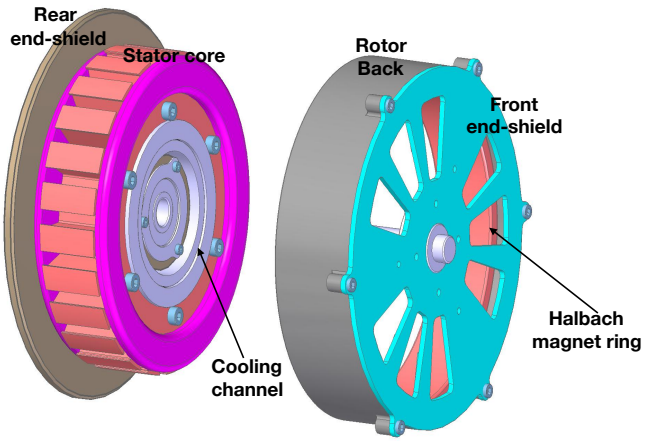

Fig. 1: Components of motor designed for easy recycling

In this article an outer rotor motor design is proposed for electric vehicles addressing issues mentioned above. The motor construction is very easy to assemble and disassemble using standard tools and process. Furthermore, the design has a single cylinder of magnet which makes extraction of magnet very easy. The magnet used for the rotor is bonded NdFeB Halbach magnet hence, ensuring easy manufacturing at low cost. The outer rotor topology and rotor assembly presented is glue free and same is also demonstrated on a sample rotor. The article also presents the measured magnetic, electrical and thermal properties of magnet used for design. The results for motor performance is also presented and compared with a SMPM motor. It can be seen that the proposed design have 19% higher torque than the SMPM motor with same dimensions.

II. Motor Design

The proposed motor designed is a PM outer rotor motor shown in figure 1. The design can be divided in two parts - stator assembly and rotor assembly. The stator assembly is comprised of rear end-sheild, stator core, copper and cooling channel. The rotor assembly is comprised of front-end shield, rotor back and Halbach magnet ring. Most of the components are fixed together either using screws or press fit to have easy assembly/disassembly of the motor. Furthermore, to improve recycling most of the components like lamination, screws, bearings etc are standard material and are easy to recycle. The rotor assembly has a single cylinder of Halbach magnet manufactured using injection molding process and the thin rotor back. Unlike, most motors the rotor back is a sheet of steel and is not laminated. The magnet used in the motor is an anisotropic bonded NdFeB magnet called MagFine 18P from Aichi Steel The stator winding has fractional slot tooth coil winding (FSTCW), which make stator design compact and simple. The design ensures not only easy extraction of magnet but also simple steps to extract other motor parts. Following are the advantages of proposed motor design for recycling.

1) Easy stator and rotor assembly separation : The rotor and stator assembly is connected only through shaft that makes separation of both the parts easy using standard tools.
2) Simple rotor assembly : The use of screw makes very easy separation of end-shield from rotor structure as shown in figure 2a.
3) Simple extraction of magnet : The magnet and rotor back is like two concentric cylinder and therefore, it is very easy to extract magnet either by heating or by cutting a small section of rotor back as shown in the figure 3. The extracted magnet was not damaged due to extraction process and can be reused in some other application however, the scenario of magnet reuse is very unlikely.
4) Glue free assembly of magnet and rotor back : The magnet is assembled inside the rotor back without any glue. Because the motor has outer rotor the centrifugal force help in keeping both magnet and rotor back together.
5) No external magnetic field : The main feature of Halbach magnet ring is that the magnetic field is only on one side of the cylinder and ideally, no field on the other side. The motor is an external rotor with all the filed only inside the cylinder. Therefore, standard tools can be used to work with the motor and this is also very important for ensuring safe working environment.

The Halbach magnet cylinder with relatively small dimensions (30 mm - 70 mm) can be made easily using injection molding without any cracks. Despite easy manufacturing of bonded magnet compared to sintered magnets manufacturing cylinder of large diameter for high torque density motor is difficult at this stage and further research needs to be done [6]. Moreover, the magnetization of thicker anisotropic bonded cylinders are also difficult. Therefore, more research has to be focused to develop manufacturing of bonded magnet. The proposed motor has almost 3.5 times the axial length. The advantage with this pan cake structure is that the major weight of the motor is on stator and can be supported from one end. The shaft has to take only the rotor weight and in this arrangement it is done with 2 bearings. However, this topology can be difficult for motors with long axial length where the point of load will be far from stator support.

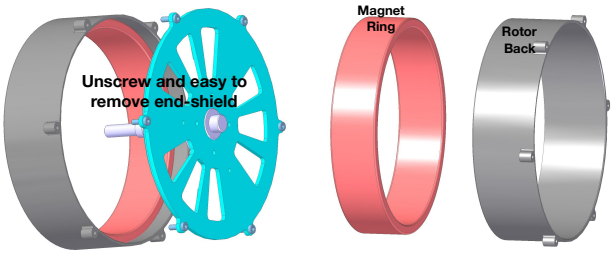

(a) Disassembly of Rotor and End-shield

(b) Separation of Rotor and Magnet ring

Fig. 2: Disassembly of Rotor

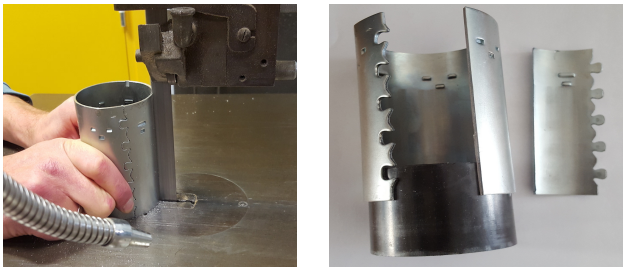

Fig. 3: Separation of rotor back and magnet

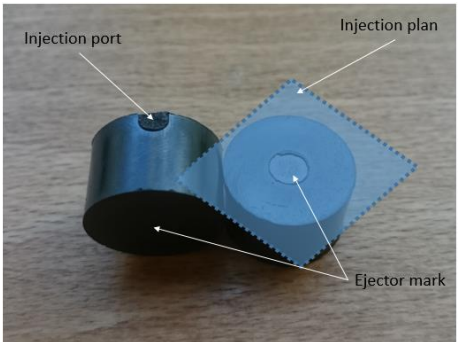

Fig. 4: Magnet sample used for measuring magnetic properties

III. Characterization of Bonded Magnet for Halbach

A. Density

The density of the magnet was measured by Archimedes thrust method in both water and ethanol. The average measured density is 4.978 $g.cm^{-3}$. If it assumed that the density of NdEeB powder and PPS binder is 7.6 $g.cm^{-3}$ and 1.35

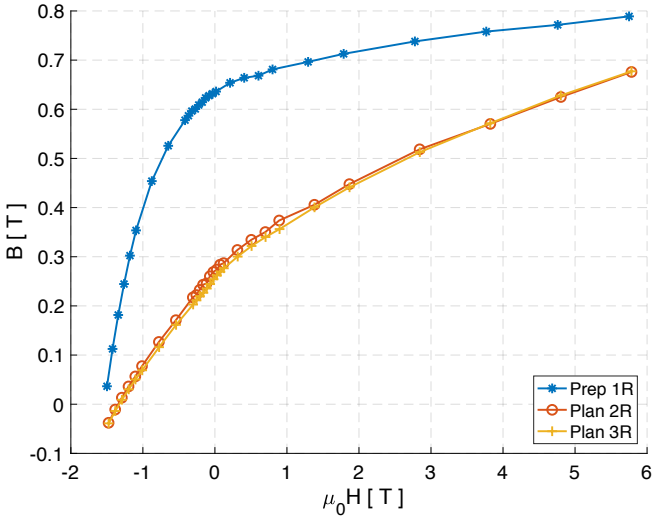

Fig. 5: Field density in different direction

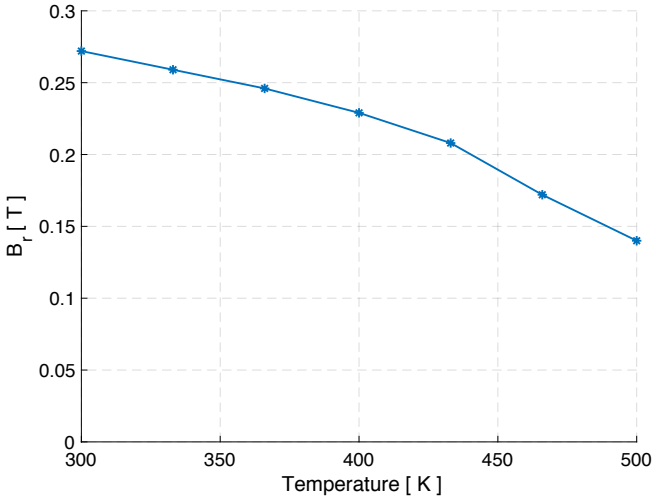

Fig. 6: Variation of remanence field density with temperature

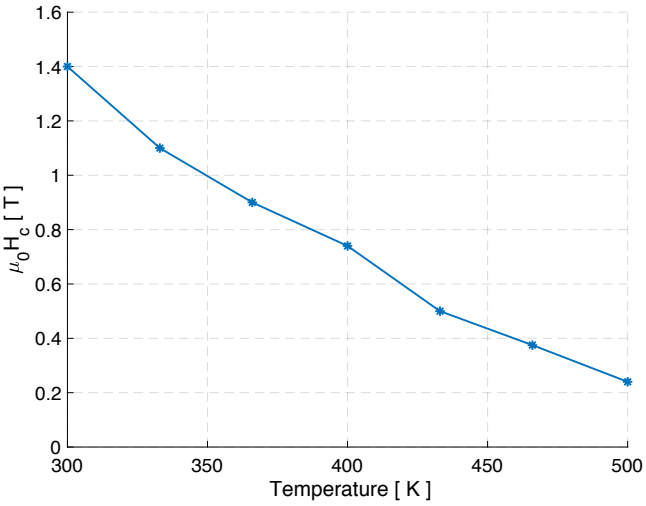

Fig. 7: Variation of coercivity with temperature

$g.cm^{-3}$ respectively. The sample magnet has 89 % NdFeB powder by weight (or 58 % by volume).

B. Magnetic properties

The magnetic properties of the sample were measured using extraction magnetometer which can apply field up to 7 T and temperature in the range of 300 K to 800 K (27 to 527 $^{\circ}C$). To perform measurement a sample of 3 mm cube was made from the magnet sample shown in figure 4.

1) Anisotropy: The demagnetization in each directions were measured and the values are shown in figure 5. The figure shows that the magnet is anisotropic. The direction named Prep 1R has high magnetic field compared to other axes and is the easy magnetization axis. The other two hard magnetization axes have very similar magnetic behaviour. The remanence of easy axis is almost 230 % higher than the other two axes. The anisotropic ratio of the magnet was around 0.42.

2) Thermal Behaviour: Figure 6 and 7 shows the variation of magnet remanence and coercivity with temperature. The values measured were for the difficult magnetic axis of the magnet sample. The thermal coefficient of remanence and coercivity of magnet is -0.066 $\%/^{\circ}C$ and 0.58 $\%/^{\circ}C$ respectively. For simple approximate calculation, the thermal coefficient of remanence for the easy axis calculated from hard axis value is -0.157 $\%/^{\circ}C$ (-0.066 $\%/^{\circ}C$/0.42). The smoothness of the curve also suggests that there was no drastic chemical or mechanical degradation of the magnet. However, as the high temperature was not applied for very long duration the behaviour of the magnet in those conditions are unknown. The variation of saturation magnetic field also shows similar trend of decrease in the value with increase in temperature see figure 8. For instance at 500 K it requires only 0.58 T to magnetize the magnet which would be much easier to produce.

C. Magnet Resistivity

The resistivity of magnet was measured using 4 wire method. Figure 9a shows the schematic of the setup used for resistivity measurement of the magnet. The magnet sample size was very small and hence, needed special preparation before measurement. Figure 9b shows the sample for the measurement. The measured value was in the range of 127 $\mu\Omega.m$ to 160 $\mu\Omega.m$. Measurement was also performed with different input currents and the impact was not significant. The difference in measured value can be because of the different sample. The resistivity of the bonded magnets are greatly influenced by the production methods and the sample obtained. Nevertheless, considering the worst case scenario the resistivity of the magnet can be taken as 120 $\mu\Omega.m$ for 57 % volume magnet.

D. Thermal Conductivity

Figure 10 shows the experiment setup for thermal conductivity measurement of bonded NdFeB magnets. The magnet sample's inner and outer radiuses are 27.3 mm and 33.4

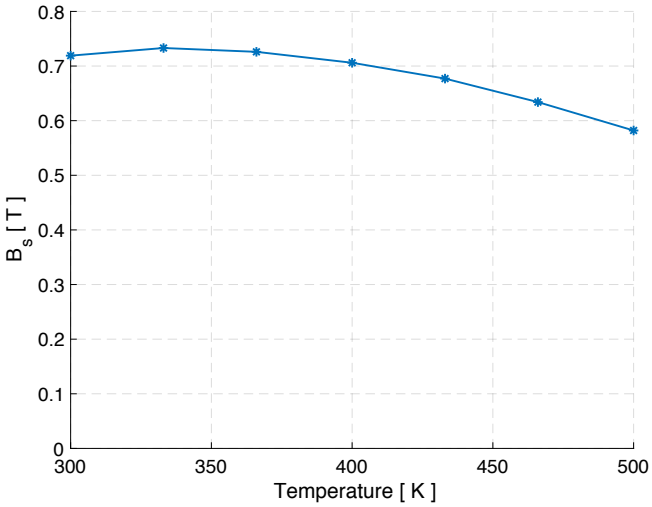

Fig. 8: Variation of saturation field density with temperature

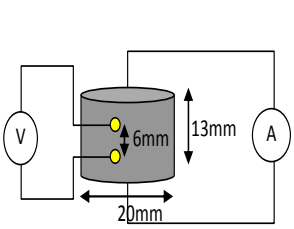

(a) Measurement Schematic

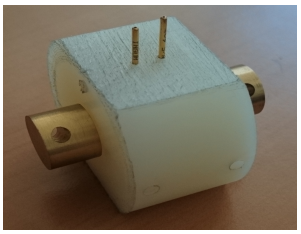

(b) Preparation of sample for measurement

Fig. 9: Resistivity measurement setup of the Bonded NdFeB magnet

mm respectively. The height of the sample is 45mm. 8 T-Type thermal sensors were used to measure the temperature at different positions on the magnet cylinder. 4 sensors were placed inside the cylinder and 4 outside making 4 pairs radially as shown in figure 10a. A cylindrical heater is used to heat the magnet and cover around the magnet sample. The heater is supplied with a controlled DC source and the input power was measured. The sample was insulated from outside so that there was no heat loss from the outer surface as shown in figure 10b. The thermal conductivity of the magnet is calculated using equation (1) - (2).

$$\Delta T = R_{th} \times P_{in} \tag{1}$$

$$\lambda_{th} = \frac{L}{A \times R_{th}} \tag{2}$$

The supply DC voltage of the heater was maintained such that the P_{in} was 7 W and 10 W. The supply was kept on till the temperatures reached steady state. Figure 11 shows the measured temperature and the temperature difference (ΔT) in steady state at different positions. From the figure it can be seen that different positions have different temperature which could be due to non-uniformity in the heating. Furthermore,

(a) Placement of temperature sensors

(b) Measurement Unit for temperature

Fig. 10: Experimental setup for thermal conductivity of the bonded NdFeB magnet

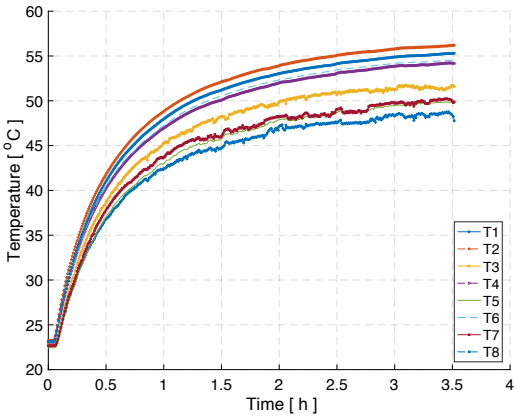

(a) Measured temperature with 7 W

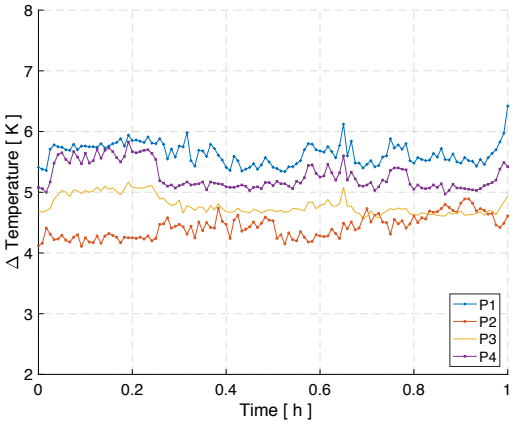

(b) Temperature difference (ΔT) at 7 W

Fig. 11: Measured temperature at different points with 7 W Input power

the difference in ΔT at different positions suggest the non-uniformity in the magnet thermal conductivity. However, the difference is not very large and hence, an average value of the thermal conductivity can be used to study the thermal behaviour of the magnet in different operating conditions. The average value of ΔT at different position is given in table I. The thermal conductivity of the magnet at 7 W and 10 W is 1.00 $W.m^{-1}.K^{-1}$ and 1.03 $W.m^{-1}.K^{-1}$.

TABLE I: ΔT at different positions on the magnet and the average thermal conductivity of the magnet

P_{in} [W]	Pos 1 [K]	Pos 2 [K]	Pos 3 [K]	Pos 4 [K]	Average [K]	Thermal Conductivity [$W/(m.K)$]
7.00	5.64	4.43	4.79	5.26	5.02	1.00
9.92	9.24	5.72	5.97	6.92	6.96	1.03
12.94	8.94	7.43	10.4	8.70	8.87	1.05
20.05	13.24	11.33	15.44	12.49	13.12	1.10
24.87	14.91	13.50	18.74	15.14	15.63	1.18

(a) 6 pole Halbach cylinder

(b) Measurement setup

Fig. 12: Halbach magnet sample and magnetic filed sample measurement setup

E. Validation of Halbach Magnet

The flux density of a 6 pole Halbach magnet cylinder was measured to analyze the magnetic field distribution. Furthermore, the validation of calculated field using FEM model was also done against the measurement. Figure 12a shows the Halbach rotor for the measurement. The spatial measurements were recorder with a radial Hall probe mounted with the fixture on the vertical drill press. The probe was moved in all three XYZ axis. To avoid any interference of environment a plastic base was used. Figure 12b shows the setup used for measuring magnetic field density inside the cylinder.

Figure 13 shows the flux density inside the Halbach cylinder at different vertical (Z direction) positions from the top. It can be seen that the axial position does not have any significant impact on the flux density values or its distribution. In figure 14 the comparison of measured and FEM calculated flux density inside the cylinder is shown. The calculated values are in very good agreement with measured flux density. The measured flux density around the circumference is sinusoidal, very close to the ideal Halbach magnetic field distribution.

F. Recycling of Bonded Magnet

In recent past, there has been some projects on recycling of NdFeB and SmCo magnets like EREAN, DEMETER, RARE[3] etc. However, the main focus was on recycling of sintered magnet due to not very wide use and low cost of bonded magnets. The presence of resins makes extraction of magnetic powder difficult without heating or chemical treatment of the magnet [7]. Another, method of recycling bonded magnet is to crush the used old magnet and mix with new magnets. The ratio of old and new magnet in the mix is very important to

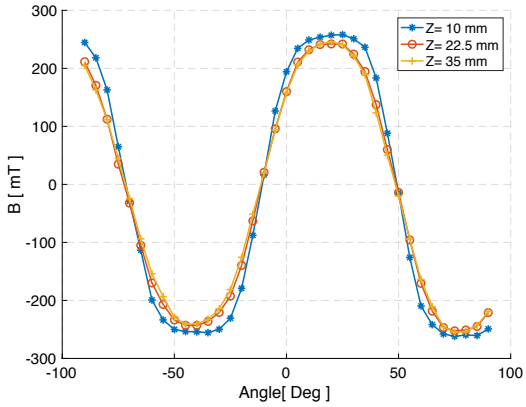

Fig. 13: Magnetic flux density at different vertical positions

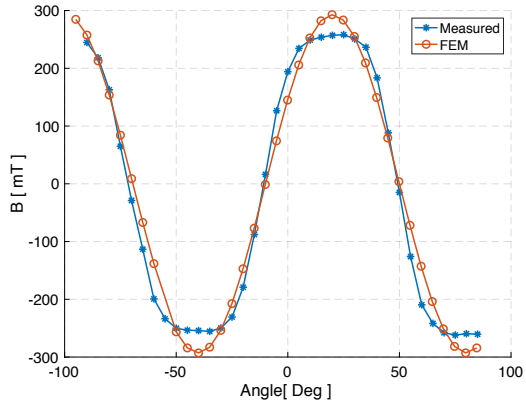

Fig. 14: Magnetic flux density at different vertical positions

have a good performance recycled magnet and it has been shown that the recycled magnet produced using mix of 30% old and 70% new does not reduce its remanance and the impact on coercivity is less than 2% [6]. Therefore, unlike sintered magnets bonded magnets can be recycled using simple process and without loosing magnetic properties.

IV. Motor Performance

The motor performance was calculated using fine element method (FEM) software Flux^{TM} 2D & 3D. The motor is designed for hybrid electric vehicle. The design specification for the motor is given in Table II. The proposed motor design has 24 slots and 26 poles with FSTCW. The impact of slot pole combination on motor is discussed in [8]- [9]. It is advantageous to use higher number of poles for Halbach rotor however, it is also important to consider inverter switching frequency and the iron loss. Hence, 26 poles was the best choice. Another, factor to select this slot pole combination is the high winding factor. Although, FSTCW causes many higher and sub harmonics, with bonded Halbach magnet rotor the impact of harmonics is not significant.

TABLE II: Motor Design Specification.

DC link Voltage	300 V	Axial length	76 mm
RMS Current	245 A	Maximum Output Power	50 kW
Outer Diameter	262 mm	Maximum Winding Temperature	180 $^{\circ}C$

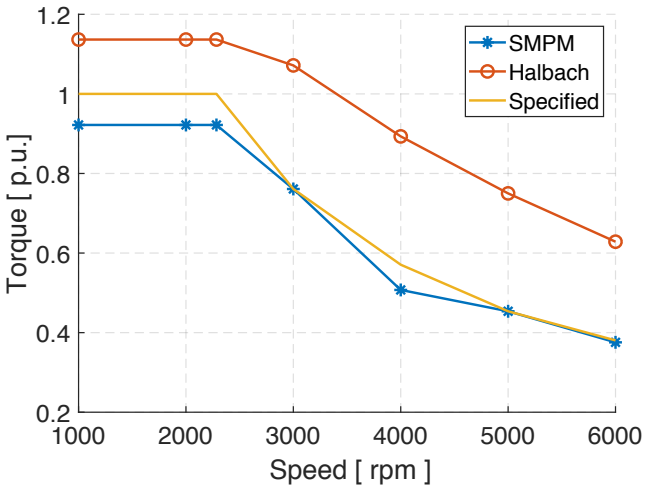

Fig. 15: Torque speed characteristic of the motor and its comparison with SMPM

A. *Torque Speed Characteristic*

Figure 15 shows the electromagnetic torque of the motor with bonded NdFeB Halbach magnet, SMPM and the specified. It can be seen that the motor fulfills the torque requirement both in constant torque and power region of the motor operation. The high torque of the motor, despite bonded magent, is due to the Halbach magnet arrangement and outer rotor configuration. Furthermore, the motor has slightly higher than 1 per unit (p.u.) inductance due to high leakage inductance of FSTCW and hence, has very wide constant power region [10]- [11]. The figure also illustrates the comparison of proposed motor with a SMPM motor. To have a fair comparison line voltage, current density, outer diameter, active length, slot pole combination, magnet volume, material and grade where kept same for both the calculation. The motor with Halbach motor has 17% higher maximum torque than the SMPM due to higher airgap flux density. In constant power region also Halbach motor has better torque than the SMPM motor.

B. *Efficiency*

The efficiency of the motor was calculated using FEM model at different load points as shown in figure 16. The efficiency of the motor does not include magnet loss (bonded magents), stray loss and other frictional loss. As can be seen that the motor has wide high efficiency area which is good for vehicle performance. Figure 17 and 18 shows the stator iron

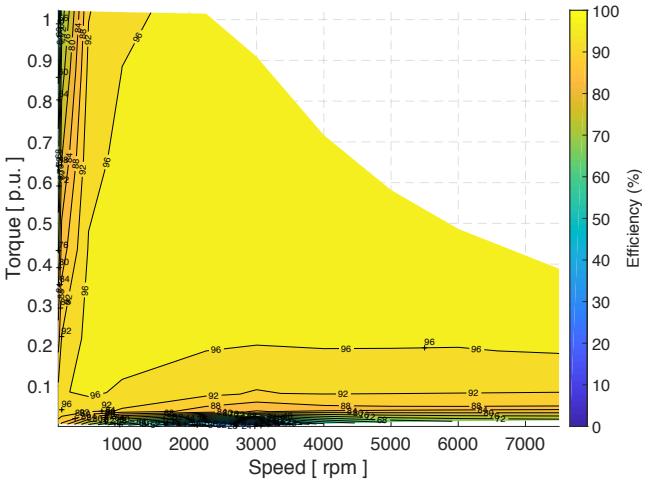

Fig. 16: Efficiency of motor over whole speed range

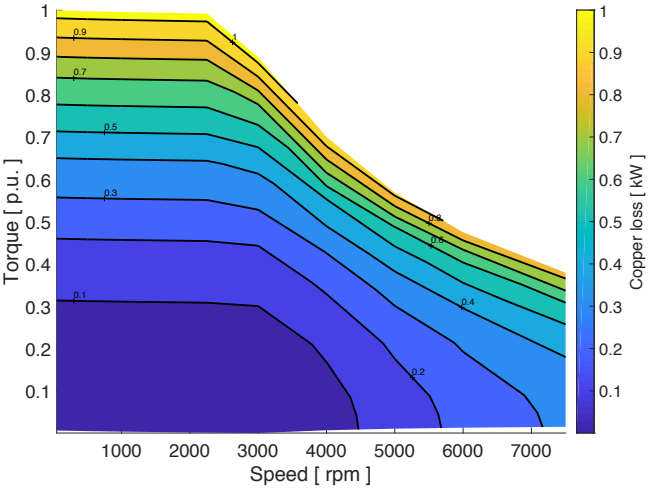

Fig. 17: Efficiency of motor over whole speed range

loss (negligible rotor loss) and copper loss of the motor. It can be seen that the iron loss at low speed, high torque is less than 10% fo the copper loss which is good for operation with many start stop.

V. Conclusion and Discussion

The proposed motor design enables easy assembly and disassembly of the motor. The simple rotor structure makes extraction of the magnet from the rotor very simple and easy. The concept of extraction has also been demonstrated on one prototype. It was observed that the extracted magnet was in very good condition and can be reused which is an added advantage of the rotor assembly. The Halbach (outer rotor) has not external magnetic field which makes extraction process very safe and hence, standard tools can be used. The rotor magnet used is Halbach anisotropic bonded magnet. The bonded magnet cylinder ring can be easily made using injection molding and the measurement results shows high anisotropic ratio which improves the magnetic properties. The

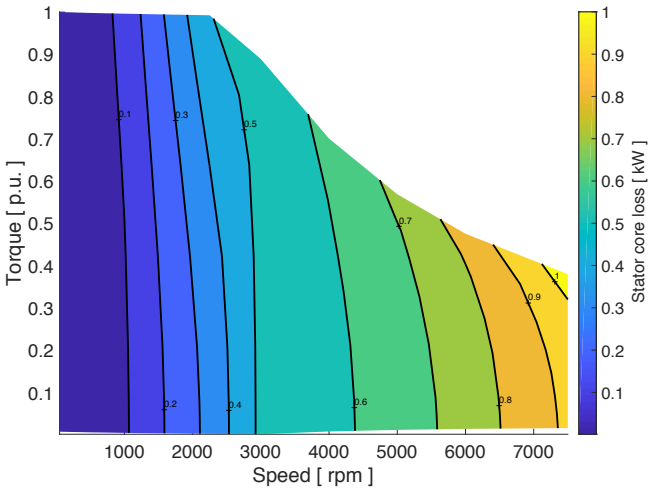

Fig. 18: Efficiency of motor over whole speed range

magnet has very stable behaviour against temperature and can easily handle 200 $^{\circ}C$ without any structural deformation. The resistance measurement of magnet shows high resistivity almost 100 time higher than sintered magnet and therefore, almost no magnet eddy loss. Due to high resistivity no magnet section is required which enables a glue free magnet rotor assembly. As expected thermal conductivity of the magnet is lower than the sintered magnet however, the temperature rise should not be high as the magnet loss is negligible and the expected heat transfer through the airgap is very small. It is also shown that the field distribution in the manufactured Halbach magnet sample is very sinusoidal and is in very good agreement with the calculated values.

The Halbach magnet has very sinusoidal field distribution and hence, FSTCW can be used for stator winding. The winding arrangement makes motor compact and improve performance by reducing the coil overhang and copper loss respectively. Furthermore, unlike motor with sintered magnets, the sub and higher order harmonics generated due to the FSTCW winding does not have any significant impact on rotor loss especially, magnet loss. The motor fulfills the torque speed requirement of a 300 V DC hybrid electric vehicle. The outer rotor topology due to higher airgap diameter augments the produced torque. It is also interesting to see that with same constraints the motor with Halbach motor generate 19% higher torque than the SMPM motor. The efficiency of the motor is also high over a wide torque-speed range. Another advantage of the Halbach is light weight rotor due to very thin rotor back which is very significant for overall vehicle performance.

ACKNOWLEDGMENT

The research leading to these results has received funding from European Communitys Horizon 2020 Programme ([H2010/2014-2019]) under Grant Agreement no. 674973 (MSCA-ETN DEMETER). This publication reflects only the authors view, exempting the Community from any liability. Project website http://etn-demeter.eu/

The authors also highly appreciate the support received from Dr. Rivoirard and Dr. Mandil from CNRS/Neel Institute for performing the measurements and Aichi Steel.

REFERENCES

[1] Countries are announcing plans to phase out petrol and diesel cars. is yours on the list? [Online]. Available: https://www.weforum.org/agenda/2017/09/countries-are-announcing-plans-to-phase-out-petrol-and-diesel-cars-is-yours-on-the-list/

[2] Internaltion Energy Agency, Ed., *Global EV Outlook 2017*.

[3] T. Elwert, D. Goldmann, F. Rmer, M. Buchert, C. Merz, D. Schueler, and J. Sutter, "Current developments and challenges in the recycling of key components of (hybrid) electric vehicles," *Recycling*, vol. 1, no. 1, pp. 25–60, 2015. [Online]. Available: http://www.mdpi.com/2313-4321/1/1/25

[4] L. Kumar and S. Jain, "Electric propulsion system for electric vehicular technology: A review," *Renewable and Sustainable Energy Reviews*, vol. 29, no. Supplement C, pp. 924 – 940, 2014. [Online]. Available: http://www.sciencedirect.com/science/article/pii/S1364032113006734

[5] U. Bast, R. Blank, M. Buchert, T. Elwert, F. Finsterwalder, G. Hornig, T. Klier, S. Langkau, F. Marscheider-Weidemann, J.-O. Muller, C. Thurigen, F. Treffer, and T. Walter, "Recycling von komponenten und strategischen metallen aus elektrischen fahrantrieben," Aug-2014.

[6] "Internal communication with Aichi Steel." [Online]. Available: https://www.aichi-steel.co.jp

[7] Y. Yamagata and F. Yamashita, "Method of recovering and recycling magnetic powder from rare earth bond magnet," Mar. 18 2003, uS Patent 6,533,837. [Online]. Available: http://www.google.com/patents/US6533837

[8] A. K. Jha, L. Garbuio, A. Kedous-Lebouc, J. P. Yonnet, and J. M. Dubus, "Design and comparison of outer rotor bonded magnets halbach motor with different topologies," in *2017 15th International Conference on Electrical Machines, Drives and Power Systems (ELMA)*, June 2017, pp. 6–10.

[9] A. K. Jha, A. Kedous-Lebouc, L. Garbuio, J. P. Yonnet, and J. M. Dubus, "Fea based analysis on effect of slot pole combination on motor torque and magnet eddy current loss with bonded ndfeb halbach rotor," in *2017 20th International Conference on Electrical Machines and Systems (ICEMS)*, Aug 2017, pp. 1–5.

[10] A. M. El-Refaie, T. M. Jahns, P. J. McCleer, and J. W. McKeever, "Experimental verification of optimal flux weakening in surface pm machines using concentrated windings," *IEEE Transactions on Industry Applications*, vol. 42, no. 2, pp. 443–453, March 2006.

[11] A. M. El-Refaie, T. M. Jahns, and D. W. Novotny, "Analysis of surface permanent magnet machines with fractional-slot concentrated windings," *IEEE Transactions on Energy Conversion*, vol. 21, no. 1, pp. 34–43, March 2006.